





Endothelial Cell-derived Extracellular Vesicles Modify Myelopoiesis in the Bone Marrow

Thesis submitted for the degree of

Doctor of Philosophy in Cardiovascular Science

University of Oxford

Lewis Timms

Division of Cardiovascular Medicine

Radcliffe Department of Medicine

&

Worcester College

Supervisors: Professor Robin Choudhury

Associate Professor Naveed Akbar

Abstract

Following a myocardial infarction (MI), there is an increase in plasma extracellular vesicles (EV). This increase correlates with the extent of myocardial damage and the EV were shown to be of endothelial cell origin. Further characterisation showed these endothelial cell-EV (EC-EV) are positive for vascular cell adhesion molecule-1 (VCAM-1) and are enriched in microRNA (miRNA) cargo, including miRNA-126-3p and miRNA-320b. EC-EV localise to the spleen and VCAM-1^{+} EC-EV rapidly mobilise monocytes and neutrophils, although it is unclear if they have a role in the bone marrow. This thesis therefore sets out to understand the role of EC-EV in the bone marrow.

Initially, I tested the hypothesis that EC-EV increases bone marrow haematopoiesis *in vivo* and found increases in several haematopoietic stem and progenitor cell (HSPC) populations. I then used transcriptomic analysis in bone marrow haematopoietic stem cells (HSC) and found an overlap in differentially expressed genes in response to EC-EV and miRNA-126-3p and miRNA-320b, which are both enriched in EC-EV, indicating a potentially novel mechanism of regulating bone marrow haematopoiesis.

I then tested a model of EC-EV on bone marrow-derived macrophages (BMDM) to determine whether they have a modulated innate immune response after the stimulus was removed. I identified modifications in the inflammatory profile of the macrophages, including lower pro-inflammatory cytokine secretion, lower cell adhesion to endothelial cell monolayers, and changes in cellular metabolism and phosphorylation signalling. These effects appeared to be VCAM-1 dependent.

Acknowledgements

I would like to start by thanking the British Heart Foundation for funding this research and for the opportunities they have extended to me in the form of travel grants and presenting my work. I would also like to thank Worcester College and the Division of Cardiovascular Medicine for providing a welcoming and nurturing environment where I could produce my best research.

Secondly, I would like to show gratitude to my supervisors. Robin, from the beginning you have helped to sculpt this project and make sure things remain on the right track. You have been an excellent leader throughout my project and, with some colourful analogies, have added some light-heartedness to the complexities of medical research. Nav, you have trained me in just about every possible technique and always did so with great patience and humour. Through daily chats and weekly meetings, you have constantly pushed me to challenge myself and become a better, more well-rounded scientist and person in general. To the rest of the Choudhury and Akbar lab members and to our external collaborators, notably Dr Robert Hedley, Professor Daniel Anthony, and Dr Daniel Radford-Smith, I would like to thank each of you for your advice and assistance throughout and without you, this work would not have been possible.

Lastly, I would like to thank all of my extended family and especially my mum and sister. Since I was young, you have always supported me in everything that I put my mind to, as a football player, a horse rider, a tennis player, a ballroom dancer, and now as a scientist. I hope to keep making you proud each and every day.

Table of Contents

Abstract 2

Acknowledgements 3

Table of Contents 4

List of Figures 8

List of Tables 13

List of Abbreviations 14

Chapter 1- Introduction 20

1.1 Cardiovascular Diseases 20

1.2 Myocardial Infarction and the Bone Marrow 25

1.3 Extracellular Vesicles 30

1.4 Extracellular Vesicles in Cardiovascular Disease 35

1.5 Endothelial Cell-Extracellular Vesicles in Cardiovascular Disease 38

1.6 Hypotheses 41

Chapter 2- Materials and Methods 42

2.1 Media Preparations 42

2.2 Endothelial Cell Culture 44

2.3 Extracellular Vesicle Isolation Using Ultracentrifugation 45

2.4 Extracellular Vesicles Characterisation 47

2.5 In Vivo Experimentation 52

2.6 Isolation of Bone Marrow, Spleen and Blood Cells for Flow Cytometry Analysis 53

2.7 Cell Staining for Flow Cytometry Analysis 54

2.8 Bone Marrow and Splenic Haematopoietic Stem and Progenitor Cell Analysis Using the In Vivo Endothelial Cell-Extracellular Vesicle Model 56

2.9 Protein Analysis by Enzyme-Linked Immunosorbent Assay (ELISA) 58

2.10 Colony-Forming Unit Assay for the Bone Marrow-Endothelial Cell-Extracellular Vesicle Model 59

2.11 Bone Marrow and Splenic Haematopoietic Stem and Progenitor Cell Analysis Using the In Vivo Endothelial Cell-Extracellular Vesicle Priming Model 62

2.12 Bone Marrow Haematopoietic Stem Cell isolation Using Fluorescence-Activated Cell Sorting for Transcriptomic Analysis 63

2.13 Gene Expression Analysis by RT-qPCR 67

2.14 Endothelial Cell-Extracellular Vesicle microRNA Isolation and Analysis 69

2.15 Endothelial Cell-Extracellular Vesicle microRNA Cargo Bioinformatics Analysis 70

2.16 Isolation and Culturing of Bone Marrow Cells to Generate Bone Marrow-Derived Macrophages 71

2.17 Bone Marrow-Derived Macrophage Characterisation Using Flow Cytometry 73

2.18 Bone Marrow-Derived Macrophage In Vitro Tolerance Model 74

2.19 Static Adhesion Assay to Assess Bone Marrow-Derived Macrophage Function 75

2.20 Isolation & Culturing of Peritoneal Macrophages for Protein Studies 76

2.21 Generating Denatured Endothelial Cell-Extracellular Vesicles 77

2.22 Human Monocyte-Derived Macrophage In Vitro Tolerance Model 78

2.23 Statistical Analysis 79

Chapter 3- Endothelial Cell Extracellular Vesicles Modulate Haematopoiesis in Bone Marrow and Spleen 81

3.1 Introduction 81

3.2 List of Methods Used in This Chapter 83

3.3 Characterisation of Endothelial Cell-Extracellular Vesicles 84

3.4 TNF-α-Stimulated Endothelial Cell-Extracellular Vesicles Increase Haematopoietic Stem Cells in Mouse Bone Marrow, But Not the Spleen 86

3.5 TNF-α-Stimulated Endothelial Cell-Extracellular Vesicles Increase Circulating Monocytes, Neutrophils, & Erythrocytes 95

3.6 TNF-α-Stimulated Endothelial Cell-Extracellular Vesicles Skew Bone Marrow Haematopoiesis Towards Granulocytes & Monocytes In Vitro 101

3.7 Priming Mice With TNF-α-Stimulated Endothelial Cell-Extracellular Vesicles Lowers Innate Immune Cells & Bone Marrow Progenitor Cells in Response to LPS 104

3.8 Proliferation of Haematopoietic Stem & Progenitor Cells is Modified Following Priming with TNF-α-Stimulated Endothelial Cell-Extracellular Vesicles In Vivo 117

3.9 Discussion 119

Chapter 4- RNA Analysis of Endothelial Cell Extracellular Vesicle Cargo and Bone Marrow Haematopoietic Stem Cells 126

4.1 Introduction 126

4.2 List of Methods Used in This Chapter 128

4.3 Transcriptional Analysis of Mouse Bone Marrow Haematopoietic Stem Cells Following Exposure to TNF-α-Stimulated Endothelial Cell-Extracellular Vesicles 129

4.4 microRNA-126-3p & microRNA-320b Are Enriched in Mouse Endothelial Cell-Extracellular Vesicles Following Stimulation with TNF-α 147

4.5 microRNA126-3p & microRNA320 are Partially Protected From RNAse Degradation in Mouse Endothelial Cell-Extracellular Vesicles 149

4.6 Identification of miRNA-mRNA Targets For Differentially Expressed miRNAs in Plasma Endothelial Cell-Extracellular Vesicles 152

4.7 Discussion 166

Chapter 5- Endothelial Cell-Extracellular Vesicles Modulate the Inflammatory Profile of Bone Marrow-derived Macrophages 171

5.1 Introduction 171

5.2 List of Methods Used in This Chapter 173

5.3 Characterisation of Mouse Bone Marrow-Derived Macrophages 174

5.4 Endothelial Cell-Extracellular Vesicles induce a Tolerance Phenotype in Pro-Inflammatory Bone Marrow-Derived Macrophages 175

5.5 The Endothelial Cell-Extracellular Vesicle Bone Marrow-Derived Macrophage Tolerance Phenotype is Conserved Between Mouse and Human Models 183

5.6 Mouse Bone Marrow-Derived Macrophages Undergo a Pro-Inflammatory Metabolic & Phosphorylation Shift in Response to TNF-α Endothelial Cell-Extracellular Vesicle Priming 187

5.7 Endothelial Cell-Extracellular Vesicle Priming Does Not Induce a Tolerance Response in Peritoneal Macrophages 190

5.8 Denaturing Endothelial Cell-Extracellular Vesicles Mitigates the Tolerance Phenotype in Bone Marrow-Derived Macrophages 192

5.9 Discussion 201

Chapter 6- Discussion 208

6.1 Key Findings 208

6.2 Study Limitations & Future Work 212

6.3 Conclusions 216

References 218

List of Figures

***Figure 1**. Lineage Tree of Bone Marrow Haematopoietic Stem and Progenitor Cells.*

***Figure 2**. Overview Schematic of Endothelial Cell-Extracellular Vesicle Culture and Isolation Using Ultracentrifugation.*

***Figure 3**. Overview Schematic of Endothelial Cell-Extracellular Vesicle Characterisation Using Nanoparticle Tracking Analysis, Western Blotting, and Cryo-TEM Imaging.*

***Figure 4**. Overview of the In Vivo Study Investigating the Effects of Endothelial Cell-Extracellular Vesicles on Bone Marrow and Splenic Haematopoiesis.*

***Figure 5**. Colony-Forming Unit Assay Involving Bone Marrow Haematopoietic Stem Cells Exposed to Endothelial Cell-Extracellular Vesicles.*

***Figure 6**. Overview of the In Vivo Study on the Effects of Endothelial Cell-Extracellular Vesicle Priming on Bone Marrow and Splenic Haematopoiesis.*

***Figure 7**. Transcriptomic Analysis of Bone Marrow Haematopoietic Stem Cells in Response to Endothelial Cell-Extracellular Vesicles.*

***Figure 8**. Schematic of Mouse Bone Marrow Isolation and Culture to Generate Bone Marrow-Derived Macrophages.*

***Figure 9**. Overview of Bone Marrow-Derived Macrophage Isolation and Stimulation with Endothelial Cell-Extracellular Vesicles for Protein, RNA, and Static Adhesion Studies.*

***Figure 10**. Schematic Detailing Human Monocyte-Derived Macrophage Isolation and Culture, followed by Endothelial Cell-Extracellular Vesicle Stimulation and Sample Harvest.*

***Figure 11**. Characterisation of Mouse sEND.1 Endothelial Cell-Extracellular Vesicles.*

***Figure 12**. Injecting Mice with Control or TNF-α-Stimulated Endothelial Cell-Extracellular Vesicles to Investigate Changes in Bone Marrow Haematopoietic Stem and Progenitor Cells.*

***Figure 13**. TNF-α-Stimulated Endothelial Cell-Extracellular Vesicles induce Haematopoiesis in Mouse Bone Marrow.*

***Figure 14**. TNF-α-Stimulated Endothelial Cell-Extracellular Vesicles Do Not Impact Haematopoiesis in Mouse Spleen.*

***Figure 15**. TNF-α-Stimulated Endothelial Cell-Extracellular Vesicles Increase Production of Innate Immune Cells.*

***Figure 16**. TNF-α-Stimulated Endothelial Cell-Extracellular Vesicles Increase Erythrocytes and Lower Platelet Counts in Mice.*

***Figure 17**. TNF-α-Stimulated Endothelial Cell-Extracellular Vesicles Skew Haematopoiesis Towards Granulocyte-Monocyte Progenitors.*

***Figure 18**. Treating Mice with Control or TNF-α-Stimulated Endothelial Cell-Extracellular Vesicles Followed by LPS to Investigate the Effects of Extracellular Vesicle Priming on Bone Marrow Haematopoietic Stem and Progenitor Cells.*

***Figure 19**. Priming Mouse Bone Marrow with TNF-α-Stimulated Endothelial Cell-Extracellular Vesicles Followed by LPS Stimulation Lowers Granulocyte-Monocyte Progenitors.*

***Figure 20**. Priming Mice with TNF-α-Stimulated Endothelial Cell-Extracellular Vesicles Followed by LPS Does Not Impact Splenic Haematopoiesis.*

Figure 21. *Priming Mice with TNF-α-Stimulated Endothelial Cell-Extracellular Vesicles Followed by LPS Treatment Lowers Bone Marrow & Splenic Neutrophils.*

***Figure 22**. Priming Mice with TNF-α-Stimulated Endothelial Cell-Extracellular Vesicles Followed by LPS Treatment Lowers Cell Proliferation in Mouse Bone Marrow.*

***Figure 23**. TNF-α EC-EV Modulates Bone Marrow Haematopoiesis and Bone Marrow and Splenic Innate Immune Cell Counts.*

***Figure 24**. Injecting Mice with Control or TNF-α-Stimulated Endothelial Cell-Extracellular Vesicles Increases Spleen Weight but Not Body Weight.*

***Figure 25**. Fluorescence-Activated Cell Sorting Analysis of Mouse Bone Marrow to Isolate Haematopoietic Stem Cells.*

***Figure 26**. Quality Control Analysis of Bone Marrow Haematopoietic Stem Cells for Bulk RNA Sequencing.*

***Figure 27**. Gene Expression Analysis of Mouse Bone Marrow Haematopoietic Stem Cells Following Treatment with Control or TNF-α Endothelial Cell-Extracellular Vesicles.*

***Figure 28**. Gene Set Enrichment Analysis of Differentially Expressed Genes in Mouse Bone Marrow Haematopoietic Stem Cells in Response to TNF-α EC-EV Exposure.*

***Figure 29**. Gene Ontology Analysis of Bone Marrow Haematopoietic Stem Cells Following In Vivo Injection of TNF-α-Stimulated Endothelial Cell-Extracellular Vesicles.*

***Figure 30**. STRING Network Analysis of Bone Marrow Haematopoietic Stem Cells Following In Vivo Injection of TNF-α-Stimulated Endothelial Cell-Extracellular Vesicles.*

***Figure 31**. KEGG Analysis of Differentially Expressed Genes in Mouse Bone Marrow Haematopoietic Stem Cells in Response to TNF-α Endothelial Cell-Extracellular Vesicle Exposure.*

***Figure 32**. microRNA-126-3p and microRNA-320b are Enriched in Mouse sEND.1 Endothelial Cell-Extracellular Vesicles.*

***Figure 33**. RNase A Treatment of Mouse Endothelial Cell-Extracellular Vesicles Leads to Degradation of microRNA-126-3p and microRNA-320b After Vesicle Rupture.*

***Figure 34**. Gene Ontology and KEGG Pathway Analysis of Putative Gene Targets of microRNA-126-3p in Mice.*

***Figure 35**. Gene Ontology and KEGG Pathway Analysis of Putative Gene Targets of microRNA-320b in Mice.*

***Figure 36**. Gene Ontology & KEGG Pathway Analysis of Putative Gene Targets of microRNA-126-3p & microRNA-320b in Mice.*

***Figure 37**. microRNA-126-3p and miRNA-320b Putative Gene Targets Overlap with Mouse Bone Marrow Haematopoietic Stem Cell Differentially Expressed Genes.*

***Figure 38**. STRING Network Analysis of Overlapping Targets from microRNA-126-3p, microRNA-320b, and Bone Marrow Haematopoietic Stem Cell Differentially Expressed Genes.*

***Figure 39**. Characterisation of Mouse Bone Marrow-Derived Macrophages.*

***Figure 40**. Mouse Bone Marrow-Derived Macrophages Have a Modified Inflammatory Response to TNF-α Endothelial Cell-Extracellular Vesicles.*

***Figure 41**. Pro-Inflammatory Cytokines Are Not Stored Within Bone Marrow-Derived Macrophages in Response to TNF-α Endothelial Cell-Extracellular Vesicles.*

***Figure 42**. TNF-α Endothelial Cell-Extracellular Vesicles Lower Macrophage Adhesion to Activated Endothelial Cell Monolayers.*

***Figure 43**. Human Monocyte-Derived Macrophages Have a Lower Inflammatory Cytokine Response to TNF-α Endothelial Cell-Extracellular Vesicle Priming.*

***Figure 44**. Mouse Bone Marrow-Derived Macrophages Undergo Changes in Metabolic and Phosphorylation Processes in Response to TNF-α Endothelial Cell-Extracellular Vesicles.*

***Figure 45**. Mouse Peritoneal Macrophages Do Not Have a Modified Inflammatory Response to TNF-α Endothelial Cell-Extracellular Vesicles.*

***Figure 46**. Characterisation of Denatured Mouse sEND.1 Endothelial Cell-Extracellular Vesicles.*

Figure 47. *Denaturation Mitigates the Effects of TNF-α Endothelial Cell-Extracellular Vesicles on Bone Marrow-Derived Macrophages.*

Figure 48. *Denaturation Mitigates the Effects of TNF-α Endothelial Cell-Extracellular Vesicle Priming on Bone Marrow-Derived Macrophage Gene Expression.*

Figure 49. *Denaturation Mitigates the Effects of TNF-α Endothelial Cell-Extracellular Vesicles on Bone Marrow-Derived Macrophage Gene Expression.*

Figure 50. *TNF-α Endothelial Cell-Extracellular Vesicles Modulate the Inflammatory Profile of Bone Marrow-Derived Macrophages in a VCAM-1-Dependent Manner.*

Figure 51. *Overview Schematic Highlighting the Key Findings from This Thesis.*

List of Tables

***Table 1**. Antibody Details for Protein Analysis by Western Blotting.*

***Table 2**. Antibody Details for Flow Cytometry Analysis.*

***Table 3.** Overview of the Haematopoiesis Stem and Progenitor Cell Populations Assessed Using Flow Cytometry.*

***Table 4**. Antibody Details for FACS Isolation of Bone Marrow Haematopoietic Stem Cells.*

***Table 5**. Quantitative PCR Primer Details.*

***Table 6**. Antibody Details for Flow Cytometry Analysis.*

List of Abbreviations

7-AAD	7-amino-actinomycin D
ALIX	Apoptosis-linked gene 2 interacting protein X
AMPKα2	Adenosine monophosphate kinase activated catalytic subunit alpha 2
ANOVA	Analysis of variance analysis
ApoB	Apolipoprotein B
ARE	Adenine and uridine-rich element
ATP	Adenosine triphosphate
ATP5A	Adenosine triphosphate synthase subunit alpha
BCA	Bicinchoninic acid
BFU-E	Burst forming unit-erythroid
BMDM	Bone marrow-derived macrophages
BSA	Bovine serum albumin
CCR2	C-c chemokine receptor 2
CD	Cluster of differentiation
CFSE	Carboxyfluorescein succinimidyl ester
CFU	Colony-forming unit
CFU-GEMM	Colony-forming unit-granulocyte-erythroid macrophage megakaryocyte
CFU-GM	Colony-forming unit-granulocyte-monocyte
CLP	Common lymphoid progenitors
CM-EV	Cardiomyocyte-derived extracellular vesicles
CMP	Common myeloid progenitors

CXCL12	C-x-c motif ligand 12
CXCR4	C-x-c motif receptor 4
DAMPs	Damage-associated molecular patterns
DAPI	4'-6-diamidino-2-phenylindole
DEG	Differentially expressed genes
DI	Deionised
DMEM	Dulbecco's modified Eagle’s medium
Dusp-26	Dual-specificity phosphatase-26
EBM-2	Endothelial basal media-2
EC-EV	Endothelial cell-extracellular vesicles
EDTA	Ethylenediaminetetraacetic acid
EdU	5-ethynyl 2'-deoxyuridine
EGF	Epidermal growth factor
ELISA	Enzyme-linked immunosorbent assay
EM	Electron microscopy
eNOS	Endothelial nitric oxide synthase
ERK1/2	Extracellular signal-regulated protein kinase 1/2
ES	Enrichment score
EV	Extracellular vesicles
FACS	Fluorescence-activated cell sorting
FBS	Foetal bovine serum
FDR	False discovery rate
FITC	Fluorescein isothiocyanate
FPKM	Fragments per kilobase of transcript sequence per million base pairs

GAPDH	Glyceraldehyde 3-phosphate dehydrogenase
GM130	Golgi matrix protein 130
GMP	Granulocyte-monocyte progenitors
GO	Gene ontology
GR-1	Glucocorticoid receptor-1
GSEA	Gene set enrichment analysis
HIF1-α	Hypoxia-inducible factor 1-alpha
HRP	Horseradish peroxidase
HSC	Haematopoietic stem cells
HSPC	Haematopoietic stem and progenitor cells
HUVEC	Human umbilical vein endothelial cells
ICAM-1	Intercellular adhesion molecule-1
IFN-γ	Interferon-gamma
IgG	Immunoglobulin G
IL	Interleukin
iNOS	Inducible nitric oxide synthase
IP	Intraperitoneal
Irg1	Immunity related guanosine triphosphatase 1
IV	Intravenous
JAK	Janus kinase
KEGG	Kyoto encyclopedia of genes and genomes
LAD	Left anterior descending
LCX	Left circumflex artery
LK	Lineage-Sca1-cKit^{+}
LPS	Lipopolysaccharides

LSK	Lineage-Sca-1+cKit+
Ly6	Lymphocyte antigen 6
M-CSF	Mammalian-colony stimulating factor
MACS	Magnetic-activated cell sorting
MAPK	Mitogen-activated protein kinase
MCMV	Multi-compartmented microvesicles
MCP-1	Monocyte chemoattractant protein-1
MDM	Monocyte-derived macrophages
MEP	Megakaryocyte-erythroid progenitors
MI	Myocardial infarction
miRNA	microRNA
MISEV	Minimal information for studies of extracellular vesicles
MPP	Multi-potent progenitors
NF-kB	Nuclear factor-kappa B
NLR	Nucleotide-binding oligomerisation domain-like receptor
NLRP3	Nucleotide-binding oligomerisation domain-like receptor family pyrin domain containing protein 3
NRES	National research ethics service
NSAIDS	Non-steroidal anti-inflammatory drugs
NTA	Nanoparticle Tracking Analysis
Padj	Adjusted P values
PBMC	Peripheral blood mononuclear cells
PBS	Phosphate-buffered saline
PCI	Primary percutaneous intervention
Peg3	Paternally expressed gene-3

Ppia	Cyclophilin
PRR	Pattern recognition receptor
PTEN	Phosphatase and tensin homolog
RAC1	Ras-related c3 botulinum toxin substrate 1
RAGE	Receptor for advanced glycation end products
RBC	Red blood cell
RIPA	Radioimmunoprecipitation assay buffer
ROS	Reactive oxygen species
RPMI	Roswell Park memorial institute
RT-qPCR	Reverse transcriptase quantitative polymerase chain reaction
Sca-1	Spinocerebellar ataxia type 1
sEND.1	Skin-derived endothelial cell 1
siRNA	small interfering RNA
SOS1	Sons of sevenless1
STAT	Signal transducer and activator of transcription
STEMI	ST-segment elevation myocardial infarction
TCA	Tricarboxylic acid
TEM	Transmission electron microscopy
TLR	Toll-like receptor
TNF-α	tumour necrosis factor-alpha
TSG-101	Tumour suppressor gene 101
VCAM-1	Vascular cell adhesion molecule-1
VLA-4	Integrin very late antigen-4
WT	Wildtype
YM1	Chitinase-like protein 3

Zeb1	Zinc-finger E-box binding homeobox 1

Chapter 1- Introduction

1.1 Cardiovascular Diseases

Cardiovascular diseases are the leading cause of global mortality and have almost doubled in 32 years from 12.4 million deaths reported in 1990, to 19.8 million deaths reported in 2022 (1). Alongside risk factors such as obesity, smoking, hyperlipidaemia, diabetes and a sedentary lifestyle, cardiovascular diseases are rising amongst those under 50 years old (2), which may exacerbate this epidemic in the near future as an increased proportion of the population develop such diseases. Cardiovascular diseases include ischemic heart disease, ischemic stroke, haemorrhage, atrial fibrillation, cardiomyopathy, and hypertensive heart disease (3). Recent data from 2021 shows that the majority of cardiovascular disease-related deaths are caused by ischemic heart disease (3), which includes myocardial infarction (MI). Diagnosis of a MI often begins with symptoms such as persistent chest pain, shortness of breath, nausea and fatigue (4, 5), and then relies on clinical tests such as elevated blood troponin levels (4), and an electrocardiogram to assess electrophysiological changes to the heart. However, these tools only confirm an MI event after the myocardial injury has occurred and cannot predict an ischaemic event.

Once an MI has been confirmed, reperfusion therapies such as primary percutaneous intervention (PCI) are initiated and have been shown to lower acute and long-term mortality rates when the delay time to treatment is limited (6-8). In addition, patients can be treated with dual anti-platelet therapy agents (9), such as aspirin in combination with either prasugrel or clopidogrel, as part of fibrinolysis therapy, although the safety implications of excessive bleeding also need to be considered and fully elucidated (10, 11). Secondary preventions and disease management strategies post-MI include

controlling blood pressure, body weight management, increasing exercise, and quitting smoking (12). Pharmacological intervention through statins is very common for patients at an increased risk of cardiovascular disease (13). Statins are low-cost, are without serious side effects for the majority of patients and lower triglycerides and low-density lipoprotein-C levels in the blood (14). Despite these interventions, the vast number of cardiovascular diseases cases annually means that a greater understanding of the processes which underlie MI has the potential to improve disease diagnosis, monitoring and therapeutic treatment.

Acute MI is caused by the sudden occlusion of a coronary artery, typically when an atherosclerotic plaque becomes unstable and ruptures, which restricts blood flow to the heart and leads to ischemic injury (15-17). Restricted blood flow to the heart deprives cells in the myocardium of key nutrients, including oxygen (18, 19), leading to the induction of cellular stress signalling pathways such as hypoxia, reactive oxygen species (ROS) generation (20), and necrosis (21). These signalling pathways activate cardiomyocytes and tissue-resident cardiac macrophages, which release tumour necrosis factor-alpha (TNF-α) and exacerbate local inflammation in the infarct site (22).

Cardiomyocyte necrosis leads to the release of ROS, generated by mitochondria, and damage-associated molecular patterns (DAMPs) which include high mobility group box-1 (23), S100 proteins, heat shock proteins (24), adenosine triphosphate (ATP), and mitochondrial DNA (16). DAMPs bind to pattern recognition receptors (PRRs) on recipient cells such as infiltrating neutrophils and monocytes, which triggers an inflammatory cascade as part of the innate immune response (17, 25).

PRRs include membrane-bound toll-like receptors (TLRs), such as TLR2 and TLR4 which are associated with cardiac remodelling following MI (17), cytosolic nucleotide-binding oligomerisation domain-like receptors (NLRs) which activates the NLR family pyrin domain containing protein 3 (NLRP3) inflammasome (26), and the receptor for advanced glycation end products (RAGE) (16). PRR activation then drives intracellular mitogen-activated protein kinase (MAPK) signalling, which involves phosphorylation of the kinases extracellular signal-regulated protein kinase 1/2 (ERK1/2) and p38-MAPK, as well as the transcription factor nuclear factor-kappa B (NF-κB), which translocate into the nucleus upon activation. This signalling cascade promotes an increase in the production and secretion of inflammatory cytokines such as TNF-α, interleukin-6 (IL-6), IL-1β, and IL-18 (27, 28), which further amplify the inflammatory response.

The innate immune response to MI consists of two components, one that promotes tissue injury and one that promotes the resolution of inflammation and tissue repair (29-32). These components are balanced, with the pro-inflammatory response occurring within the first 24-hours of injury, where pro-inflammatory cytokines are secreted by cardiomyocytes, cardiac fibroblasts and endothelial cells surrounding the damage site through the NLRP3 and TLR signalling pathways described above (27, 28). Pro-inflammatory cytokine signalling further amplifies inflammation by recruiting neutrophils and monocytes to the damage site (29, 30, 33). By contrast, anti-inflammatory signalling is prominent in the repair phase of innate immune signalling and occurs up to several months after the initial MI (34).

Monocytes and neutrophils are mobilised from the spleen post-MI, with the extent of myocardial damage positively correlating with the number of monocytes and

neutrophils released into the blood, and also correlating with the likelihood of patient mortality (29, 30, 33, 35). The migration and mobilisation of neutrophils is regulated by interactions between C-X-C motif ligand 12 (CXCL12) and C-X-C motif receptor 4 (CXCR4) (36) within the bone marrow, and can be induced through cytokine, chemokine, or complement signalling (36, 37). However, studies have shown blood chemokine levels peak 24 hours post-MI whereas blood neutrophil counts peak ~2 hours post-MI, therefore indicating neutrophil mobilisation that occurs post-MI may not be induced by circulating chemokines (33, 34).

Endothelial cells line the blood vessels in the heart and become activated in response to external stimuli such as hypoxia, chemokines (38) and cytokines (39). Stimulated endothelial cells increase expression of cell adhesion molecules such as vascular cell adhesion molecule 1 (VCAM-1) and intercellular adhesion molecule 1 (ICAM-1) (39, 40), which interact with integrins to allow neutrophils to infiltrate the damaged region of the heart and clear debris and dead cells from the infarcted region (21, 41).

The importance of regulating rather than eliminating neutrophils in the response to MI has been highlighted through findings from several studies. By inhibiting the clearance of neutrophils from the infarcted heart, there was an increase in scar size and an increased susceptibility to cardiac rupture due to dysfunctional collagen deposition within the heart (42). Elsewhere, neutrophils were shown to produce additional ROS during the process of removing dead cells in the injury site which amplifies the inflammatory response excessively and has the capacity to damage healthy myocardium (34). However, neutrophils also play a key role in regulating the tissue reparative responses to MI by promoting the polarisation of macrophages towards a reparative M2-like phenotype (34), highlighting the importance of neutrophils and how

intercellular communication between different innate immune cell populations regulates the post-MI response and could have future therapeutic relevance.

Similar to neutrophils, monocytes are mobilised from the spleen and recruited to the injury site post-MI (29, 30). Monocytes are mobilised in response to pro-inflammatory cytokines, chemokines and monocyte chemoattractant protein 1 (MCP-1) (43) and can be detected in the infarct site 30 minutes post-injury and peak at ~3 days post-injury (44). In the initial monocyte recruitment phase, NF-κB is activated through phosphorylation as part of intracellular signalling within macrophages which increases the production of cytokines such as IL-1β, IL-6, IL-12 and TNF-α (44), and also promotes extensive extracellular matrix remodelling through the secretion of matrix metalloproteases and the activation of myofibroblasts (45).

A subset of monocytes differentiates into M2-like macrophages 5 days post-injury in response to glucocorticoid receptor signalling and anti-inflammatory IL-14 and IL-3 cytokine signalling (46). This phase of the monocyte-macrophage response to MI involves collagen deposition and angiogenesis to promote wound healing (45). Studies investigating the role of early-phase monocytes in the response to MI injury have used small interfering RNA (siRNA) to suppress pro-inflammatory macrophage activity by targeting CCR2, which was shown to decrease infarct size and curb left ventricular remodelling (47, 48). These findings demonstrate the potential of developing novel therapeutics to target the innate immune system in order to decrease the infarct size, which can improve patient outcomes (17). However, such therapies must involve a degree of precision in targeting the innate immune system since general inhibitors of inflammation such as non-steroidal anti-inflammatory drugs

(NSAIDs) can increase the size of the infarct or increase the risk of ventricular wall rupture (49-51).

In addition to the role of the innate immune system in the response to MI, the importance of lymphocytes as part of the adaptive immune system should also be mentioned. $CD4^+$ T cells are activated in response to MI and promote reparative fibrosis (52). Furthermore, T cell-deficient mice generated using a CD4 knockout model showed increased left ventricular dilation and a limited capacity to remove pro-inflammatory monocytes compared to wildtype mice (53). The CD4 knockout mice also had dysregulated collagen deposition in the infarct zone, highlighting the importance of understanding the cross-communication between the innate and adaptive immune responses to MI. Sustained T cell activation in chronic ischemic heart failure has been shown to promote adverse remodelling and hypertrophy in mouse models, indicating that T cell activity can worsen patient outcomes in chronic conditions (54, 55).

1.2 Myocardial Infarction and the Bone Marrow

As the primary site of haematopoiesis, the bone marrow has an important role in regulating the innate and adaptive immune response to MI (56-58). Although a degree of inflammation and innate immune cell activity is necessary to promote healing post-MI, excessive and unresolved immune cell activity in the heart leads to adverse cardiac remodelling and results in heart failure (32).

The bone marrow is a complex organ which consists of haematopoietic, endothelial, vascular smooth muscle, mesenchymal, and neural lineages (59). These cell types are arranged into specialised niches, which regulate the maintenance and

differentiation of stem cells including haematopoietic stem and progenitor cells (HSPC) and protect progenitor cells from overstimulation and dysregulated proliferation (60). In addition to haematopoietic stem cells (HSC), there are several more differentiated progenitor cells which are either biased or committed to specific lineages within the bone marrow (61, 62). These cells are short-lived compared to HSC (63) and include multi-potent progenitors (MPP), common lymphoid progenitors (CLP), common myeloid progenitors (CMP), megakaryocyte erythroid progenitors (MEP), and granulocyte monocyte progenitors (GMP), amongst others. Although MPP are multipotent, they demonstrate lineage bias which resembles the transcriptional profile of differentiated cells (64, 65), including MEP bias (MPP2), CMP bias (MPP3), & CLP bias (MPP4) (66).

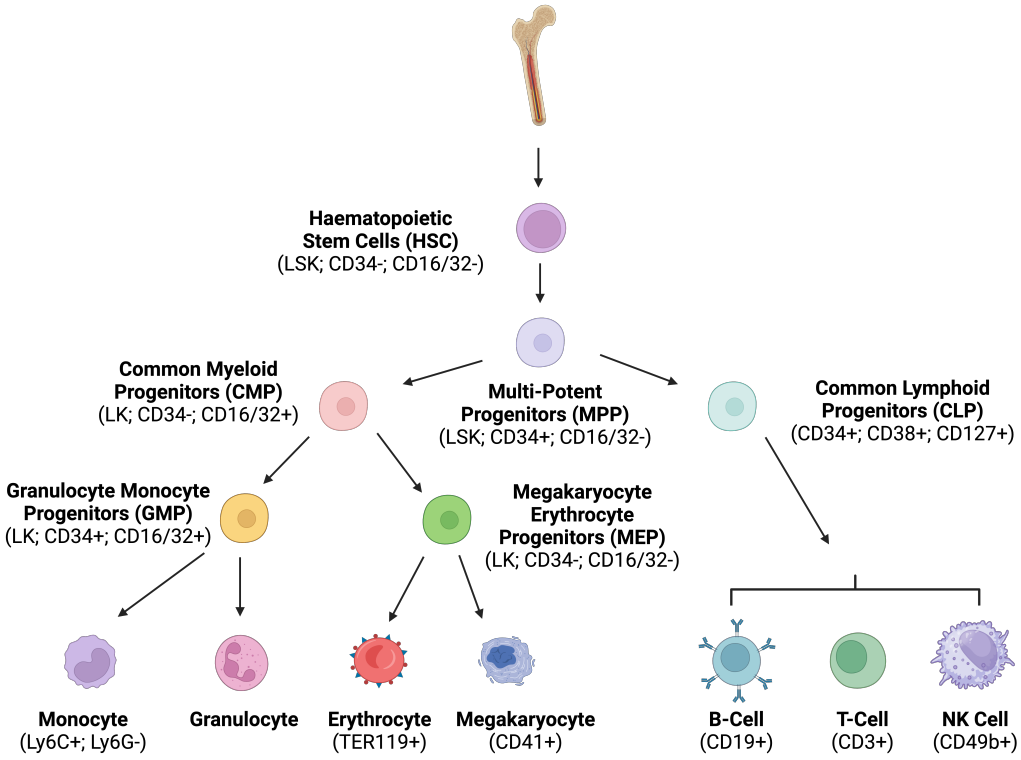

Figure 1. Lineage Tree of Bone Marrow Haematopoietic Stem and Progenitor Cells. Associated markers for each cell type are shown in parentheses.

Recent evidence from single cell sequencing experiments has highlighted the heterogeneity that exists between HSPC subpopulations and also within HSC populations (67, 68). Genetic lineage tracing has demonstrated that HSC can bypass intermediate stages during differentiation such as by differentiating directly from HSC into MEP without the CMP intermediary. This suggests the traditional hierarchy of haematopoiesis may not be the complete picture and instead a more dynamic and flexible model of HSC cell fate should be considered (69, 70).

In the bone marrow, CXCL12 regulates the mobilisation of HSC through interactions with the CXCR4 receptor, and studies have shown that selective deletion of CXCL12 from different cell types in the bone marrow promotes different outcomes in HSC maintenance and mobilisation (71). Deleting CXCL12 from endothelial cells restricts the ability of HSC to repopulate sufficiently by inducing senescence, whilst deleting CXCL12 from stromal cells has no impact on HSC function but decreases B-lymphoid progenitors (72). This provides evidence for HSC existing in specific bone marrow niches which are tightly controlled, rather than non-specific niches which are shared with other progenitor cell types.

Most HSC are found in the trabecular region of the bone marrow and reside within 5 μm of sinusoids (73, 74), allowing HSC to easily mobilise into circulation (75). The location of HSC also enables a rapid response to stimuli, which may be acute, chronic or recurrent, to modify haematopoiesis. Acute infections such as the bacterial cell wall component, liposaccharides (LPS) (76), induces a pro-inflammatory response in the bone marrow, leading to neutrophil mobilisation. Activation of the bone marrow prompts structural remodelling of sinusoids, and stromal cells respond to increased

ROS generation by transferring mitochondria to HSC, leading to HSC entering a proliferative phase (77, 78).

When acute inflammatory responses are not resolved, such as in chronic inflammatory diseases, bone marrow haematopoiesis becomes dysregulated and can drive disease progression further. Chronic inflammatory conditions, such as obesity and type 2 diabetes, increase myeloid-biased haematopoiesis and are mediated by hyperlipidaemia, which increases the release of DAMPs such as S100A8 and S100A9 from adipose tissue (79). In obese mice, tissue-resident and circulating macrophages detect S100 protein through the TLR4 receptor and activate the NLRP3 inflammasome pathway, leading to IL-1β secretion and bone marrow myelopoiesis. In hyperglycaemia, circulating neutrophils secrete DAMPs and activate the RAGE receptor expressed on both macrophages and CMP (80).

Over time, the bone marrow can receive repeated exposure from the same stimuli. Recurrent MI is a common clinical problem for patients with 20% dying within 7 days of a second MI (81). One study used a rodent model to induce multiple MI by ligating the left circumflex (LCX) artery, followed by the left anterior descending (LAD) artery and assessed the impact on haematopoiesis in the bone marrow (82). A single MI event increased the overall HSPC count in the bone marrow as well as GMP populations, indicating the induction of haematopoiesis and a skew in favour of granulocyte and monocyte production. Interestingly, the LAD ligation produced a greater haematopoietic response than the LCX ligation, indicating the location of the infarct impacts the size of the response in the bone marrow.

In the recurrent model, the haematopoietic response was reversed with fewer HSC, fewer GMP and fewer blood myeloid cells (82). This study is remarkable in showing a

modified bone marrow response between the first and second MI within the same mouse. Despite performing a parabiosis experiment, which connects the circulatory systems of two mice (one receiving MI, one was uninjured), both mice had the recurrent MI phenotype, suggesting a circulating factor was responsible for this haemopoietic priming effect. Further experiments are needed to discern the identity of this circulating factor.

A recent study has investigated the impact of heart failure on bone marrow haematopoiesis (83). By performing a transplant of bone marrow from heart failure mice to heart failure-naïve mice, this study showed cardiac dysfunction and fibrosis in recipient mice, with the process driven by bone marrow HSC. Chromatin and RNA sequencing analysis were used to show that heart failure memory in bone marrow HSC suppressed transforming growth factor-β signalling and promoted the formation of pro-inflammatory M1-polarised macrophages.

The impact of repeated exposures of LPS on the bone marrow during infection (84) or in combination with MI has also been assessed (85, 86), with repeat LPS doses targeting bone marrow macrophages to have a muted inflammatory response which was associated with a lower inflammatory cytokine secretion profile. Furthermore, epigenetic modifications to acetylated histones were identified with a reduction in H3K27ac at promoter sites leading to suppressed gene expression. These changes suggest priming the bone marrow promotes long-term reprogramming and fundamental changes to the cell biology of mature myeloid cells.

This phenotype in bone marrow-derived macrophages (BMDM) was extended to LPS-treated bone marrow progenitor cells (86), which produced more myeloid-derived cells in response to the initial stimulus and these mice therefore appeared to be resistant to

chemotherapy-induced myelosuppression after the second stimulus. MI has also been shown to imprint an immunosuppressive innate immune response on the bone marrow, leading to dysregulated macrophage activity and worse mortality outcomes in patients (87). These studies provide evidence for innate immune cells and progenitor cells in the bone marrow being reprogrammed with an initial stimulus to produce a modified immune response to the secondary stimulus. Understanding this mechanism could allow for tighter regulation of the size and timeframe of both the pro-inflammatory and pro-reparative immune response to MI to improve patient outcomes.

1.3 Extracellular Vesicles

Following MI, an increase in extracellular vesicles (EV) in the plasma of patients and mice is detected within ~3 hours of presentation (88, 89). Similar to how the initial number of mobilised monocytes and neutrophils positively correlates with the extent of myocardial injury, the number of plasma EV detected also positively correlates with the extent of myocardial damage, as measured by oedema quantification using T2-weighted MRI analysis (88).

EV are lipid bilayer membrane-enclosed particles which are secreted by a diverse array of cell types (90-92). EV play an active role in cell-cell communication in healthy physiology and in diseased states (93, 94) and can act both locally (95), and remotely by secretion into the blood (96). EV-mediated communication between cells occurs through a wide variety of bioactive cargo present within EV, including protein (97), lipid (98), RNA (99), DNA (100), metabolites, and mitochondria (101).

The term EV includes many different sub-groups, which can be divided based on the biogenesis of the particles (90). Exosomes are a population of small EV, with a diameter of less than 200 nm (90), and originate from early endosomes which invaginate to form intraluminal vesicles within multi-vesicular bodies. These vesicles are released from the cell as exosomes (93). Ectosomes typically have a size range of 100 – 1000 nm and are generated by the outward budding from the plasma membrane (102), whilst apoptotic bodies are produced by outward blebbing and fragmentation of the plasma membrane of cells undergoing apoptosis (102). The dynamic nature of EV research means the definitions of each sub-group are frequently being updated to reflect new findings in the field. For example, new and improved techniques for studying EV have uncovered new subpopulations such as exomeres, exophers, and migrasomes, with the latter reportedly containing internal vesicles (102). One recent study used serial thin electron microscopy to identify multi-compartmented microvesicles (MCMV), which are microvesicles containing multi-vesicular bodies (103). This finding proposes a novel mechanism of EV signalling, with EV released from non-cellular entities and could pave the way to better understanding the complex nature of EV biogenesis and signalling mechanisms.

A major limitation of early EV research was a lack of standardisation across the field for the methods of isolation and characterisation used, including the use of technical terms such as ‘exosome’ and ‘microvesicle’. In order to address this, the minimal information for the studies of extracellular vesicles (MISEV) guidelines were created and are responsible for setting guidelines for how EV research is reported and the types of characterisation that should be used (90).

The conditions and isolation methods used in EV studies are important to define due to the significant variation in EV depending on the type of sample and how the sample is processed (104). For example, when isolating EV from the cell culture media of a homogenous cell line, the EV population isolated will be different compared to isolating EV from plasma, where EV derived from a range of cell types and non-EV particles such as lipoproteins will also be present (105).

The heterogeneity produced by different isolation methods includes the total number of EV particles isolated, the EV subpopulations which are isolated, the protein and lipid content of the EV, and the presence or absence of impurities such as lipoproteins, albumin and protein complexes (98, 104). These impurities often have a similar size profile to the EV populations and therefore are difficult to exclude during isolation, and difficult to distinguish during characterisation (90). This provides a significant challenge in isolating highly pure EV populations, especially from plasma, either for the purpose of diagnosing or monitoring disease using a blood test, or for the development of EV-based therapeutics which can reproducibly be manufactured at scale (91, 104, 106).

Though the methods of isolating EV are being constantly improved and refined, five of the most commonly used methods include: ultracentrifugation, size exclusion chromatography, immunoaffinity capture, precipitation, and acoustic trapping (90). These methods vary in how the EV are isolated. For example, immunoaffinity capture isolation uses magnetic or polystyrene beads conjugated to antibodies specific for EV associated surface markers such as cluster of differentiation 9 (CD9), CD63, or CD81 (107). This allows the isolation of highly specific EV populations but requires the use of appropriate controls including an IgG control to account for non-specific protein binding. Other methods such as ultracentrifugation and size exclusion

chromatography rely instead on biophysical properties of the EV, such as the size and density of the particles. The drawback of such methods is lower purity than immunoaffinity capture, since non-EV particles with similar properties are co-isolated during this process.

Characterisation of EV is required to show the presence of intact EV, for an estimation of the quantity of EV, and to determine the presence of non-EV impurities. Due to the benefits and drawbacks of each characterisation technique, no single method of analysis is sufficient for complete EV characterisation. Particle size analysis includes Nanoparticle Tracking Analysis (NTA) (108), flow cytometry (109), resistive pulse sensing (110), and cryogenic electron microscopy (EM). Many of these methods rely on assumptions as part of the analysis such as the particles are spherical (111) and, despite being high throughput, can overestimate the size of particles. NTA uses the Brownian motion of particles in solution to measure particle size and tracks single particle trajectories to calculate particle concentration. Cryogenic EM is one of the most accurate techniques (112), but can be destructive to particles and modify particle size during sample preparation. Furthermore, cryogenic EM can only measure particles within a narrow size window and therefore is not appropriate for highly heterogenous populations.

EV morphology and the presence of non-EV impurities can also be assessed using cryogenic EM as well as other imaging techniques. Analysis of smaller EV populations (<200 nm) requires high-resolution imaging techniques such as scanning EM (113), transmission EM (114) or atomic force microscopy (115). The development of cryogenic EM, which does not dehydrate samples during preparation unlike other EM techniques, allows for better preservation of EV morphology, which is more

representative of their size and shape in aqueous solutions (116). Other methods of characterisation include total RNA and lipid content, as well as non-protein EV content such as modified lipids (90).

Protein analysis of EV can include total protein content using a bicinchoninic acid (BCA) assay or, for specific protein markers, western blotting, flow cytometry analysis, fluorescence microscopy, and proteomic analysis (117). Due to EV heterogeneity, MISEV guidelines does not mandate the use of specific EV molecular markers but instead have several categories of proteins which must either be positively or negatively identified (90). These categories include transmembrane EV-associated proteins such as tetraspanins (CD9, CD63 and CD81), cytosolic proteins associated with EV such as TSG101, ALIX and heat shock proteins, both of which confirm the presence of EV, and non-EV components such as albumin, GM130 and apolipoproteins to show the presence of co-isolates, which are regarded as impurities in the sample (90, 107).

Like many areas of research, the development of higher resolution techniques such as single cell or single vesicle analysis enables EV researchers to better understand different subpopulations of EV, including EV surface markers and cargo within vesicles. Improved resolution of EV has the potential for use as a diagnostic tool following MI and to identify EV subpopulations that assist or worsen myocardial repair post-injury.

1.4 Extracellular Vesicles in Cardiovascular Disease

In addition to the increase in circulating monocytes and neutrophils, studies have also shown that MI increases the number of circulating EV (29, 88, 94, 118), which return to baseline levels 6-months post-injury (119). These EV are derived from multiple cell types including cardiomyocytes (caveolin 3^{+}), endothelial cells ($CD31^{+}CD41^{-}$), fibroblasts ($CD90.2^{+}$), and platelets ($CD41^{+}$), based on the protein markers assessed by flow cytometry (94). The circulating EV were also positive for Endoglin and VCAM-1 (89), indicating potential endothelial cell origin although VCAM-1 is also expressed by other cell types such as cardiomyocytes, macrophages and HSPC and therefore is not an exclusive endothelial marker (120, 121). Elsewhere, research has shown that patients with coronary artery disease have elevated endothelial cell-EV, defined by the presence of Endoglin and VE-Cadherin (122), and patients with acute coronary syndrome had elevated EV, largely of platelet origin (123). These studies indicate the potential significance of specific sub-populations of EV in the pathophysiology of cardiovascular diseases.

Furthermore, EV from healthy rats and human volunteers improved ischaemic reperfusion injury outcomes in animal models through TLR-4-mediated cell survival pathways (124). A separate study also found healthy rat EV lowered ischaemic reperfusion injury through inhibition of the pro-inflammatory complement cascade (125). The improved response to ischaemic reperfusion injury could be reversed through the inhibition of the EV-associated protein heat shock protein 90, providing evidence for the importance of specific EV cargo as part of this process (125).

Under hypoxic or ischaemic conditions, cardiomyocyte-derived EV (CM-EV) cargo becomes modified and these modified EV are taken up by neighbouring cells,

including cardiomyocytes (126), fibroblasts (127), macrophages (128) and endothelial cells (129), which affects the downstream functions of the target cells. For example, EV-associated heat shock protein 60 is enriched in CM-EV following hypoxia-reoxygenation stimulation (126), and promotes cardiomyocyte apoptosis in neighbouring cells, suggesting CM-EV may mediate and amplify cardiomyocyte damage following cardiac ischaemia. In macrophages, CM-EV reprogramming in an ischaemic rat model leads to a decrease in pro-inflammatory M1 activation (128), suggesting a potential cardio-protective role for these EV. CM-EV derived from H9c2 cardiomyocytes downregulated p38-MAPK phosphorylation, leading to lower expression of inducible nitric oxide synthase (iNOS), IL-1β, and IL-6. These effects were then replicated using neonatal cardiomyocytes and in human macrophage models and suggest CM-EV signalling within pro-inflammatory M1-polarised macrophages helps to regulate the extent of the initial response to ischaemic injury.

Several studies have also provided evidence for EV-miRNA-driven reprogramming in cardiovascular disease. In rodent heart failure models, hypoxic cardiomyocytes increase expression of miRNA-30d, which activates MAPK-associated cell survival in cardiomyocytes, and restrains cardiac fibroblast proliferation by targeting integrin α5 (130). Lowering miRNA-30d induces adverse remodelling in both rodents and humans, indicating a functional role for miRNA in cardiac ischaemia pathology. Furthermore, CM-EV enriched in miRNA-1, miRNA-208, and miRNA-499 and taken up by the bone marrow were found to downregulate CXCR4, which tethers HSPC to restrict cell mobilisation (96). Cell motility is required for HSPC proliferation and suppressing CXCR4 activity in bone marrow reversed this effect on HSPC mobilisation. However, it was not determined whether the proliferative capacity of these HSPC populations were modified in response to CM-EV.

As described above, the recruitment and polarisation of macrophages has a notable impact on patient outcomes to MI. Pro-inflammatory M1-polarised macrophages regulate angiogenesis and fibroblast proliferation in the heart through the EV-associated miRNA-155, which is upregulated post-MI (131). miRNA-155 downregulates endothelial cell proliferation by inhibiting sirtuin 1, adenosine monophosphate kinase activated catalytic subunit alpha 2 (AMPKα2), and Ras-related c3 botulinum toxin substrate 1 (RAC1). Furthermore, miRNA-155 restricts sons of sevenless 1 (SOS1) in fibroblasts to restrict fibroblast proliferation and further myocardial injury (132).

Cardiac fibroblast expansion along with the clearance of dying cardiomyocytes regulates the extent of cardiac fibrosis. Cardiac fibroblasts can protect cardiomyocytes from cell death following ischaemic injury through fibroblast-EV signalling both *in vivo* and *in vitro* (133) and studies indicate a role of miRNAs in this process. miRNA-423-3p is upregulated in cardiac fibroblasts post-injury and downregulating miRNA-423-3p using an antagomir was sufficient to reverse the cardioprotective effects of fibroblast-EV on cardiomyocytes *in vivo*. This study also provided data through a miRNA-423-3p rescue assay to suggest this microRNA may have therapeutic relevance to limit ischaemic-reperfusion injury. These studies highlight the importance of investigating EV-miRNA cargo in cardiovascular diseases and their downstream effects which can be manipulated for therapeutic benefits.

In addition to protein and RNA cargo within EV, which appear to either drive or reverse post-MI pathology, EV cargo can be used as diagnostic markers of disease. Lipidomic analysis of plasma EV in ST-segment elevation myocardial infarction (STEMI) and healthy patient control samples revealed an increase in ceramides and sphingolipids

(134). By comparing the protein and sphingolipid content of healthy and post-MI plasma EV samples (98), research indicates significant differences in the proteomic and sphingolipidomic profiles between healthy and post-MI groups. Further investigation into these differences will improve our understanding of the pathological effects of plasma EV in MI.

1.5 Endothelial Cell-Extracellular Vesicles in Cardiovascular Disease

The endothelium maintains tissue homeostasis and vascular tone in each vascularised tissue and organ to allow a constant flow of nutrients such as oxygen (135, 136). Endothelial cells also serve an essential role in the immune response and are activated by a variety of stimuli including LPS, the inflammatory cytokines TNF-α, IL-1β, IL-6, interferon-gamma (IFN-γ), and ROS (137, 138).

Dysfunction of the endothelium is a known predictor of a range of cardiovascular and metabolic diseases, including MI, and involves the dysregulation of nitric oxide production (139). Following MI, endothelial cells in close proximity to the injury site are similarly activated, as shown by an upregulation of cell adhesion molecules VCAM-1 and ICAM-1, and the secretion of inflammatory cytokines IL-1 and IL-8 (140). These changes, along with a loss of vascular integrity, facilitate increased leukocyte binding and localisation, respectively, leading to leukocyte extravasation and diapedesis at the damage site (141).

VCAM-1 is endothelial cell associated, and studies have shown VCAM-1 is enriched on the surface of plasma EV following MI (89), and that myocardial expression of VCAM-1 is linked with an increased risk of heart failure (142). One study showed that

both MI and endothelial-EV promoted the mobilisation of neutrophils and monocytes from the spleen, but this phenotype was lost when the endothelial-EV were CRISPR-Cas9 edited to knock out VCAM-1 (88, 89). This indicates VCAM-1 may be a relevant therapeutic target to improve outcomes for MI patients. Despite being associated with endothelial cells, VCAM-1 is also expressed in smooth muscle cells, macrophages and HSC, meaning the marker is not exclusive to endothelial cells (120, 121). Also, the transcriptional heterogeneity of endothelial cells is dependent on the environment they are exposed to, meaning not all individual endothelial cells in a blood vessel express VCAM-1 equally following stimulation, if at all (143).

miRNA-126-3p and miRNA-126-5p, are two of the most abundant microRNAs in endothelial cells (144, 145). The importance of miRNA-126, the precursor to miRNA-126-3p and miRNA-126-5p, to endothelial cells was demonstrated in one mouse study through targeted deletion of the miRNA, which produced defects in angiogenesis and disrupted vascular integrity (146). In the context of cardiovascular disease, these miRNA-126-defective mice also had dysfunctional myocardial neovascularisation post-MI, indicating an important role for miRNA-126 in post-MI tissue repair (146).

Furthermore, the genetic depletion of miRNA-126-5p in atherosclerosis-prone, apolipoprotein E-deficient mice lowered endothelial cell proliferation and worsened atherosclerosis (145). This phenotype could be rescued through the administration of miRNA-126 which highlights the possibility of using miRNA-126 as a therapeutic to slow or limit the progression of atherosclerosis.

A microRNA array was used to demonstrate that both miRNAs are enriched in plasma EV following MI at the time of presentation compared to a 6-month follow up timepoint (88), and analysis of neutrophil transcriptome changes post-MI shows an overlap with

miRNA-126-3p and miRNA-126-5p targets (89). This indicates innate immune cells may be downstream targets of endothelial-EV-associated miRNA-126-3p and miRNA-126-5p following an MI.

In patients with acute coronary syndrome, serum miRNA-126 levels were also elevated relative to healthy controls and correlate with the severity of coronary artery stenosis (147). This study was also noteworthy because the authors developed a model for predicting acute coronary syndrome in patients based on serum miRNA-126, miRNA-21, and phosphatase and tensin homolog (PTEN) levels and predicted the severity of coronary stenosis. These findings suggest miRNA-126 can be developed as a diagnostic marker for disease prognosis and severity in cardiovascular disease.

This introduction highlights the importance of understanding the role of the immune system in the response to MI, particularly in the bone marrow as the primary source of haematopoiesis. Furthermore, it describes the relevance of endothelial-EV in disease progression and signalling following MI, with the potential of developing novel diagnostic and therapeutic tools to improve patient outcomes. The following chapters will assess transcriptional changes in bone marrow HSC in response to endothelial-EV and test the relevance of miRNAs to the endothelial-EV model. The second chapter will investigate the *in vivo* role of endothelial-EV on the bone marrow, with a particular focus on interactions with HSPC. The third chapter will explore how endothelial-EV can reprogramme BMDM to lower the inflammatory profile of these cells.

1.6 Hypotheses

- *Hypothesis 1: MI reprogramming of the bone marrow is mediated by endothelial cell-EV.*
- *Hypothesis 2: Endothelial cell-EV transcriptionally reprogramme HSC in the bone marrow to induce haematopoiesis.*
- *Hypothesis 3: Endothelial cell-EV cargo has reprogramming effects on innate immune cells in the bone marrow.*
- *Hypothesis 4: Endothelial cell-EV modulate the inflammatory phenotype of bone marrow-derived macrophages following MI.*

Chapter 2- Materials and Methods

2.1 Media Preparations

sEND.1 cell culture media

Mouse skin-derived endothelial cell 1 (sEND.1) cell culture was conducted in 25 mM glucose Dulbecco's Modified Eagle's Medium (DMEM) (Sigma Aldrich, UK) supplemented with 10% foetal bovine serum (FBS) (Life Technologies, UK), 2% v/v penicillin-streptomycin (Sigma Aldrich, UK), and 2 mM L-glutamine (Life Technologies, UK). This medium will be referred to throughout as 'sEND.1 cell culture media'.

EV-depleted sEND.1 cell culture media

EV-depleted medium for sEND.1 cell culture studies was generated by combining 25 mM glucose DMEM supplemented with 2% v/v penicillin-streptomycin, 2 mM L-glutamine and 10% EV-depleted FBS, which was generated by ultracentrifugation of FBS in Polyallomer Quick-Seal ultra clear 16 mm x 76 mm tubes (Beckman Coulter, USA) for 16 hours at 120,000 x *g* at 4 °C (Beckman Coulter, Optima MAX-XP Ultracentrifuge, MLA-55 fixed-angle rotor, k-adjusted value = 125). This medium will be referred to as 'EV-depleted sEND.1 cell culture media'.

L929 media & L929-conditioned media

Mouse fibroblast cell line, L929, cell culture was conducted in Roswell Park Memorial Institute (RPMI) medium supplemented with 10% FBS, 2% v/v penicillin streptomycin

and 2 mM L-glutamine. L929-conditioned medium was generated by culturing L929 cells to confluency for 5 days, removing the conditioned medium and centrifuging at 400 x *g* for 5 minutes. The supernatant was stored at -20 °C and will be referred to throughout as 'L929-conditioned media'.

Bone marrow-derived macrophage differentiation media

Mouse bone marrow cells were cultured in 5 mM glucose DMEM supplemented with 10% FBS, 2% v/v penicillin-streptomycin, and 20% L929-conditioned medium to generate bone marrow-derived macrophages. This medium will be referred to throughout as ‘BMDM Differentiation media’.

Macrophage Stimulation media

Mouse BMDM, human monocytes, and human monocyte-derived macrophages were cultured in 5 mM glucose DMEM supplemented with 10% FBS, and 2% v/v penicillin-streptomycin. This medium will be referred to throughout as ‘Macrophage Stimulation media’.

EV-depleted bone marrow-derived macrophage stimulation media

Mouse BMDM were cultured in 5 mM glucose DMEM supplemented with 10% EV-depleted FBS, and 2% v/v penicillin-streptomycin. This medium will be referred to throughout as ‘EV-depleted BMDM Stimulation media’.

HUVEC culture media

Human umbilical vein endothelial cell (HUVEC) culture was conducted in 5.5 mM glucose endothelial basal media 2 (EBM-2) (Lonza, UK) supplemented with endothelial growth media 2 (EGM-2) kit (Lonza, UK). This medium will be referred to throughout as 'HUVEC culture media'.

EV-depleted HUVEC culture media

EV-depleted HUVEC culture medium was generated using EBM-2 medium supplemented with the EGM-2 kit and 2% EV-depleted FBS, which replaced the FBS provided in the EGM-2 kit. This medium will be referred to throughout as 'EV-depleted HUVEC culture media'.

2.2 Endothelial Cell Culture

sEND.1 endothelial cells were cultured in T175 (surface area = 175 cm^2) cell culture flasks (Corning, UK) containing 3 x 10^6 cells and 14 mL of sEND.1 cell culture media in a humified incubator with 5% CO_2 at 37 °C. sEND.1 cells were passaged by aspirating cell culture media, washing with 10 mL of sterile PBS (Thermo Fisher, UK), adding 4 mL of 2.5% trypsin-EDTA (Life Technologies, UK), and incubating cells for 5 minutes at 37 °C until adhered cells became dislodged. Trypsin was neutralised by adding 10 mL of sEND.1 cell culture media and the solution was collected and centrifuged at 400 x *g* for 5 minutes. The cell pellet was resuspended in 1 mL of sterile PBS and cells were counted using an automated cell counter (Countess II FL

Automated Cell Counter) (Thermo Fisher, UK) using 10 μL of the sEND.1 cell suspension and 10 μL of 0.4% Trypan Blue (Thermo Fisher, UK) solution. HUVEC were cultured and passaged using the same conditions as sEND.1 cells using HUVEC culture media.

2.3 Extracellular Vesicle Isolation Using Ultracentrifugation

Endothelial-EV were isolated from cell culture supernatants using ultracentrifugation (**Figure 2**). 3 x 10^6 endothelial cells were seeded into 8 x T175 flasks and grown to ~80% cell confluency. One day later, the medium was aspirated, cells were washed with 10 mL of sterile PBS and replaced with 14 mL of either EV-depleted sEND.1 cell culture media or EV-depleted HUVEC culture media, for sEND.1 and HUVECs, respectively. Endothelial cells were exposed to vehicle-control (sterile PBS), or 10 ng / mL of recombinant mouse TNF-α (410-MT, R&D Systems, UK) or recombinant human TNF-α (210-TA, R&D Systems, UK) for 18 hours (88, 89).

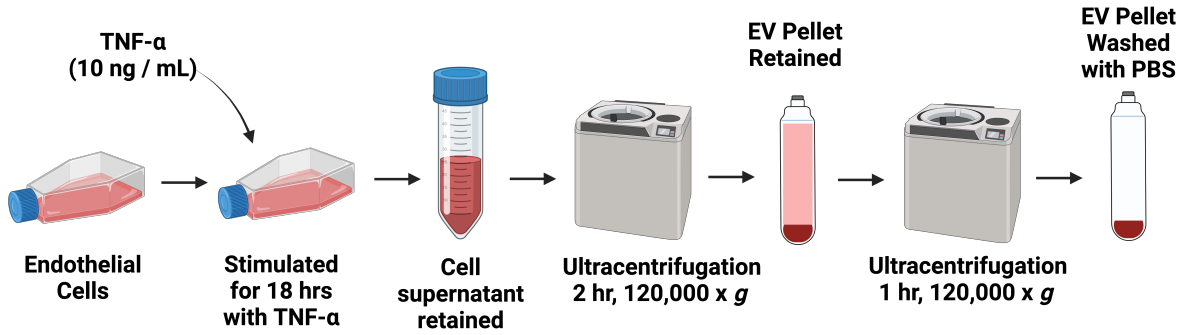

Figure 2. Overview Schematic of Endothelial Cell-Extracellular Vesicle Culture and Isolation Using Ultracentrifugation.

Cell culture medium was removed from each flask and centrifuged at 1,000 x *g* for 10 minutes at 4 °C. The supernatants were retained and transferred to 13.1 mL QuickSeal ultra clear 16 mm x 76 mm ultracentrifuge tubes (Beckman Coulter, USA) using a 16 G hypodermic needle (Terumo, VWR, UK) and were topped up with sterile PBS. The ultracentrifugation tubes were sealed using a soldering iron (Amazon, UK) and centrifuged for 2 hours at 120,000 x *g* at 4 °C (Beckman Coulter, Optima MAX-XP Ultracentrifuge, MLA-55 fixed-angle rotor, k-adjusted value = 125).

The ultracentrifugation tubes were cut open and the supernatant was removed. The endothelial-EV pellet was resuspended using 1 mL of sterile PBS and transferred into new 13.1 mL ultracentrifugation tubes. The samples were topped up with sterile PBS, sealed, and centrifuged at 120,000 x *g* for 60 minutes at 4 °C. Endothelial-EV pellets were retained and resuspended in 100 µL of either sterile PBS or RIPA lysis buffer (Cell Signalling, UK) with protease and phosphatase inhibitors (Complete protease inhibitor cocktail, Roche).

2.4 Extracellular Vesicles Characterisation

Endothelial-EV were characterised to comply with MISEV guidelines (90) (**Figure 3**).

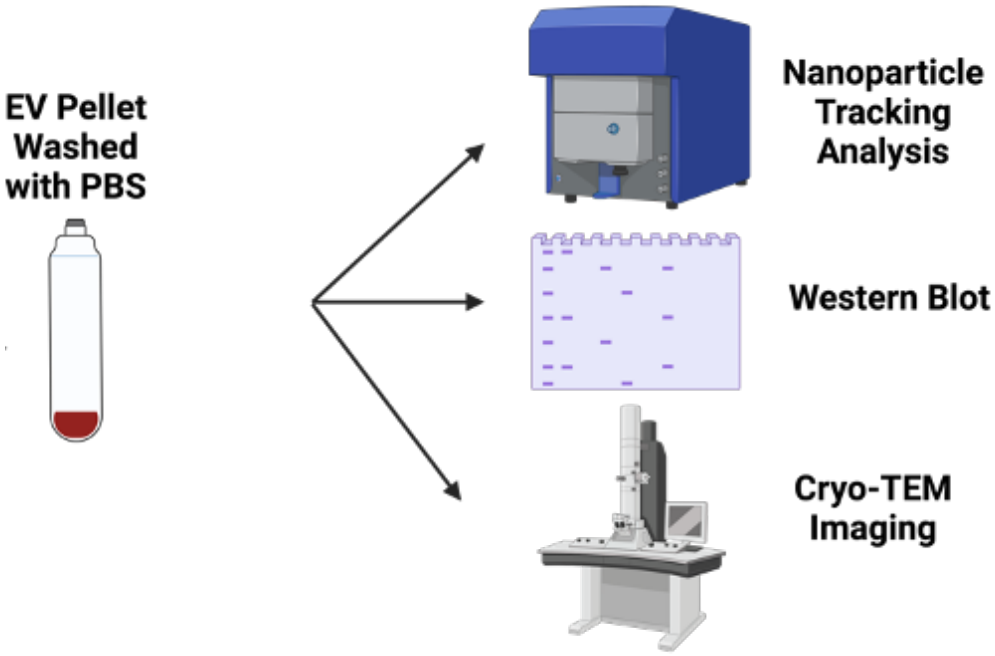

Figure 3. Overview Schematic of Endothelial Cell-Extracellular Vesicle Characterisation Using Nanoparticle Tracking Analysis, Western Blotting, and Cryo-TEM Imaging.

Nanoparticle Tracking Analysis

The size and concentration profiles of endothelial-EV were determined using the Particle Metrix, Zetaview as described elsewhere (29, 148). Silica 100 nm microspheres (Polysciences Inc., USA) were analysed to calibrate the instrument. Endothelial-EV were diluted in sterile PBS to a concentration of ~1 x 10^8 particles / mL. 1 mL of each sample was loaded into the sample chamber and analysed according to the following Zetaview settings: 11 positions in 2 cycles, medium video resolution. Pre-acquisition settings: sensitivity 80, fame 30, shutter speed 100. Post-

acquisition settings: minimum brightness 25, maximum size 1000, minimum size 5, trace length 15, nm / class 30.

Lysis and Sample Preparation for Western Blotting Analysis

Samples for western blotting analysis were lysed using RIPA buffer containing protease inhibitors and phosphatase inhibitors. Samples were needle sonicated at 33% power for 15 seconds using a SonoPuls HD2070 (Bandelin Sonopuls, Germany), were stored on ice at 4 °C, and were centrifuged at 5,000 x *g* for 5 minutes. The supernatants were retained and stored on ice at 4 °C until the protein concentration of each sample was determined.

Protein Concentration Determination

The protein concentration of each sample was measured to ensure equal loading of protein during western blotting analysis. Protein concentration was determined using a bicinchoninic acid (BCA) assay (Pierce BCA Protein Assay kit, Thermo Fisher, UK, UK) with a standard curve of a known quantity of bovine serum albumin (BSA) as per the manufacturer's instructions. Samples were diluted 1:5 and 1:10 in RIPA buffer and 25 μL of each diluted sample or standard was incubated in duplicate with 200 μL of combined Reagent A and Reagent B solution. Samples were incubated at 37 °C for 30 minutes and the absorbance was measured at 562 nm using a FLUOstart Omega plate reader (BMG Labtech, UK).

SDS-Page Electrophoresis

20 μg of protein from each sample was diluted with RIPA buffer and NuPAGE 4x LDS sample buffer agent (Invitrogen, USA) and loaded onto a 1.5 mm 4-12% NuPage Bis-Tris gradient gel (Thermo Fisher, UK) with 10 μL of Amersham ECL Rainbow Full Range ladder (Cytiva Life Sciences, USA). Electrophoresis was conducted at 125 V for 100 minutes.

Protein Analysis by Western Blotting Analysis

Separated samples were transferred onto nitrocellulose membranes using the iBlot 2 Western Blot Transfer Device (Thermo Fisher, UK) and iBlot 2 transfer stacks (Thermo Fisher, UK) as per the manufacturer's instructions. The successful transfer of samples was confirmed with a 5-minute Ponceau stain (Ponceau S solution, Sigma Aldrich, UK) through the appearance of protein bands. Ponceau was removed through a wash step for 5 minutes in PBS-Tween (PBS plus 0.05% Tween-20 (Sigma Aldrich, UK)), and membranes were blocked to limit non-specific binding in 15 mL of PBS-Tween plus 5% skimmed milk powder (Marvel Original, UK) on a rocking device for one hour at room temperature. Membranes were incubated overnight at 4 °C with 8 mL of primary antibodies (**Table 1**) diluted in PBS-Tween plus 5% milk on a rocking device.

Membranes were washed three times with PBS-Tween for 5 minutes on a rocking device and incubated with 10 mL of either anti-mouse IgG (Promega, UK) or anti-rabbit IgG (Promega, UK) secondary antibodies conjugated to horse radish peroxidase (HRP) for one hour at room temperature on a rocking device. Membranes were washed three times with PBS-Tween for 5 minutes at room temperature on a rocking

device and were exposed to enhance chemiluminescence substrate (Pierce ECL, Thermo Fisher, UK) for 5 minutes at room temperature, and were immediately imaged on a Bio-Rad ChemiDoc MP Imaging system.

Target	**Molecular Weight (kDa)**	**Dilution**	**Species**	**Isotype**	**Supplier; Cat#**
ApoB	515	1 in 5,000	Rabbit	Rabbit IgG	Abcam, AB139401
eNOS	133	1 in 1,000	Mouse	Mouse IgG1, κ	BDBioscience, 610296
GM130	130	1 in 3,000	Rabbit	Rabbit IgG	Abcam, ab52649
VCAM-1	101	1 in 2,000	Rabbit	Rabbit IgG	Abcam, EPR5047
p-NF-κB	65	1 in 1,000	Rabbit	Rabbit IgG	CellSignalling, 3033T
NF-κB	65	1 in 1,000	Rabbit	Rabbit, IgG	CellSignalling, 4764T
ATP5A	53	1 in 5,000	Mouse	Mouse IgG2b, κ	Abcam, 15H4C4
TSG-101	44	1 in 1,000	Mouse	Mouse IgG1	Abcam, ab83
p-ERK1/2	44	1 in 1,000	Mouse	Mouse IgG2a, κ	Biolegend, 699951

ERK1/2	44	1 in 1,000	Rat	Rat IgG1, κ	Biolegend, 699951
p-p38-MAPK	40	1 in 1,000	Mouse	Mouse IgG1 κ	Biolegend, 690201
p38-MAPK	40	1 in 1,000	Rabbit	Rabbit IgG	CellSignalling, 8690T
Syntenin-1	31	1 in 1,000	Rabbit	Rabbit IgG	Abcam, 133267
CD9	24	1 in 1,000	Mouse		Thermo Fisher, TS63
Histone H3	17	1 in 2,000	Rabbit	Rabbit IgG	CellSignalling, D1H2/4499P
Mouse IgG HRP Conjugate		1 in 25,000	Goat		Promega, W402B
Rabbit IgG HRP Conjugate		1 in 50,000	Goat		Promega, W401B

Table 1. Antibodies Details for Protein Analysis by Western Blotting.

Imaging Analysis by Transmission Electron Microscopy (TEM) and Cryo-TEM

sEND.1 endothelial-EV samples generated by Dr Naveed Akbar were sent for TEM imaging. TEM images were taken by Dr Errin Johnson from the Dunn school of Pathology, University of Oxford, UK. For negative staining TEM, grids (300 mesh Cu carbon film) were glow discharged for 20 seconds at 15 mA (Leica EM ACE 200). Isolated endothelial-EV samples were applied to the grid for 2 minutes, blotted and stained with 2% uranyl acetate for 20 seconds, blotted and allowed to air dry. Images were acquired using a 120 kV Tecnai 12 TEM (Thermo Fisher, UK) equipped with a OneView digital camera (Gatan). For cryo-TEM imaging, grids (Quantifoil 200 mesh Cu 2/1 or lacey carbon grids) were prepared with a graphene oxide layer. Isolated endothelial-EV were then applied to the grid for 2 minutes before being plunge-frozen in ethane using a Vitrobot IV (Thermo Fisher, UK). Grids were imaged using SerialEM (149) on a Talos Arctica (operated at 200 kV) equipped with a Falcon III camera (Thermo Fisher, UK).

2.5 In Vivo Experimentation

C57BL/6 mice (Biomedical Services, Oxford, UK and Charles River, USA) were housed in a pathogen-free facility under standard conditions with food and water provided *ad libitum*. All licensed procedures were performed under UK Home Office license P996B4A4E by a personal license holder.

2.6 Isolation of Bone Marrow, Spleen and Blood Cells for Flow Cytometry Analysis

Adult wildtype male C57BL/6 mice (10 weeks old) were terminally anaesthetised, and a cardiac puncture was performed followed by cervical dislocation. Bone marrow tissue was isolated by cutting the ends of each femur and tibia and flushing the bone marrow contents with 10 mL of ice-cold sterile PBS and a 25 G needle (Terumo, UK) attached to a syringe. Cell suspensions were passed through a 70 μm sterile cell strainer (BD Falcon, UK) to create a single cell suspension and remove bone fragments and tissue debris. Samples were centrifuged at 1000 x *g* for 10 minutes and the cell pellet was retained and resuspended in 1 mL of fluorescence-activated cell sorting (FACS) buffer (2% FBS in sterile PBS). Cells were counted using an automated cell counter and were stained for flow cytometry analysis.

Spleens were removed, weighed using a weighing boat and balance, and were dissociated through mechanical agitation using the plunger of a 1 mL syringe through a 70 μm sterile cell strainer in red blood cell (RBC) lysis buffer (80.2 g / L NH_4Cl, 8.4 g / L $NaHCO_3$ and 3.7 g / L EDTA in DI water) and incubated for 10 minutes at room temperature. Samples were centrifuged at 1000 x *g* for 10 minutes and the cell pellet was retained and resuspended in 1 mL of FACS buffer. Cells were counted using an automated cell counter and were stained for flow cytometry.

The blood was collected by cardiac puncture in K2-EDTA-coated tubes (BD Vacutainer, USA). Samples were centrifuged at 1000 x *g* for 10 minutes and the cell pellet, containing PBMC, was retained and resuspended in 1 mL of FACS buffer and transferred using a Pasteur pipette (Thermo Fisher, UK) to 45 mL of 1x RBC lysis buffer and incubated for 10 minutes at room temperature. The plasma supernatant was also retained to isolate platelets and produce platelet-poor-plasma through

centrifugation at 5,000 x *g* for 10 minutes. The PBMC were centrifuged at 1,000 x *g* for 5 minutes and the cell pellet was retained and resuspended in 1 mL of FACS buffer. Cells were counted using an automated cell counter and were stained for flow cytometry analysis.

2.7 Cell Staining for Flow Cytometry Analysis

Bone marrow and splenic samples were stained in a 96-well plate to identify HSPC, monocytes and neutrophils. Blood samples were stained in a 96-well plate to identify monocytes and neutrophils. 5 x 10^6 cells were centrifuged at 500 x *g* for 5 minutes at room temperature and the pellet was retained and resuspended in 200 μL of FACS buffer plus 1% Fc receptor blocking buffer (Miltenyi Biotec, UK) and 5% 7-amino-actinomycin D (7-AAD) dye (eBioscience, UK) at 4 °C for 20 minutes. Samples were washed in 200 μL FACS buffer, centrifuged at 500 x *g* for 5 minutes, and then were resuspended in antibodies diluted in 200 μL of FACS buffer (**Table 2**) and incubated for 30 minutes at 4 °C. Samples were then washed with 200 μL of FACS buffer and centrifuged at 500 x *g* for 5 minutes. Samples were resuspended in 200 μL of BD Cytofix buffer (BD Biosciences, UK) and incubated for 20 minutes at 4 °C, and were then centrifuged at 500 x *g* for 5 minutes and resuspended in 200 μL of FACS buffer and stored at 4 °C in tin foil until the samples were analysed. Samples were analysed using a BD Fortessa X20 (BD Biosciences, UK) and analysed using FlowJo software (FlowJo, Treestar).

To determine the background fluorescence levels during the analysis, compensation was calculated for each channel using unstained samples and fluorescence-minus

one samples. In the latter, each antibody-fluorophore conjugate that was used in the flow cytometry analysis was added except the antibody-fluorophore conjugate that corresponded to the fluorescence channel being measured. This established the background signal for each antibody and was used to create the gating strategy by excluding counts that did not meet the background signal threshold.

Target	**Clone**	**Isotype**	**Supplier; Cat#**	**Fluorophore**	**Dilution**
CD3-epsilon	145-2C11	Armenian Hamster IgG	Biolegend	Biotin	1 in 200
CD4	RM4-5	Rat IgG2a κ	Biolegend	Biotin	1 in 200
TER-119	TER-119	Rat IgG2b κ	Biolegend	Biotin	1 in 200
B220	RA3-6B2	Rat IgG2a κ	Biolegend	Biotin	1 in 200
GR-1	RB6-8C5	Rat IgG2b κ	Biolegend	Biotin	1 in 200
Streptavidin			Biolegend	BV785	1 in 200
c-Kit/ CD117	S18020H	Rat IgG2a κ	Biolegend	PE	1 in 100
Sca-1	D7	Rat IgG2a κ	Biolegend	AF700	1 in 150
CD34	SA376A4	Rat IgG2a λ	Biolegend	PE/Cy7	1 in 200
CD16/32	S17011E	Rat IgG2b κ	Biolegend	FITC	1 in 100
CD45	30-F11	Rat IgG2b κ	Biolegend	AF647	1 in 100
CD11b	M1/70	Rat IgG2b κ	Biolegend	FITC	1 in 100
Ly6C	HK1.4	Rat IgG2c κ	Biolegend	APC/Cy7	1 in 200

Ly6G	1A8	Rat IgG2a κ	Biolegend	Pacific Blue	1 in 200

Table 2. Antibody Details for Flow Cytometry Analysis.

2.8 Bone Marrow and Splenic Haematopoietic Stem and Progenitor Cell Analysis Using the In Vivo Endothelial Cell-Extracellular Vesicle Model

Adult wildtype male C57BL/6 mice (10 weeks old) were injected by Professor Daniel Anthony's Laboratory (Department of Pharmacology, University of Oxford). Mouse weights were recorded and mice received either an intraperitoneal injection of LPS (1 mg / kg body weight) (Sigma Aldrich, UK) or an intravenous injection of sterile PBS (100 μL), control EC-EV (1 x 10^9 particles derived from unstimulated endothelial cells) or TNF-α EC-EV (1 x 10^9 particles derived from TNF-α (10 ng / mL)-stimulated endothelial cells), using a 1 mL syringe and 30 G needle (Terumo, UK) (**Figure 4**). After 72 hours (150), mice were re-weighed and received a cardiac puncture followed by cervical dislocation (performed by Dr Naveed Akbar). Bone marrow, splenic and blood cells were isolated and stained for flow cytometry analysis as described above (**Method 2.6** & **2.7**) (**Table 3**).

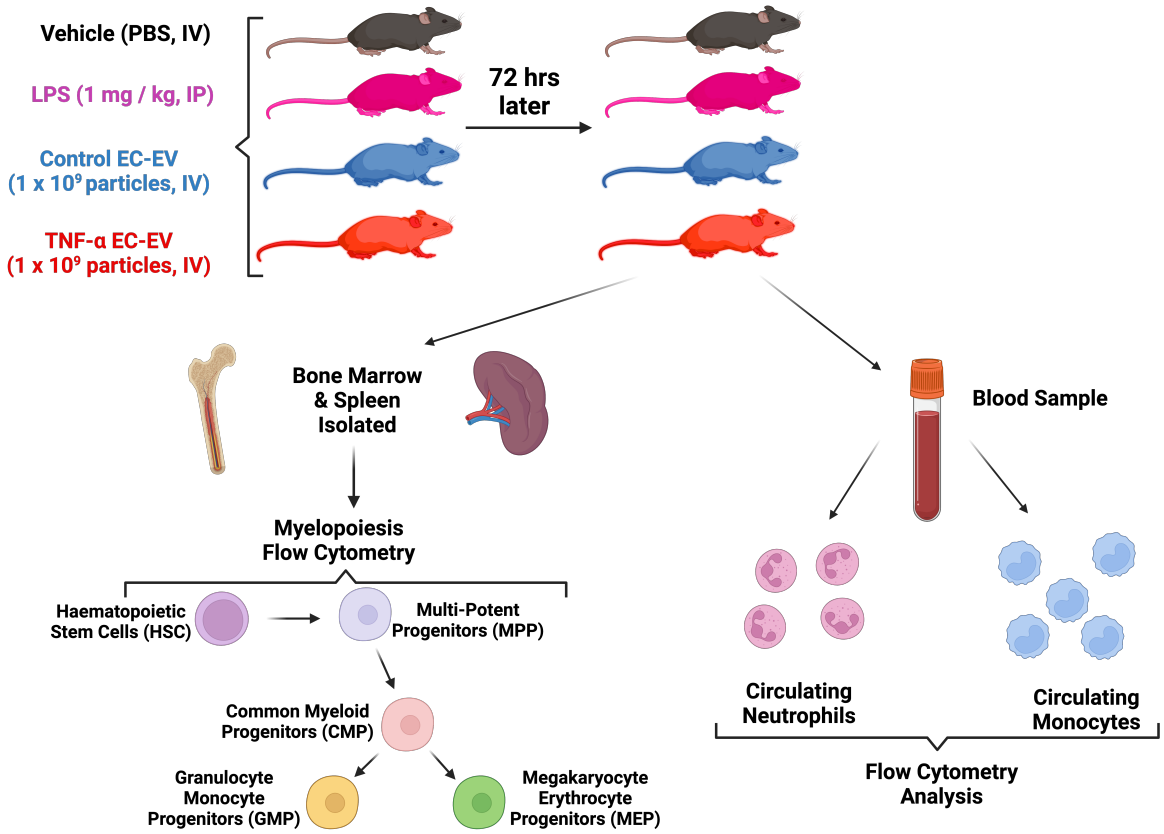

Figure 4. Overview of the In Vivo Study Investigating the Effects of Endothelial Cell-Extracellular Vesicles on Bone Marrow and Splenic Haematopoiesis.

Cell Type	Lineage Committed	Sca-1	c-Kit/ CD117	CD34	CD16/32
HSC	-	+	+	-	-
MPP	-	+	+	+	-
CMP	-	-	+	-	+
GMP	-	-	+	+	+
MEP	-	-	+	-	-

Table 3. Overview of the Haematopoiesis Stem and Progenitor Cell Populations Assessed by Flow Cytometry.

2.9 Protein Analysis by Enzyme-Linked Immunosorbent Assay (ELISA)

Inflammatory cytokines from plasma samples (**Method 2.8**) and from BMDM supernatants (**Method 2.18**) were assessed using enzyme-linked immunosorbent assay (ELISA) kits (R&D Systems, UK). Samples stored at -80 °C were thawed on wet ice and were centrifuged at 500 x *g* for 5 minutes to remove cellular debris. Samples were diluted for mouse TNF-α (DY410, R&D Systems) and human TNF-α (DY210, R&D Systems) ELISA kits at 1:10 and 1:20, for mouse IL-6 (DY406, R&D Systems) and human IL-6 (DY206, R&D Systems) kits at 1:20 and 1:50, for mouse IL-1β (DY401, R&D Systems) and human IL-1β (DY201, R&D Systems) kits at 1:10 and 1:20, and mouse VCAM-1 (DY643, R&D Systems) and human VCAM-1 (DY809, R&D Systems) kits at 1:1 and 1:10. Dilutions were performed using reagent diluent (R&D systems, UK) which was supplied by the manufacturer, and diluted samples were analysed

using the DuoSet ELISA kit (R&D Systems, UK) and the DuoSet ELISA Ancillary Reagent kit 2 (R&D Systems, UK) as per the manufacturer's instructions. Wash steps were performed using the Hydroflex Plus microplate washer (Tecan, UK).

2.10 Colony-Forming Unit Assay for the Bone Marrow-Endothelial Cell-Extracellular Vesicle Model

Adult wildtype male C57BL/6 mice (10 weeks old) were culled using a cardiac puncture followed by cervical dislocation. Bone marrow cells were isolated and counted as outlined above (**Method 2.6**). Bone marrow samples were stained in FACS tubes (StemCell Technologies, UK) in order to isolate HSC. 2 x 10^7 cells were centrifuged at 500 x *g* for 5 minutes at room temperature and the cell pellet was retained and resuspended in 1 mL of FACS buffer plus 1% Fc receptor blocking buffer and 5% 7-AAD dye at 4 °C for 20 minutes. Samples were washed in 1 mL of FACS buffer, centrifuged at 400 x *g* for 5 minutes at room temperature, and then resuspended in antibodies diluted in 1 mL of FACS buffer (**Table 4**) and incubated for 30 minutes at 4 °C, were washed with 1 mL of FACS buffer and centrifuged at 400 x *g* for 5 minutes. Samples were resuspended in 1 mL of FACS buffer and stored at 4 °C until the samples were ready for FACS analysis. HSC were harvested using a BD FACSAria III (BD Biosciences) and FlowJo software (FlowJo, Treestar) was used to quantify cell numbers. Cells were placed on wet ice until they were seeded onto plates (**Figure 5**).

Target	Clone	Isotype	Supplier; Cat#	Fluorophore	Dilution
Lineage Antibody Cocktail	145-2C11; RB6-8C5; RA3-6B2; Ter119; M1/70	Armenian Hamster IgG; Rat IgG2a; Rat IgG2b	Biolegend	FITC	1 in 10
c-Kit/ CD117	2B8	Rat IgG2b κ	Biolegend	PE	1 in 100
Sca-1	E13-161.7	Rat IgG2a κ	Biolegend	PECy7	1 in 150
CD48	HM48-1	Armenian Hamster IgG	Biolegend	AF700	1 in 200
CD150	TC15-12F12.2	Rat IgG2a λ	Biolegend	Pacific Blue	1 in 100

Table 4. Antibody Details for FACS Isolation of Bone Marrow Haematopoietic Stem Cells.

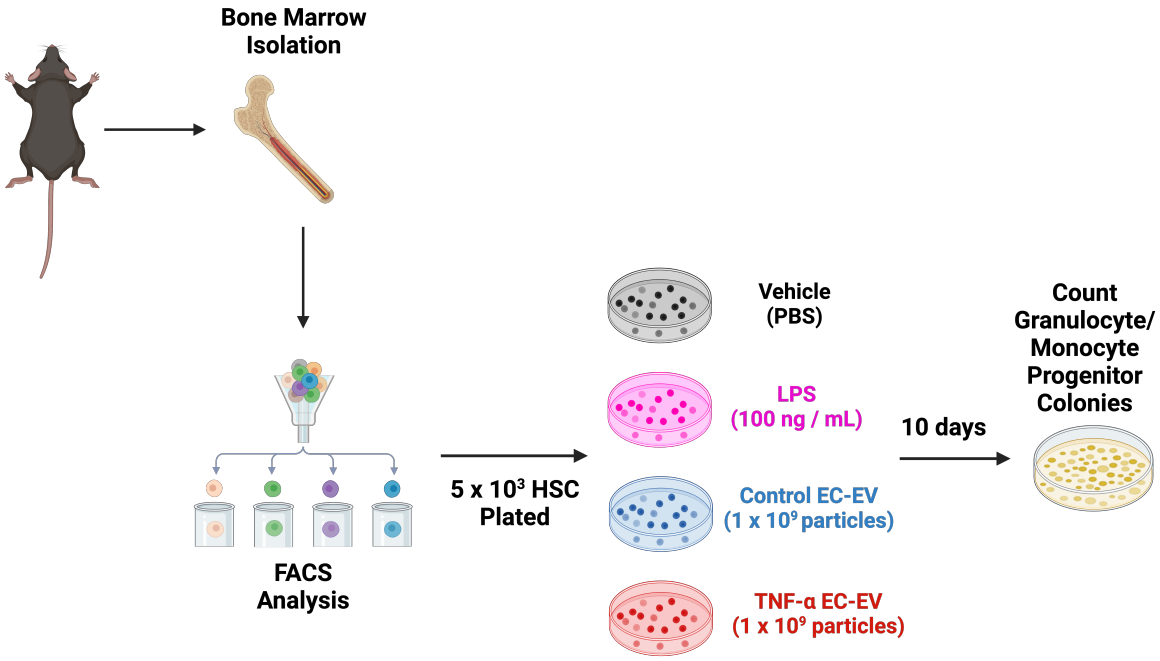

Figure 5. Colony-Forming Unit Assay Involving Bone Marrow Haematopoietic Stem Cells Exposed to Endothelial Cell-Extracellular Vesicles.

Bone marrow HSC populations were counted, and 5 x 10^3 cells were plated in triplicate in 1.5 mL of methylcellulose MethoCult M3434 media (StemCell Technologies, UK), supplemented with recombinant mouse IL-3, recombinant mouse IL-6, recombinant mouse erythropoietin and recombinant mouse stem cell factor (StemCell Technologies, UK). Cells were treated with vehicle-control (100 μL of sterile PBS), LPS (100 ng / mL), control EC-EV (1 x10^9 particles derived from unstimulated endothelial cells) or TNF-α EC-EV (1 x10^9 particles derived from TNF-α (10 ng / mL)-stimulated endothelial cells) and were incubated for 18 hours at 37 °C. After incubation, the medium was replaced without the PBS, LPS or EC-EV and colonies from each condition were imaged daily using a Brightfield microscope at 10x magnification. After 10 days, granulocyte-monocyte (colony forming unit-granulocyte macrophage CFU-GM) colonies, colonies derived from erythroid progenitors (burst forming unit-erythroid

BFU-E), and multilineage colonies (colony forming unit-granulocyte erythroid macrophage megakaryocyte CFU-GEMM) were counted manually. The threshold for a 'colony' was a cluster containing more than 20 cells.

2.11 Bone Marrow and Splenic Haematopoietic Stem and Progenitor Cell Analysis Using the In Vivo Endothelial Cell-Extracellular Vesicle Priming Model

Adult wildtype male C57BL/6 mice (10 weeks old) were weighed and injected with one of vehicle-control (100 μL of sterile PBS), LPS (1 mg / kg body weight), control EC-EV (1×10^9 particles derived from unstimulated endothelial cells), TNF-α EC-EV (1×10^9 particles derived from TNF-α (10 ng / mL)-stimulated endothelial cells) or VCAM-1 knockout TNF-α EC-EV (1×10^9 particles derived from TNF-α (10 ng / mL)-stimulated endothelial cells CRISPR-edited to knock out VCAM-1 (89)), as described above (**Method 2.6**) (**Figure 6**). After 24 hours, mice were weighed and received a second injection (all intravenous) of LPS (1 mg / kg body weight) combined with 5-ethynyl 2'deoxyuridine (EdU) (Click-iT Plus EdU kit, Thermo Fisher, UK). After 72 hours, mice were re-weighed and received a cardiac puncture followed by cervical dislocation (performed by Dr Naveed Akbar). Tissue harvesting of bone marrow, spleen, and blood cells was as described above (**Method 2.6**) and cell staining for flow cytometry analysis was performed (**Method 2.7**). Samples were analysed using a BD Fortessa X20 and data analysis was performed using FlowJo software (FlowJo, Treestar).

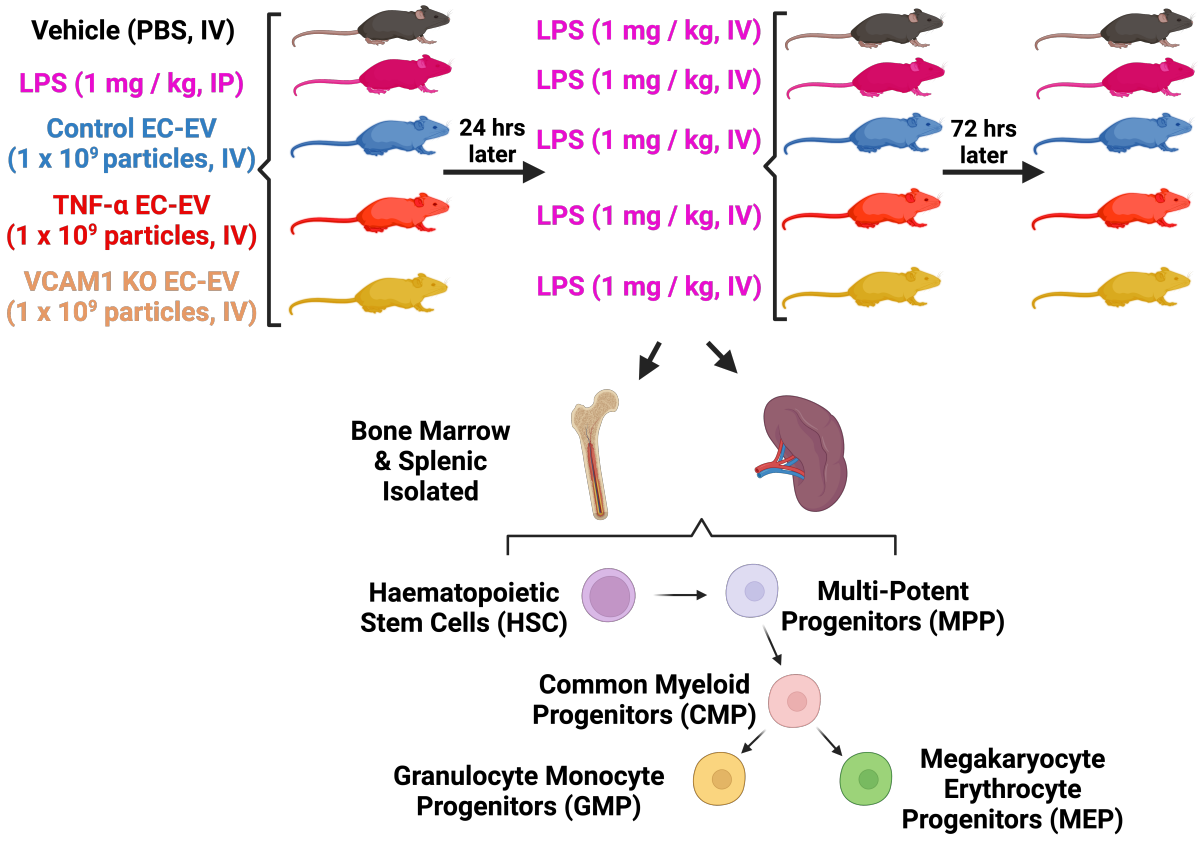

Figure 6. Overview of the In Vivo Study on the Effects of Endothelial Cell-Extracellular Vesicle Priming on Bone Marrow and Splenic Haematopoiesis.

2.12 Bone Marrow Haematopoietic Stem Cell isolation Using Fluorescence-Activated Cell Sorting for Transcriptomic Analysis

For transcriptomic analysis of bone marrow HSC, mice were injected with either control EC-EV (1 x 10^9 particles) or TNF-α EC-EV (1 x 10^9 particles) as described above (**Method 2.8**) (**Figure 7**). Bone marrow cells were harvested (**Method 2.6**) and stained (**Method 2.7**) (**Table 4**) and HSC were isolated using FACS. HSC were collected in 1.5 mL Eppendorf tubes containing 300 μL of buffer RLT solution (Qiagen, UK) and were stored on dry ice at -20 °C.

Samples were thawed on wet ice for RNA extraction. Total RNA was isolated from HSC for sequencing using a miRNeasy Mini Kit (Qiagen, UK) according to the manufacturer's instructions. RNA was eluted in 30 μL of RNAse-free water (Qiagen, UK). The RNA yield and purity was calculated using a Nanodrop 100 spectrophotometer (Thermo Fisher, UK) and RNA purity was determined by the A260/280 ratio of each sample. RNA samples were flash frozen at -80 °C and were shipped to the NovoGene sequencing facility for quality control, pre-amplification, sequencing, and post-sequencing analysis (NovoGene, UK).

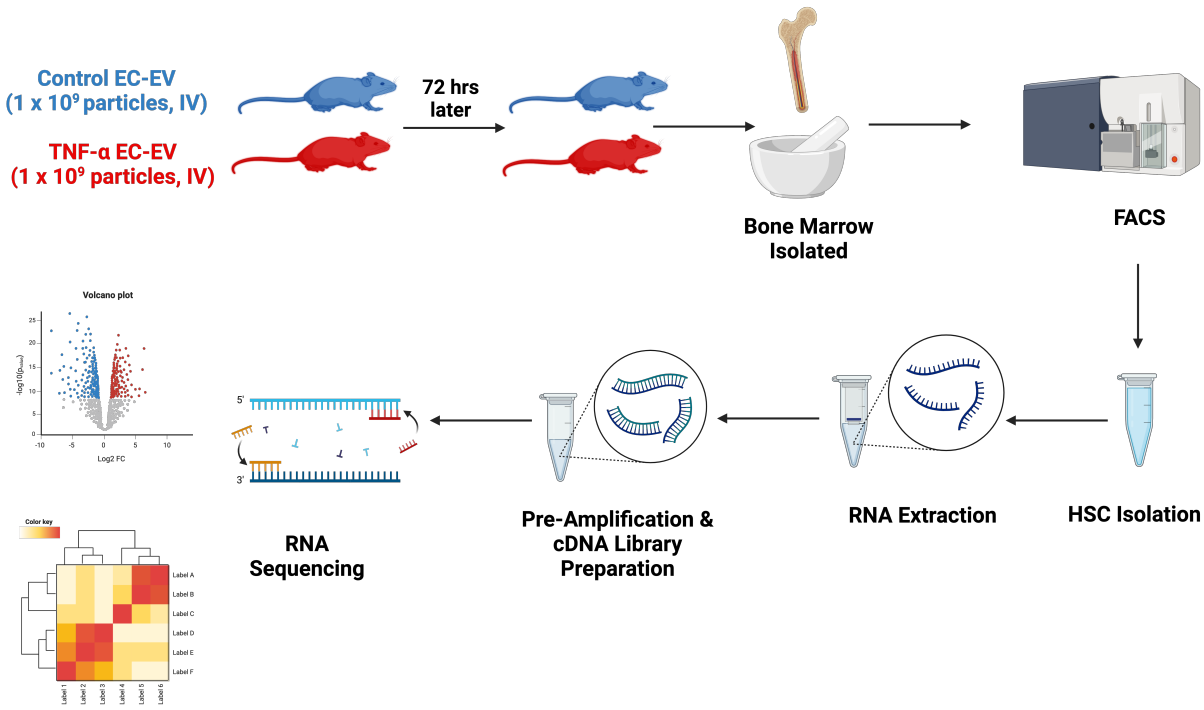

Figure 7. Transcriptomic Analysis of Bone Marrow Haematopoietic Stem Cells in Response to Endothelial Cell-Extracellular Vesicles.

For quality control steps, Qubit (Life Technologies, UK) and the Agilent 2100 Bioanalyser (Agilent, UK) were used to measure RNA purity and the degree of RNA degradation during extraction. To ensure high RNA quality, all samples met the following requirements for sequencing: A260/280>2.0, A260/230>2.0, and the RNA integrity number (RIN)>4.0. During library construction, a pre-amplification step was used to overcome the low cell number using SMART-seq v4 Ultra Low Input RNA kit (Takara Bio, Japan). The library was then sequenced using the Illumina NovaSeq 6000 Sequencing System (Illumina, USA) and the paired-end 150 base pair configuration. Reads were mapped to the mouse genome 'GRCm39' (Ensembl) using *Hisat2* v2.05 (151) and mapped reads were assembled using *StringTie* v1.3.3b. *FeatureCounts* v1.5.0-p3 (152) was used to count the number of reads mapped to each gene. The expected number of fragments per kilobase of transcript sequence per million base pairs (FPKM) of each gene was calculated based on the gene length and the number of reads mapped to the gene. This accounts for the sequencing depth and corrects for the bias towards larger fragments and more highly expressed genes.

Principal component analysis (PCA) was used to condense the number of mapped reads for each sample using R-studio packages *factoextra* and *FactoMineR* for analysis and *ggplot2m* for data visualisation. Differential gene expression analysis was performed using the *DESeq2* R-studio package and ggplot2m to create a Volcano plot. The P values were modified using the Benjamini and Hochberg approach, which controls the False Discovery Rate (FDR) to correct for multiple comparisons and creates adjusted P values (Padj). The threshold for statistical significance was set at Padj<0.05 for differentially expressed genes.

Gene ontology (GO) analysis for terms associated with Biological Process, Molecular Function, and Cellular Component was performed on the set of differentially expressed genes. A Fisher's Exact test was used to determine which GO terms were significantly overrepresented in the differentially expressed genes dataset compared to the reference database. The threshold for statistical significance was set at Padj<0.05 and was determined by calculating P values which were adjusted using the Benjamini and Hochberg test to control the FDR to correct for multiple comparisons.

Kyoto Encyclopedia of Genes and Genomes (KEGG) pathway analysis was also performed on the set of differentially expressed genes. P values were adjusted using the Benjamini and Hochberg test to control the FDR to correct for multiple comparisons/. The threshold for statistically significant KEGG pathways was set at Padj<0.05.

Gene set enrichment analysis (GSEA) (153, 154) was performed using the *clusterProfiler* package in R-studio. Analysis was performed on all genes expressed in control EC-EV (12,922 genes) and TNF-α EC-EV (11,196 genes) groups. From the 22,762 gene sets on the Molecular Signatures Database (MSigDB), 15,850 gene sets were excluded based on gene set size filters which were imposed (minimum size = 15, maximum size = 5,000). Genes were ranked according to the equation:

$$\text{Rank} = -\log10(\text{Padj}) * \textit{sign}(\text{FoldChange})$$

Significant or overrepresented gene sets were identified using a Kolmogorov-Smirnov test and the Benjamini and Hochberg test was used to control the FDR to correct for multiple comparisons and create adjusted P values. The threshold for statistical significance was set at Padj<0.05. STRING Network analysis (155) was performed on

the statistically significant genes within overrepresented gene sets in order to identify clusters of interacting genes. The minimum required confidence score for identified interactions was greater than 0.400 (>0.400). Gene clusters were identified using the Markov Cluster algorithm. The Benjamini and Hochberg test was used to control the FDR to correct for multiple comparisons to produce Padj. Significant Padj was set to Padj<0.05.

2.13 Gene Expression Analysis by RT-qPCR

Cells were washed with 1 mL of sterile PBS and lysed using 300 μL of buffer RLT solution (Qiagen, UK). Macrophage samples were stored at -80 °C and were thawed on wet ice at 4 °C prior to RNA isolation, whilst HSC samples were transported on dry ice following FACS and were then thawed at 4 °C prior to RNA isolation. Total RNA was isolated using a miRNeasy Mini Kit (Qiagen, UK) and RNA was eluted in 30 μL RNAse-free water (Qiagen, UK). The RNA yield and purity was determined using a Nanodrop 100 spectrophotometer (Thermo Fisher, UK) and the A260/280 ratio. High purity RNA with an A260/280>1.8 was used for cDNA synthesis. cDNA was synthesised using a QuantiTect Reverse Transcription PCR kit (Qiagen, UK) by eliminating genomic DNA (gDNA) using the gDNA wipeout buffer for 2 minutes at 42 °C as per the manufacturer's instructions on a 96-well Thermal Cycler (Veriti, Thermo Fisher, UK). cDNA was then generated using the Quantiscript Reverse Transcriptase, Quantiscript RT buffer, and Reverse Transcriptase primer mix for 15 minutes at 42 °C, as per the manufacturer's instructions. To denature and inactivate the reverse transcriptase enzyme, the samples were incubated at 95 °C for 3 minutes. Samples were stored at -80 °C for qPCR analysis. qPCR reactions were performed using the

TaqMan Gene Expression Assay system (Thermo Fisher, UK), TaqMan Universal Master Mix II with UNG (Applied Biosystems, UK) and TaqMan probes (see **Table 5**) according to the manufacturer's instructions. qPCR analysis was performed by the QuantStudio 7 Flex (Thermo Fisher, UK). Housekeeper genes normalised gene expression for each experiment. $\delta\delta$Ct values were calculated to normalise the housekeeper gene for each gene of interest.

Reagent	**Company**	**Identifier Code**
Mouse *tnf* Taqman assay	Applied Biosystems	Cat#: 4331182; Assay ID: Mm00443260
Mouse *il6* Taqman assay	Applied Biosystems	Cat#: 4331182; Assay ID: Mm00446190
Mouse *ym1* (c*hil3*) Taqman assay	Applied Biosystems	Cat#: 4331182; Assay ID: Mm00657889_mH
Mouse *gapdh* Taqman assay	Applied Biosystems	Cat# 4448489; Assay ID: Mm99999915_g1
Mouse *hif1-*α Taqman assay	Applied Biosystems	Cat#: 4331189; Assay ID: Mm00468869_m1
Mouse *ppia* Taqman assay	Applied Biosystems	Cat#: 4448489; Assay ID: Mm01273726_m1
Mouse *il1*β Taqman assay	Applied Biosystems	Cat#: 4331182; Assay ID: Mm00434228_m1

Mouse *zeb1* Taqman assay	Applied Biosystems	Cat#: 4331182; Assay ID: Mm00495564_m1

Table 5. Quantitative PCR Primer Details.

2.14 Endothelial Cell-Extracellular Vesicle microRNA Isolation and Analysis

sEND.1-EV were isolated as described in **Method 2.3**, resuspended in 150 μL of sterile PBS and the number of isolated particles were counted using NTA (**Method 2.4**). Each sample was split evenly into 3 groups. The untreated EC-EV samples were placed immediately in 300 μL of Qiazol (from the miRNeasy Mini Kit) and were snap frozen on dry ice and stored at -80 ºC until further isolation. The RNAse-treated group were incubated with 10 μg / mL of RNase A (Thermo Fisher, UK) for 30 minutes at 37 °C, and the enzyme was inactivated by heating at 95 °C for 10 minutes. 300 μL of Qiazol was then added and samples were snap frozen on dry ice and stored at -80 ºC.

The sonicated RNase-treated group was needle sonicated at 33% power for 15 seconds using a SonoPuls HD2070 (Bandelin Sonopuls, Germany), stored on ice at 4 °C and were centrifuged at 500 x *g* for 1 minute. Samples were then exposed to RNase A as described above and 300 μL of Qiazol was added and samples were snap frozen on dry ice and stored at -80 ºC. RNA was extracted as described in **Method 2.13**. Total RNA was diluted to 5 ng / μL for each sample and cDNA was generated from miRNA transcripts and transcripts were quantified for miRNA-126-3p and miRNA-320b using the miRCURY LNA miRNA PCR Starter Kit (Qiagen, UK). Unisp6 RNA was used as a spike-in control. The protocol was carried out in line with the manufacturer's instructions. qPCR analysis was performed as described above (**Method 2.13**).

2.15 Endothelial Cell-Extracellular Vesicle microRNA Cargo Bioinformatics Analysis

A previous microRNA array of plasma EV miRNA samples from patients following MI at the time of presentation and three months post-MI identified several differentially expressed miRNAs by filtering for fold change (log2fold change>1) and $p<0.05$ including miRNA-126-3p and miRNA-320 (88). A list of predicted putative gene targets in mice was generated for both enriched miRNAs using miRDB (156), miRWalk (157) and TargetScan (158) databases. Targets lists were deduplicated and those targets identified in multiple databases were imputed into GO to identify overrepresented terms associated with Biological Processes, Molecular Functions, and Cellular Components. A Fisher's exact test was used to identify enriched GO terms and was ranked by fold enrichment. Statistical significance was assessed using P values which were adjusted to control the FDR and correct for multiple comparisons. The threshold for statistically significant GO terms was set at $Padj<0.05$. KEGG pathway analysis was also performed to identify enriched KEGG pathways. P values were adjusted to control the FDR and correct for multiple comparisons. The threshold for statistically significant KEGG pathways was set at $Padj<0.05$.

The overlapping putative target lists and GO terms for miRNA-126-3p and miRNA-320b were then compared to identify common gene targets and enriched GO pathways between both miRNAs. These overlapping gene targets were compared with the differentially expressed genes in the HSC analysis (**Method 2.12**). The overrepresented GO terms for miRNA-16-3p and miRNA-320b were also compared with the overrepresented HSC GO terms using the same statistical analyses as described above.

STRING network analysis was performed on the overrepresented GO terms which overlapped between the HSC differentially expressed genes and either the miRNA-126-3p or the miRNA-320b putative gene targets in order to identify clusters of interacting genes. The minimum required confidence score for identified interactions was greater than 0.400 (>0.400). Gene clusters were identified using the Markov Cluster algorithm. P values were adjusted to control the FDR and correct for multiple comparisons. Significant Padj was set to Padj<0.05.

2.16 Isolation and Culturing of Bone Marrow Cells to Generate Bone Marrow-Derived Macrophages

Adult wildtype C57/BL6 female mice (10 weeks old) with a body weight between 23 - 27 g were culled through cardiac puncture followed by cervical dislocation. Bone marrow was isolated by severing each femur and tibia and flushing the bone marrow contents using 10 mL of ice-cold sterile PBS and a 25 G needle (Terumo, UK) attached to a syringe (**Figure 8**). Cell suspensions were passed through a 70 μm cell strainer to create a single cell suspension and remove bone fragments and tissue debris. Samples were centrifuged at 1,000 x *g* for 5 minutes at room temperature and the pellet was retained and resuspended in 1 mL of BMDM Differentiation media (**Method 2.1**).

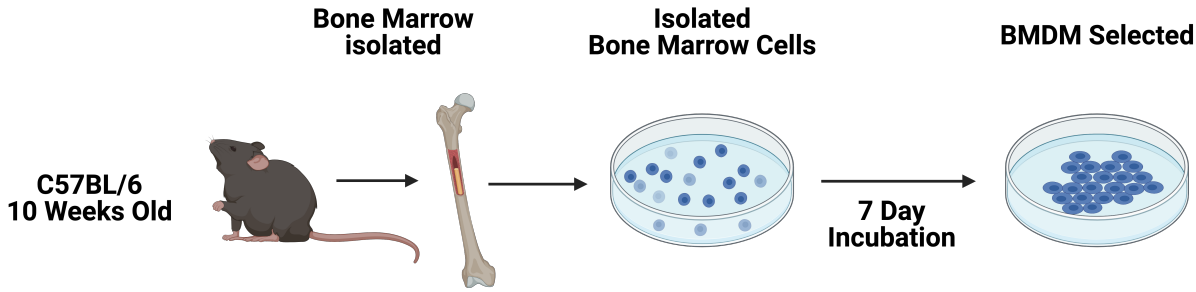

Figure 8. Schematic of Mouse Bone Marrow Isolation and Culture to Generate Bone Marrow-Derived Macrophages.

Samples were plated onto four non-tissue culture-treated Petri dishes (101VR20, Thermo Fisher, UK) in 10 mL of BMDM Differentiation media and incubated at 37 °C. Cells were supplemented with an additional 5 mL per dish of BMDM Differentiation media on Day 4 and mature BMDM were positively selected by adhesion on Day 7. Briefly, media was aspirated to remove dead and undifferentiated cells followed by the addition of 4 mL of 2.5% trypsin-EDTA for 5 minutes at 37 °C to dislodge adhered macrophages. 10 mL of BMDM Differentiation media was added to neutralise trypsin. Samples were centrifuged at 500 x *g* for 5 minutes and the pellet was retained and resuspended in 10 mL of BMDM Stimulation media (**Method 2.1**). The cell suspensions were transferred into two Petri dishes and incubated at 37 °C. After 20 minutes, the media was aspirated to remove non-adhered cells and leave BMDM adhered to the dish which was supplemented with 10 mL of fresh BMDM Stimulation media. After a 24-hour rest period, BMDM were either harvested or stimulated for future experiments.

2.17 Bone Marrow-Derived Macrophage Characterisation Using Flow Cytometry

BMDM were cultured as described (**Method 2.16**), were resuspended in 1 mL of sterile PBS and centrifuged at 500 x *g* for 5 minutes. Cell pellets were resuspended in 1 mL of FACS buffer, and 1 x 10^6 cells were aliquoted into wells on a 96-well plate (Corning Incorporated, UK) in 200 μL of FACS buffer plus 1% Fc receptor blocking buffer and 5% 7-AAD for 15 minutes at 4 °C. Samples were washed in 200 μL of FACS buffer and centrifuged at 500 x *g* for 5 minutes. Cell pellets were retained and resuspended in antibodies diluted in FACS buffer (**Table 6**) for 20 minutes at 4 °C in the dark. Samples were washed with 200 μL of FACS buffer and centrifuged at 500 x *g* for 5 minutes. Cell pellets were retained and resuspended in 200 μL of BD Cytofix buffer for 20 minutes at 4 °C in the dark. Samples were then centrifuged at 500 x *g* for 5 minutes and cell pellets were resuspended in 200 μL of FACS buffer and stored for analysis at 4 °C in the dark. Samples were analysed using a BD Fortessa X20 and analysed using FlowJo software.

To determine the background fluorescence levels during the analysis, compensation was calculated for each channel using unstained samples and fluorescence-minus one samples. In the latter, each antibody-fluorophore conjugate that was used in the flow cytometry analysis was added except the antibody-fluorophore conjugate that corresponded to the fluorescence channel being measured. This established the background signal for each antibody and was used to create the gating strategy by excluding counts that did not meet the background signal threshold.

Target	Clone	Isotype	Supplier; Cat#	Fluorophore	Dilution
CD45	30-F11	Rat IgG2b, κ	Biolegend 103124	AF647	1 in 200
CD11b	M1/70	Rat IgG2b, κ	Biolegend 101206	FITC	1 in 100
F4/80	BM8	Rat IgG2a, κ	Biolegend 123110	PE	1 in 100

Table 6. Antibody Details for Flow Cytometry Analysis.

2.18 Bone Marrow-Derived Macrophage In Vitro Tolerance Model

Isolated BMDM were plated onto 12-well plates (Corning Incorporated) in BMDM Stimulation media (**Method 2.1**) at a seeding density of 3 x 10^5 cells / mL / well. Cells were stimulated for 18 hours with either LPS (100 ng / mL), β-glucan (10 μg / mL), hyperglycaemia (20 mM glucose), mannitol (15 mM mannitol + 5 mM glucose), control EC-EV (1 x 10^9 particles / mL, isolated from unstimulated sEND.1 cells), TNF-α EC-EV (1 x 10^9 particles / mL, isolated from TNF-α-stimulated sEND.1 cells) (**Method 2.3**), or a vehicle-control (sterile PBS) (**Figure 9**). The medium was aspirated and replaced with 1 mL of BMDM Stimulation media overnight. Cells were then stimulated for 18 hours with either PBS or a combination of LPS (100 ng / mL) and IFN-γ (10 ng / mL) (R&D Systems, UK) and then were harvested.

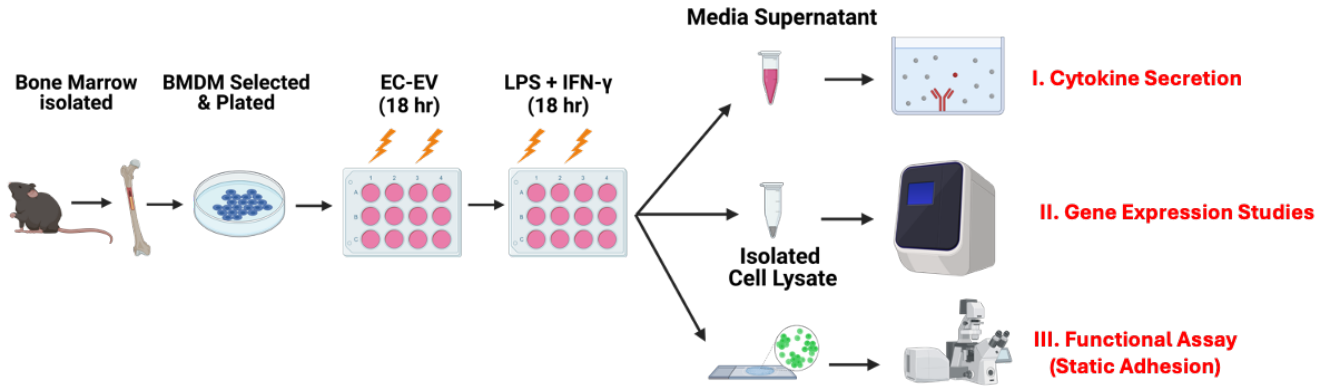

Figure 9. Overview of Bone Marrow-Derived Macrophage Isolation and Stimulation with Endothelial Cell-Extracellular Vesicles for Protein, RNA, and Static Adhesion Studies.

2.19 Static Adhesion Assay to Assess Bone Marrow-Derived Macrophage Function

sEND.1 cells were seeded at 2 x 10^6 cells / flask in a T75 flask and were grown to confluency on 10 mm glass coverslips (VWR, UK) in 12-well plates. Cells were activated using 10 ng / mL of recombinant mouse TNF-α for 18 hours in sEND.1 cell culture media (**Method 2.1**). Bone marrow cells were isolated and cultured to generate BMDM (**Method 2.16**) and plated on 12-well plates in 1 mL of Macrophage Stimulation media at a density of 3 x 10^5 cells / mL / well. Cells were stimulated as previously described (**Method 2.18**) and BMDM were dislodged using 500 µL of 2.5% trypsin-EDTA for 5 minutes at 37 °C. Samples were collected and centrifuged at 500 x *g* for 5 minutes at room temperature and resuspended in 500 µL of sterile PBS. BMDM were fluorescently labelled using CFSE (Abcam, UK).

Briefly, 1 µL of CFSE dye was added to each cell suspension and incubated for 10 minutes at 37 °C. Samples were washed with 500 µL of sterile PBS, centrifuged at

500 x *g* for 5 minutes, and resuspended in 1 mL of Macrophage Stimulation media. 5 x 10^4 BMDM were added per coverslip in 500 μL of Macrophage Stimulation media. After a 1-hour incubation at 37 °C, the medium was aspirated and washed with 500 μL of sterile PBS to retain only adhered BMDM on the coverslip. Coverslips were fixed and mounted on glass microscope slides (VWR, UK) using ProLong Gold Antifade Mountant with DAPI (Thermo Fisher, UK), allowed to air dry for 1 hour and were imaged. DAPI images confirmed the presence of endothelial monolayers and FITC images at matching locations captured adhered BMDM. Images were captured using a Leica DM 6000 CFS fluorescent microscope (Leica Microsystems, Germany) at x10 magnification. The number of adhered cells was quantified using ImageJ software. The data displayed is the average of quantified adhered cells from 4 images per sample. Images were taken from the same pre-determined region of each coverslip.

2.20 Isolation & Culturing of Peritoneal Macrophages for Protein Studies

To isolate mouse peritoneal macrophages, adult wildtype C57/BL6 female mice (10 weeks old) were culled by cardiac puncture followed by cervical dislocation. The fur and skin around the abdomen were removed and 5 mL of ice-cold sterile PBS was injected using a 28 G needle attached to a syringe. The abdomen was massaged for 2 minutes to dislodge the peritoneal cells, and the samples were collected using a 21 G needle attached to a syringe. Samples were centrifuged at 400 x *g* for 5 minutes and the cell pellet was resuspended in 1 mL of Macrophage Stimulation media (**Method 2.1**). Samples were plated onto two sterile, non-tissue culture-treated Petri dishes (101VR20, Thermo Fisher, UK) in 10 mL of Macrophage Stimulation media, and after incubating at 37 °C for 20 minutes, peritoneal macrophages were positively

selected by aspirating the medium to remove non-adhered cells and leave viable macrophages attached to the dish. After a 24-hour rest period, macrophages were seeded onto 12-well plates in BMDM Stimulation media (**Method 2.1**) at a seeding density of 3 x 10^5 cells / mL / well. Macrophages were stimulated with LPS (100 ng / mL), β-glucan (10 μg / mL), control EC-EV (1 x 10^9 particles / mL, isolated from unstimulated endothelial cells), TNF-α EC-EV (1 x 10^9 particles / mL, isolated from TNF-α-stimulated endothelial cells), or vehicle-control (sterile PBS). After 18 hours, the medium was aspirated and replaced with 1 mL of fresh media overnight. Cells were then exposed to a combination of LPS (100 ng / mL) and IFN-γ (10 ng / mL) for 18 hours or given a vehicle-control (sterile PBS). Cell supernatants were removed for TNF-α ELISA studies (**Method 2.9**).

2.21 Generating Denatured Endothelial Cell-Extracellular Vesicles

To generate denatured EC-EV, wildtype sEND.1 cells were cultured (**Method 2.2**) and EC-EV were isolated by ultracentrifugation (**Method 2.3**) as previously described. Following isolation, EC-EV samples were resuspended in 100 μL of sterile PBS. 50 μL of each EV sample was stored at 4 °C and the remaining 50 μL of each EV sample was placed on an electronic heat block at 95 °C for 10 minutes, followed by centrifugation at 500 x *g* for 1 minute at room temperature. EC-EV were then characterised using NTA (**Method 2.4**) as previously described.

2.22 Human Monocyte-Derived Macrophage In Vitro Tolerance Model

All clinical investigations were completed in accordance with the Declaration of Helsinki. Ethical approval was obtained from National Research Ethics Service (NRES), and samples were processed in accordance with the Human Tissue Act 2004. Leukapheresis cones were obtained from the NHS Blood Bank and layered onto Ficoll Paque Plus and were centrifuged at 600 x *g* for 30 minutes at room temperature. Peripheral blood mononuclear cells (PBMC) were collected from the buffy coat, were combined with 50 mL of sterile PBS, and were washed by centrifugation at 500 x *g* for 15 minutes at 4 °C (**Figure 10**).

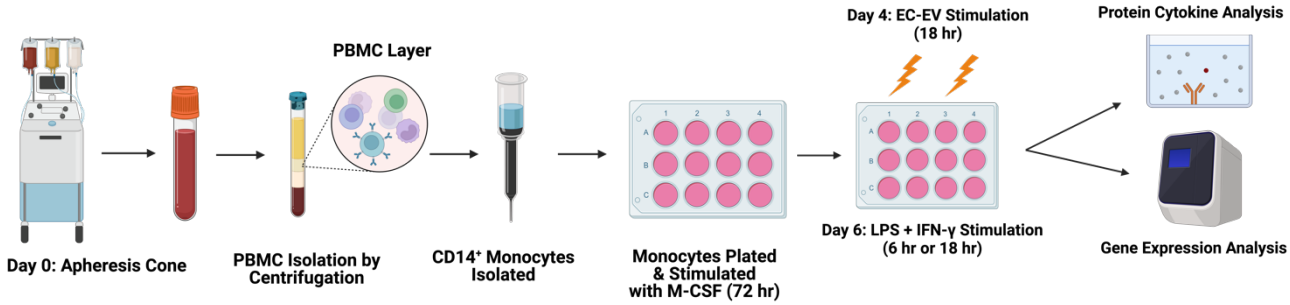

Figure 10. Schematic Detailing Human Monocyte-Derived Macrophage Isolation and Culture, Followed by Endothelial Cell-Extracellular Vesicle Stimulation and Sample Harvest.

Isolated PBMC were resuspended in 1 mL of sterile PBS, counted using an automated cell counter, and 1 x 10^7 cells were diluted in sterile PBS plus 0.5% BSA and 2 mM EDTA by diluting MACS BSA stock solution (Miltenyi, Germany) 1:20 in autoMACS Rinsing Solution (Miltenyi, Germany). Human anti-CD14 beads (Miltenyi, Germany) were diluted 1:10 with the PBMC resuspended solution and incubated for 15 minutes

at 4 °C. 2 mL of MACS buffer was added to the monocyte-anti-CD14 antibody solution and was centrifuged at 400 x *g* for 5 minutes at room temperature. Monocytes were resuspended in 0.5 mL of MACS buffer and were passed through the pre-washed MS column (Miltenyi, Germany).

Monocytes were removed through washing in 1 mL of ice-cold MACS buffer, were centrifuged at 500 x *g* for 5 minutes at room temperature and were resuspended in 1 mL of sterile PBS. Cells were counted using an automated cell counter and isolated monocytes were seeded on 48-well plates at a density of 2 x 10^5 cells / well in 0.5 mL Macrophage Stimulation media (**Method 2.1**). 50 ng / mL of recombinant human M-CSF (R&D Systems, UK) was added to generate monocyte-derived macrophages. Cells were rested for 3 days prior to stimulation with 1 x 10^9 particles / mL of HUVEC-EV (cultured using **Method 2.2** and isolated using **Method 2.3**) for 18 hours. After a 1-day rest period, cells were stimulated with 100 ng / mL of LPS and 10 ng / mL of recombinant human interferon-γ (Invitrogen, USA) for either 6 hours or 18 hours. Cell supernatants were retained and stored at -80 °C for protein cytokine analysis (**Method 2.9**) and monocyte-derived macrophages were lysed using miRvana miRNA isolation kit (Thermo Fisher, UK) and stored at -80 °C for gene expression studies (**Method 2.13**).

2.23 Statistical Analysis

All statistical analysis was performed using GraphPad Prism software. The Gaussian distribution of parameters was assessed using a Shapiro-Wilk normality test (α = 0.05, $p<0.05$). Outliers in each dataset were identified using a Grubb's test (α = 0.05,

$p<0.05$). Comparisons between two groups were calculated by either paired or unpaired two-tailed Student's t-tests or a Mann-Whitney U test, for parametric or non-parametric data, respectively. The statistical significance of differences between more than two groups was calculated for parametric data by one-way or two-way ANOVA analysis with Bonferonni post-hoc correction test to correct for multiple comparisons. For non-parametric data, a Kruskal-Wallis test with Dunn's post-hoc correction analysis was used to correct for multiple comparisons. At a value of $p<0.05$ the null hypothesis was rejected.

Chapter 3- Endothelial Cell Extracellular Vesicles Modulate Haematopoiesis in Bone Marrow and Spleen

3.1 Introduction

An MI induces a rapid and large innate immune response within the body (159-162), including localised cytokine and chemokine secretion at the infarct site, and an increase in circulating innate immune cells such as monocytes and neutrophils in the peripheral blood (88, 89, 163, 164). The bone marrow contributes to the supply of innate immune cells through haematopoiesis, a process that promotes the production of myeloid-lineage cells and is activated by acute injury, such as MI (57, 165, 166). These cells are then able to localise to the damaged myocardium where they are responsible for promoting phagocytosis of necrotic cells and debris by pro-inflammatory M1 macrophages (44, 164, 167, 168), and for amplifying the inflammatory cytokine response through the secretion of TNF-α and IL-6 (164).

The signalling mechanisms between the bone marrow and damaged myocardium to initiate haematopoiesis has not been fully elucidated, but studies have shown a role for the sympathetic nervous system in promoting norepinephrine signalling in response to MI (169, 170). Norepinephrine activity stimulates chemokine signalling and the structural remodelling of the bone marrow niche through matrix metalloprotease signalling (171) and by repressing HSC maintenance factors such as CXCL12 and VCAM-1. This leads to the expansion of HSPC in the bone marrow and the production of new myeloid cells (82, 171).

Studies have also shown the effects of repeated MI on the bone marrow in patients who survive an initial infarction and found that recurrent MI suppresses

haematopoiesis in the bone marrow (82), evidenced by fewer HSC, GMP, monocytes and neutrophils. Furthermore, these reprogramming effects can be transferred through the blood between an MI-injured mouse to a naïve mouse (82). However, the signalling factors mediating this process remains unknown.

VCAM-1$^+$ EV are elevated in the peripheral blood following MI (88, 89, 98) and promote the mobilisation and transcriptional activation of monocytes and neutrophils from the spleen (88, 89). The cellular origin of these VCAM-1$^+$ EV post-MI is not known with certainty, but the EV are enriched in endothelial cell-associated miRNA cargo such as miRNA-126-3p, and miRNA-126-5p (88, 146, 172), suggesting endothelial cell origin, as well as miRNA-320 (173, 174). Furthermore, VCAM-1 expression is upregulated upon activation of endothelial cells and on EC-EV (88) and *in vitro*, in a model of endothelial cell activation with pro-inflammatory TNF-α (88, 89). Using this *in vitro* model and knocking out VCAM-1 using CRISPR-Cas9 gene base-editing of the same endothelial cells mitigates the splenic mobilisation of monocytes and neutrophils in mice (89), suggesting that VCAM-1 is required for this response.

Given the signalling mechanism between the bone marrow and injured heart is not known and there is evidence that the regulation of haematopoiesis in the bone marrow can be mediated by components of the blood (89, 98), VCAM-1$^+$ EC-EV could be highly relevant to this process, especially given the established role of VCAM-1$^+$ EC-EV on the spleen. Therefore, here, I hypothesise that VCAM-1$^+$ EC-EV, generated by stimulating endothelial cells with TNF-α, regulate haematopoiesis within the bone marrow.

3.2 List of Methods Used in This Chapter

- *2.1 Media Preparations*
- *2.2 Endothelial Cell Culture*
- *2.3 Extracellular Vesicle Isolation Using Ultracentrifugation*
- *2.4 Extracellular Vesicle Characterisation*
- *2.5 In Vivo Experimentation*
- *2.6 Isolation of Bone Marrow, Spleen & Blood Cells for Flow Cytometry Analysis*
- *2.7 Cell Staining for Flow Cytometry Analysis*
- *2.8 Bone Marrow and Splenic Haematopoietic Stem & Progenitor Cell Analysis Using the In Vivo Endothelial Cell-Extracellular Vesicle Model*
- *2.9 Protein Analysis by Enzyme-Linked Immunosorbent Assay (ELISA)*
- *2.10 Colony-Forming Unit Assay for the Bone Marrow-Endothelial Cell-Extracellular Vesicle Model*
- *2.11 Bone Marrow & Splenic Haematopoietic Stem & Progenitor Cell Analysis Using the In Vivo Endothelial Cell-Extracellular Vesicle Priming Model*
- *2.23 Statistical Analysis*

3.3 Characterisation of Endothelial Cell-Extracellular Vesicles

Mouse endothelial cell-EV were derived from sEND.1 cells stimulated with either vehicle-control (PBS) or mouse recombinant TNF-α (10 ng / mL) (TNF-α) and were characterised in line with MISEV guidelines (90). In accordance with previous work (88, 89), NTA showed that TNF-α-stimulated endothelial cells released significantly more particles relative to the controls ($p<0.0001$, **Figure 11A**) and both groups had similar size distribution profiles and a particle size peak of ~110 nm (**Figure 11B**). Cryo-TEM (**Figure 11C**) and TEM (**Figure 11D**) imaging shows the morphology of EV-like particles and western blot analysis showed the presence of ALIX, TSG-101 and Syntenin-1 (typical EV markers), the presence of eNOS (an endothelial marker) and the absence of GM130 and ATP5A (cellular contamination markers) in EV fractions (**Figure 11E**). Histone H3 was present in EC-EV and VCAM-1 was enriched in the TNF-α EC-EV fraction relative to the control EC-EV fraction, indicating endothelial cells were successfully activated by TNF-α.

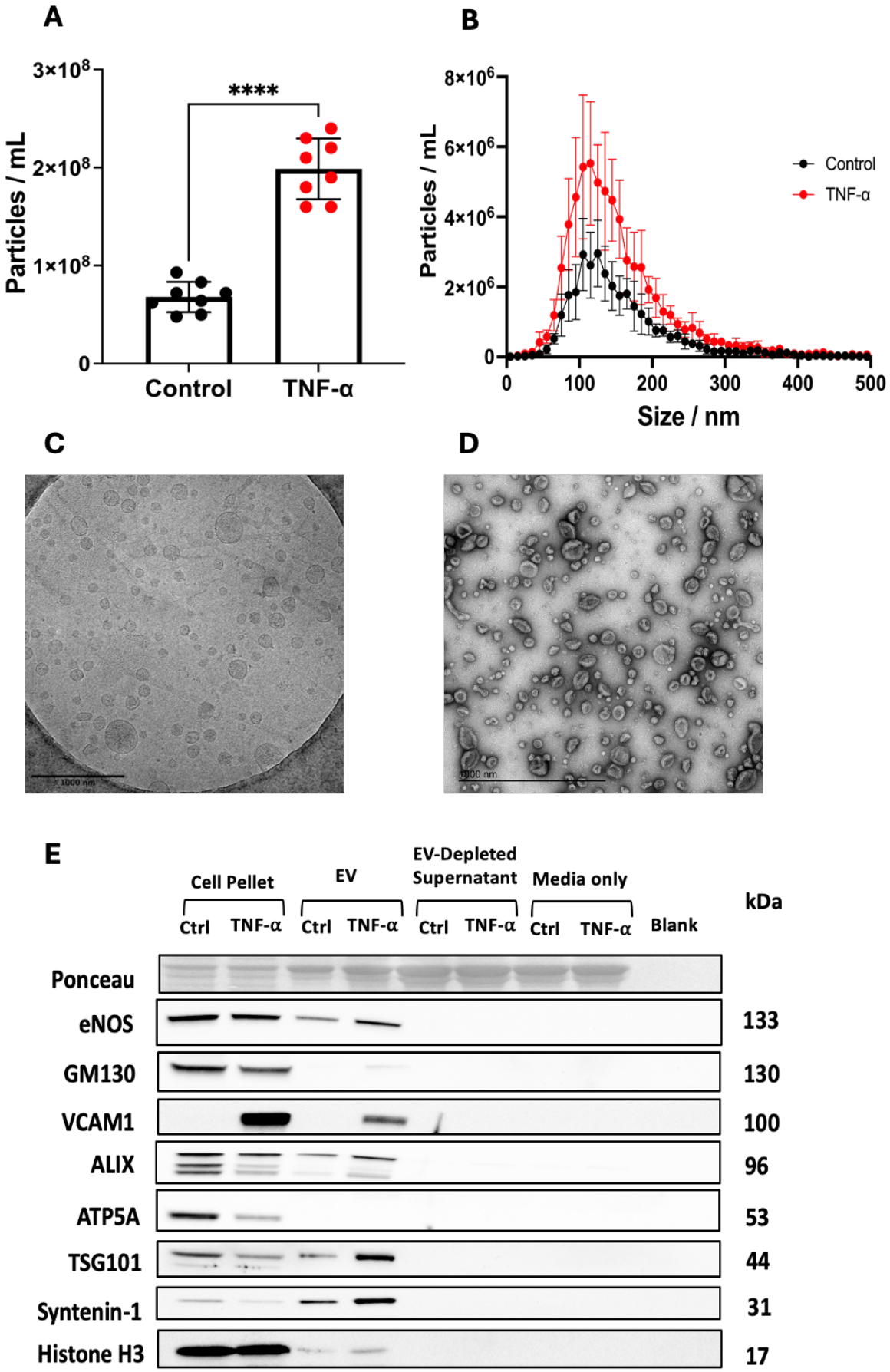
A
B
C
D
E
Particles / mL
3×10^8
2×10^8
1×10^8
0
****
Control
TNF-α
8×10^6
6×10^6
4×10^6
2×10^6
0
100
200
300
400
500
Size / nm
Control
TNF-α
1000 nm
Cell Pellet
EV
EV-Depleted Supernatant
Media only
Ctrl
TNF-α
Blank
kDa
Ponceau
eNOS
133
GM130
130
VCAM1
100
ALIX
96
ATP5A
53
TSG101
44
Syntenin-1
31
Histone H3
17

Figure 11. Characterisation of Mouse sEND.1 Endothelial Cell-Extracellular Vesicles. *(**A**) Particle count analysis of mouse sEND.1 endothelial cells under basal conditions or following stimulation with recombinant mouse TNF-α (10 ng / mL) (n = 8 per group). (**B**) Size and concentration profile analysis of endothelial cell-derived particles under basal conditions or following stimulation with recombinant mouse TNF-α (10 ng / mL) (n = 8 per group). (**C**) Cryo-TEM and (**D**) TEM images of endothelial cell-derived particles (scale bar 1000 nm). (**E**) Ponceau stain and western blot imaging of endothelial cell-derived particles under basal conditions or following stimulation with recombinant mouse TNF-α (10 ng / mL) for eNOS, GM130, VCAM-1, ALIX, ATP5A, TSG-101, Syntenin-1 and Histone H3. sEND.1 cell pellets, EV-depleted cell culture supernatants and cell culture media (Media only) were used as controls. n = Number of replicates. Data are reported as mean $\pm$ standard deviation. A Shapiro-Wilk test was used to determine data normality (α = 0.05, p<0.05), and a Grubbs test was used to identify outliers (α = 0.05). Data was parametric and statistical significance between the groups was assessed using an unpaired two-tailed t-test. Significance is represented on the graph by ****p<0.0001.*

3.4 TNF-α-Stimulated Endothelial Cell-Extracellular Vesicles Increase Haematopoietic Stem Cells in Mouse Bone Marrow, But Not the Spleen

An MI induces changes in the local myocardium as well as distant organs such as the liver (175, 176) and spleen (177). In the bone marrow, MI induces haematopoiesis leading to an increase in HSCs, monocytes and neutrophils, which can be mobilised into the blood (32, 57), although the mechanism driving this process has not been

elucidated. MI also increases VCAM-1$^+$ EC-EV (88, 89, 98), which are taken up by the spleen (88, 89), but the impact on the bone marrow remains unclear.

In order to determine the *in vivo* effects of TNF-α-stimulated EC-EV (TNF-α EC-EV) on mouse bone marrow, mice received an intravenous injection of either control EC-EV or TNF-α EC-EV, derived from sEND.1 endothelial cells and isolated by ultracentrifugation (see **Method 2.3**). Vehicle-control (sterile PBS) was used as a negative control group and LPS, a known inducer of haematopoiesis as part of the septicaemia response (178, 179) in the bone marrow and spleen, was used as a positive control group (**Figure 12A**). After 72 hours, the minimum time required to detect sufficient haematopoiesis (150, 180, 181), tissues were harvested and mice showed little difference in body weight pre- and post-injection (**Figure 12B**) across all conditions. Mice injected with LPS ($p<0.01$) or TNF-α EC-EV ($p<0.05$) had a significantly heavier spleen relative to the vehicle-control and control EC-EV groups (**Figure 12C**). Spleen weight can be influenced by bodyweight; therefore the spleen weight values were normalised to the body weight of each mouse and the significant difference for the LPS ($p<0.01$) and TNF-α EC-EV ($p<0.05$) groups, relative to the vehicle-control, was maintained.

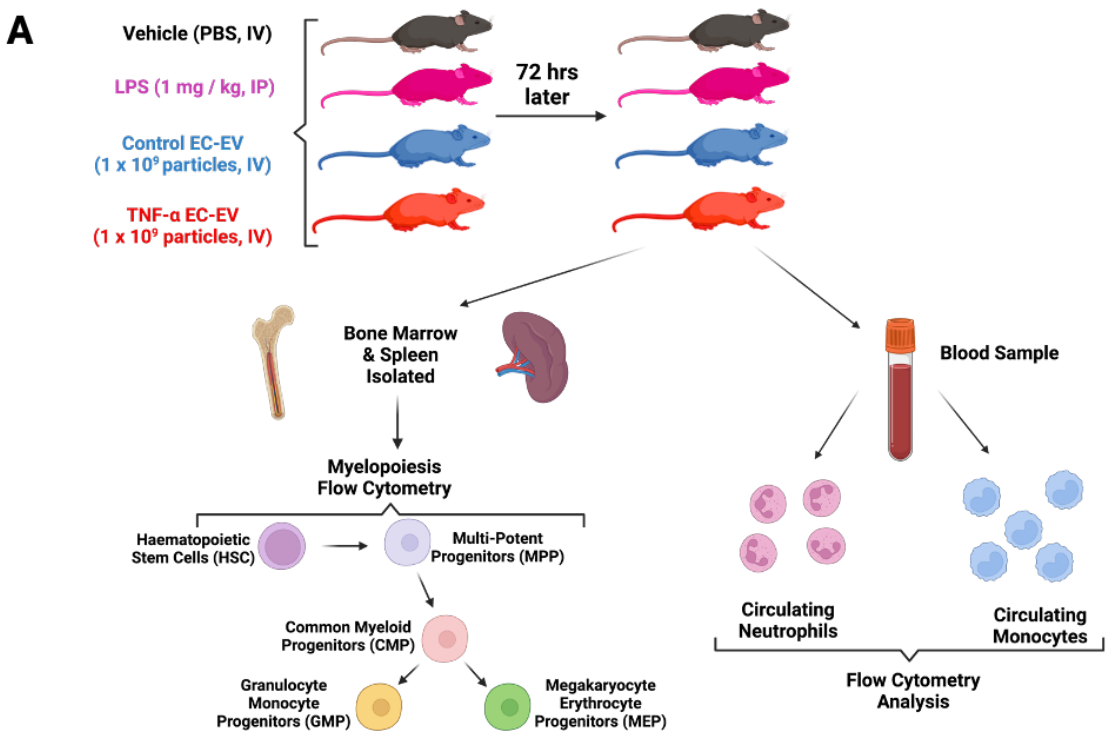
A
Vehicle (PBS, IV)
LPS (1 mg / kg, IP)
Control EC-EV
(1 x 10⁹ particles, IV)
TNF-α EC-EV
(1 x 10⁹ particles, IV)
72 hrs later
Bone Marrow & Spleen Isolated
Blood Sample
Myelopoiesis Flow Cytometry
Haematopoietic Stem Cells (HSC)
Multi-Potent Progenitors (MPP)
Common Myeloid Progenitors (CMP)
Granulocyte Monocyte Progenitors (GMP)
Megakaryocyte Erythrocyte Progenitors (MEP)
Circulating Neutrophils
Circulating Monocytes
Flow Cytometry Analysis

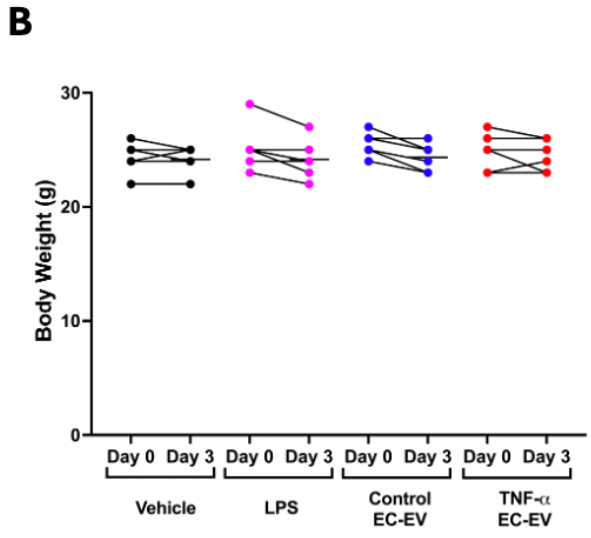
B
Body Weight (g)
30
20
10
0
Day 0 Day 3 Day 0 Day 3 Day 0 Day 3 Day 0 Day 3
Vehicle
LPS
Control EC-EV
TNF-α EC-EV

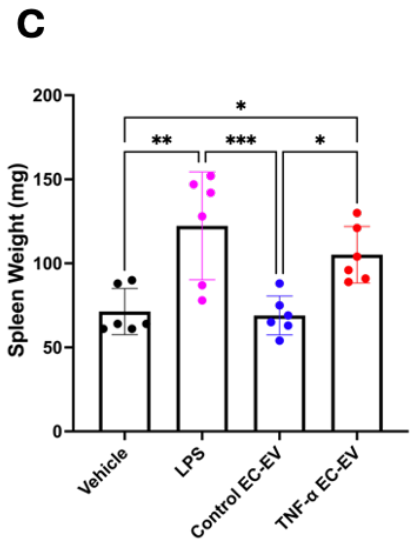
C
Spleen Weight (mg)
200
150
100
50
0
*
**
***
*
Vehicle
LPS
Control EC-EV
TNF-α EC-EV

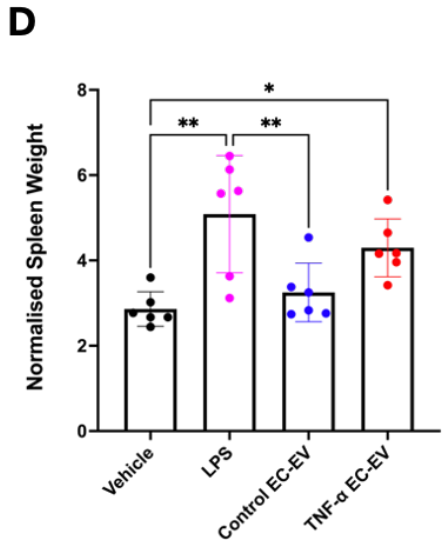
D
Normalised Spleen Weight
8
6
4
2
0
*
**
**
Vehicle
LPS
Control EC-EV
TNF-α EC-EV

Figure 12. Injecting Mice with Control or TNF-α-Stimulated Endothelial Cell-Extracellular Vesicles to Investigate Changes in Bone Marrow Haematopoietic Stem and Progenitor Cells. *(**A**) Overview experimental schematic. (**B**) Body weight changes in mice measured between the time of injection (Day 0) with one of vehicle-control (sterile PBS), LPS (1 mg / kg body weight), control EC-EV (1 x 10^9 particles) or TNF-α EC-EV (1 x 10^9 particles), and the time of tissue harvest (Day 3) (n = 6 per group). (**C**) Spleen weight at the time of bone marrow tissue harvest (Day 3). (**D**) Normalised spleen weight against body weight for each individual. n = Number of replicates. Data are reported as mean ± standard deviation. A Shapiro-Wilk test was used to determine data normality (α = 0.05, p<0.05), and a Grubbs test was used to identify outliers (α = 0.05). Data was parametric and one-way ANOVA with Bonferroni post-hoc correction was used to determine the statistical significance of differences between the groups. Significance is represented on the graph by *p<0.05, **p<0.01, or ***p<0.001.*

<u>*Bone Marrow*</u>

Following bone marrow harvest from the injected mice, the bone marrow cells were filtered to remove debris and counted. There was no significant difference in the total number of bone marrow cells across all groups (**Figure 13A**). Bone marrow cells were stained with antibodies specific to lineage-committed cells (CD3-ε, CD4, TER-119, CD45R/B220 and GR-1), followed by Sca-1, CD117/c-Kit, CD34 & CD16/32 to identify five populations of HSPC (**Method 2.7**) through flow cytometry analysis: HSC, MPP, CMP, GMP, and MEP (**Figure 13B**). The cells in each HSPC population were quantified to give a raw cell count (**Figure 13C-D**) and showed the number of HSC

significantly increased following TNF-α EC-EV injection ($p<0.05$) relative to the control EC-EV group. By contrast, the number of MPP decreased for the TNF-α EC-EV group, relative to control EC-EV ($p<0.05$), indicating the direction of change in HSPC in response to TNF-α EC-EV differs depending on the cell type being investigated. Furthermore, there were no significant changes in CMP across all conditions, but GMP were significantly elevated ($p<0.001$), and there were significantly fewer MEP ($p<0.0001$) for the TNF-α EC-EV group relative to control EC-EV. Since both GMP and MEP are produced through the expansion of CMP, these data suggest a skew of haematopoiesis away from megakaryocyte, platelet and erythrocyte production, and towards granulocyte and monocyte production. This supports findings from the wider literature (82) that GMP are elevated in bone marrow following MI and may contribute to the wider immune response. **Figure 13E** summarises the changes in HSPC populations as a fold-change relative to the vehicle-control, with lines connecting HSPC populations from the same mouse.

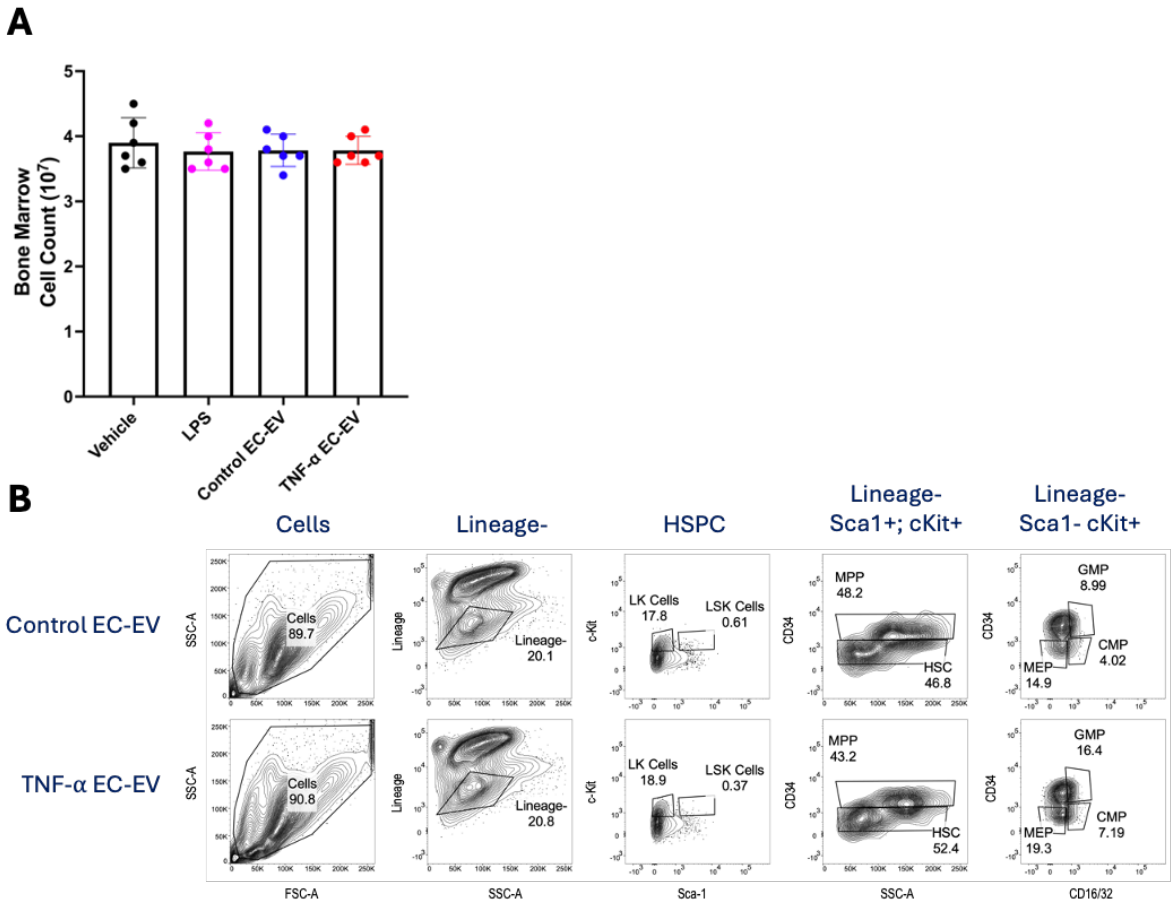
A
Bone Marrow Cell Count (10^7)
Vehicle
LPS
Control EC-EV
TNF-α EC-EV
B
Cells
Lineage-
HSPC
Lineage- Sca1+; cKit+
Lineage- Sca1- cKit+
Control EC-EV
TNF-α EC-EV
Cells 89.7
Lineage- 20.1
LK Cells 17.8
LSK Cells 0.61
MPP 48.2
HSC 46.8
GMP 8.99
CMP 4.02
MEP 14.9
Cells 90.8
Lineage- 20.8
LK Cells 18.9
LSK Cells 0.37
MPP 43.2
HSC 52.4
GMP 16.4
CMP 7.19
MEP 19.3
FSC-A
SSC-A
Sca-1
CD16/32
C
Vehicle
LPS
Control EC-EV
TNF-α EC-EV
Cells / Femur
HSC
MPP
D
Cells / Femur
CMP
GMP
MEP
E
Cells Fold Change (vs. Vehicle)
HSC
MPP
CMP
GMP
MEP
Vehicle
LPS
Control EC-EV
TNF-α EC-EV

Figure 13. TNF-α-Stimulated Endothelial Cell-Extracellular Vesicles Induce Haematopoiesis in Mouse Bone Marrow. *(**A**) Bone marrow cell counts from mice 72 hours post-injection with either vehicle-control (sterile PBS), LPS (1 mg / kg body weight), control EC-EV (1 x 10^9 particles) or TNF-α EC-EV (1 x 10^9 particles) (n = 6 per group). (**B**) Flow cytometry gating strategy for analysis of isolated bone marrow cells to calculate changes in bone marrow HSPC populations. (**C**) Changes in mouse bone marrow HSC and MPP populations following treatment with LPS or EC-EV. (**D**) Changes in mouse bone marrow CMP, GMP and MEP populations following exposure to LPS or EC-EV. (**E**) Fold-change of each HSPC population relative to the vehicle-control. HSPC = Haematopoietic stem and progenitor cells, LSK = Lineage$^-$Sca1$^+$cKit$^+$, LK = Lineage$^-$Sca1$^-$cKit$^+$, HSC = Haematopoietic stem cells, MPP = Multipotent progenitors, CMP = Common myeloid progenitor, GMP = Granulocyte-monocyte progenitor, MEP = Megakaryocyte-Erythrocyte progenitor, n = Number of replicates. Data are reported as mean ± standard deviation. A Shapiro-Wilk test was used to determine data normality (α = 0.05, p<0.05), and a Grubbs test was used to identify outliers (α = 0.05). Data was parametric and one-way ANOVA with Bonferroni post-hoc correction was used to determine the statistical significance of differences between the groups. Significance is represented on the graph by *p<0.05, **p<0.01, ***p<0.001 or ****p<0.0001*.

<u>*Spleen*</u>

Although the primary site of haematopoiesis is the bone marrow, the spleen also has the capacity to generate new blood cells, such as during MI, infection (182), anaemia (182) or myelofibrosis (183), in aiding the bone marrow to replenish the body

sufficiently. Since TNF-α EC-EV are known to localise to the spleen (88), haematopoiesis was also investigated in the spleen to determine if the effects of TNF-α EC-EV were exclusive to HSPC in the bone marrow.

To do this, splenic HSPC from the same mice described in **Figure 13** were isolated and analysed using flow cytometry. In line with the changes in spleen weight (**Figure 12C**), the spleen total cell count was significantly higher for LPS ($p<0.001$) and TNF-α EC-EV ($p<0.05$) groups relative to the vehicle-control and control EC-EV (**Figure 14A**). Normalising the spleen total cell count to the spleen weight showed no significant difference between TNF-α EC-EV and control EC-EV groups (**Figure 14B**), indicating the increase in the spleen weight was proportional to the increase in the spleen cell count.

Flow cytometry analysis of splenic samples used the same gating strategy as for the bone marrow (**Figure 14C**). The quantified data for each population of HSPC appeared to show no significant differences across each of the conditions (**Figure 14D-E**). This suggests that although the spleen weight and cell count increase in response to LPS and TNF-α EC-EV, HSPC populations do not increase in the spleen during this process and instead are only significantly elevated in the bone marrow.

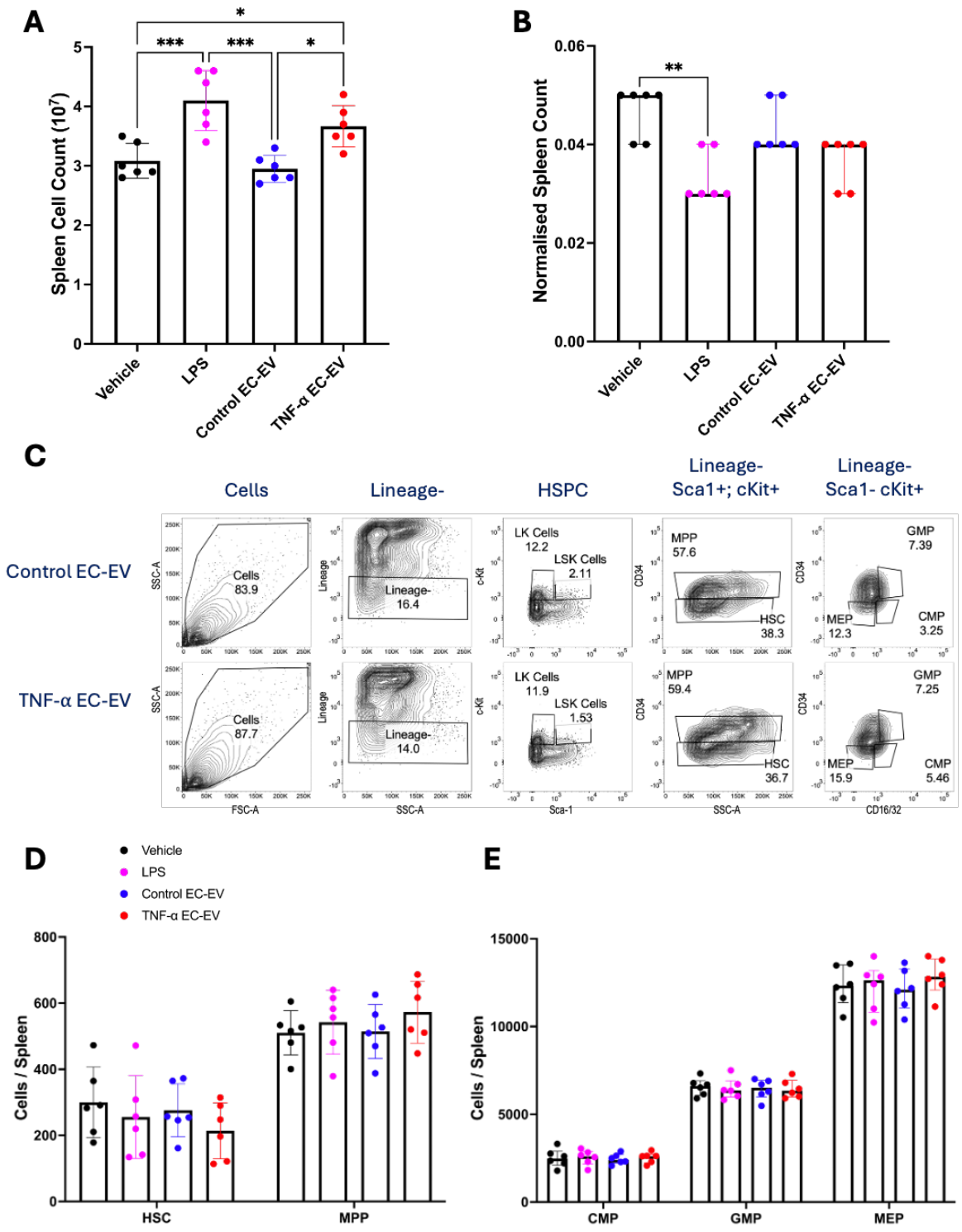

Figure 14. TNF-α-Stimulated Endothelial Cell-Extracellular Vesicles Do Not Impact Haematopoiesis in Mouse Spleen. *(**A**) Spleen cell counts from mice 72*

*hours post-injection with either vehicle-control (sterile PBS), LPS (1 mg / kg body weight), control EC-EV (1 x 10^9 particles) or TNF-α EC-EV (1 x 10^9 particles) (n = 6 per group). (**B**) Spleen cell counts normalised to the spleen weight 72 hours post-injection. (**C**) Flow cytometry gating strategy for analysis of isolated splenic cells to calculate changes in HSPC populations. (**D**) Changes in mouse splenic HSC and MPP populations following treatment with LPS or EC-EV. (**E**) Changes in mouse splenic CMP, GMP and MEP populations following exposure to LPS or EC-EV. HSPC = Haematopoietic stem and progenitor cells, LSK = Lineage$^-$Sca1$^+$cKit$^+$, LK = Lineage$^-$ Sca1$^-$cKit$^+$, HSC = Haematopoietic stem cells, MPP = Multipotent progenitors, CMP = Common myeloid progenitor, GMP = Granulocyte-monocyte progenitor, MEP = Megakaryocyte-Erythrocyte progenitor, n = Number of replicates. Parametric data are reported as mean $\pm$ standard deviation, and non-parametric data are reported as median and interquartile ranges. A Shapiro-Wilk test was used to determine data normality (α = 0.05, p<0.05), and a Grubbs test was used to identify outliers (α = 0.05). Data was parametric for graphs (**A**) & (**D**) and a one-way ANOVA with Bonferroni post-hoc correction was used to determine statistical significance of differences between the groups. Data was non-parametric for graphs (**B**) and (**E**) and a Kruskal-Wallis test with Dunn's post-hoc correction analysis was used to assess statistical significance. Significance is represented on the graph by *p<0.05, **p<0.01, or ***p<0.001*.

3.5 TNF-α-Stimulated Endothelial Cell-Extracellular Vesicles Increase Circulating Monocytes, Neutrophils, & Erythrocytes

Innate immune cells such as monocytes and neutrophils are mobilised from the bone marrow and spleen into the blood as part of the MI response (28, 57, 166). In this

study, TNF-α EC-EV are shown to modulate HSPC populations in the bone marrow with a skew towards increased GMP, which I hypothesise contributes to increased neutrophils and monocytes in circulation. Blood, spleen and bone marrow were collected from mice following injections with either vehicle-control, LPS, control EC-EV or TNF-α EC-EV as described above (**Section 3.4**), in order to assess changes in monocytes and neutrophils. The overall blood cell counts indicated a significant increase in the total number of cells in response to LPS and to TNF-α EC-EV (both $p<0.05$, **Figure 15A**).

Cells from bone marrow, spleen & blood were isolated and stained with CD45, CD11b, Ly6C and Ly6G (**Method 2.7**) for flow cytometry analysis (**Figure 15B**). Quantitative analysis shows in the bone marrow (**Figure 15C**, $p<0.05$), spleen (**Figure 15D**, $p<0.05$) and blood (**Figure 15E**, $p<0.01$), that monocytes increase in response to TNF-α EC-EV compared to control EC-EV. Similarly, neutrophil levels are elevated in the bone marrow ($p<0.01$), spleen ($p<0.01$) and blood ($p<0.05$) after treatment with TNF-α EC-EV relative to control EC-EV. These data offer an explanation for the increase in spleen weight (**Figure 12C**) and spleen count (**Figure 14A**) that was observed and is consistent with the broader literature that the spleen acts as a reserve for innate immune cells (30, 184) .

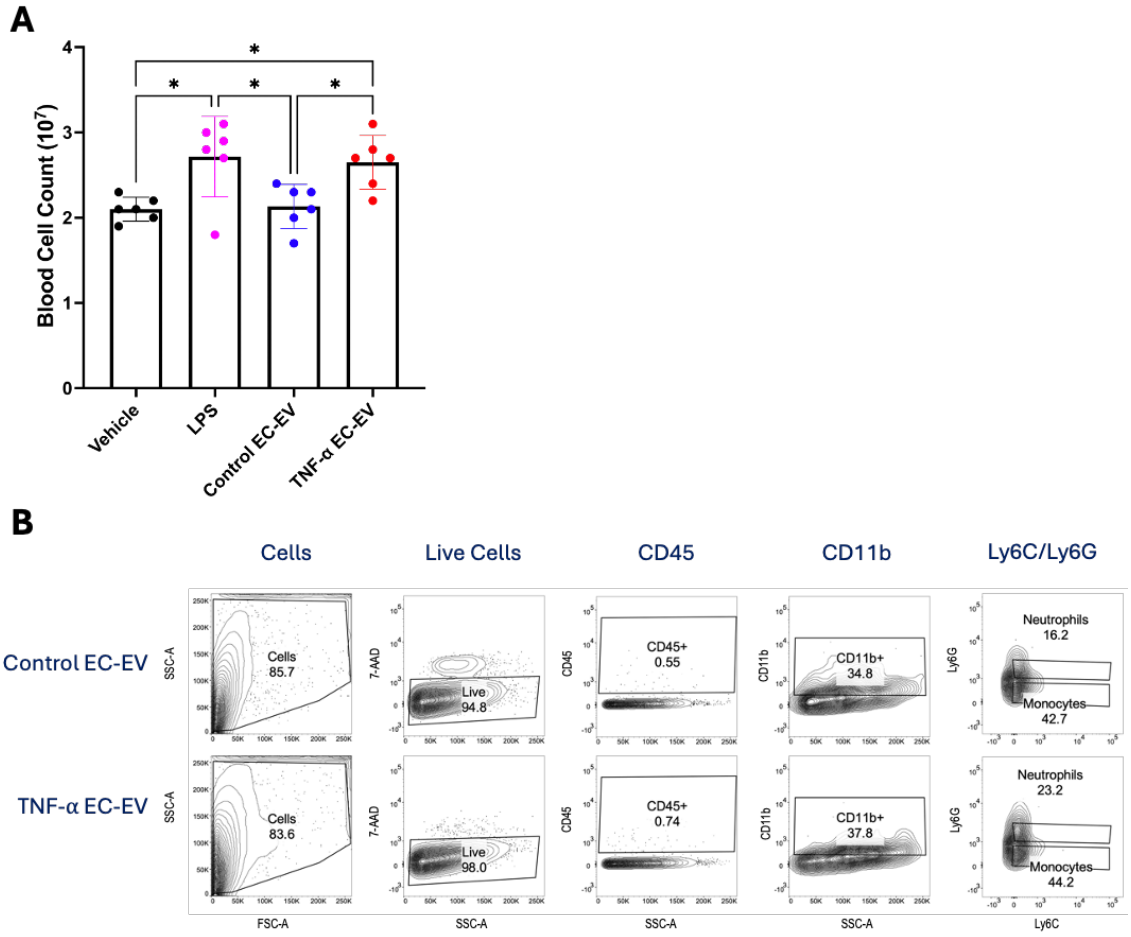
A
Blood Cell Count (10^7)
Vehicle
LPS
Control EC-EV
TNF-α EC-EV
B
Cells
Live Cells
CD45
CD11b
Ly6C/Ly6G
Control EC-EV
TNF-α EC-EV
Cells 85.7
Live 94.8
CD45+ 0.55
CD11b+ 34.8
Neutrophils 16.2
Monocytes 42.7
Cells 83.6
Live 98.0
CD45+ 0.74
CD11b+ 37.8
Neutrophils 23.2
Monocytes 44.2
FSC-A
SSC-A
7-AAD
CD45
CD11b
Ly6G
Ly6C
C
Vehicle
LPS
Control EC-EV
TNF-α EC-EV
Cells / Femur
Monocytes
Neutrophils
D
Cells / Spleen
Monocytes
Neutrophils
E
Cells / 100 µL Blood
Monocytes
Neutrophils

Figure 15. TNF-α-Stimulated Endothelial Cell-Extracellular Vesicles Increase Production of Innate Immune Cells. *(**A**) Blood cell counts from mice 72 hours post-injection with either vehicle-control (sterile PBS), LPS (1 mg / kg body weight), control EC-EV (1 x 10^9 particles) or TNF-α EC-EV (1 x 10^9 particles) (n = 6 per group). (**B**) Flow cytometry gating strategy for analysis of isolated cells from blood samples to calculate changes in circulating innate immune cell populations. Changes in bone marrow (**C**), splenic (**D**), and blood (**E**) monocytes and neutrophils following treatment with LPS or EC-EV (n = 6 per group). n = Number of replicates. Data are reported as mean ± standard deviation. A Shapiro-Wilk test was used to determine data normality (α = 0.05, p<0.05), and a Grubbs test was used to identify outliers (α = 0.05). Data was parametric and one-way ANOVA with Bonferroni post-hoc correction was used to determine the statistical significance of differences between the groups. Significance is represented on the graph by *p<0.05, **p<0.01, ***p<0.001, or ****p<0.0001*.

In order to fully elucidate the *in vivo* changes that occur in response to TNF-α EC-EV, the blood was collected, and erythrocytes, platelets, and inflammatory cytokines were assessed (**Figure 16**). The total blood erythrocyte counts (**Figure 16A**) and platelet counts (**Figure 16B**) from each mouse was analysed and showed TNF-α EC-EV increase erythrocytes ($p<0.05$) and decrease platelets ($p<0.01$) 72 hours-post injection. This aligns with findings in the literature, which found MI lowers platelet counts (185). Furthermore, hypoxia in the liver induces erythropoiesis as part of the stress response mediated by HIF1-α (186), which could play a role post-MI. Whether these responses are mediated by TNF-α EC-EV, however, is unknown.

The inflammatory cytokine response to TNF-α EC-EV injection was also measured by assessing TNF-α (**Figure 16C**), IL-6 (**Figure 16D**) & IL-1β (**Figure 16E**) changes in plasma. There were no significant differences in inflammatory cytokine levels across all conditions and the cytokine levels were below the detection threshold, which may be due to the 72-hour timepoint that was used for this experiment. The inflammatory cytokine response to acute stimuli such as MI has been well characterised and typically peaks several hours after injury and then recedes (187, 188) meaning 72 hours may not be the optimal timepoint to measure changes in inflammatory cytokine levels.

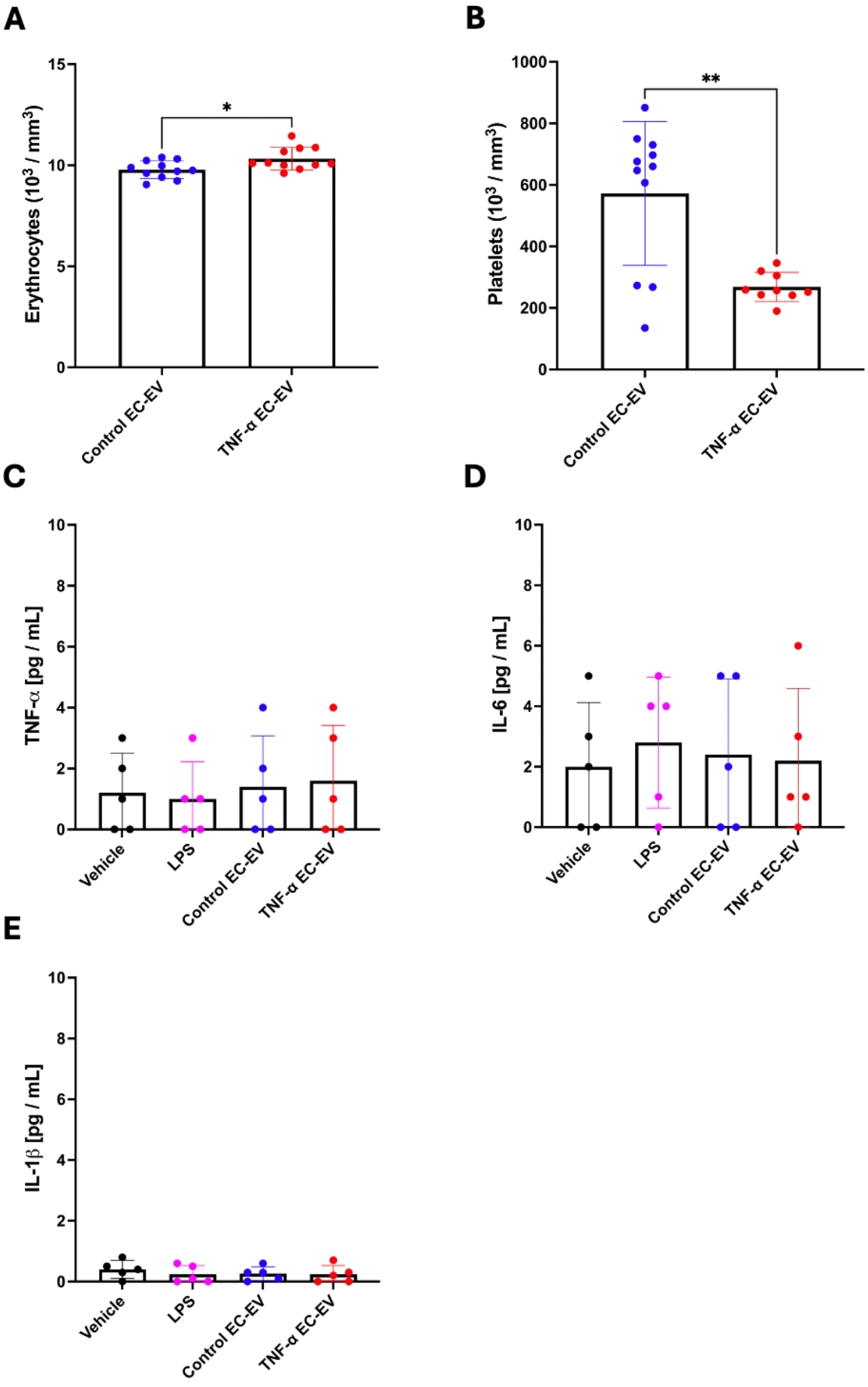
A
Erythrocytes (10³ / mm³)
15
10
5
0
*
Control EC-EV
TNF-α EC-EV
B
Platelets (10³ / mm³)
1000
800
600
400
200
0
**
Control EC-EV
TNF-α EC-EV
C
TNF-α [pg / mL]
10
8
6
4
2
0
Vehicle
LPS
Control EC-EV
TNF-α EC-EV
D
IL-6 [pg / mL]
10
8
6
4
2
0
Vehicle
LPS
Control EC-EV
TNF-α EC-EV
E
IL-1β [pg / mL]
10
8
6
4
2
0
Vehicle
LPS
Control EC-EV
TNF-α EC-EV

Figure 16. TNF-α-Stimulated Endothelial Cell-Extracellular Vesicles Increase Erythrocytes and Lower Platelet Counts in Mice. *(**A**) Erythrocyte, and (**B**) platelet counts from mice 72 hours post-injection with control EC-EV (1 x 10^9 particles) or TNF-α EC-EV (1 x 10^9 particles) (n = 11 per group). Plasma cytokine analysis of (**C**) TNF-α, (**D**) IL-6, and (**E**) IL-1β from mice 72 hours post-injection with vehicle-control (sterile PBS), LPS (1 mg / kg body weight), control EC-EV (1 x 10^9 particles) or TNF-α EC-EV (1 x 10^9 particles) (n = 5 per group). n = Number of replicates. Data are reported as mean ± standard deviation. A Shapiro-Wilk test was used to determine data normality (α = 0.05, p<0.05), and a Grubbs test was used to identify outliers (α = 0.05). Data was parametric and an unpaired two-way t-test (Graphs **A** & **B**) or a one-way ANOVA with Bonferroni post-hoc correction (Graphs **C**, **D** & **E**) was used to determine the statistical significance of differences between the groups. Significance is represented on the graph by *p<0.05*.

3.6 TNF-α-Stimulated Endothelial Cell-Extracellular Vesicles Skew Bone Marrow Haematopoiesis Towards Granulocytes & Monocytes In Vitro

The data described so far suggests that TNF-α EC-EV can modulate the bone marrow to induce haematopoiesis, leading to increased numbers of HSC and GMP populations. However, which cell type(s) within the bone marrow directly interact with TNF-α EC-EV is not clear. Studies elsewhere provide evidence for EV-mediated reprogramming of the bone marrow indicate multiple avenues for reprogramming (189-193). Direct reprogramming of HSPC through the uptake of EV has been shown (189, 190), whilst alternate routes of indirect HSPC reprogramming include EV uptake by

mast cells (192) or stromal cells (194). These cells can then induce secondary effects on bone marrow HSPC leading to modified haematopoiesis (195).

To better understand how TNF-α EC-EV affects haematopoiesis in the bone marrow, a CFU assay was used on isolated HSC (**Figure 17A**). This would determine whether TNF-α EC-EV directly interact with HSC and provide evidence of lineage-bias haematopoiesis in response to TNF-α EC-EV. Bone marrow HSC were isolated from untreated mice and sorted using FACS (**Figure 17B**). Isolated bone marrow HSC were then stimulated *in vitro* with either vehicle-control, LPS, control EC-EV or TNF-α EC-EV.

After 10 days, representative brightfield images were taken (**Figure 17C**) and the number of erythroid colonies, granulocyte-monocyte colonies, and mixed colonies (containing granulocyte, erythroid, megakaryocyte and monocyte colonies) were counted (**Figure 17D**). Since exposure to TNF-α EC-EV increased HSC populations *in vivo* (**Figure 13C**), the data are presented as a proportion of the total colonies for each condition. TNF-α EC-EV increased ($p<0.001$) the percentage of granulocyte-monocyte colonies compared to control EC-EV and decreased the percentage of erythroid colonies. This aligns with the findings *in vivo* that TNF-α EC-EV increase GMP populations and lower MEP in the bone marrow and therefore suggests that the model of studying TNF-α EC-EV and bone marrow haematopoiesis *in vivo* and *in vitro* is consistent.

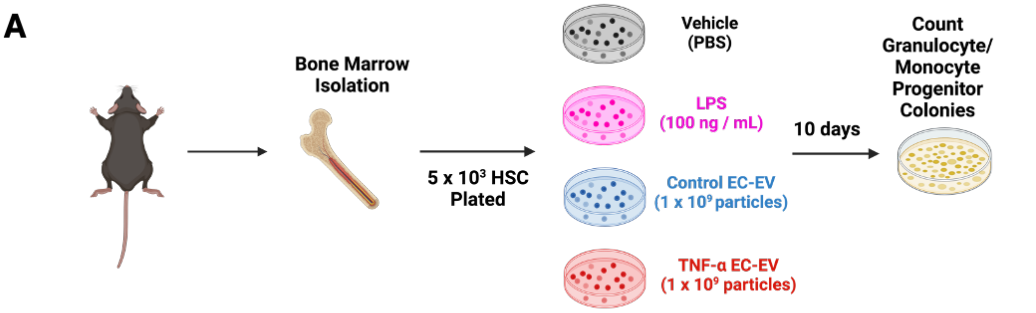
A
Bone Marrow Isolation
5 x 10³ HSC Plated
Vehicle (PBS)
LPS (100 ng / mL)
Control EC-EV (1 x 10⁹ particles)
TNF-α EC-EV (1 x 10⁹ particles)
10 days
Count Granulocyte/ Monocyte Progenitor Colonies

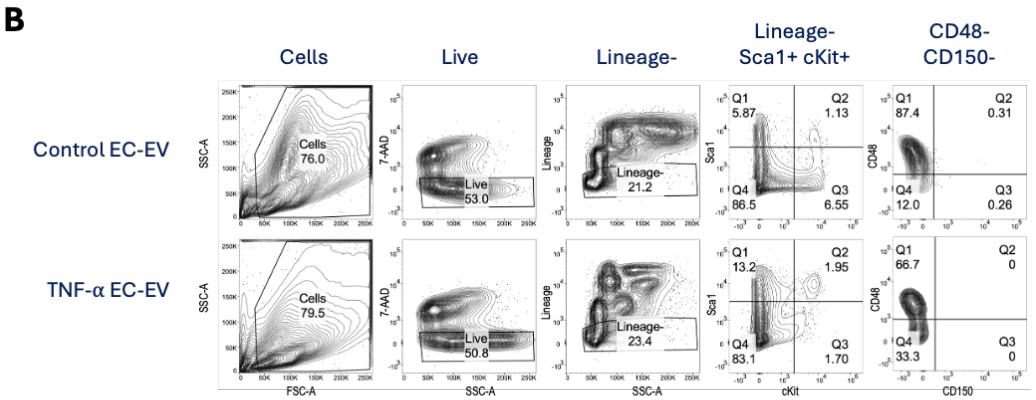
B
Cells
Live
Lineage-
Lineage- Sca1+ cKit+
CD48- CD150-
Control EC-EV
TNF-α EC-EV
Cells 76.0
Live 53.0
Lineage- 21.2
Q1 5.87
Q2 1.13
Q4 86.5
Q3 6.55
Q1 87.4
Q2 0.31
Q4 12.0
Q3 0.26
Cells 79.5
Live 50.8
Lineage- 23.4
Q1 13.2
Q2 1.95
Q4 83.1
Q3 1.70
Q1 66.7
Q2 0
Q4 33.3
Q3 0
SSC-A
FSC-A
7-AAD
Lineage
Sca1
cKit
CD48
CD150

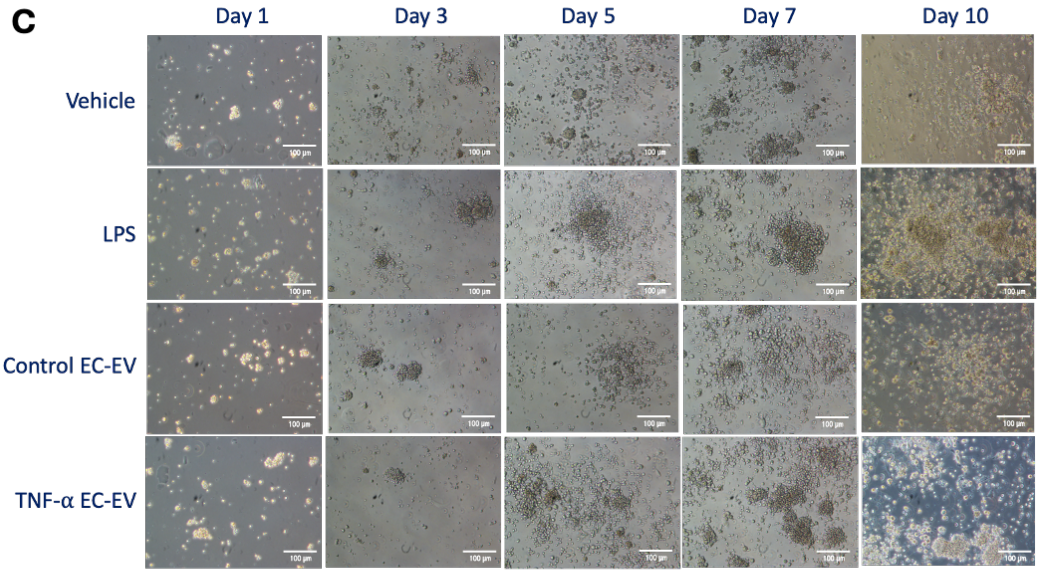
C
Day 1
Day 3
Day 5
Day 7
Day 10
Vehicle
LPS
Control EC-EV
TNF-α EC-EV

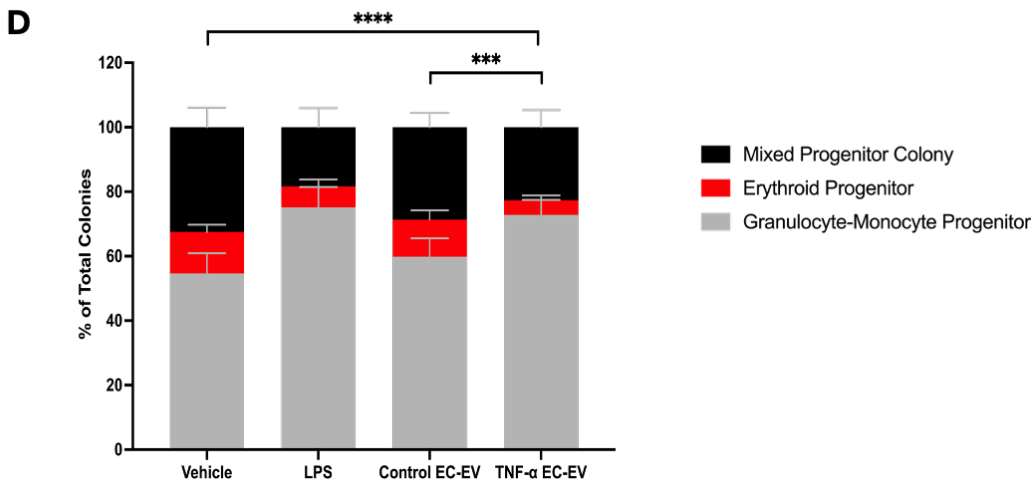
D
****
***
% of Total Colonies
120
100
80
60
40
20
0
Vehicle
LPS
Control EC-EV
TNF-α EC-EV
Mixed Progenitor Colony
Erythroid Progenitor
Granulocyte-Monocyte Progenitor

Figure 17. TNF-α-Stimulated Endothelial Cell-Extracellular Vesicles Skew Haematopoiesis Towards Granulocyte-Monocyte Progenitors. *(**A**) Experimental schematic. (**B**) FACS gating strategy and analysis to isolate HSC from bone marrow samples. (**C**) Representative brightfield images of plated bone marrow HSC following exposure to vehicle-control (sterile PBS), LPS (100 ng / mL), control EC-EV (1 x 10^9 particles) or TNF-α EC-EV (1 x 10^9 particles) (n = 6 per group) at timepoints Day 1, Day 3, Day 5, Day 7 and Day 10. (**D**) Quantification of the number of colonies formed from bone marrow HSC exposed to LPS or EC-EV. n = Number of replicates. Data are reported as mean % of total colonies ± standard deviation. A Shapiro-Wilk test was used to determine data normality (α = 0.05, p<0.05), and a Grubbs test was used to identify outliers (α = 0.05). Data was parametric and a one-way ANOVA with Bonferroni post-hoc correction was used to determine the statistical significance of differences between the groups. Significance is represented on the graph by ***p<0.05 and ****p<0.0001*.

3.7 Priming Mice With TNF-α-Stimulated Endothelial Cell-Extracellular Vesicles Lowers Innate Immune Cells & Bone Marrow Progenitor Cells in Response to LPS

The *in vivo* investigations described so far in this chapter have focused on understanding the immediate impact of TNF-α EC-EV on the bone marrow, and how this might contribute to the reprogramming effects of an MI on the bone marrow that have been described (57, 82, 196). In order to understand the longer-term impact on the bone marrow of patients who survive an initial MI, several studies have investigated the effects of multiple stimuli to the bone marrow (81, 82). This includes

giving mice recurrent MI and determining the effects on haematopoiesis at different timepoints (82, 86), and also combining MI with different pro-inflammatory stimuli such as acute infection.

To understand the longer-term impact of TNF-α EC-EV on haematopoiesis in the bone marrow, mice received an injection of one of vehicle-control, LPS, control EC-EV or TNF-α EC-EV and after a rest period of 24 hours, received a second injection with LPS (**Figure 18A**). In order to determine if the effects of TNF-α EC-EV were mediated by VCAM-1, which is enriched in TNF-α EC-EV compared to control EC-EV (**Figure 11E**), EV from the CRISPR-Cas9-edited sEND.1 VCAM-1 knockout cell line were also used in this study. There was no significant change in body weight between Day 0 (first injection) and Day 4 (tissue harvest) across all experimental conditions (**Figure 18B**) and there was no significant change in the spleen weight across all conditions (**Figure 18C)**, including when the spleen weight was normalised to the mouse body weight 72-hours post-LPS injection (Day 4) (**Figure 18D**).

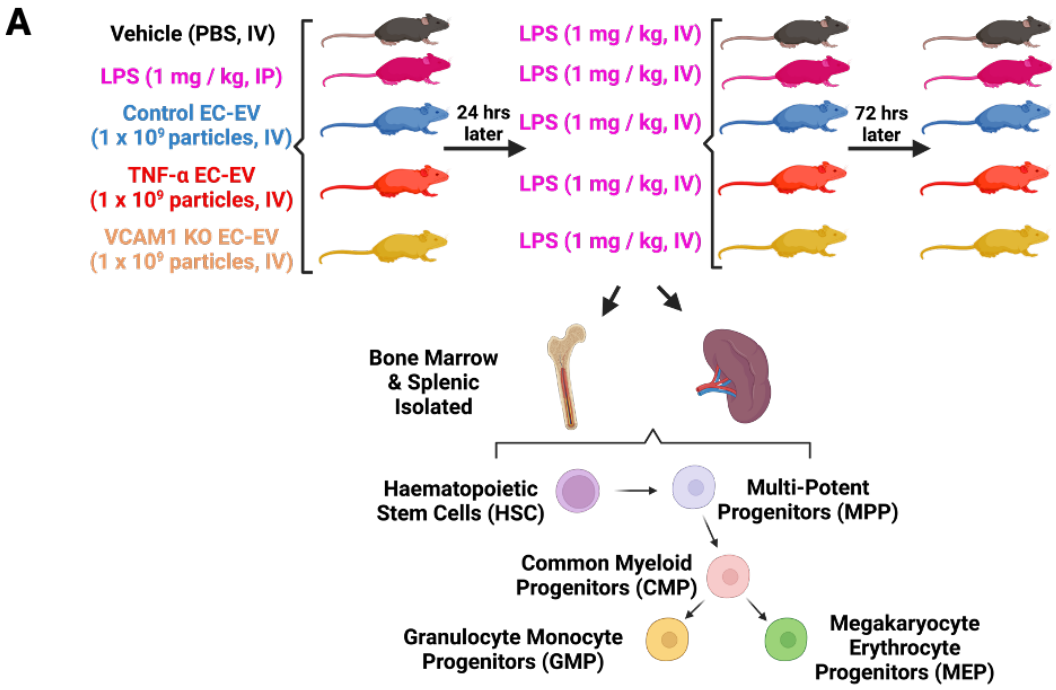
A
Vehicle (PBS, IV)
LPS (1 mg / kg, IP)
Control EC-EV
(1 x 10⁹ particles, IV)
TNF-α EC-EV
(1 x 10⁹ particles, IV)
VCAM1 KO EC-EV
(1 x 10⁹ particles, IV)
24 hrs later
LPS (1 mg / kg, IV)
LPS (1 mg / kg, IV)
LPS (1 mg / kg, IV)
LPS (1 mg / kg, IV)
LPS (1 mg / kg, IV)
72 hrs later
Bone Marrow & Splenic Isolated
Haematopoietic Stem Cells (HSC)
Multi-Potent Progenitors (MPP)
Common Myeloid Progenitors (CMP)
Granulocyte Monocyte Progenitors (GMP)
Megakaryocyte Erythrocyte Progenitors (MEP)

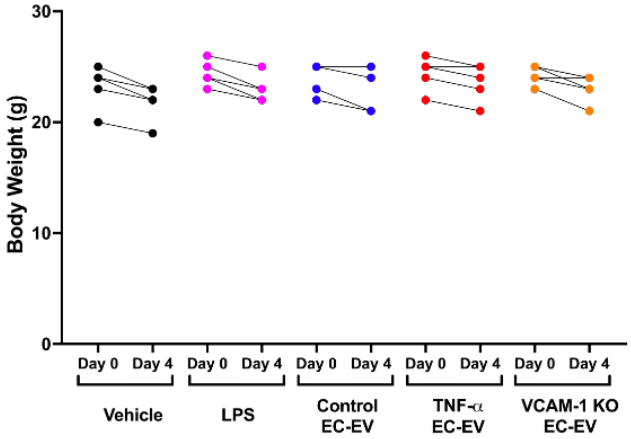
B
Body Weight (g)
30
20
10
0
Day 0
Day 4
Vehicle
LPS
Control EC-EV
TNF-α EC-EV
VCAM-1 KO EC-EV

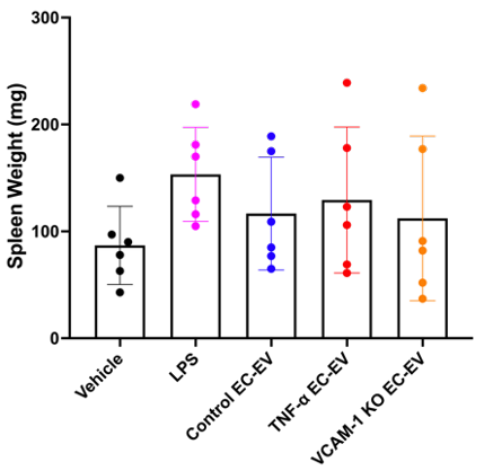
C
Spleen Weight (mg)
300
200
100
0
Vehicle
LPS
Control EC-EV
TNF-α EC-EV
VCAM-1 KO EC-EV

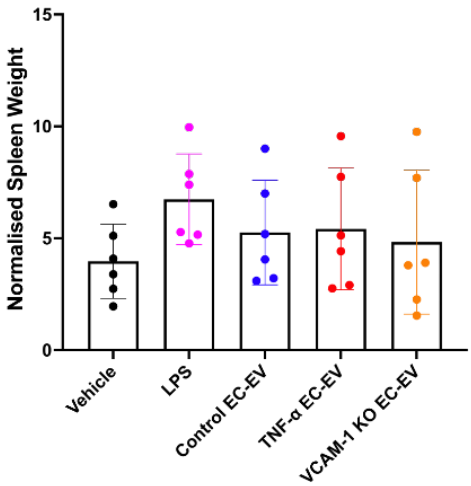
D
Normalised Spleen Weight
15
10
5
0
Vehicle
LPS
Control EC-EV
TNF-α EC-EV
VCAM-1 KO EC-EV

Figure 18. Treating Mice with Control or TNF-α-Stimulated Endothelial Cell-Extracellular Vesicles Followed by LPS to Investigate the Effects of Extracellular Vesicle Priming on Bone Marrow Haematopoietic Stem and Progenitor Cells. *(**A**) Overview experimental schematic. (**B**) Body weight changes in mice measured at the time of the first injection (Day 0) with vehicle-control (sterile PBS), LPS (1 mg / kg body weight), control EC-EV (1 x 10^9 particles), TNF-α EC-EV (1 x 10^9 particles) or VCAM-1 knockout EC-EV (1 x 10^9 particles), and the time of tissue harvest (Day 4) (n = 6 per group). (**C**) Spleen weight at the time of tissue harvest (Day 4). (**D**) Normalised spleen weight against body weight for each individual. n = Number of replicates. Data are reported as mean ± standard deviation. A Shapiro-Wilk test was used to determine data normality (α = 0.05, p<0.05), and a Grubbs test was used to identify outliers (α = 0.05). Data was parametric and a one-way ANOVA with Bonferroni post-hoc correction was used to determine the statistical significance of differences between the groups.*

Upon tissue harvest on Day 4, the bone marrow was isolated, and the total bone marrow cell counts showed no significant differences across all experimental conditions (**Figure 19A**). Bone marrow cells were stained for flow cytometry analysis (**Figure 19B**) to characterise changes in the five HSPC populations assessed in **Figure 13**. By contrast to the changes observed in response to a single injection of TNF-α EC-EV in **Figure 13C**, there were no significant differences in the number of HSC or MPP across all groups (**Figure 19C**). There were also no significant differences in the number of CMP (**Figure 19D**), but GMP populations were significantly lower in TNF-α EC-EV ($p<0.05$), and MEP populations were significantly elevated ($p<0.0001$), relative to the control EC-EV group. Combined, this data

suggests that priming the bone marrow with TNF-α EC-EV followed by LPS treatment impacts haematopoiesis in the bone marrow, but the direction of change for GMP and MEP are reversed compared to a single dose of TNF-α EC-EV (**Figure 13**). These results suggest a depleted capacity for myeloid-bias haematopoiesis in the bone marrow.

Furthermore, the injection of VCAM-1 knockout EC-EV followed by LPS produced significantly more GMP cells in the bone marrow ($p<0.05$) than TNF-α EC-EV but was not significantly different compared to control EC-EV. The number of MEP cells was significantly elevated in the TNF-α EC-EV group compared to the VCAM-1 knockout EC-EV group ($p<0.0001$), which is also the reverse of the single injection TNF-α EC-EV effect. **Figure 19E** represents the changes in bone marrow HSPC as a fold-change relative to the vehicle-control to show matched HSPC populations from the same mouse.

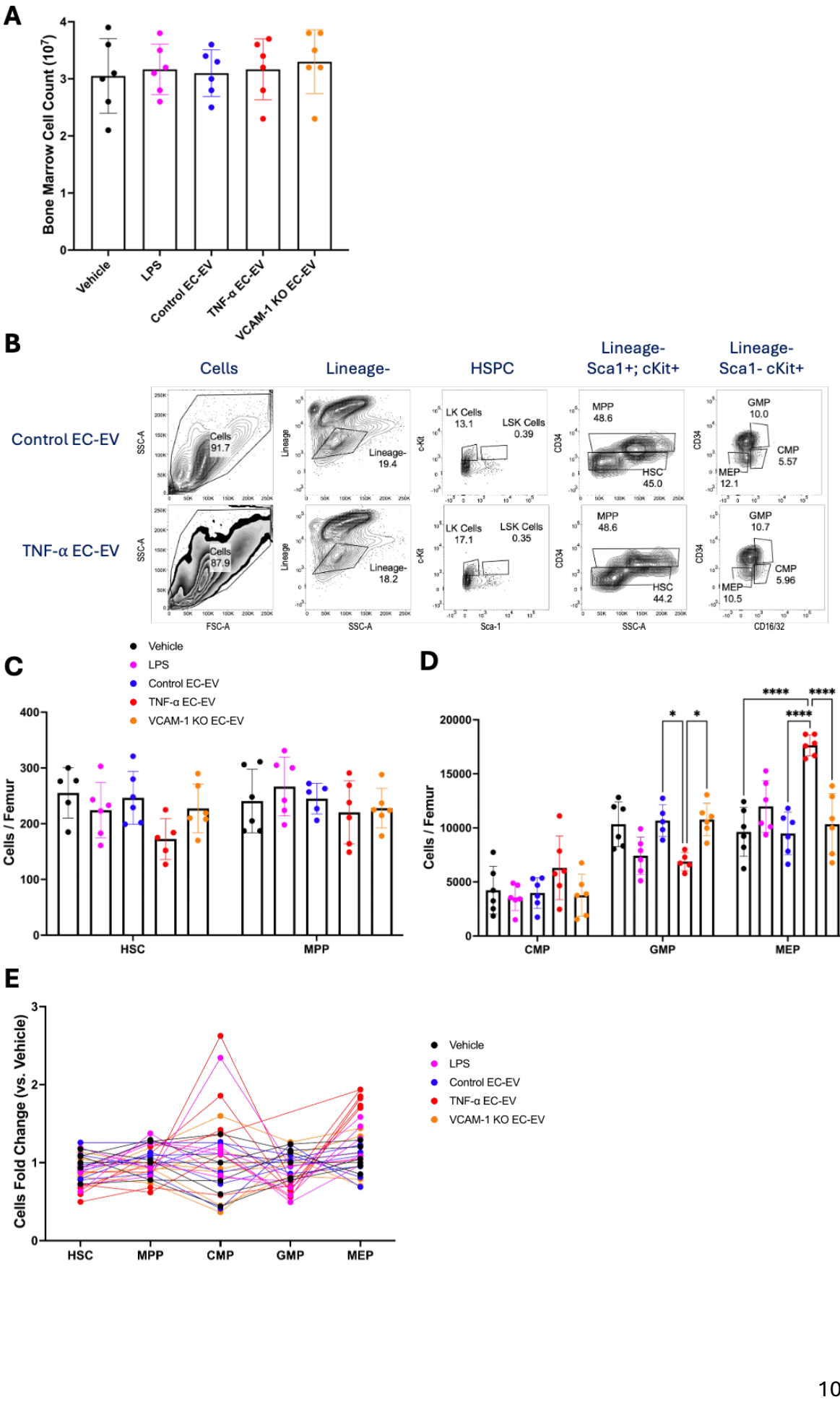
A
Bone Marrow Cell Count (10^7)
Vehicle
LPS
Control EC-EV
TNF-α EC-EV
VCAM-1 KO EC-EV
B
Cells
Lineage-
HSPC
Lineage- Sca1+; cKit+
Lineage- Sca1- cKit+
Control EC-EV
TNF-α EC-EV
Cells 91.7
Lineage- 19.4
LK Cells 13.1
LSK Cells 0.39
MPP 48.6
HSC 45.0
GMP 10.0
CMP 5.57
MEP 12.1
Cells 87.9
Lineage- 18.2
LK Cells 17.1
LSK Cells 0.35
MPP 48.6
HSC 44.2
GMP 10.7
CMP 5.96
MEP 10.5
FSC-A
SSC-A
Lineage
c-Kit
Sca-1
CD34
CD16/32
C
Vehicle
LPS
Control EC-EV
TNF-α EC-EV
VCAM-1 KO EC-EV
Cells / Femur
HSC
MPP
D
Cells / Femur
CMP
GMP
MEP
E
Cells Fold Change (vs. Vehicle)
HSC
MPP
CMP
GMP
MEP
Vehicle
LPS
Control EC-EV
TNF-α EC-EV
VCAM-1 KO EC-EV

Figure 19. Priming Mouse Bone Marrow with TNF-α-Stimulated Endothelial Cell-Extracellular Vesicles Followed by LPS Stimulation Lowers Granulocyte-Monocyte Progenitors. *(**A**) Bone marrow cell counts from mice 72 hours post-LPS injection (1 mg / kg body weight) following priming with either vehicle-control (sterile PBS), LPS (1 mg / kg body weight), control EC-EV (1 x 10^9 particles), TNF-α EC-EV (1 x 10^9 particles) or VCAM-1 knockout EC-EV (1 x 10^9 particles) (n = 6 per group). (**B**) Flow cytometry gating strategy for the analysis of isolated bone marrow cells to calculate changes in bone marrow HSPC populations. (**C**) Changes in mouse bone marrow HSC and MPP populations following priming with EC-EV or control groups, followed by LPS. (**D**) Changes in mouse bone marrow CMP, GMP and MEP populations following priming with EC-EV or control groups, followed by LPS. (**E**) Fold-change of each HSPC population relative to the vehicle-control. HSPC = Haematopoietic stem and progenitor cells, LSK = Lineage$^-$Sca1$^+$cKit$^+$, LK = Lineage$^-$Sca1$^-$cKit$^+$, HSC = Haematopoietic stem cells, MPP = Multipotent progenitors, CMP = Common myeloid progenitor, GMP = Granulocyte-monocyte progenitor, MEP = Megakaryocyte-Erythrocyte progenitor, n = Number of replicates. Data are reported as mean ± standard deviation. A Shapiro-Wilk test was used to determine data normality (α = 0.05, p<0.05), and a Grubbs test was used to identify outliers (α = 0.05). Data was parametric and a one-way ANOVA with Bonferroni post-hoc correction was used to determine the statistical significance of differences between the groups. Significance is represented on the graph by *p<0.05 or ****p<0.0001*.

The effects of TNF-α EC-EV priming followed by LPS treatment on haematopoiesis were also assessed in the spleen. There was no significant change in total spleen cell

counts across all experimental conditions (**Figure 20A**), although the cell counts were slightly elevated compared to the single dose response (**Figure 14A**). The normalised spleen cell counts / per mg of spleen weight was also unchanged across each condition (**Figure 20B**). Flow cytometry analysis of the five subpopulations of HSPC showed no significant differences across all experimental conditions (**Figure 20D-E**) and these results corroborate with earlier findings in this chapter that TNF-α EC-EV does not appear to impact haematopoiesis in the spleen.

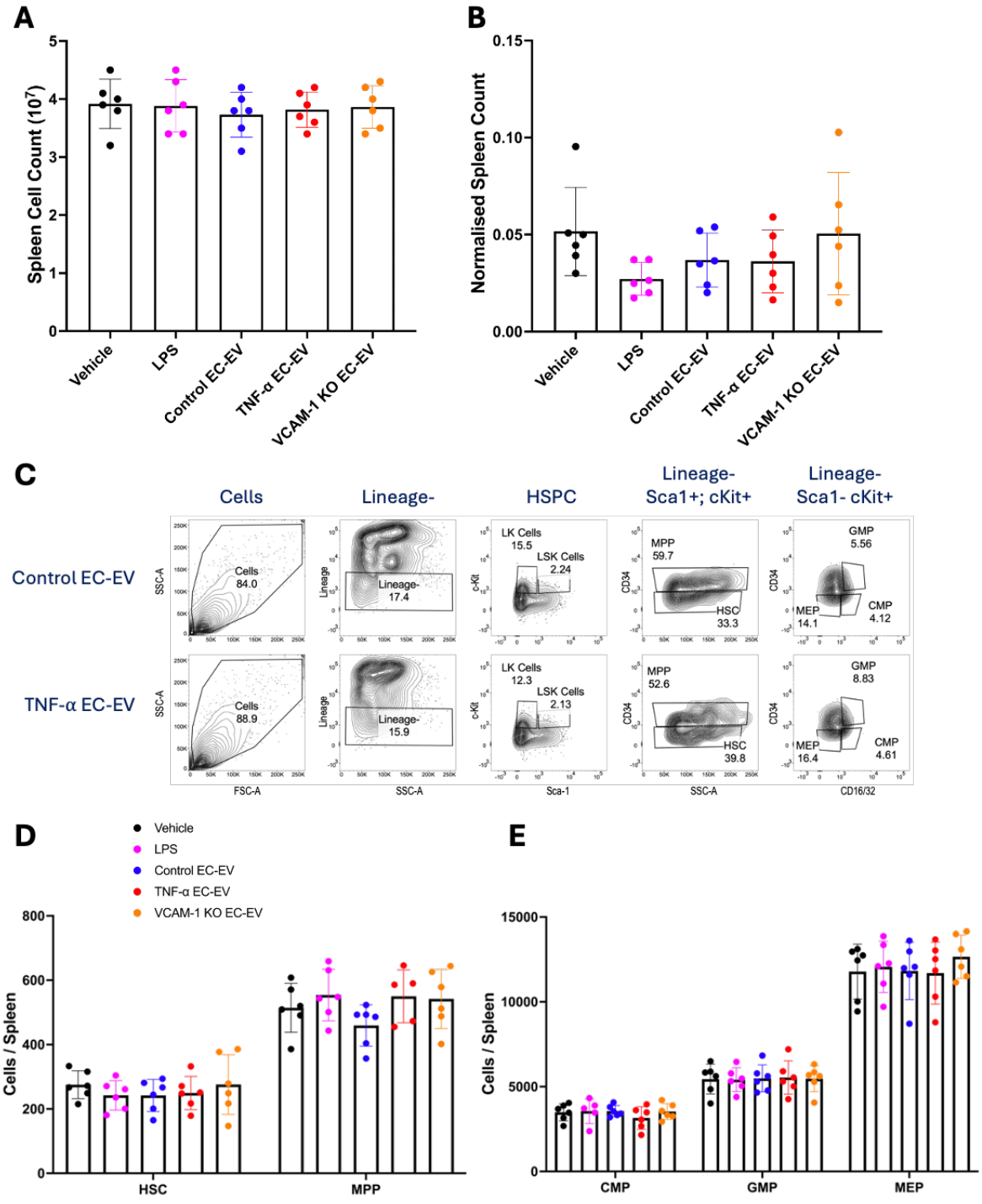

Figure 20. Priming Mice with TNF-α-Stimulated Endothelial Cell-Extracellular Vesicles Followed by LPS Does Not Impact Splenic Haematopoiesis*. (**A**) Spleen cell counts from mice 72 hours post-LPS injection (1 mg / kg body weight) following*

*priming with either vehicle-control (sterile PBS), LPS (1 mg / kg body weight), control EC-EV (1 x 10^9 particles), TNF-α EC-EV (1 x 10^9 particles) or VCAM-1 knockout EC-EV (1 x 10^9 particles) (n = 6 per group). (**B**) Spleen cell counts normalised to spleen weight 72 hours post-LPS injection. (**C**) Flow cytometry gating strategy for analysis of isolated splenic cells to calculate changes in splenic HSPC populations. (**D**) Changes in mouse splenic HSC and MPP populations following priming with EC-EV or control groups, and LPS treatment. (**E**) Changes in mouse splenic CMP, GMP and MEP populations following priming with EC-EV or control groups, and LPS treatment. HSPC = Haematopoietic stem and progenitor cells, LSK = Lineage$^-$Sca1$^+$cKit$^+$, LK = Lineage$^-$ Sca1$^-$cKit$^+$, HSC = Haematopoietic stem cells, MPP = Multipotent progenitors, CMP = Common myeloid progenitor, GMP = Granulocyte-monocyte progenitor, MEP = Megakaryocyte-Erythrocyte progenitor, n = Number of replicates. Data are reported as mean $\pm$ standard deviation. A Shapiro-Wilk test was used to determine data normality (α = 0.05, p<0.05), and a Grubbs test was used to identify outliers (α = 0.05). Data was parametric and a one-way ANOVA with Bonferroni post-hoc correction was used to determine the statistical significance of differences between the groups*.

To investigate the effects of TNF-α EC-EV priming followed by LPS on innate immune cells, mice were injected with TNF-α EC-EV or control groups, followed by LPS 24-hours later. The total blood cell counts were determined 72 hours post-LPS injection (**Figure 21A**). Isolated cells from the blood, the bone marrow and the spleen were stained with antibodies to assess changes in monocyte and neutrophil populations using flow cytometry analysis (**Figure 21B**). Monocytes in the bone marrow (**Figure 21C**) and spleen (**Figure 21D**) were unchanged across all conditions, however,

neutrophil populations were significantly lower in the bone marrow ($p<0.01$) and spleen (0.0001) after priming with TNF-α EC-EV compared to the control EC-EV group. The repeated dose of LPS also yielded fewer neutrophils in the bone marrow compared to vehicle-control ($p<0.01$), but not in the spleen. Furthermore, the VCAM-1 knockout EC-EV group had significantly higher levels of neutrophils in the spleen ($p<0.0001$) compared to TNF-α EC-EV and was similar to the control EC-EV group. This indicates a potential role for VCAM-1 in mediating this response, although there were no differences in neutrophil populations between TNF-α EC-EV and VCAM-1 knockout EC-EV in the bone marrow. In the blood, there were no significant changes in monocytes and neutrophils across all conditions (**Figure 21E**).

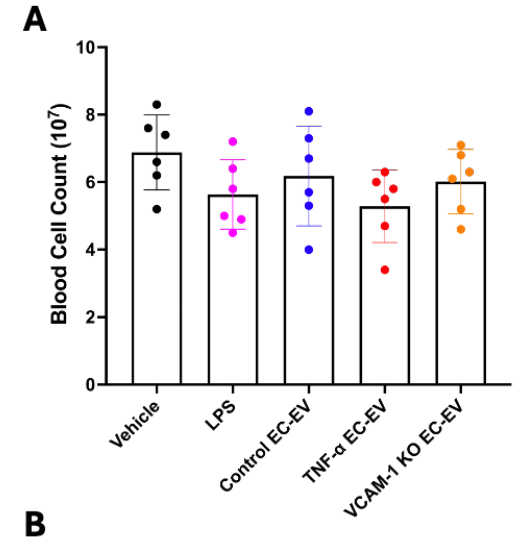
A
Blood Cell Count (10^7)
10
8
6
4
2
0
Vehicle
LPS
Control EC-EV
TNF-α EC-EV
VCAM-1 KO EC-EV

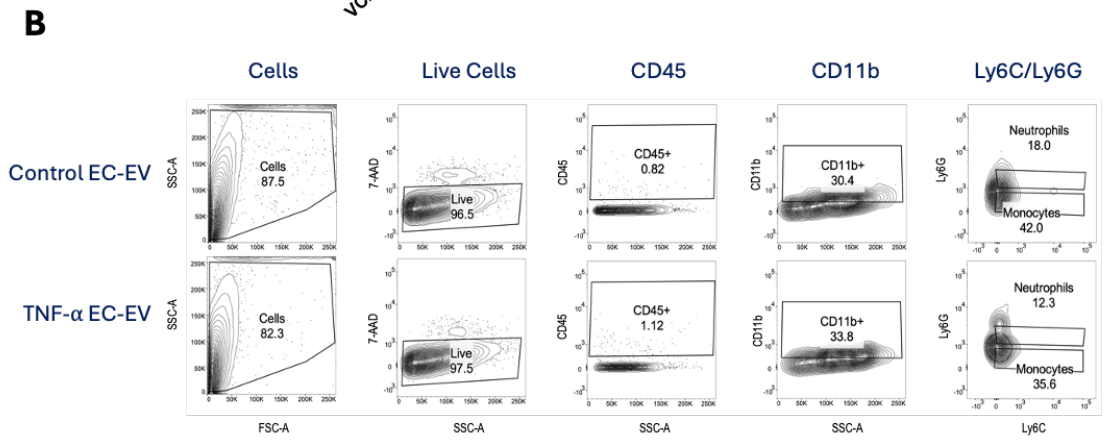
B
Cells
Live Cells
CD45
CD11b
Ly6C/Ly6G
Control EC-EV
TNF-α EC-EV
SSC-A
Cells
87.5
Cells
82.3
7-AAD
Live
96.5
Live
97.5
CD45
CD45+
0.82
CD45+
1.12
CD11b
CD11b+
30.4
CD11b+
33.8
Ly6G
Neutrophils
18.0
Monocytes
42.0
Neutrophils
12.3
Monocytes
35.6
FSC-A
SSC-A
SSC-A
SSC-A
Ly6C

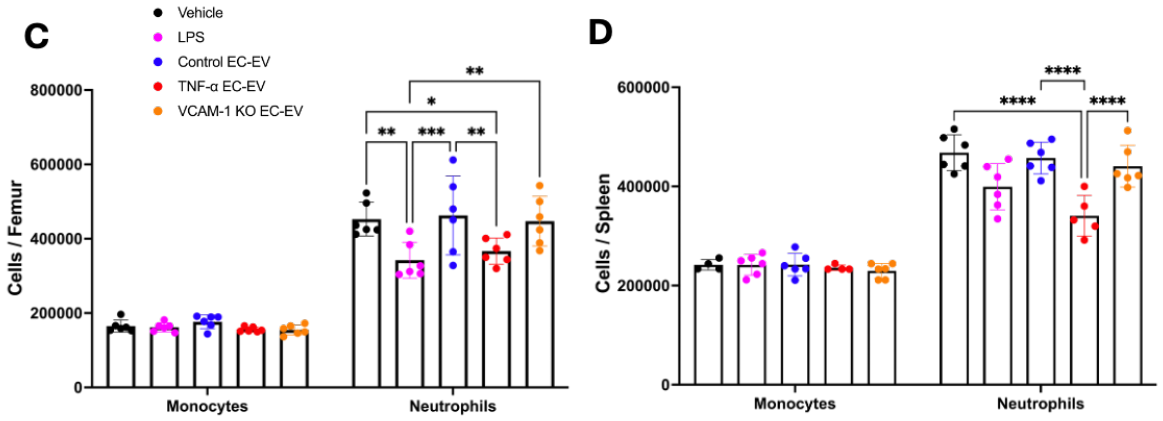
C
Vehicle
LPS
Control EC-EV
TNF-α EC-EV
VCAM-1 KO EC-EV
Cells / Femur
800000
600000
400000
200000
0
**
*
**
***
**
Monocytes
Neutrophils
D
Cells / Spleen
600000
400000
200000
0
****
****
****
Monocytes
Neutrophils

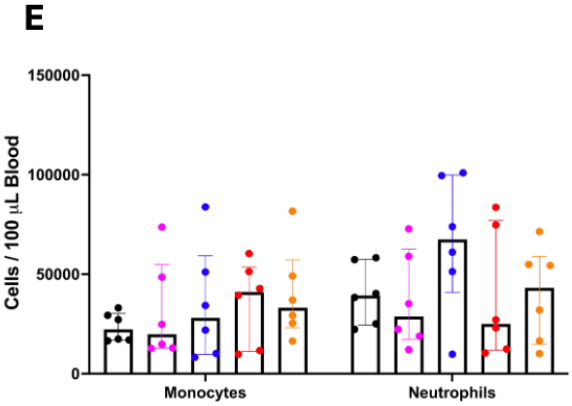
E
Cells / 100 µL Blood
150000
100000
50000
0
Monocytes
Neutrophils

Figure 21. Priming Mice with TNF-α-Stimulated Endothelial Cell-Extracellular Vesicles Followed by LPS Treatment Lowers Bone Marrow & Splenic Neutrophils. *(**A**) Blood cell counts from mice 72 hours post-LPS injection (1 mg / kg body weight) following priming with either vehicle-control (sterile PBS), LPS (1 mg / kg body weight), control EC-EV (1 x 10^9 particles), TNF-α EC-EV (1 x 10^9 particles) or VCAM-1 knockout EC-EV (1 x 10^9 particles) (n = 6 per group). (**B**) Flow cytometry gating strategy for analysis of isolated cells from blood samples to calculate changes in circulating innate immune cell populations. Changes in mouse (**C**) bone marrow, (**D**) splenic, and (**E**) blood monocytes and neutrophils following priming with EC-EV or control groups, followed by LPS treatment (n = 6 per group). n = Number of replicates. Parametric data are reported as mean $\pm$ standard deviation, and non-parametric data are reported as median and interquartile ranges. A Shapiro-Wilk test was used to determine data normality (α = 0.05, p<0.05), and a Grubbs test was used to identify outliers (α = 0.05). Data was parametric for graphs (**A**), (**C**), and (**D**) and a one-way ANOVA with Bonferroni post-hoc correction was used to determine the statistical significance between groups. Data was non-parametric for graph (**E**) and a Kruskal-Wallis test with Dunn's post-hoc analysis was used to determine statistical significance. Significance is represented on the graph by *p<0.05, **p<0.01, ***p<0.001, or ****p<0.0001*.

3.8 Proliferation of Haematopoietic Stem & Progenitor Cells is Modified Following Priming with TNF-α-Stimulated Endothelial Cell-Extracellular Vesicles In Vivo

The model of priming mice with TNF-α EC-EV followed by LPS treatment after a rest period has shown changes to bone marrow and splenic neutrophils, and importantly with regards to haematopoiesis, changes to GMP and MEP populations in the bone marrow. However, whether these differences in cell number are caused by changes to the proliferation rate of HSPC or by another mechanism e.g. cell migration from the bone marrow, was not clear. To understand this better, EdU, a reagent used to track proliferating cells by binding to newly synthesised DNA, was injected into mice with LPS 24 hours after priming with TNF-α EC-EV or control groups. HSPC populations from the bone marrow and spleen were then isolated, stained and analysed by flow cytometry.

The number of proliferating cells was measured as a proportion of the total subpopulation for each HSPC group. In the bone marrow (**Figure 22A**), TNF-α EC-EV priming induced significant differences to the rate of HSPC proliferation, including a lower proliferating rate for HSC ($p<0.05$) and MPP ($p<0.01$) relative to the control EC-EV groups. Furthermore, GMP proliferation (**Figure 22B**) ($p<0.01$) significantly decreased in response to TNF-α EC-EV, whilst MEP proliferation increased ($p<0.01$) compared to control EC-EV. These data support my hypothesis that haematopoiesis within the bone marrow is modified following treatment with TNF-α EC-EV by highlighting changes to the rate of HSPC proliferation within the bone marrow. In the spleen (**Figure 22C-D**), there were no significant differences in the rate of proliferation for HSC or GMP populations, but there was a decrease in MPP proliferation in TNF-α EC-EV and LPS relative to the control EC-EV groups.

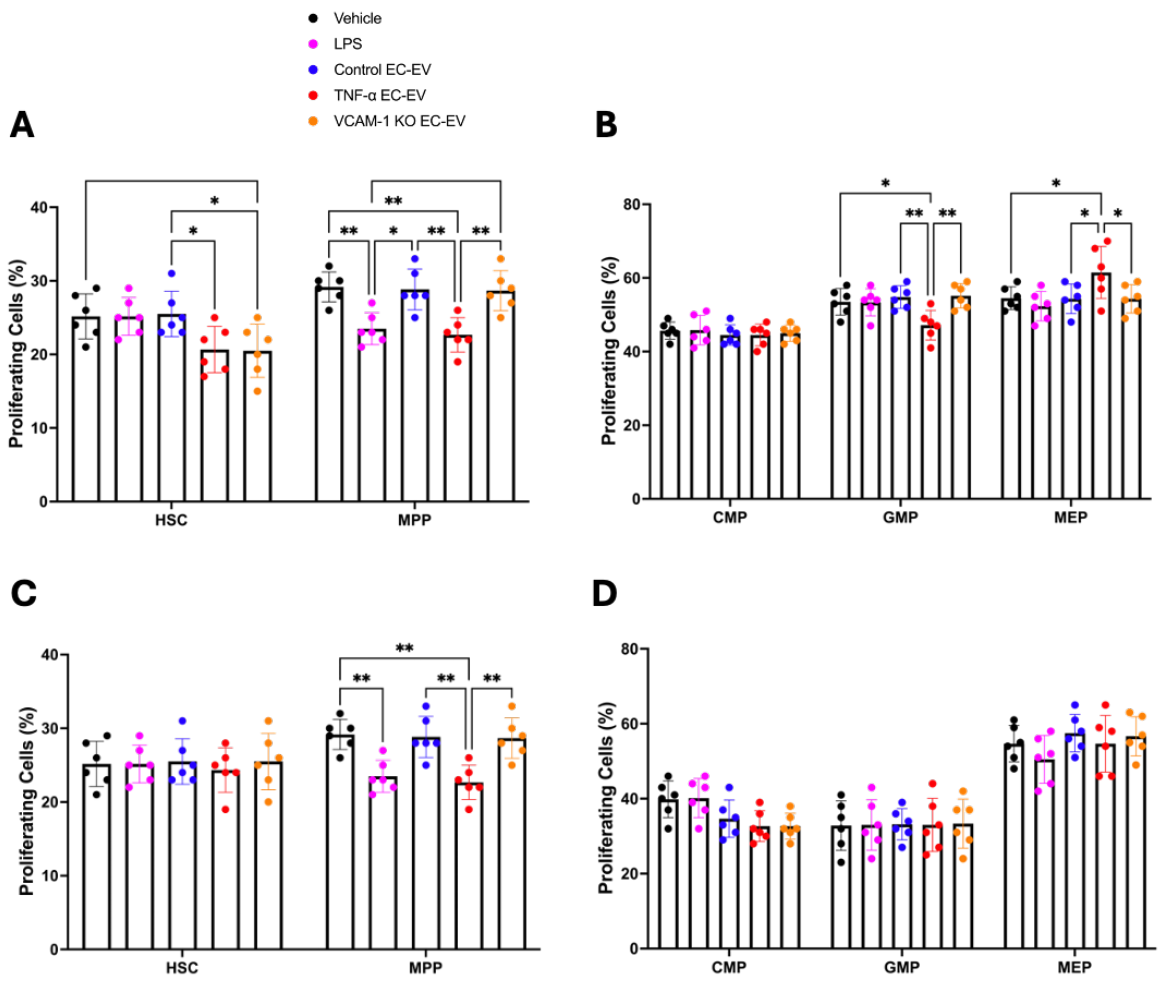

Figure 22. Priming Mice with TNF-α-Stimulated Endothelial Cell-Extracellular Vesicles Followed by LPS Treatment Lowers Cell Proliferation in Mouse Bone Marrow. *The percentage of proliferating (**A**) HSC and MPP, and (**B**) CMP, GMP and MEP populations in mouse bone marrow in response to priming with either vehicle-control (sterile PBS), LPS (1 mg / kg body weight), control EC-EV (1 x 10^9 particles), TNF-α EC-EV (1 x 10^9 particles) or VCAM-1 knockout EC-EV (1 x 10^9 particles), followed by LPS (1 mg / kg body weight) for 72 hours (n = 6 per group). The percentage of proliferating (**C**) HSC and MPP, and (**D**) CMP, GMP and MEP populations in mouse spleens in response to the conditions listed above (n = 6 per group). n = Number of*

*replicates. Data are reported as mean ± standard deviation. A Shapiro-Wilk test was used to determine data normality (α = 0.05, p<0.05), and a Grubbs test was used to identify outliers (α = 0.05). Data was parametric and a one-way ANOVA with Bonferroni post-hoc correction was used to determine the statistical significance of differences between the groups. Significance is represented on the graph by *p<0.05, or **p<0.01*.

3.9 Discussion

VCAM-1$^+$ EC-EV are elevated in the blood following MI (88, 89, 98, 197) and contribute to the MI response by localising to organs such as the spleen (88, 89), where they induce the mobilisation of innate immune cells (88). The role of VCAM-1$^+$ EC-EV in the bone marrow has not been established and this chapter aimed to understand the effects of VCAM-1$^+$ EC-EV on bone marrow haematopoiesis using TNF-α-stimulated EC-EV. This chapter found; (I) TNF-α EC-EV increase HSC and GMP in the bone marrow *in vivo* relative to control EC-EV, (II) TNF-α EC-EV appear to skew HSC haematopoiesis towards GMP and away from MEP *in vitro*, and (III) exposing the bone marrow to several inflammatory stimuli such as TNF-α EC-EV followed by LPS suppresses bone marrow GMP production and lowers GMP cell proliferation. The key findings are summarised in **Figure 23.**

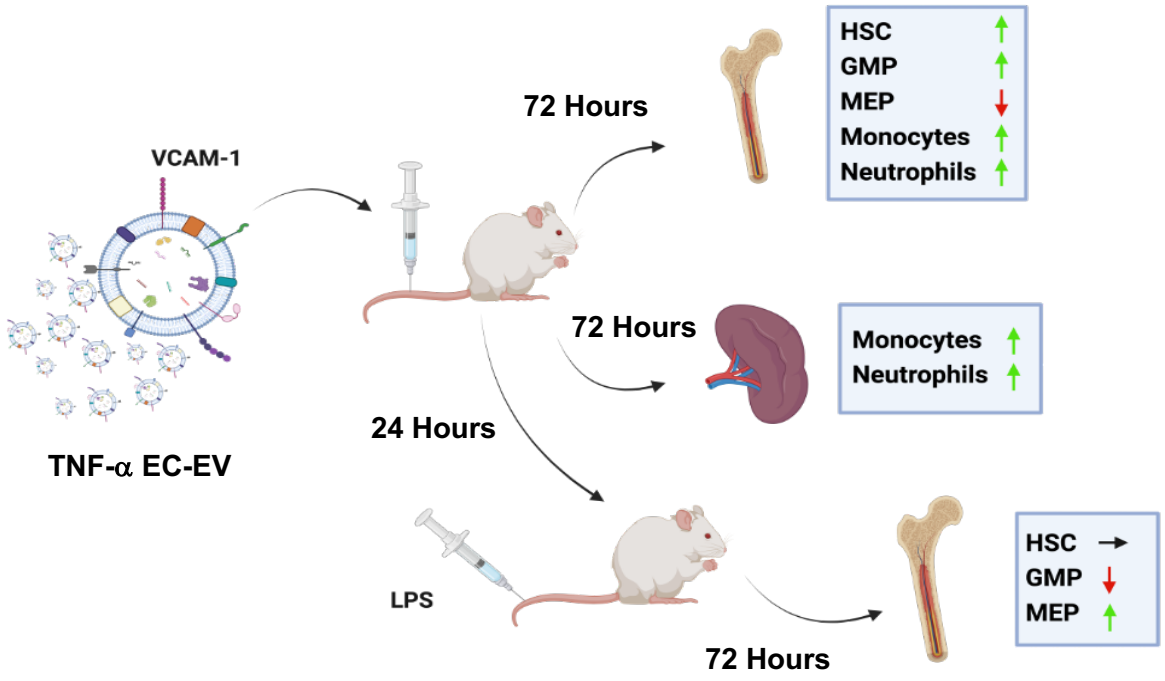

Figure 23. TNF-α EC-EV Modulates Bone Marrow Haematopoiesis and Bone Marrow and Splenic Innate Immune Cell Counts. *Green arrow = Cells increase. Black Arrow = Cells unchanged. Red arrow = Cells decrease*.

The use of sEND.1 as the source of EC-EV for these studies allowed for the rapid generation of the EC-EV. The EC-EV model selected has been validated in previous studies (89) to show that stimulation with TNF-α yields an increase in the number of EC-EV released which is proportional to what has been observed *in vivo* and therefore can be considered pathologically relevant. Furthermore, *in vitro* activation of endothelial cells with TNF-α leads to a similar change in protein and miRNA cargo as was observed in plasma EV post-MI, with VCAM-1 and miRNA-126-3p and miRNA-126-5p similarly elevated in both (88).

The studies in this chapter have assessed changes in haematopoiesis at 72 hours. This was based on research elsewhere in the literature which identified 72 hours as the minimum timepoint for detecting changes in HSPC populations due to haematopoiesis (150, 180, 181). Other studies also used longer timepoints to assess haematopoiesis, such as at 10 days or 28 days post-injection (82, 189). Therefore, expanding this study to include multiple timepoints would allow the longer-term effects on haematopoiesis to be studied and would indicate whether the effects of TNF-α EC-EV reprogramming are permanent or reversible. Measuring earlier timepoints would also provide crucial data on the dynamics of TNF-α EC-EV reprogramming in the bone marrow and would overcome the limitations of measuring at a single timepoint. Changes in blood cytokine levels could also be examined at these earlier timepoints, which would be insightful since the 72-hour post-injection measurements in this chapter did not reach the detection threshold and likely peaked at earlier timepoints.

Nevertheless, the results from experiments that used longer timepoints for haematopoiesis broadly aligned with the results of this chapter, notably that bone marrow HSC populations increase in response to MI or TNF-α EC-EV (82, 198, 199), and that recurrent stimulations appeared to suppress myelopoiesis in the bone marrow (82). Furthermore, the results in **Figure 15** highlight the effects of TNF-α EC-EV on circulating monocytes and neutrophils and on splenic monocytes and neutrophils. This is consistent with previous reports which have shown that although MI significantly increases circulating monocytes and neutrophils (28, 57), recurrent MI leads to decreasing numbers of monocytes and neutrophils in the blood (82).

The results in **Figure 16** demonstrated differences in circulating platelet and erythrocyte levels following exposure to TNF-α EC-EV. Erythropoietin is produced in

the kidney and is a known inducer of erythropoiesis in the bone marrow (200). Erythropoietin binds to erythropoietin receptors in the bone marrow and spleen in response to hypoxia and has interesting therapeutic potential for diseases such as MI and ischemic brain injury (201, 202). In a rodent MI model, erythropoietin injection lowered the infarct size by up to 25% after 8 weeks (202). Under hypoxic conditions, erythropoietin may promote erythropoiesis in the bone marrow, leading to increased numbers of circulating erythrocytes in response to TNF-α EC-EV injection. Therefore, assessing changes in the level of circulating erythropoietin following TNF-α EC-EV injection would be a useful next experiment to potentially explain the changes in erythrocyte levels that were observed.

TNF-α EC-EV treatment modified bone marrow haematopoiesis *in vivo* and specifically promoted a bias in HSC proliferation towards granulocytes and monocytes *in vitro*. This corresponds with an increase in circulating monocytes and neutrophils which are seen elsewhere following MI and are required for the initial pro-inflammatory phase of the immune response to MI (88, 89, 199). As part of the initial pro-inflammatory response, DAMPs are recognised by PRRs on the surface of resident bone marrow cells including monocytes and HSPCs, leading to bone marrow niche remodelling and HSC proliferation and expansion (170). It is not clear whether TNF-α EC-EV function involves remodelling of the bone marrow and therefore future experiments could involve live cell imaging of bone marrow sections following TNF-α EC-EV to compare changes in the bone marrow structure.

This chapter has focused on the effects of TNF-α EC-EV on HSPC, monocytes and neutrophils and is due to the rapid mobilisation of innate immune cells to promote tissue repair in the damaged myocardium (28, 30, 57, 82). Lymphocytes also play an

important role in the response to MI (203, 204), such as by secreting pro-inflammatory cytokines to amplify the inflammatory immune response (205, 206), the regulation of fibrosis and tissue remodelling with cardiac fibroblasts (207), and in promoting angiogenesis (203). Therefore, changes to the number of lymphocytes and the different lymphocyte subpopulations in response to TNF-α EC-EV would create a more detailed picture compared to the current model and may offer a novel insight into TNF-α EC-EV-induced reprogramming of the bone marrow.

Furthermore, there is evidence that haematopoiesis in response to acute injury increases common lymphoid progenitor production in the bone marrow (208). CLP populations then either expand to form mature lymphocytes, or migrate from the bone marrow to other lymphoid organs such as the spleen or lymph nodes to promote the rapid response to acute injury (203). As a result, future experiments would first identify if lymphoid progenitors play a key role in TNF-α EC-EV-driven haematopoiesis in the bone marrow, and secondly investigate the direction of change for specific subsets of mature lymphocytes, such as natural killer T-cells (209) and Regulatory T-cells (203, 210).

Finally, the studies in this chapter showed changes in haematopoiesis in the bone marrow in response to TNF-α EC-EV *in vivo* and then isolated HSC to show that TNF-α EC-EV directly modify these cells. However, further studies are required to determine whether TNF-α EC-EV are internalised by bone marrow HSC or if the EV have an effect at the cell surface. In addition, the specific role of the TNF-α EC-EV cargo was not uncovered during these experiments. Previous research has shown the effects of TNF-α EC-EV on the spleen in mobilising monocytes and neutrophils, and these effects are mitigated through the CRISPR-Cas9-mediated knockout of VCAM-1

(89). The use of the VCAM-1 knockout endothelial cells in this chapter indicates this protein may be essential for the reprogramming effects of TNF-α EC-EV on the bone marrow, potentially to allow docking of the vesicle to the target cell. Nevertheless, the specific molecular pathways downstream of this docking were not investigated in this study.

Using plasma VCAM-1$^+$ EV isolated from mice post-MI rather than using the TNF-α EC-EV model may have produced a model which was more physiologically relevant. The difficulties in obtaining sufficient VCAM-1$^+$ EV from mouse plasma to conduct these experiments prohibited this option during these studies. Since endothelial cells are highly sensitive to extracellular conditions such as flow rate *in vivo* (211-213) , our TNF-α EC-EV model could also be improved by placing the sEND.1 cells under a flow system (214, 215). Furthermore, improvements in Omics technologies have helped to uncover endothelial cell heterogeneity between different populations (136, 216, 217), including within the same organ such as in the heart (218, 219). These transcriptional changes are produced by differences in epigenetic landscapes (220) and reflect the different micro-environments that each endothelial cell subpopulation is exposed to, including flow rate and oxygen concentration, which endothelial cells are highly sensitive to (211-213). Studies also identified differences in VCAM-1 expression between different vascular beds (216, 221). As a result, future experiments would potentially need to perform a comparison between the EV secreted from different sections of the heart and whether each subpopulation respond uniquely to TNF-α.

To conclude, this chapter showed that TNF-α EC-EV function *in vivo* to modulate the bone marrow and increase haematopoiesis, leading to an increase in HSC populations. *In vitro* analysis shows HSC skews haematopoiesis towards myeloid

lineages, which favours the amplification of monocytes and neutrophils. These are crucial to the initial MI response and therefore TNF-α EC-EV may mediate interactions between the bone marrow and infarcted heart and could therefore be an important therapeutic target for managing the post-MI response in patients.

Chapter 4- RNA Analysis of Endothelial Cell Extracellular Vesicle Cargo and Bone Marrow Haematopoietic Stem Cells

4.1 Introduction

The previous chapter details the effects of TNF-α EC-EV on bone marrow haematopoiesis, however the specific cellular mechanisms which contribute to this phenotype have not been explored. EV from a variety of cellular origins including macrophages (189, 190), skeletal muscle (222), pulmonary epithelium (223), and platelets (224) have been shown to target the bone marrow, leading to modified haematopoiesis and skewed innate immune signalling (223, 224). Furthermore, several studies have shown how HSPC are specifically targeted by EV in order to regulate haematopoiesis and cell survival (225). In one study, primary bone marrow stromal cell-EV increased cell survival in HSPC by activating the JAK-STAT pathway and also increased the proliferation of myeloid progenitor cells (226).

The effects of EV on target cells are mediated by cargo within the EV lumen. These include miRNA (227-229), which regulate gene expression within target cells by hybridising to complementary mRNA sequences and altering the rate of translation. Research on how EV regulate haematopoiesis provides evidence that mesenchymal stem cell-EV promote the proliferation of HSPC through EV-miRNA cargo which lower β-catenin expression (230). Bioinformatics analysis of mesenchymal stem cell-EV miRNAs indicated 17 miRNAs which downregulate β-catenin and promote HSPC differentiation. miRNA-126 was also identified in this study as a mesenchymal stem cell-EV miRNA which regulates haematopoiesis (231).

miRNA-126-3p and miRNA-126-5p are two well-characterised miRNA and were shown to increase in patient plasma EV following MI (88, 89). Interestingly, mice treated with a miRNA-126 antagomir sequence had a smaller infarct size compared to control-treated mice (89). Studies elsewhere have shown that Plexin-B2 is a potential target of miRNA-126, leading to modified cell motility and adhesion of innate immune cells such as monocytes (232). Furthermore, miRNA-126 appears to specifically target the bone marrow and promote the mobilisation of HSPC by downregulating VCAM-1, which disrupts HSPC anchoring within the bone marrow niche and leads to HSPC migration and mobilisation from the bone marrow (233). A separate study into the role of miRNA-126 in promoting erythropoiesis also proposes that VCAM-1 downregulation induces erythropoiesis based on expression patterns of miRNA-126 and *vcam1,* and that *vcam1* expression increases 2.3-fold in a conditional knockout model of miRNA-126 (231).

In addition to miRNA-126, other miRNAs are involved in regulating the response to MI. Following ischemic reperfusion, cardiomyocyte apoptosis is regulated by the MAPK phosphorylation cascade involving Akt-PTEN signalling (234). PTEN is upregulated following MI and functions to inactivate Akt, which inhibits *il10* expression and cell survival, and also promotes the expression of *tnf* and matrix metalloproteinase-2 in order to facilitate myocardial remodelling. miRNA-320 inhibits PTEN and targeting miRNA-320 in the myocardium post-MI was shown to lower cardiomyocyte apoptosis (235-237). One study showed miRNA-320 is upregulated in response to myocardial ischaemic reperfusion injury and miRNA-320 expression levels correlate with the extent of cardiac apoptosis (237). However, research elsewhere indicates that miRNA-320 is downregulated following ischaemic reperfusion injury (236), and therefore the role of miRNA-320 in MI needs to be studied further.

TNF-α EC-EV may also exert its effects on the bone marrow post-MI through EV-miRNA cargo including miRNA-126-3p and miRNA-320. Therefore, this chapter hypothesises that bone marrow HSC undergo transcriptional changes in response to TNF-α EC-EV. Secondly, this chapter hypothesises that the effects of TNF-α EC-EV are mediated by miRNA cargo.

4.2 List of Methods Used in This Chapter

- *2.1 Media Preparations*
- *2.2 Endothelial Cell Culture*
- *2.3 Extracellular Vesicle Isolation Using Ultracentrifugation*
- *2.4 Extracellular Vesicle Characterisation*
- *2.5 In Vivo Experimentation*
- *2.12 Bone Marrow Haematopoietic Stem Cell Isolation Using Fluorescence Activated Cell Sorting (FACS) for Transcriptomics Analysis*
- *2.13 Gene Expression Analysis by RT-qPCR*
- *2.14 Endothelial Cell-Extracellular Vesicle microRNA Isolation and Analysis*
- *2.15 Endothelial Cell-Extracellular Vesicle microRNA Cargo Bioinformatics Analysis*
- *2.23 Statistical Analysis*

4.3 Transcriptional Analysis of Mouse Bone Marrow Haematopoietic Stem Cells Following Exposure to TNF-α-Stimulated Endothelial Cell-Extracellular Vesicles

Data in **Section 3.4** showed that the injection of TNF-α EC-EV induced changes in haematopoiesis within the bone marrow and, specifically, increased the number of HSC (**Figure 13**). To understand the transcriptional effects on bone marrow HSC, mice were injected with either control EC-EV or TNF-α EC-EV (**Figure 24A**) and after 72 hours, the bone marrow was harvested. There were no significant differences in body weight between the control and TNF-α EC-EV groups at the time of harvest (**Figure 24B**), but the spleen weight was significantly greater in TNF-α EC-EV ($p<0.0001$, **Figure 24C-D**), which was consistent with the findings from Chapter 3 (**Figure 12C**).

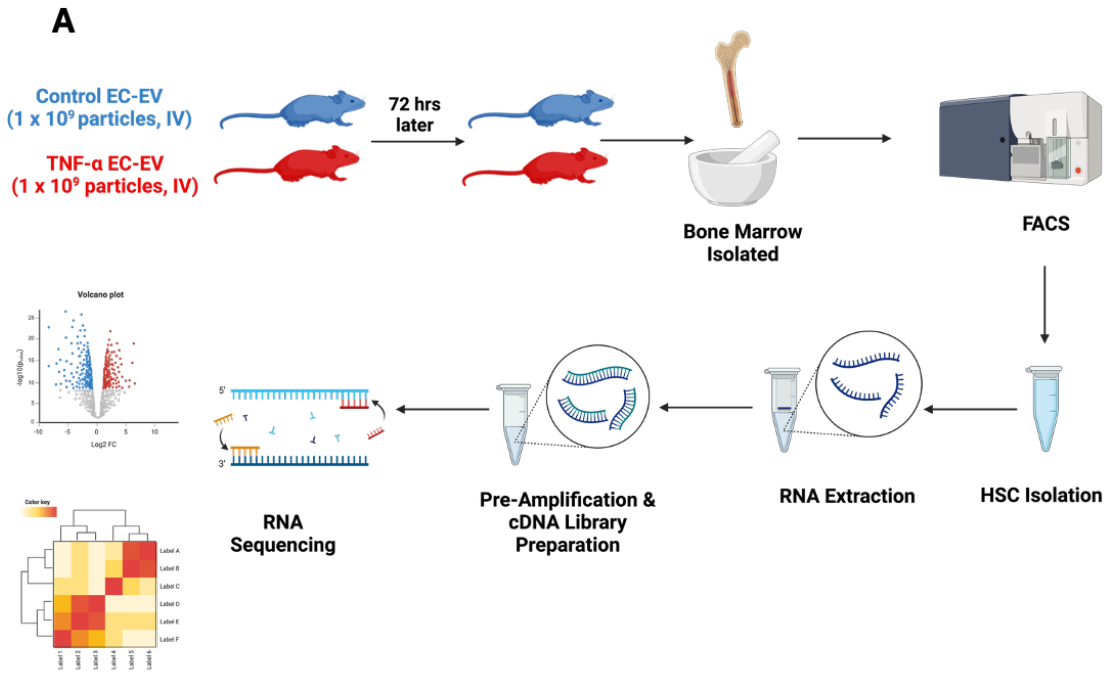
A
Control EC-EV
(1 x 10⁹ particles, IV)
TNF-α EC-EV
(1 x 10⁹ particles, IV)
72 hrs
later
Bone Marrow
Isolated
FACS
HSC Isolation
RNA Extraction
Pre-Amplification &
cDNA Library
Preparation
RNA
Sequencing
Volcano plot

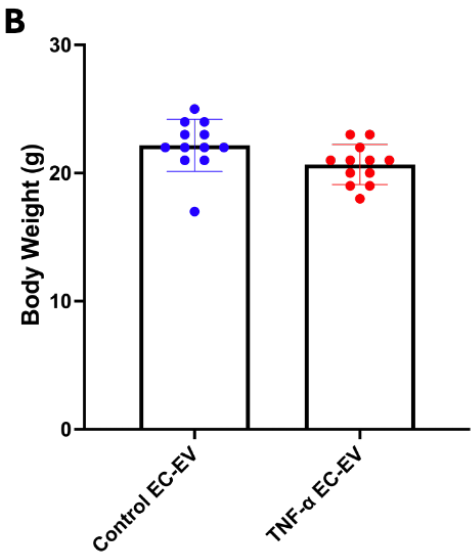
B
Body Weight (g)
30
20
10
0
Control EC-EV
TNF-α EC-EV

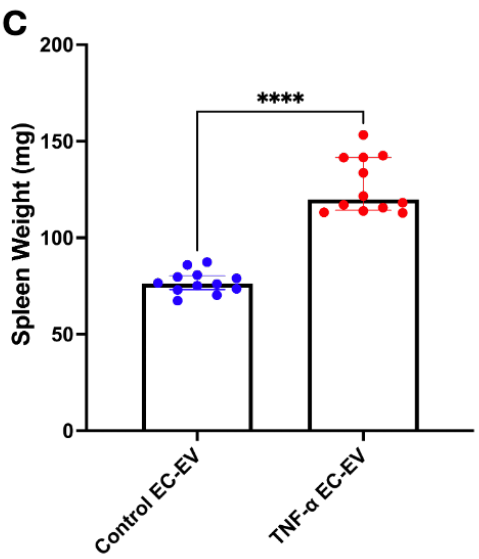
C
Spleen Weight (mg)
200
150
100
50
0
****
Control EC-EV
TNF-α EC-EV

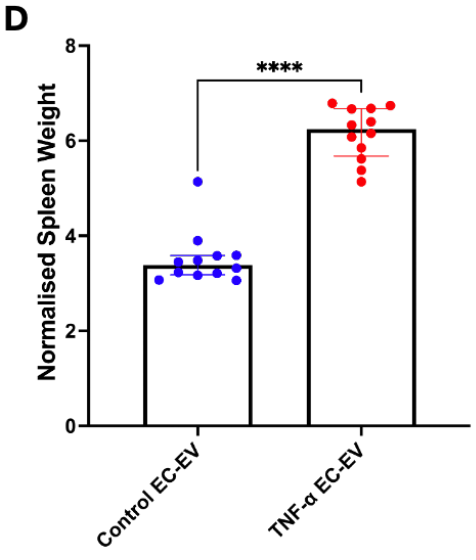
D
Normalised Spleen Weight
8
6
4
2
0
****
Control EC-EV
TNF-α EC-EV

Figure 24. Injecting Mice with Control or TNF-α-Stimulated Endothelial Cell-Extracellular Vesicles Increases Spleen Weight But Not Body Weight. *(**A**) Overview experimental schematic. (**B**) Body weight in mice at the time of bone marrow harvest (72 hours) after injection with either control EC-EV (1 x 10^9 particles) or TNF-α EC-EV (1 x 10^9 particles) (n = 12 per group). (**C**) Spleen weight at the time of bone marrow tissue harvest (72 hours). (**D**) Normalised spleen weight against body weight for each individual. n = Number of replicates. Parametric data are reported as mean ± standard deviation, and non-parametric data are reported as median and interquartile ranges. A Shapiro-Wilk test was used to determine data normality (α = 0.05, p<0.05), and a Grubbs test was used to identify outliers (α = 0.05). Data was parametric for graph (**B**) and non-parametric for graphs (**C**) and (**D**). Statistical significance for parametric data was assessed using a two-way unpaired t-test and for non-parametric data, a Mann-Whitney test. Significance is represented on the graph by ****p<0.0001.*

Bone marrow HSC were isolated from each sample using FACS (**Figure 25A**). Bone marrow cells were first stained with lineage antibodies (CD3-ε, CD4, TER-119, CD45R/B220 and GR-1) to identify lineage-committed cells for exclusion, followed by Sca-1, CD117/c-Kit, CD48 and CD150 to isolate the HSC population. Quantifying the $Lineage^-Sca1^+cKit^+$ (LSK) population shows a statistically significant increase in bone marrow LSK (p<0.05, **Figure 25B**) following exposure to TNF-α EC-EV, compared to control EC-EV, although there were no significant increases in the number of bone marrow HSC (**Figure 25C**).

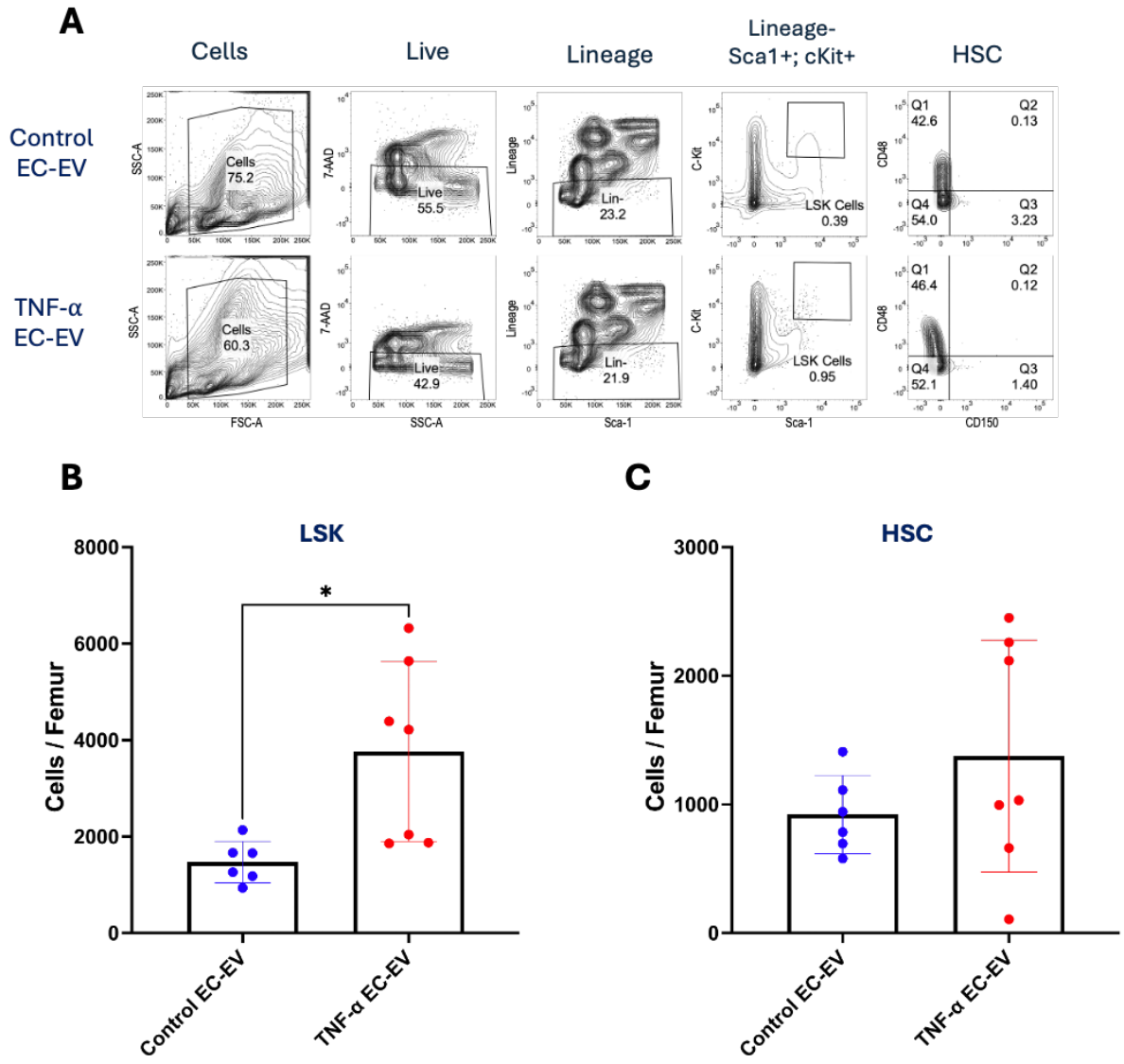

Figure 25. Fluorescence-Activated Cell Sorting Analysis of Mouse Bone Marrow to Isolate Haematopoietic Stem Cells. *(**A**) FACS gating strategy for isolation of bone marrow HSC. Changes in mouse bone marrow (**B**) LSK and (**C**) HSC populations following exposure to either control EC-EV (1 x 10^9 particles / mL) or TNF-α EC-EV (1 x 10^9 particles / mL) (n = 6-7 per group). LSK = Lineage$^-$Sca1$^+$cKit$^+$, HSC = Haematopoietic stem cells. n = Number of replicates. Data are reported as mean ± standard deviation. A Shapiro-Wilk test was used to determine data normality (α = 0.05, p<0.05), and a Grubbs test was used to identify outliers (α = 0.05). Data was*

*parametric and post-hoc analysis included a two-way unpaired t-test. Significance is represented on the graph by *p<0.05.*

Following isolation, RNA from the HSC samples for each group was extracted, quantified (**Figure 26A**), and assessed for purity (**Figure 26B**) (**Method 2.12**). Samples were then sequenced in order to identify differentially expressed genes between each group. From the total number of reads, the number of clean reads was determined by eliminating 'error reads' which include those that still contain adapter or primer sequences, reads containing >10% unknown nucleotides, and low-quality reads based on a Phred Quality Score of 30 (Q30). The Quality Score is calculated by:

$$Q = -10 \log_{10} P$$

where P is the probability of calling a base error. Q30 base call accuracy is 99.9%. The number of clean reads was similar between each group (**Figure 26C**), and analysis of the total reads (**Figure 26D**) shows the low level of error reads across each group. The number of reads containing adapter sequences was higher in TNF-α EC-EV compared to control EC-EV, and all error reads were excluded from the final analysis. The clean reads were mapped to the GRCm39 mouse genome, with ~95% of reads being successfully mapped for each group (**Figure 26E**), and ~90% of mapped reads corresponding to unique regions of the genome (**Figure 26F**).

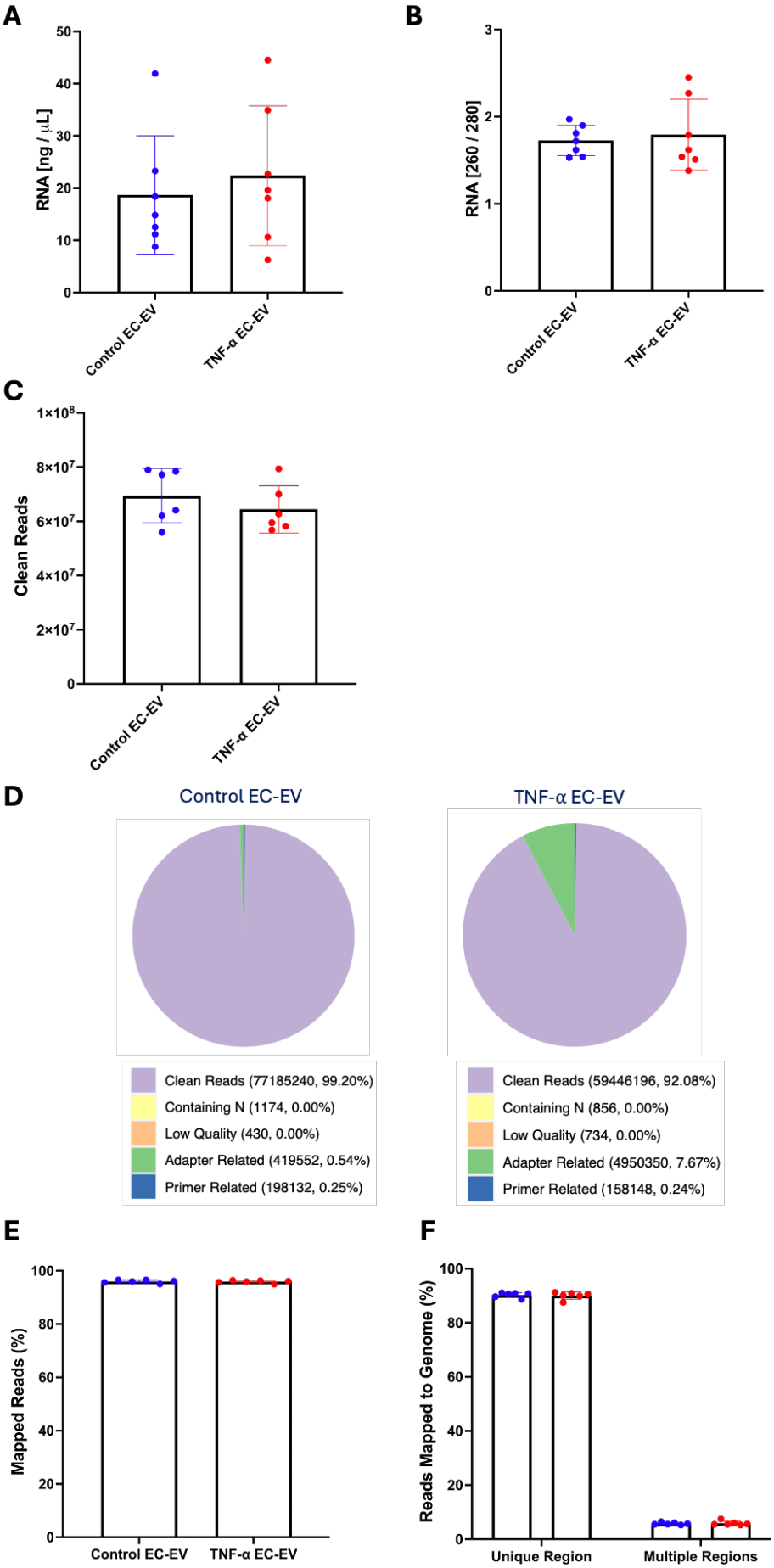
A
RNA [ng / μL]
50
40
30
20
10
0
Control EC-EV
TNF-α EC-EV
B
RNA [260 / 280]
3
2
1
0
Control EC-EV
TNF-α EC-EV
C
Clean Reads
1×10^8
8×10^7
6×10^7
4×10^7
2×10^7
0
Control EC-EV
TNF-α EC-EV
D
Control EC-EV
TNF-α EC-EV
Clean Reads (77185240, 99.20%)
Containing N (1174, 0.00%)
Low Quality (430, 0.00%)
Adapter Related (419552, 0.54%)
Primer Related (198132, 0.25%)
Clean Reads (59446196, 92.08%)
Containing N (856, 0.00%)
Low Quality (734, 0.00%)
Adapter Related (4950350, 7.67%)
Primer Related (158148, 0.24%)
E
Mapped Reads (%)
100
80
60
40
20
0
Control EC-EV
TNF-α EC-EV
F
Reads Mapped to Genome (%)
100
80
60
40
20
0
Unique Region
Multiple Regions

Figure 26. Quality Control Analysis of Bone Marrow Haematopoietic Stem Cells for Bulk RNA Sequencing. *(**A**) Quantification of RNA isolated from HSC following exposure to control EC-EV and TNF-α EC-EV (n = 7 per group). (**B**) Analysis of the quality of RNA isolated from HSC using A260/280. Quality control analysis comparing (**C**) the number of clean RNA reads, and (**D**) the % of clean reads in isolated HSC RNA samples (n = 6 per group). (**E**) The number of reads successfully mapped to the reference genome (GRCm39), and (**F**) the number of reads mapped to either unique regions or multiple regions of the reference genome (n = 6 per group). n = Number of replicates. Data are reported as mean $\pm$ standard deviation. A Shapiro-Wilk test was performed on (**A**), (**B**), (**C**) and (**E**) to determine data normality (α = 0.05, p<0.05), and a Grubbs test was used to identify outliers (α = 0.05). Data from (**A**), (**B**), (**C**) and (**E**) was parametric and post-hoc analysis included an unpaired t-test.*

Gene expression was quantified in both groups (**Figure 27A**) using *featureCounts* v1.5.0-p3 software to count the number of reads mapped to each gene. FPKM was calculated to account for a bias towards larger fragments and highly expressed genes. The analysis found 11,271 genes were commonly expressed in both the control EC-EV and TNF-α EC-EV groups, 1,041 genes were expressed solely in control EC-EV, and 655 genes were expressed exclusively in the TNF-α EC-EV group. This number of genes expressed by HSC was similar to the reported HSC sequencing literature (238, 239). In order to understand the pattern of gene expression between control EC-EV and TNF-α EC-EV groups, the data was converted into principal components using PCA (**Figure 27B**) which showed separation between the control EC-EV and TNF-α EC-EV groups. Between the two components (PCA1 and PCA2), PCA accounted for

44.09% of the total variance. From the 11,271 genes expressed in both groups, differential gene expression analysis was performed, and the resulting Volcano plot (**Figure 27C**) mapped log2(Fold Change) vs -$\log_{10}$(adjusted p-value). The plot shows significant differences between the control EC-EV and TNF-α EC-EV groups with 129 genes significantly upregulated (orange) in the TNF-α EC-EV group and 218 genes were significantly downregulated (green) in the TNF-α EC-EV group. GSEA takes the total set of expressed genes in control EC-EV and TNF-α EC-EV and ranks each gene based on the log2(Fold change) and padj values(153, 154). This eliminates the bias of pre-selecting genes which is used in other methods, such as overrepresentation analysis, where only DEG are used in downstream gene set analysis.

Genes with the highest log2(Fold change) increase and the lowest padj values were ranked the highest and those with the highest log2(Fold change) decrease and the lowest padj values were ranked the lowest. From this data, a heat map was generated (**Figure 27D**) showing gene expression of the top 50 ranked genes and bottom 50 ranked genes for each sample.

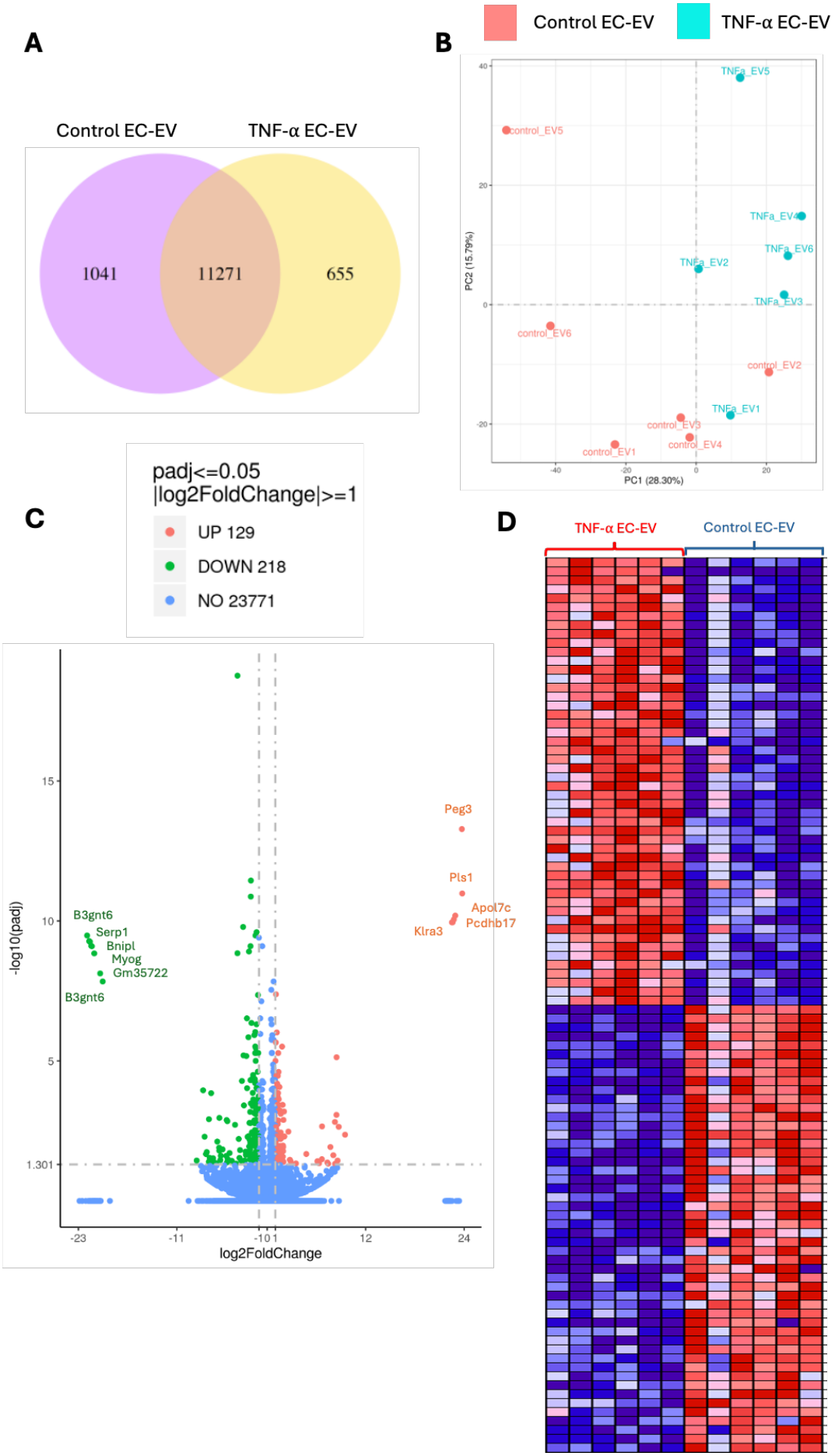
A
Control EC-EV
TNF-α EC-EV
1041
11271
655
B
Control EC-EV
TNF-α EC-EV
TNFa_EV5
control_EV5
TNFa_EV4
TNFa_EV6
TNFa_EV2
TNFa_EV3
control_EV6
control_EV2
TNFa_EV1
control_EV3
control_EV4
control_EV1
PC2 (15.79%)
PC1 (28.30%)
C
padj<=0.05
|log2FoldChange|>=1
UP 129
DOWN 218
NO 23771
Peg3
Pls1
Apol7c
Pcdhb17
Klra3
B3gnt6
Serp1
Bnipl
Myog
Gm35722
B3gnt6
-log10(padj)
log2FoldChange
D
TNF-α EC-EV
Control EC-EV

Figure 27. Gene Expression Analysis of Mouse Bone Marrow Haematopoietic Stem Cells Following Treatment with Control or TNF-α Endothelial Cell-Extracellular Vesicles. *(**A**) Comparison of the number of genes expressed in mouse bone marrow HSC samples following treatment with control EC-EV or TNF-α EC-EV (n = 6 per group). (**B**) A Principal Component Analysis of control EC-EV and TNF-α EC-EV groups. The integrated data was condensed to components PC1 and PC2. (**C**) A Volcano plot to show differential gene expression in bone marrow HSC between control EC-EV and TNF-α EC-EV groups. Non-significant genes are shown in blue, with significantly upregulated genes (log2FoldChange>1 and Padj<0.05) shown in orange, and significantly downregulated genes (log2FoldChange<-1 and Padj<0.05) shown in green. (**D**) A heat map was generated to show the gene expression of the top 50 ranked genes and bottom 50 ranked genes following GSEA of bone marrow HSC between control EC-EV and TNF-α EC-EV groups. (N = number of replicates per group). P values were adjusted (Padj) using the Benjamini and Hochberg method to control the FDR. The threshold for significant differential gene expression was Padj<0.05 and absolute fold change >= 2.*

From 6,912 gene sets used for GSEA, 3,712 were upregulated in TNF-α EC-EV group. **Figure 28A** shows the enrichment score (ES) for each of the gene sets as a histogram, those with a low or negative enrichment score are downregulated in TNF-α EC-EV compared to control EC-EV, whilst those with a high enrichment score are upregulated. A ranked gene list correlation profile (**Figure 28B**) was also produced to show elevated ES at the top of the gene list, and lower ES at the bottom of the ranked list. Enrichment plots for two of the significantly upregulated gene sets, ‘Chromosome centromeric

region GO:0000775' (**Figure 28C**) and 'Kinetochore GO:0000776' (**Figure 28D**), are included. The enrichment profile curves (green line) for each plot show a high proportion of genes within each of these gene sets are highly ranked genes (high ES). The 'barcode' section of each graph, which uses a vertical line to show the distribution of ranked genes in each gene set, also demonstrates that a high proportion of genes in the 'Chromosome centromeric region' and 'Kinetochore' gene sets are highly ranked and therefore are the most differentially expressed genes between TNF-α EC-EV and control EC-EV groups.

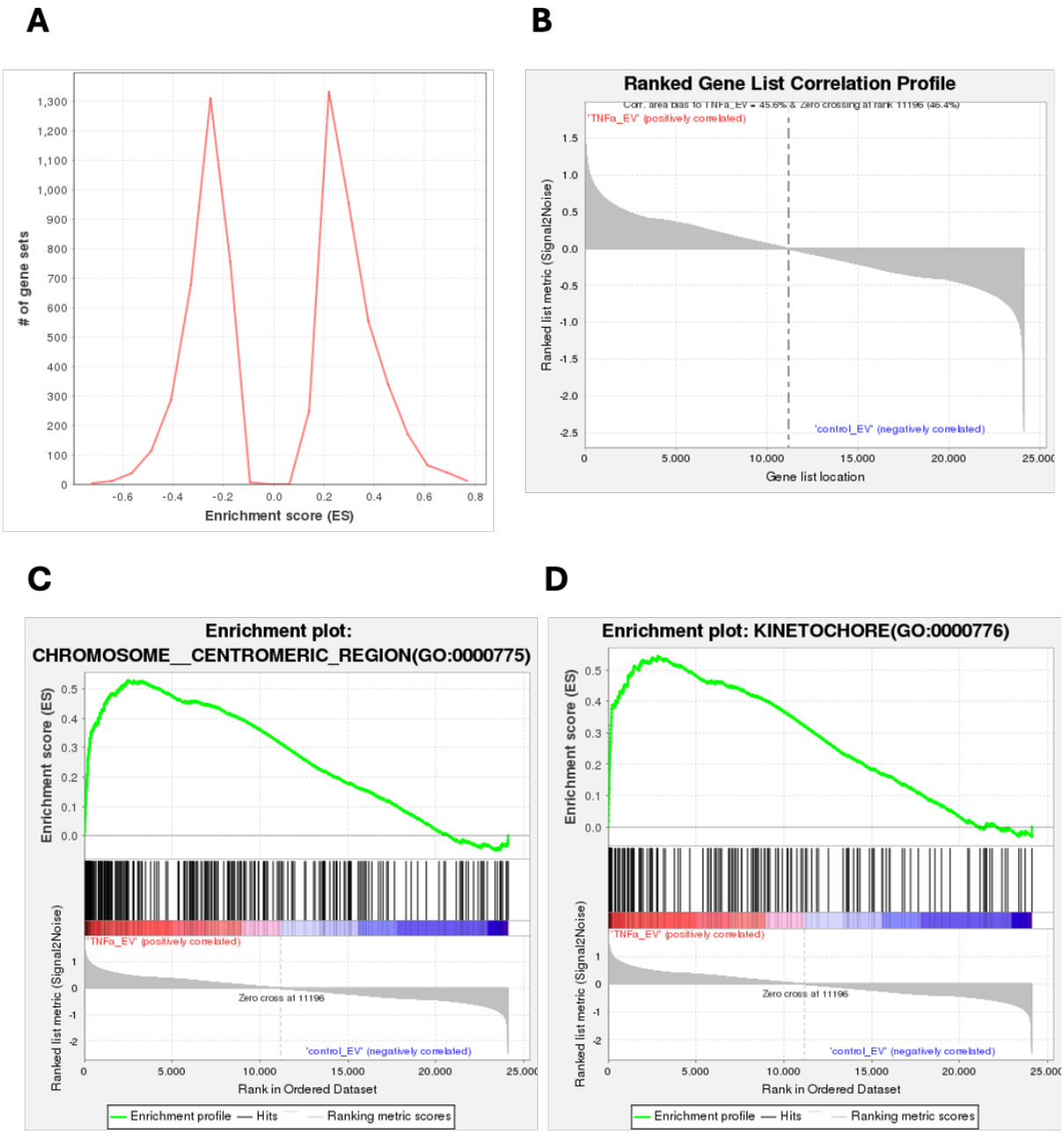

Figure 28. Gene Set Enrichment Analysis of Differentially Expressed Genes in Mouse Bone Marrow Haematopoietic Stem Cells in Response to TNF-α EC-EV Exposure. *(**A**) Histogram showing the enrichment score for each gene set from the 6,912 gene sets which were assessed. (**B**) Ranked gene list correlation profile for gene set enrichment analysis shows differences in expression across the ranked list of differentially expressed genes in HSC for control EC-EV and TNF-α EC-EV groups. Representative enrichment plots for GO terms (**C**) 'Chromosome-Centromeric Region*

*GO:0000775' and (**D**) 'Kinetochore GO:0000776' to demonstrate changes in the enrichment score and distribution of genes in the ranked gene list. Statistical significance was measured using p-adjusted values (padj), using the Benjamini and Hochberg method to control the FDR and the threshold for significance was set at Padj<0.05.*

In order to identify how the differentially expressed genes affect the downstream function within HSC populations, GO analysis was performed. Significant GO terms associated with Biological Process, Molecular Function, and Cellular Component were represented as a dot plot (**Figure 29A**). Terms containing a greater proportion of differentially expressed genes have a higher gene ratio and therefore may be of particular interest for downstream therapeutic targeting. For example, 'Myeloid cell differentiation GO:0030099 p=0.0144', 'Chromosome, centromeric region GO:0000775 p=0.0177', and 'Negative regulation of phosphorus metabolic process GO:0010563 p=0.0144' are some of the most enriched GO terms to emerge from this analysis and therefore may be important processes in TNF-α EC-EV-mediated reprogramming of HSC which could be targeted.

The 50 GO terms which were significantly enriched were then analysed to identify which genes were most frequently upregulated across these 50 pathways (**Figure 30A**). The 129 upregulated genes which were identified were then analysed using STRING network analysis to determine which upregulated genes cluster together into specific pathways (**Figure 30B**). The upregulated genes formed four main clusters with 28% of those genes associated with 'Cell cycle phase transition and mitotic spindle checkpoint' (red), 25% of genes forming the 'MAPK activation and

phosphatase activity' cluster (beige), 7% of genes were part of the 'LPS signalling and myeloid cell activation' cluster (dark green), and 6% were part of 'NK cell chemotaxis' (mint green). This data indicates that over half of the upregulated genes from the GO analysis are associated with either cell cycle regulation or MAPK signalling activity and therefore TNF-α EC-EV may induce transcriptional changes in bone marrow HSC through these pathways. Interestingly, these findings align with previous data on TNF-α EC-EV in bone marrow haematopoiesis (**Figure 13**), which requires the activation of mitosis for cell proliferation.

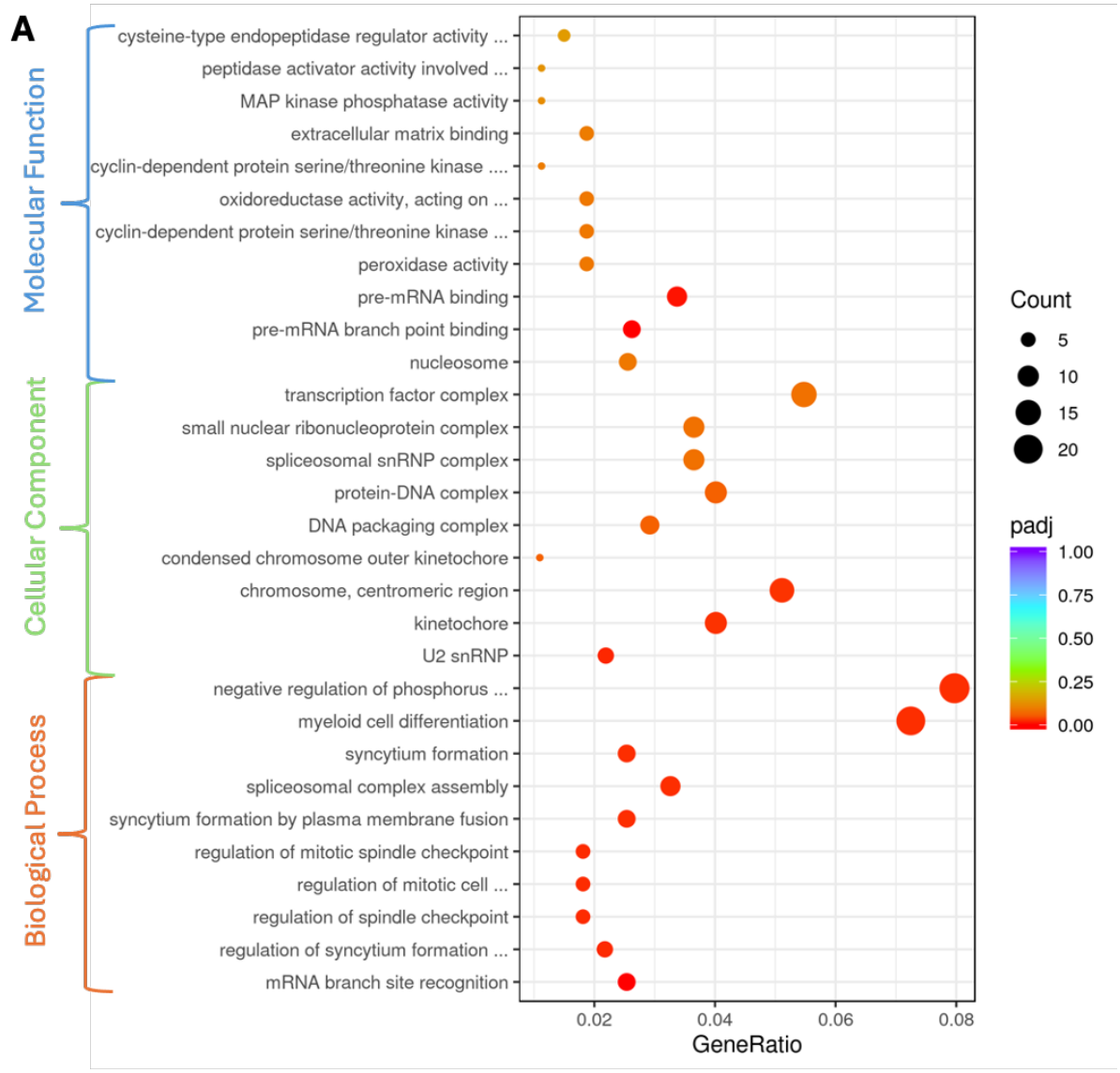

Figure 29. Gene Ontology Analysis of Bone Marrow Haematopoietic Stem Cells Following In Vivo Injection of TNF-α-Stimulated Endothelial Cell-Extracellular Vesicles. *(**A**) Dot plot showing significantly upregulated GO terms associated with Molecular Function, Cellular Component, and Biological Process for bone marrow HSC following in vivo injection with control EC-EV (1 x 10^9 particles) or TNF-α EC-EV (1 x 10^9 particles) (n = 6 per group). The diameter of each dot correlates with the number of enriched genes in each GO term. Statistical significance was measured using p-adjusted values (padj), using the Benjamini and Hochberg method to control the FDR and the threshold for significance was set at Padj<0.05.*

A

Gene Name	% of Enriched GO Terms
Ccnb1	48
Dusp1	42
Mad2l1	40
Birc5	40
Ndc80	40
Spc24	34
Myog	20
Tyrobp	20
Fos	20
Ocstamp	20
Jun	18
Ccl3	18
Cd53	16
Flt3l	16
Klf10	12
Ier3	12
Cdkn1c	12

B

Cluster Name	% of Genes in Cluster
Cell Cycle Phase Transition & Mitotic Spindle Checkpoint	28
MAPK Activation & Phosphatase	25
LPS Signalling & Myeloid Cell Activation	7
NK Cell Chemotaxis	6

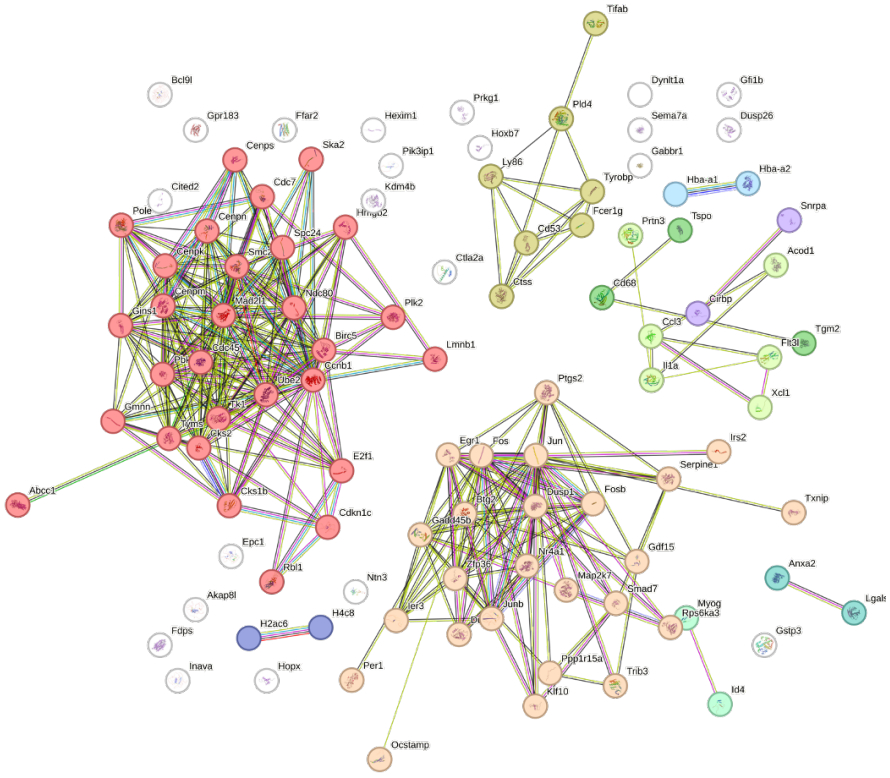

Figure 30. STRING Network Analysis of Bone Marrow Haematopoietic Stem Cells Following In Vivo Injection of TNF-α-Stimulated Endothelial Cell-Extracellular Vesicles. *(**A**) Table demonstrating the most common upregulated genes from the enriched GO terms shown in **Figure 29A**. 129 genes were upregulated in total. Cut-off was >10% of significantly enriched GO terms. (**B**) Clustering of 129 upregulated genes found in enriched GO terms in **Figure 29A** using STRING network analysis. Gene clusters were identified using the Markov Cluster algorithm.*

KEGG analysis was also performed on the differentially expressed genes to identify which pathways may be targeted within bone marrow HSC. The dot plot (**Figure 31**) highlights 'Apoptosis', 'MAPK signalling pathway', and 'Cell cycle' as pathways of interest. However, these pathways were not significantly different between control EC-EV and TNF-α EC-EV based on adjusted p-values, and therefore STRING network analysis was not performed on these pathways.

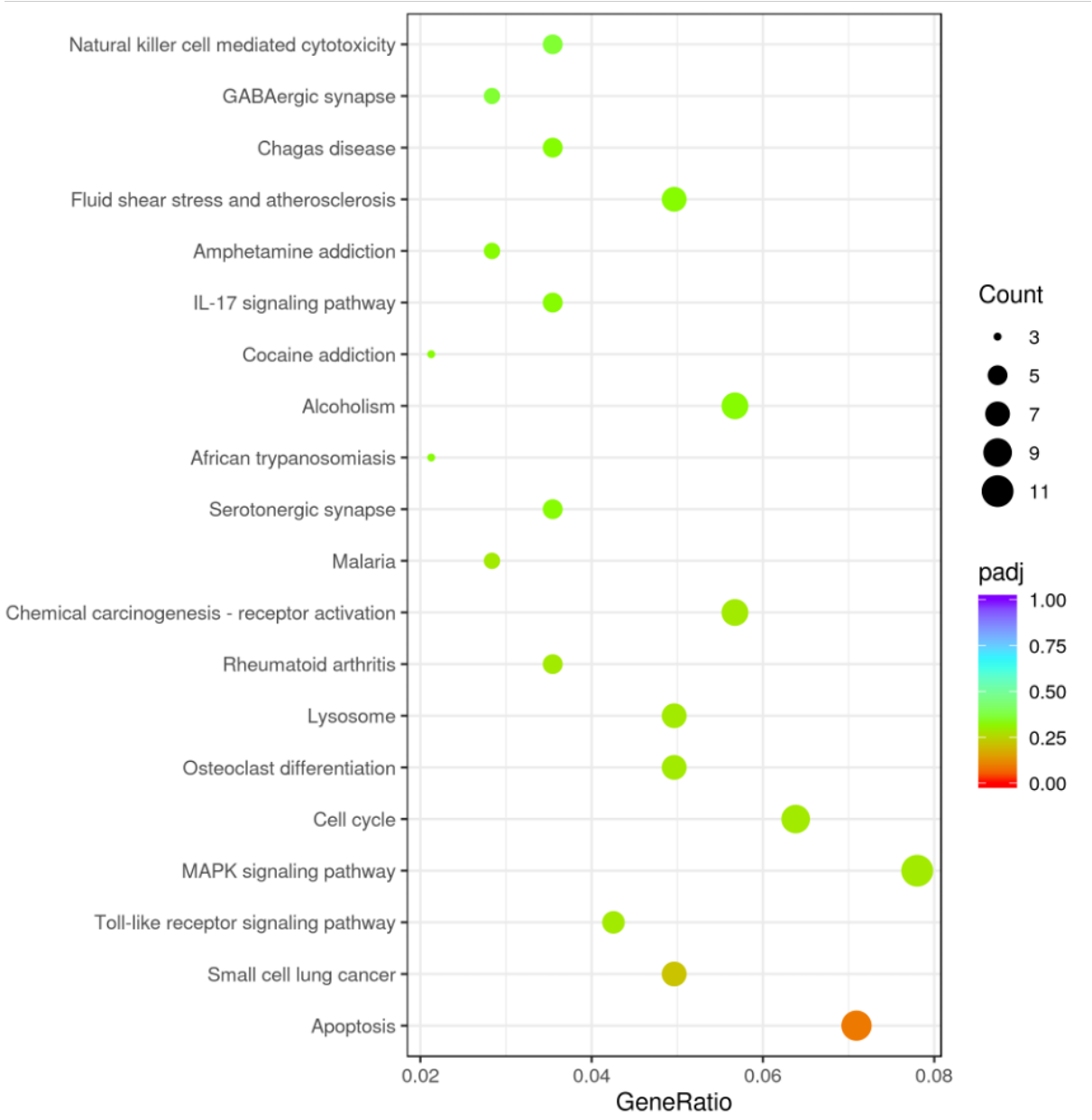

Figure 31. KEGG Analysis of Differentially Expressed Genes in Mouse Bone Marrow Haematopoietic Stem Cells in Response to TNF-α EC-EV Exposure. ***(A)*** *Dot plot for KEGG Pathway analysis for differentially expressed genes from bone marrow HSC in response to control EC-EV or TNF-α EC-EV. Diameter of the dot correlates with the number of differentially expressed genes (count). Statistical significance was measured using p-adjusted values (padj), using the Benjamini and*

Hochberg method to control the FDR. The threshold for significant KEGG Pathways was padj<0.05.

4.4 microRNA-126-3p & microRNA-320b Are Enriched in Mouse Endothelial Cell-Extracellular Vesicles Following Stimulation with TNF-α

The quantity of miRNAs increases following MI in patient plasma (240-242) and it is therefore hypothesised that specific miRNAs act as signalling mediators in the MI response. The enrichment of plasma VCAM-1$^+$ EV post-MI is accompanied by an enrichment in miRNA cargo, including miRNA-126-3p and miRNA-126-5p (88, 89). Unpublished work in our group has also shown a 7.35-fold increase in miRNA-320b at the time of presentation to hospital post-MI.

To test the enrichment of these MI-associated miRNA in the TNF-α EC-EV model, endothelial cell pellets and EC-EV were analysed in control and TNF-α-stimulated conditions to determine the presence of miRNA-126-3p and miRNA-320b. Following the extraction of RNA (**Figure 32A-C**), miRNA-126-3p was significantly enriched in TNF-α EC-EV relative to the control EC-EV group (**Figure 32D**, $p<0.01$), which is consistent with previous findings in plasma EC-EV samples following MI (88). miRNA-320b was also significantly enriched (**Figure 32E**, $p<0.05$) in the TNF-α EC-EV group relative to control EC-EV.

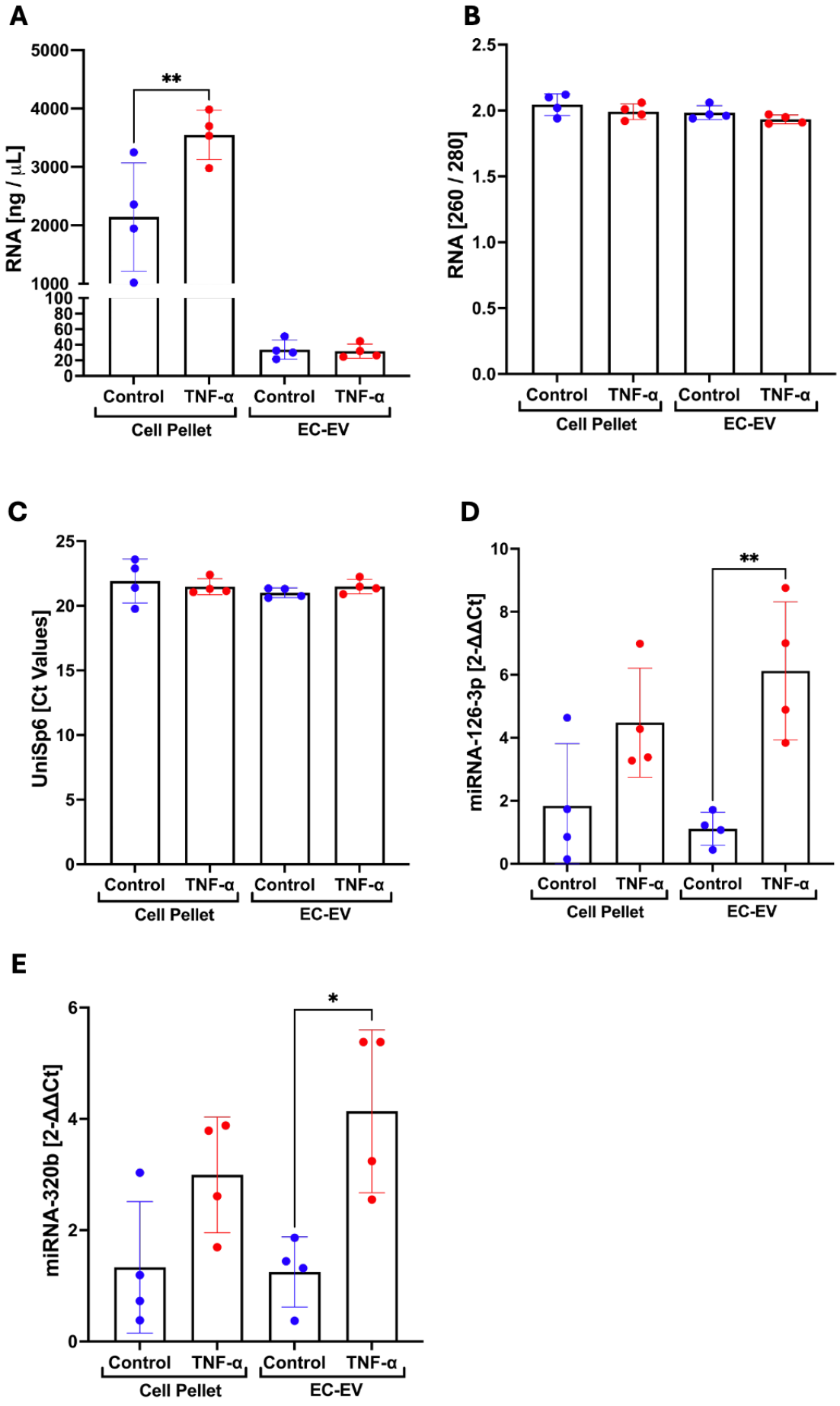
A
RNA [ng / µL]
5000
4000
3000
2000
1000
100
80
60
40
20
0
**
Control
TNF-α
Control
TNF-α
Cell Pellet
EC-EV
B
RNA [260 / 280]
2.5
2.0
1.5
1.0
0.5
0.0
Control
TNF-α
Control
TNF-α
Cell Pellet
EC-EV
C
UniSp6 [Ct Values]
25
20
15
10
5
0
Control
TNF-α
Control
TNF-α
Cell Pellet
EC-EV
D
miRNA-126-3p [2-ΔΔCt]
10
8
6
4
2
0
**
Control
TNF-α
Control
TNF-α
Cell Pellet
EC-EV
E
miRNA-320b [2-ΔΔCt]
6
4
2
0
*
Control
TNF-α
Control
TNF-α
Cell Pellet
EC-EV

Figure 32. microRNA-126-3p and microRNA-320b are Enriched in Mouse sEND.1 Endothelial Cell-Extracellular Vesicles. *(**A**) RNA quantity and (**B**) RNA purity values of sEND.1 cell pellets and EC-EV under basal conditions and after stimulation with TNF-α (10 ng / mL) (n = 4 per group). (**C**) Cycle threshold values for spike-in control (Unisp6) for sEND.1 cell pellets and EC-EV samples. Cycle threshold values for (**D**) miRNA-126-3p and (**E**) miRNA-320b in sEND.1 cell pellets and EC-EV under basal conditions and after stimulation with TNF-α (10 ng / mL) (n = 4 per group). Both (**D**) and (**E**) were normalised to Unisp6 control. Data are reported as mean $\pm$ standard deviation. n = Number of replicates. A Shapiro-Wilk test was performed to determine data normality (α = 0.05, p<0.05), and a Grubbs test was used to identify outliers (α = 0.05). Data was parametric and one-way ANOVA with Bonferroni post-hoc correction was used to determine the statistical significance of changes between groups. Significance is represented on the graph by *p<0.05, or **p<0.01.*

4.5 microRNA126-3p & microRNA320 are Partially Protected From RNAse Degradation in Mouse Endothelial Cell-Extracellular Vesicles

miRNA are associated with EV primarily within the vesicle lumen (243), but recent evidence suggests the presence of nucleic acids on the surface of EV (244), which introduces a novel mechanism of action for EV-associated miRNA cargo. To determine whether the enriched miRNA-126-3p and miRNA-320b cargo in TNF-α EC-EV are intraluminal or surface-bound, control EC-EV and TNF-α EC-EV were isolated and exposed to RNase A. EC-EV not incubated with RNAse A acted as a negative control and the positive control used EC-EV which were first sonicated to rupture the vesicle membrane, then were exposed to RNAse A. Following the extraction of RNA (**Figure**

33A-C), miRNA-126-3p was more abundant (**Figure 33D**, $p<0.001$) in TNF-α EC-EV relative to control EC-EV. In TNF-α EC-EV, miRNA-126-3p was significantly lower following exposure to RNAse A ($p<0.01$) and when the sample was sonicated prior to RNAse A exposure ($p<0.0001$). The relative decrease in miRNA-126-3p in samples sonicated prior to RNAse A degradation was not significant compared to RNAse A treated samples. This indicates miRNA-126-3p is partially protected from RNAse A degradation and therefore may be present within the EV lumen. However, there is a degree of degradation in the RNAse A-treated group for miRNA-126-3p and miRNA-320b and therefore a proportion of each miRNA may be present on the external region of the EV membrane.

For miRNA-320b, TNF-α EC-EV were enriched with miRNA-320b relative to control EC-EV (**Figure 33E**, $p<0.0001$) and there was a statistically significant decrease in miRNA-320b in response to RNAse A treatment ($p<0.001$). TNF-α EC-EV samples exposed to sonication followed by RNAse A treatment also had significantly lower miRNA-320b ($p<0.05$) relative to those exposed only to RNAse A. This indicates that miRNA-320b is partially protected from degradation by the vesicle membrane and therefore is present within the EV lumen.

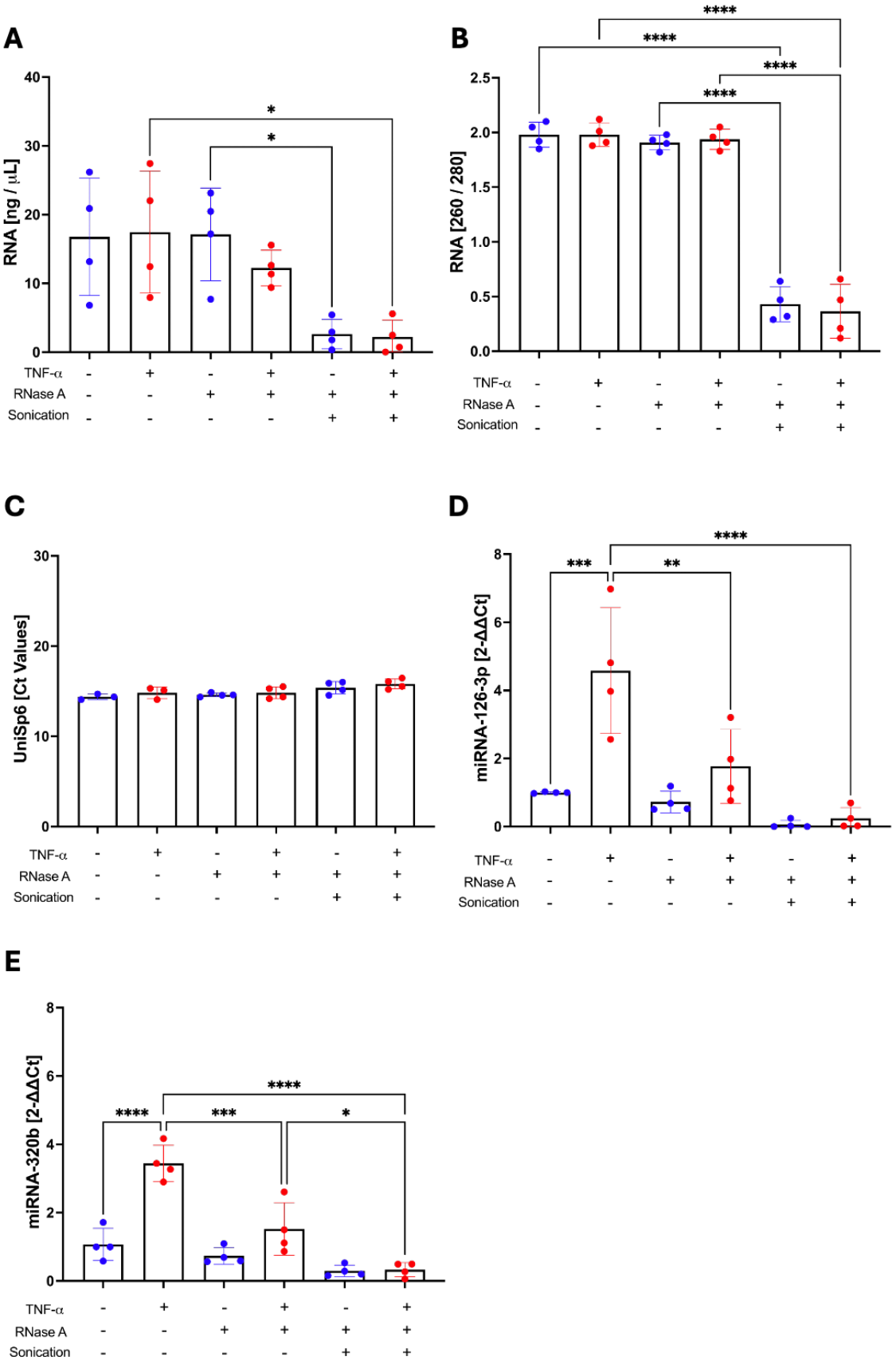
A
RNA [ng / µL]
40
30
20
10
0
*
*
TNF-α - + - + - +
RNase A - - + + + +
Sonication - - - - + +
B
RNA [260 / 280]
2.5
2.0
1.5
1.0
0.5
0.0
****
****
****
****
TNF-α - + - + - +
RNase A - - + + + +
Sonication - - - - + +
C
UniSp6 [Ct Values]
30
20
10
0
TNF-α - + - + - +
RNase A - - + + + +
Sonication - - - - + +
D
miRNA-126-3p [2-ΔΔCt]
8
6
4
2
0
***
**
****
TNF-α - + - + - +
RNase A - - + + + +
Sonication - - - - + +
E
miRNA-320b [2-ΔΔCt]
8
6
4
2
0
****
***
*
****
TNF-α - + - + - +
RNase A - - + + + +
Sonication - - - - + +

Figure 33. RNase A Treatment of Mouse Endothelial Cell-Extracellular Vesicles Leads to Degradation of microRNA-126-3p and microRNA-320b After Vesicle Rupture. *(**A**) RNA quantity and (**B**) RNA purity values of sEND.1 cell pellets and EC-EV under basal conditions and after stimulation with TNF-α (10 ng / mL) (n = 4 per group). (**C**) Cycle threshold values for spike-in control (Unisp6) for sEND.1 cell pellets and EC-EV samples. (n = 3-4 per group). Cycle threshold values for (**D**) miRNA126-3p and (**E**) miRNA-320 in sEND.1 cell pellets and EC-EV under basal conditions and after stimulation with TNF-α (10 ng / mL) (n = 4 per group). Data are reported as mean $\pm$ standard deviation. n = Number of replicates. A Shapiro-Wilk test was performed to determine data normality (α = 0.05, p<0.05), and a Grubbs test was used to identify outliers (α = 0.05). Data was parametric and one-way ANOVA with Bonferroni post-hoc correction was used to determine the statistical significance of changes between groups. Significance is represented on the graph by *p<0.05, **p<0.01, ***p<0.001, or ****p<0.0001.*

4.6 Identification of miRNA-mRNA Targets For Differentially Expressed miRNAs in Plasma Endothelial Cell-Extracellular Vesicles

Having found evidence that miRNA-126-3p and miRNA-320b are present in sEND.1 EC-EV and shown that these miRNAs are enriched in TNF-α EC-EV, bioinformatics analysis was performed to better understand the mRNA targets of these miRNAs. A list of putative miRNA-mRNA targets was generated using miRWalk (157), miRDB (156), and TargetScan (158, 245) mouse databases for miRNA-126-3p. The lists were compared using a Venn diagram (**Figure 34A**) and targets found in multiple databases

formed a single, deduplicated list. The 1,409 putative gene targets were inputted into GO analysis (246, 247) to generate lists of predicted biological function at a pathway level. The most significant GO terms for Biological Process are shown (**Figure 34B**). KEGG pathway analysis was also performed on the putative gene target list and the most significant pathways are also shown (**Figure 34C**). The GO analysis found significant increases in terms associated with EV biology (Exosomal secretion GO:1990182 p=0.0024, Extracellular exosome biogenesis GO:0097734 p=0.0201, Vesicle transport along actin filament GO:0030050 p=0.0312, and Extracellular vesicle biogenesis GO:0140112 p=0.0449), Stem cell regulation (Negative regulation of stem cell differentiation GO:2000737 p=0.0373, and Positive regulation of stem cell proliferation GO:2000648 p=0.0444), and epidermal growth factor (EGF) signalling (ERBB2-EGFR signalling pathway GO:0038134 p=0.0017, and regulation of inositol 1,4,5-triphosphate-sensitive calcium-release channel activity GO:0031585 p=0.0420). KEGG pathway analysis included EGF signalling (ErbB signalling pathway mmu04012 p=0.0004, EGFR tyrosine kinase inhibitor resistance mmu01521 p=0.00216, mTOR signalling pathway mmu04150 p<0.0001, MAPK signalling pathway mmu04010 p<0.0001, and Ras signalling pathway mmu04014 p<0.0001) and stem cell activity (Signalling pathways regulating pluripotency of stem cells mmu04550 p=0.0002). These findings suggest miRNA-126-3p regulates stem cell proliferation, MAPK signalling, and cellular differentiation and therefore may be relevant to the TNF-α EC-EV HSC reprogramming model and haematopoiesis.

A

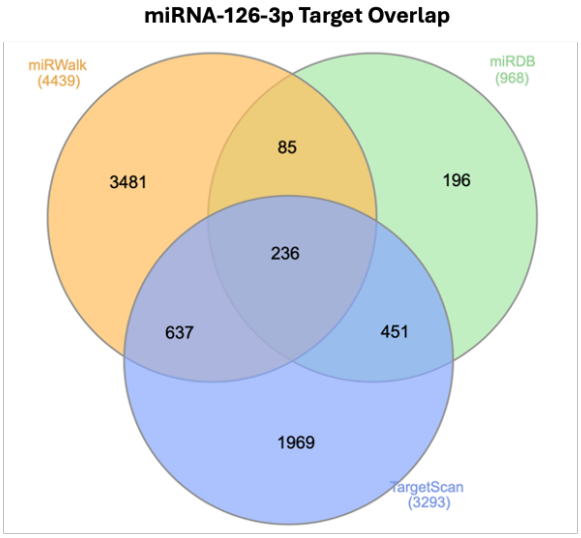
miRNA-126-3p Target Overlap
miRWalk (4439)
miRDB (968)
TargetScan (3293)
3481
85
196
236
637
451
1969

B

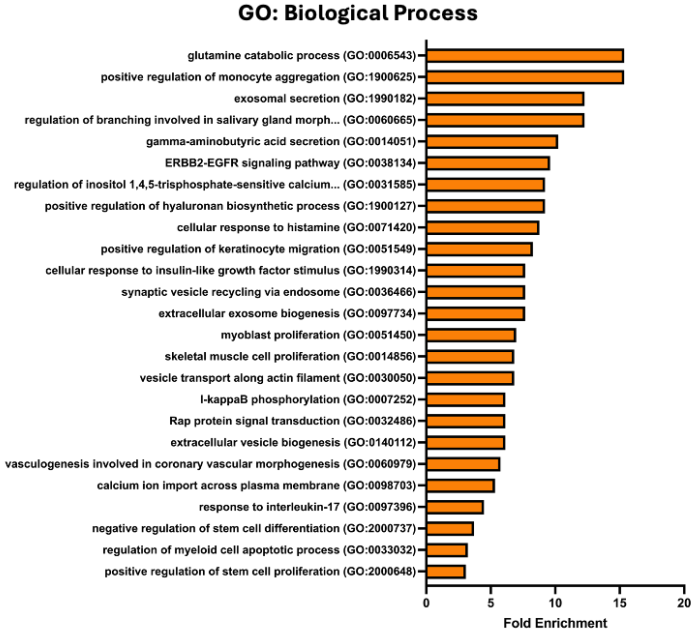
GO: Biological Process
glutamine catabolic process (GO:0006543)
positive regulation of monocyte aggregation (GO:1900625)
exosomal secretion (GO:1990182)
regulation of branching involved in salivary gland morph... (GO:0060665)
gamma-aminobutyric acid secretion (GO:0014051)
ERBB2-EGFR signaling pathway (GO:0038134)
regulation of inositol 1,4,5-trisphosphate-sensitive calcium... (GO:0031585)
positive regulation of hyaluronan biosynthetic process (GO:1900127)
cellular response to histamine (GO:0071420)
positive regulation of keratinocyte migration (GO:0051549)
cellular response to insulin-like growth factor stimulus (GO:1990314)
synaptic vesicle recycling via endosome (GO:0036466)
extracellular exosome biogenesis (GO:0097734)
myoblast proliferation (GO:0051450)
skeletal muscle cell proliferation (GO:0014856)
vesicle transport along actin filament (GO:0030050)
I-kappaB phosphorylation (GO:0007252)
Rap protein signal transduction (GO:0032486)
extracellular vesicle biogenesis (GO:0140112)
vasculogenesis involved in coronary vascular morphogenesis (GO:0060979)
calcium ion import across plasma membrane (GO:0098703)
response to interleukin-17 (GO:0097396)
negative regulation of stem cell differentiation (GO:2000737)
regulation of myeloid cell apoptotic process (GO:0033032)
positive regulation of stem cell proliferation (GO:2000648)
0
5
10
15
20
Fold Enrichment

C

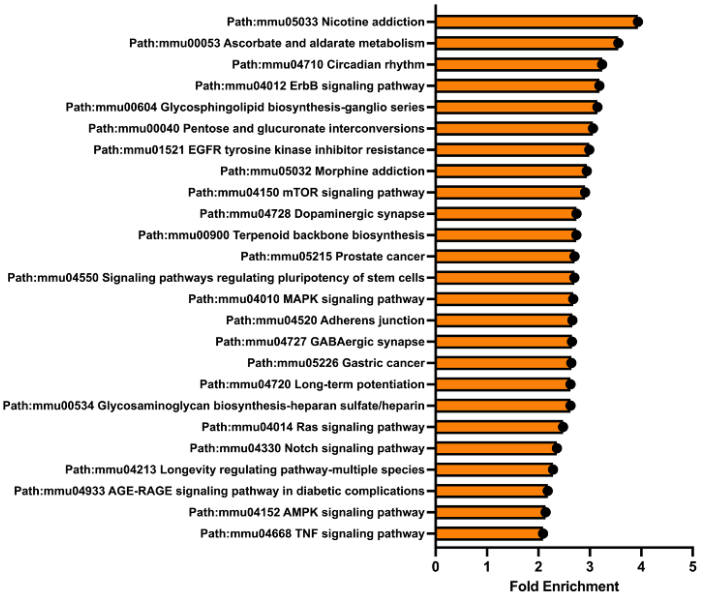
KEGG Pathway Analysis
Path:mmu05033 Nicotine addiction
Path:mmu00053 Ascorbate and aldarate metabolism
Path:mmu04710 Circadian rhythm
Path:mmu04012 ErbB signaling pathway
Path:mmu00604 Glycosphingolipid biosynthesis-ganglio series
Path:mmu00040 Pentose and glucuronate interconversions
Path:mmu01521 EGFR tyrosine kinase inhibitor resistance
Path:mmu05032 Morphine addiction
Path:mmu04150 mTOR signaling pathway
Path:mmu04728 Dopaminergic synapse
Path:mmu00900 Terpenoid backbone biosynthesis
Path:mmu05215 Prostate cancer
Path:mmu04550 Signaling pathways regulating pluripotency of stem cells
Path:mmu04010 MAPK signaling pathway
Path:mmu04520 Adherens junction
Path:mmu04727 GABAergic synapse
Path:mmu05226 Gastric cancer
Path:mmu04720 Long-term potentiation
Path:mmu00534 Glycosaminoglycan biosynthesis-heparan sulfate/heparin
Path:mmu04014 Ras signaling pathway
Path:mmu04330 Notch signaling pathway
Path:mmu04213 Longevity regulating pathway-multiple species
Path:mmu04933 AGE-RAGE signaling pathway in diabetic complications
Path:mmu04152 AMPK signaling pathway
Path:mmu04668 TNF signaling pathway
0
1
2
3
4
5
Fold Enrichment

Figure 34. Gene Ontology and KEGG Pathway Analysis of Putative Gene Targets of microRNA-126-3p in Mice. *(**A**) Venn diagram showing the overlapping putative gene targets for miRNA-126-3p using miRWalk, miRDB & TargetScan databases. Bar charts showing (**B**) the enriched GO terms for Biological Process, and (**C**) the KEGG Pathway Analysis from the overlapping mouse miRNA-126-3p gene target list. GO analysis was performed using a Fisher's Exact Test and the threshold for significance was set at Padj<0.05. For KEGG analysis, the threshold for significant pathways was set at Padj<0.05.*

The same analysis was applied to miRNA-320b using miRWalk, miRDB, and Target Scan (**Figure 35A**) to generate a single, deduplicated list of 820 putative targets. The targets were inputted into GO analysis to identify overrepresented terms associated with Biological Process (**Figure 35B**) and KEGG pathway analysis (**Figure 35C**). GO analysis identified enriched terms associated with heart development (Regulation of cardiac muscle cell proliferation GO:0060043 p=0.0042, Cardiac muscle tissue growth GO:0.0055017 p=0.0153, Heart growth GO:0060419 p=0.0221, and Ventricular septum morphogenesis GO:0060412 p=0.0458) and cell proliferation (Stem cell differentiation GO:0048863 p=0.00167, Positive regulation of cell population proliferation GO:0008284 p<0.0001).

Enriched KEGG pathways from this analysis included cancer (Glioma mmu05214 p<0.0001, Chronic myeloid leukaemia mmu05220 p<0.0001, Non-small cell lung cancer mmu05223 p<0.0001, and Renal cell carcinoma mmu05211 p=0.0023), and growth factor signalling (VEGF signalling pathway mmu04370 p=0.0076, EGFR tyrosine kinase inhibitor resistance mmu01521 p=0.0023, and Growth hormone

synthesis secretion and action mmu04935 p=0.0004) were also upregulated. The predicted role for miRNA-320b in growth factor signalling, cell proliferation and myocardial cell proliferation is highly relevant to the TNF-α EC-EV-HSC model and the most enriched gene targets and GO terms should be explored further.

A

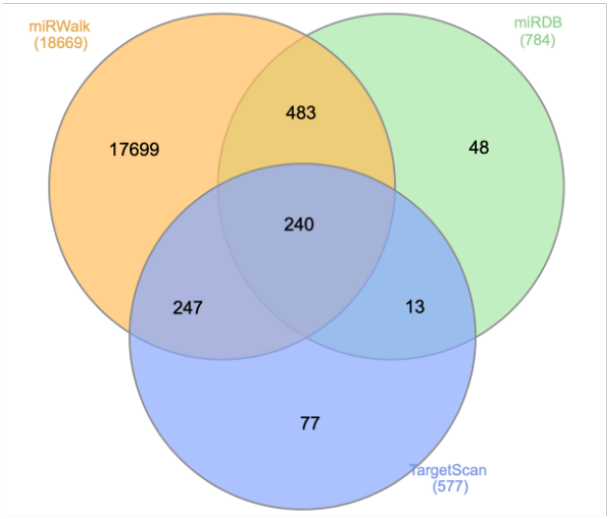
miRNA-320b Target Overlap
miRWalk
(18669)
miRDB
(784)
TargetScan
(577)
17699
483
48
240
247
13
77

B

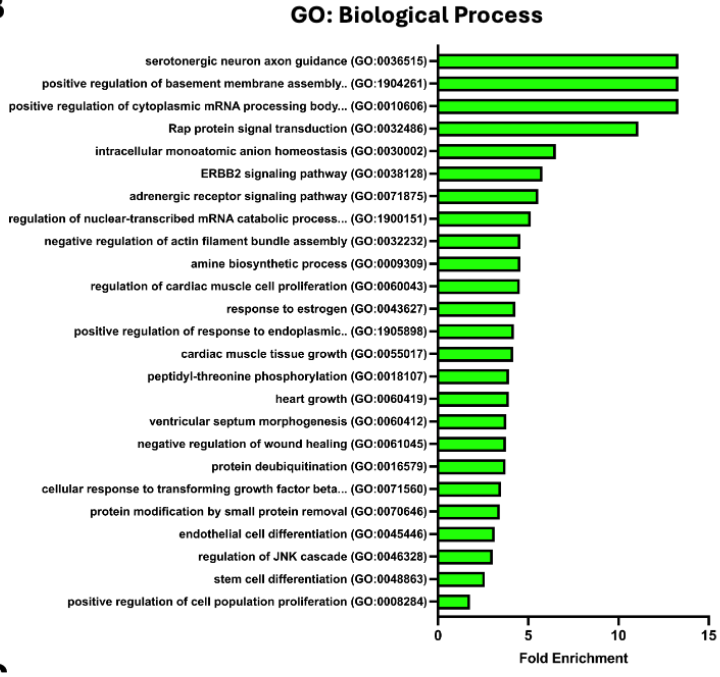
GO: Biological Process
serotonergic neuron axon guidance (GO:0036515)
positive regulation of basement membrane assembly.. (GO:1904261)
positive regulation of cytoplasmic mRNA processing body... (GO:0010606)
Rap protein signal transduction (GO:0032486)
intracellular monoatomic anion homeostasis (GO:0030002)
ERBB2 signaling pathway (GO:0038128)
adrenergic receptor signaling pathway (GO:0071875)
regulation of nuclear-transcribed mRNA catabolic process... (GO:1900151)
negative regulation of actin filament bundle assembly (GO:0032232)
amine biosynthetic process (GO:0009309)
regulation of cardiac muscle cell proliferation (GO:0060043)
response to estrogen (GO:0043627)
positive regulation of response to endoplasmic.. (GO:1905898)
cardiac muscle tissue growth (GO:0055017)
peptidyl-threonine phosphorylation (GO:0018107)
heart growth (GO:0060419)
ventricular septum morphogenesis (GO:0060412)
negative regulation of wound healing (GO:0061045)
protein deubiquitination (GO:0016579)
cellular response to transforming growth factor beta... (GO:0071560)
protein modification by small protein removal (GO:0070646)
endothelial cell differentiation (GO:0045446)
regulation of JNK cascade (GO:0046328)
stem cell differentiation (GO:0048863)
positive regulation of cell population proliferation (GO:0008284)
0
5
10
15
Fold Enrichment

C

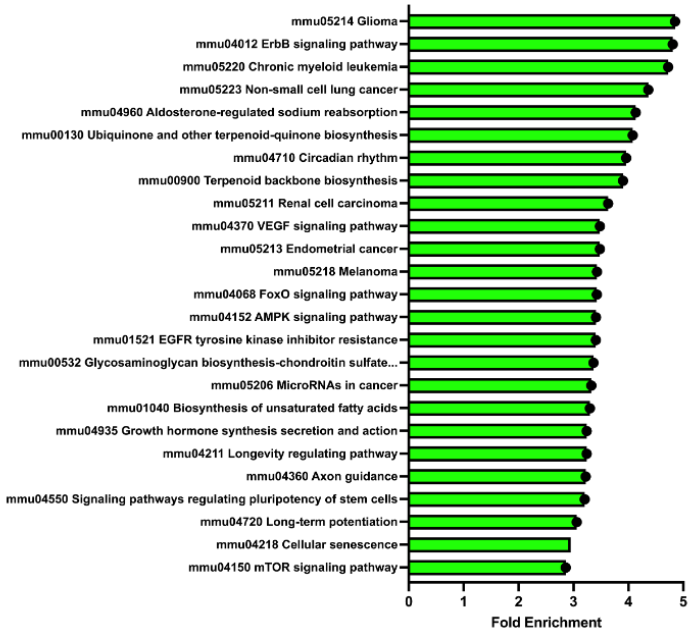
KEGG Pathway Analysis
mmu05214 Glioma
mmu04012 ErbB signaling pathway
mmu05220 Chronic myeloid leukemia
mmu05223 Non-small cell lung cancer
mmu04960 Aldosterone-regulated sodium reabsorption
mmu00130 Ubiquinone and other terpenoid-quinone biosynthesis
mmu04710 Circadian rhythm
mmu00900 Terpenoid backbone biosynthesis
mmu05211 Renal cell carcinoma
mmu04370 VEGF signaling pathway
mmu05213 Endometrial cancer
mmu05218 Melanoma
mmu04068 FoxO signaling pathway
mmu04152 AMPK signaling pathway
mmu01521 EGFR tyrosine kinase inhibitor resistance
mmu00532 Glycosaminoglycan biosynthesis-chondroitin sulfate...
mmu05206 MicroRNAs in cancer
mmu01040 Biosynthesis of unsaturated fatty acids
mmu04935 Growth hormone synthesis secretion and action
mmu04211 Longevity regulating pathway
mmu04360 Axon guidance
mmu04550 Signaling pathways regulating pluripotency of stem cells
mmu04720 Long-term potentiation
mmu04218 Cellular senescence
mmu04150 mTOR signaling pathway
0
1
2
3
4
5
Fold Enrichment

Figure 35. Gene Ontology and KEGG Pathway Analysis of Putative Gene Targets of microRNA-320b in Mice. *(**A**) Venn diagram showing the overlapping putative gene targets for miRNA-320b using miRWalk, miRDB & TargetScan databases. Bar charts showing (**B**) the enriched GO terms associated with Biological Processes, and (**C**) the KEGG Pathway analysis from the overlapping mouse miRNA-320b target list. GO analysis was performed using a Fisher's Exact Test and the threshold for significance was set at Padj<0.05. For KEGG analysis, the threshold for significant pathways was set at Padj<0.05.*

In order to better understand the potential role of EC-EV miRNA-mediated signalling in MI, the list of putative mRNA targets for miRNA-126-3p generated in **Figure 34A** and miRNA-320b generated in **Figure 35A** were compared to generate a single list of 180 gene targets (**Figure 36A**). Furthermore, enriched GO terms for Biological Process were compared between miRNA-126-3p (**Figure 34B**) and miRNA-320b (**Figure 35B**) to identify 281 overlapping GO terms for Biological Process which are overrepresented for both miRNAs (**Figure 36B**).

The most significant GO terms for Biological Process are shown in **Figure 36C**. GO terms for Molecular Function and Cellular Components were also assessed however returned only 1 significant result and were therefore not included. From the lists, GO terms relating to MAPK phosphorylation (regulation of MAPK cascade GO:0043408 p=0.005, positive regulation of MAPK cascade GO:0043410 p=0.043, protein phosphorylation GO:0006468 p=0.043), inflammatory cytokine signalling (IL-17-mediated signalling pathway GO:0097400 p=0.012, cellular response to Transforming Growth Factor beta stimulus GO:0071560 p=0.045), and macrophage function

(negative regulation of cell motility GO:2000146 $p<0.001$, negative regulation of cell migration GO:0030336 $p<0.001$) were enriched overlapping terms for both miRNA-126-3p and miRNA-320b.

Enriched KEGG pathways for both miRNA-126-3p and miRNA-320b putative targets were also compared (**Figure 36D**) and identify 75 KEGG pathways which were enriched for both miRNAs. The most enriched KEGG pathways are shown in **Figure 36E** and can be grouped into MAPK-Akt signalling (mTOR signalling pathway mmu04150 $p=0.030$, and MAPK signalling pathway mmu04010 $p=0.030$), inflammatory cytokine signalling (TGF-beta signalling pathway mmu04350 $p=0.066$, and IL-17 signalling pathway mmu04657 $p=0.171$), and HSPC proliferation (stem cell pluripotency regulation mmu04550 $p=0.022$, and chronic myeloid leukaemia mmu05220 $p=0.038$). The overrepresentation of terms associated with HSPC proliferation supports the hypothesis that miRNA-126-3p and miRNA-320b, which are enriched in TNF-α EC-EV, are responsible for modifying haematopoiesis in the bone marrow.

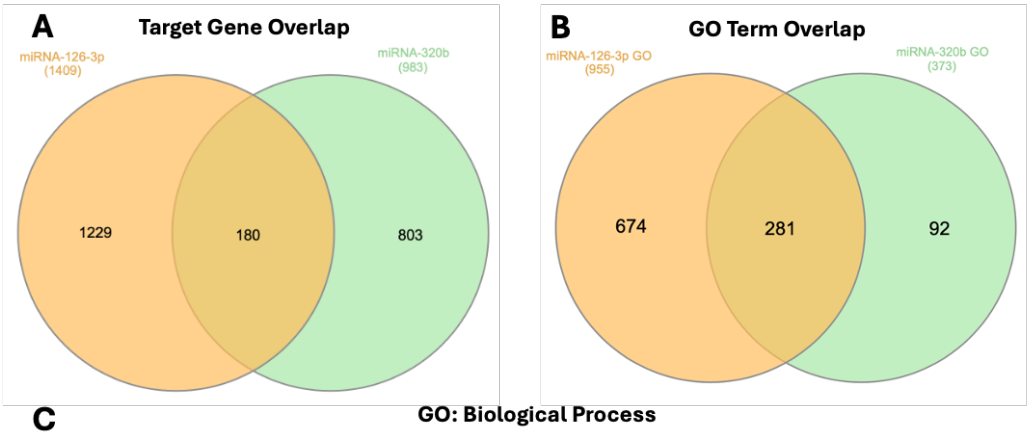
A
Target Gene Overlap
miRNA-126-3p
(1409)
miRNA-320b
(983)
1229
180
803
B
GO Term Overlap
miRNA-126-3p GO
(955)
miRNA-320b GO
(373)
674
281
92

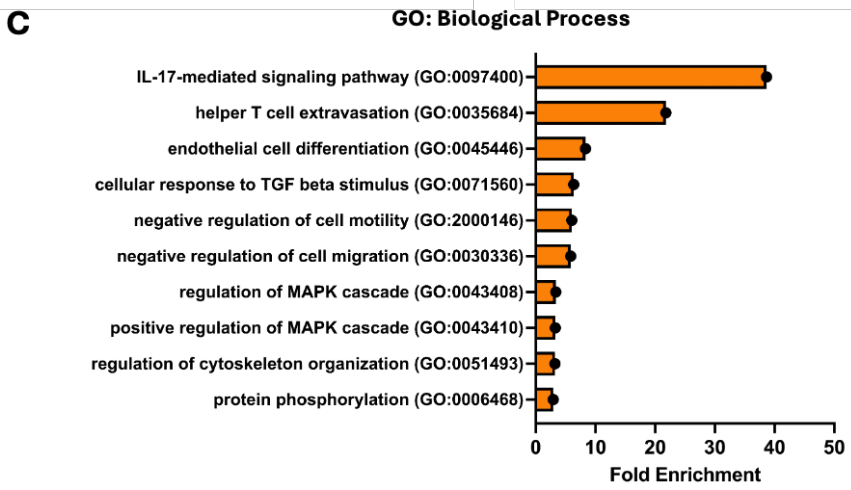
C
GO: Biological Process
IL-17-mediated signaling pathway (GO:0097400)
helper T cell extravasation (GO:0035684)
endothelial cell differentiation (GO:0045446)
cellular response to TGF beta stimulus (GO:0071560)
negative regulation of cell motility (GO:2000146)
negative regulation of cell migration (GO:0030336)
regulation of MAPK cascade (GO:0043408)
positive regulation of MAPK cascade (GO:0043410)
regulation of cytoskeleton organization (GO:0051493)
protein phosphorylation (GO:0006468)
0
10
20
30
40
50
Fold Enrichment

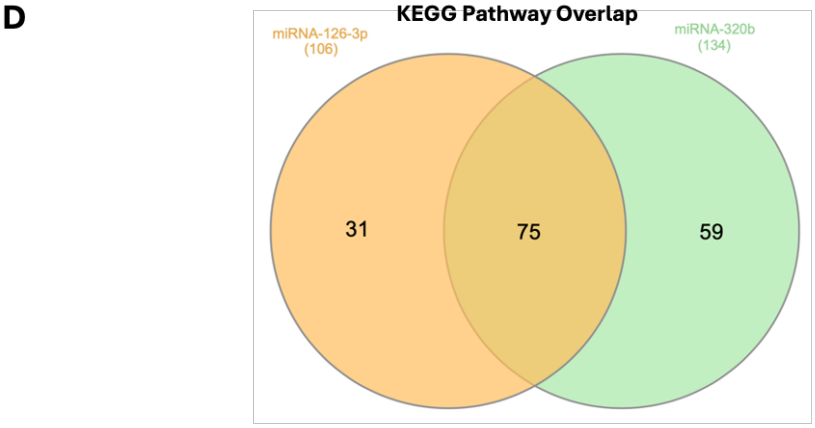
D
KEGG Pathway Overlap
miRNA-126-3p
(106)
miRNA-320b
(134)
31
75
59

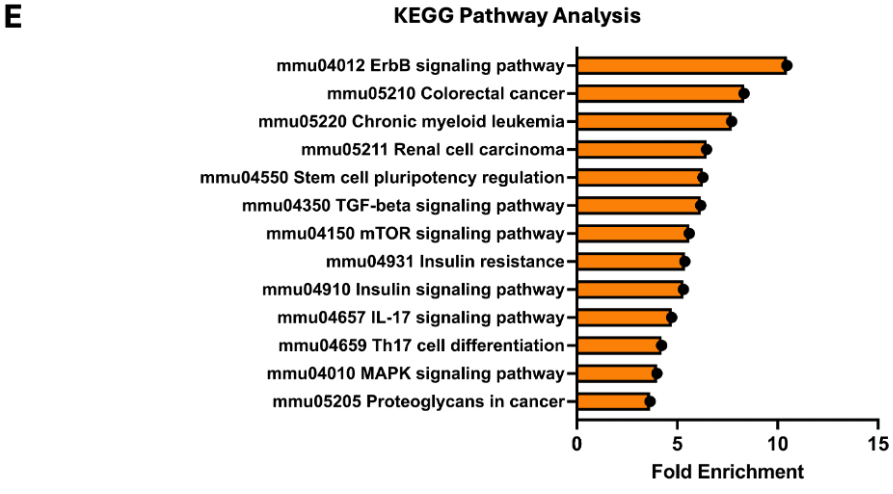
E
KEGG Pathway Analysis
mmu04012 ErbB signaling pathway
mmu05210 Colorectal cancer
mmu05220 Chronic myeloid leukemia
mmu05211 Renal cell carcinoma
mmu04550 Stem cell pluripotency regulation
mmu04350 TGF-beta signaling pathway
mmu04150 mTOR signaling pathway
mmu04931 Insulin resistance
mmu04910 Insulin signaling pathway
mmu04657 IL-17 signaling pathway
mmu04659 Th17 cell differentiation
mmu04010 MAPK signaling pathway
mmu05205 Proteoglycans in cancer
0
5
10
15
Fold Enrichment

Figure 36. Gene Ontology & KEGG Pathway Analysis of Putative Gene Targets of microRNA-126-3p & microRNA-320b in Mice. *(**A**) Venn diagram showing the overlapping putative gene targets for miRNA-126-3p and miRNA-320b using miRWalk, miRDB & TargetScan databases. (**B**) Venn diagram showing overlapping GO terms for Biological Process between mouse miRNA-126-3p and miRNA-320b-associated GO terms. (**C**) Bar chart showing the enriched GO terms for Biological Process from overlapping mouse miRNA-126-3p and miRNA-320b enriched terms. (**D**) Venn diagram showing overlapping KEGG pathways between mouse miRNA-126-3p and miRNA-320b enriched pathways. (**E**) Bar chart showing the KEGG pathway analysis from the overlapping mouse miRNA-126-3p and miRNA-320b enriched pathways. GO analysis was performed using a Fisher's Exact Test and the threshold for significance was set at Padj<0.05. For KEGG analysis, the threshold for significant pathways was set at Padj<0.05.*

Analysis of the overlapping enriched GO terms and KEGG pathways for miRNA-126-3p and miRNA-320b putative gene targets (**Figure 36**) highlighted some interesting pathways which may be regulated by these miRNAs, including Akt-MAPK signalling and cell motility. MAPK signalling appeared to be enriched in the bone marrow HSC transcriptomic analysis in response to TNF-α EC-EV treatment compared to control EC-EV. Due to the predicted role of miRNA-126-3p and miRNA-320b in regulating MAPK signalling, I hypothesised the transcriptional changes in bone marrow HSC may be mediated by miRNA-126-3p and miRNA-320b within TNF-α EC-EV. To test this hypothesis, the overlapping putative gene targets for miRNA-126-3p and miRNA-320b (generated in **Figure 36A**) were compared with the differentially enriched genes from

bone marrow HSC in response to TNF-α EC-EV (**Figure 27-29**). **Figure 37A** shows 28 differentially expressed genes in TNF-α EC-EV-treated bone marrow HSC overlap as putative targets for either miRNA-126-3p, miRNA-320b, or both. **Figure 37B** shows 8 overlapping GO terms which are overrepresented in bone marrow HSC exposed to TNF-α EC-EV, and either miRNA-126-3p or miRNA-320b. The 8 overlapping GO terms (**Figure 37B**) which were significantly enriched in bone marrow HSC were then identified (**Figure 37C**) and the most frequently upregulated genes across each of these GO terms was determined (**Figure 38A**). The 51 upregulated genes which were identified from the overrepresented GO terms were analysed using STRING network analysis to determine which genes cluster together and which molecular pathways these gene clusters are associated with (**Figure 38B**). The upregulated genes formed two main clusters: 43% of genes were associated with 'Cell cycle phase transition and mitotic spindle checkpoint' (red), and 20% of genes formed the 'MAPK activation and phosphatase activity' cluster (yellow). This data correlates with **Figure 30B** and indicates these two processes may be regulated by miRNA-126-3p and miRNA-320b signalling in bone marrow HSC.

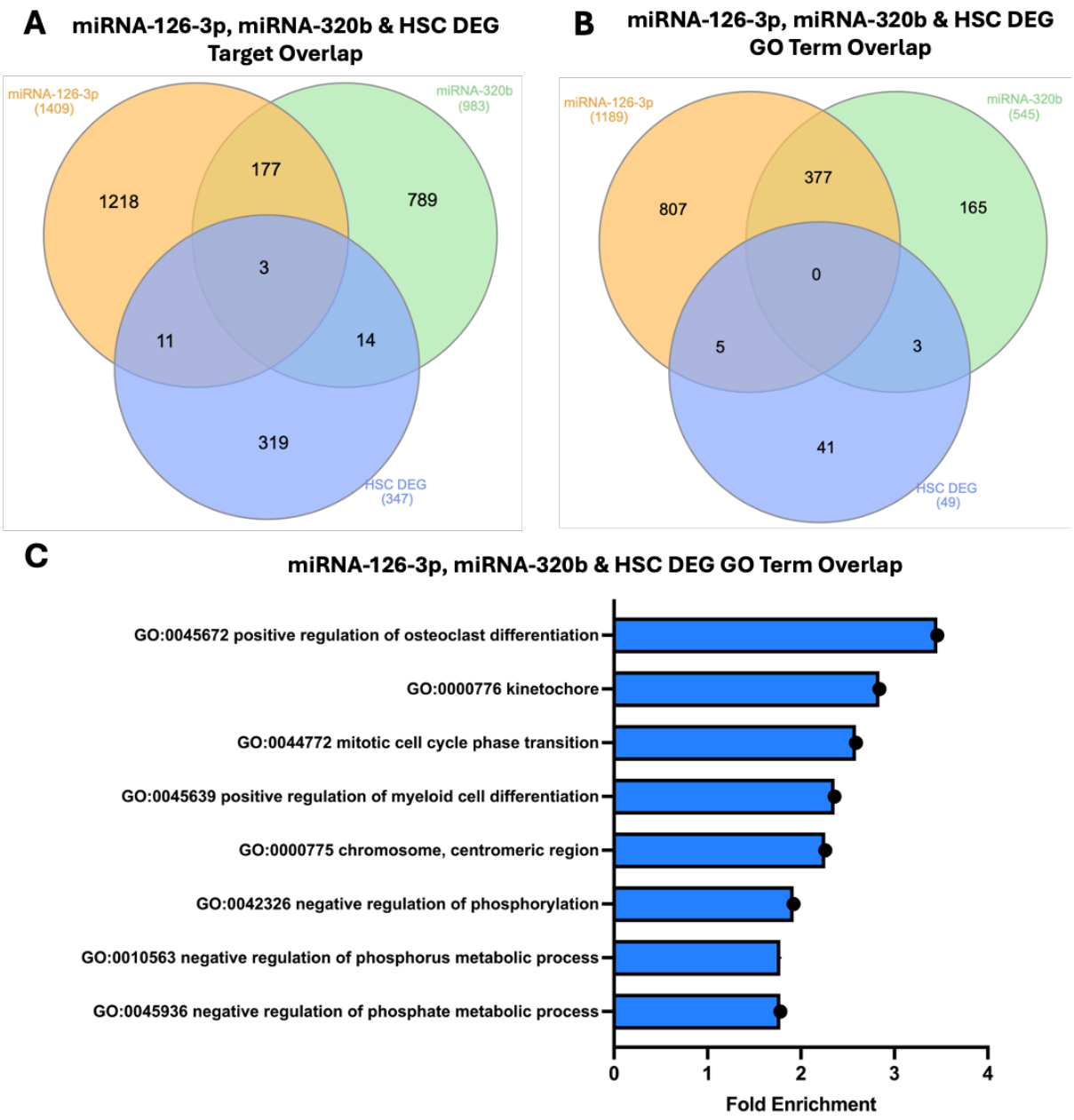

Figure 37. microRNA-126-3p and miRNA-320b Putative Gene Targets Overlap with Mouse Bone Marrow Haematopoietic Stem Cell Differentially Expressed Genes. *(**A**) Venn diagram showing the overlapping gene targets for mouse miRNA-126-3p, miRNA-320b, which were identified using miRWalk, miRDB & TargetScan databases, and differentially expressed genes from bone marrow HSC after treatment with control EC-EV or TNF-α EC-EV. (**B**) Venn diagram showing the overlapping Gene Ontology terms for Biological Process for miRNA-126-3p, miRNA-320b, and*

*differentially expressed genes from bone marrow HSC after treatment with control EC-EV or TNF-α EC-EV. (**C**) The 8 enriched Gene Ontology terms for Biological Process which overlap for differentially expressed genes from bone marrow HSC and either miRNA-126-3p and miRNA-320b. GO analysis was performed using a Fisher's Exact Test and the threshold for significance was set at Padj<0.05.*

A

Gene Name	% of Enriched GO Terms
Jun	75
Ccnb1	75
Dusp1	50
Ier3	50
Cdkn1c	50
Dusp2	38
Mad2l1	38
Pik3ip1	38
Dusp26	38
Plk2	38

B

Cluster Name	% of Genes in Cluster
Cell Cycle Phase Transition & Mitotic Spindle Checkpoint	43
MAPK Activation & Phosphatase	20
Granulocyte Activation	4

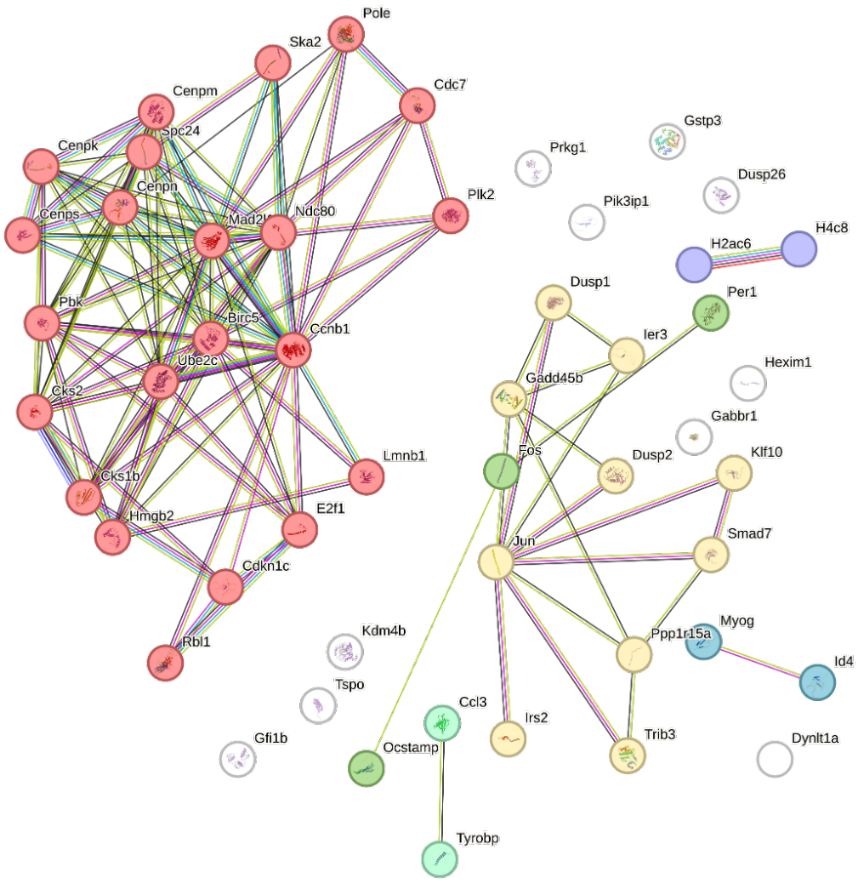

Figure 38. STRING Network Analysis of Overlapping Targets from microRNA-126-3p, microRNA-320b and Bone Marrow Haematopoietic Stem Cell Differentially Expressed Genes. *(**A**) Table showing the most common upregulated genes from the enriched GO terms identified in **Figure 37B**. 51 genes were upregulated in total. The cut-off threshold was 37% of significantly enriched GO terms. (**B**) Clustering analysis of the 51 upregulated genes identified in 8 enriched overlapping GO terms in (**A**) using STRING network analysis. Gene clusters were identified in STRING analysis using the Markov Cluster algorithm. GO analysis was performed using a Fisher's Exact Test and the threshold for significance was set at Padj<0.05.*

4.7 Discussion

MI has reprogramming effects on the bone marrow, which can modify haematopoiesis (82, 165) and induce downstream immune responses (57, 88, 89). Although studies have shown an elevation in plasma EV in response to MI (88, 89), they have not investigated a direct reprogramming effect of EC-EV on bone marrow HSPC in response to MI. Through RNA sequencing of bone marrow HSC and the assessment of miRNA cargo within EC-EV, this chapter found; (I) TNF-α EC-EV induces transcriptional changes in bone marrow HSC relative to control EC-EV, (II) miRNA-126-3p and miRNA-320b are enriched in TNF-α EC-EV, (III) miRNA-126-3p and miRNA-320b have overlapping putative targets associated with MAPK signalling and cell motility, and (IV) miRNA-126-3p and miRNA-320b putative targets overlap with differentially expressed genes in bone marrow HSC in response to TNF-α EC-EV exposure.

The RNA sequencing data highlights distinct transcriptional profiles in bone marrow HSC between TNF-α EC-EV and control EC-EV. Plastin1 (Pls1) expression was significantly enriched in the TNF-α EC-EV group (**Figure 27**) and has an important role in definitive haematopoiesis during embryonic development by acting as an actin-bundling protein (248). There is also evidence that Pls1 promotes the expression of matrix metalloproteinase 2 & 9, leading to increased migration of cells in colorectal cancer (249). This process is mediated by ERK1/2, a key component of the MAPK signalling cascade which is also significantly enriched in the GO term analysis of HSC in response to TNF-α EC-EV (**Figure 30B**). Matrix metalloproteinases including matrix metalloproteinase-9 (MMP-9) are established in remodelling the bone marrow and are crucial modulators of HSC migration and proliferation (250). MMP-9 knockout mice were shown to have restricted HSC motility and haematopoietic recovery as HSC are unable to migrate to repopulate bone marrow niches. Therefore, Pls1 may act as an important regulator of HSC motility by regulating MMP-9 expression. Future experiments should assess how the motility of HSC within the bone marrow changes in response to TNF-α EC-EV. This could be performed by imaging sections of the bone marrow at different timepoints post-injection with TNF-α EC-EV and using labelled HSC to track cell motility.

Dual-specificity phosphatase-1 (Dusp-1) were significantly downregulated in TNF-α EC-EV-treated HSC (**Figure 38A**) and is associated with the GO term MAP Kinase Phosphatase Activity (GO:0033549), the second most downregulated GO term in the HSC gene set enrichment analysis (**Figure 38B**). The HSC transcriptional analysis indicates that TNF-α EC-EV may mediate MAPK signalling activity through the downregulation of Pls1 and Dusp-1. Paternally expressed gene3 (Peg3) was also

significantly enriched in the TNF-α EC-EV group and one study found that Peg3 is regulated by anti-inflammatory bone marrow macrophage-EV in a model of glioma (251). Here, Peg3 inhibits tumour growth and tumour migration, and restoring Peg3 in mice led to increased cellular apoptosis. Therefore, Peg3 could be an important regulator of cellular mobilisation and proliferation in the bone marrow in response to TNF-α EC-EV which will require further study.

miRNA-126 is a well-studied endothelial cell-associated miRNA (144-146, 172) that regulates endothelial cell activation and suppresses the progression of atherosclerosis in mice (145). miRNA-126-3p is enriched in plasma EV following MI vs. 6 months post-injury (88). Similarly, studies in this chapter have shown miRNA-126-3p is enriched in TNF-α-stimulated EC-EV and have shown that this miRNA is partially protected from degradation by RNase A, which indicates the miRNA is intra-luminal. Further studies will need to be performed to understand why there was a partial degradation of the miRNAs in the presence of RNAse A and if some of the miRNA is present on the outer surface of the membrane. In the bone marrow, one investigation suggests miRNA-126 mobilises HSPC by downregulating VCAM-1 in bone marrow cells (233). Decreasing VCAM-1 in HSPC and neighbouring stromal and endothelial cells allows HSPC to be mobilised in response to granulocyte colony-stimulating factor and proliferate in haematopoiesis.

Given the roles of microvesicle-miRNA-126 already highlighted in the bone marrow to promote HSPC proliferation (233), and that miRNA-126-3p is enriched in plasma EV post-MI (88) and in TNF-α EC-EV (**Figure 32D**), further investigations should be conducted into the function of miRNA-126-3p within the bone marrow post-MI. The KEGG pathway analysis (**Figure 36E**) highlighted the regulation of stem cell

pluripotency (mmu04550) by miRNA-126-3p, which may corroborate the findings of previous studies. Furthermore, GO and KEGG pathway analysis highlighted MAPK (GO:0043408) and mTOR (mmu04150) signalling are targeted by both miRNA-126-3p and miRNA-320b (**Figure 36**). Akt-mTOR signalling promotes cell survival and proliferation (234, 235) and is activated through TLR4 signalling (79, 150). miRNA-320b targets PTEN, an inhibitor of Akt phospho-activation (234, 235), and therefore delivery of TNF-α EC-EV enriched in miRNA-320b cargo is likely to drive Akt-mTOR signalling further, leading to increased cell survival and the induction of proliferation. This hypothesis should be tested in future work, potentially through the delivery of a miRNA-320b mimic in liposomes into bone marrow HSC and by assessing changes in the rate of HSC proliferation. Furthermore, changes in phospho-kinase activity could be assessed to determine whether the transcriptomics analysis matches the phosphorylation changes that occur within bone marrow HSC.

The miRNA studies that were performed could be expanded to also investigate the role of miRNA-126-3p on TNF-α EC-EV signalling and whether miRNA-126-3p alone is sufficient to modify haematopoiesis in the bone marrow. If this is possible, it might allow for the fine-tuning of the innate immune response to MI as well as chronic inflammatory diseases such as diabetes (252) and obesity (79, 137). Therefore, it would be an attractive therapeutic target to pursue. Using the current model, HSC could first be treated with a miRNA-126 antagomir (88) and then treated with TNF-α EC-EV to determine the impact of specifically downregulating miRNA-126-3p on target cells. Combining this model with a MAPK phosphorylation array would also determine whether the *in silico* analysis performed on miRNA-126-3p is consistent and translates into the TNF-α EC-EV HSC model.

To conclude, this chapter has shown that TNF-α EC-EV induces transcriptional changes in bone marrow HSC, relative to control EC-EV. Through HSC transcriptomic sequencing, gene set enrichment analysis provided a powerful tool to identify overexpressed gene sets, including those associated with stem cell maintenance, the regulation of cell division, and of MAPK signalling. Overlap analysis between two miRNA of interest, miRNA-126-3p and miRNA-320b then identified 28 genes which are differentially enriched in HSC following TNF-α EC-EV exposure and therefore will be exciting targets to explore for their therapeutic potential in cardiovascular disease.

Chapter 5- Endothelial Cell-Extracellular Vesicles Modulate the Inflammatory Profile of Bone Marrow-derived Macrophages

5.1 Introduction

Following MI, cardiomyocyte cell death and hypoxia mediate the increased production and mobilisation of monocytes (16, 17, 29) to the infarct site from organs such as the bone marrow. Upon entering the infarct site, the initial monocytes differentiate towards a pro-inflammatory M1 phenotype, which is mediated by pro-inflammatory cytokine and chemokine signalling, and by an increase in TLR4-NF-κB signalling (25, 44). Furthermore, plasma EV mobilise splenic monocytes and mediate the reprogramming of monocytes prior to recruitment to the infarct site (29, 88). After the initial recruitment of pro-inflammatory monocytes, a second wave of monocytes are mobilised and recruited to the heart, where they differentiate into pro-reparative M2 macrophages (32, 46).

Macrophage differentiation into these two phenotypes involves morphological, functional, and phenotypic changes (253, 254) and is regulated by signalling pathways including Janus kinase (JAK) / Signal transducer and activator of transcription (STAT) and Akt-mTOR (255), with the latter forming part of a phosphorylation cascade with the transcription factor, NF-κB. In pro-inflammatory M1 macrophages, NF-κB phosphorylation increases which promotes NF-κB translocation into the nucleus and increases gene expression of inflammatory cytokines such as *tnf, il6,* and *il1β* (256). There is also a metabolic switch in M1 pro-inflammatory macrophages to favour glycolysis through increased expression of *hypoxia-inducible factor 1-α* (*hif1-α*) and

glycolytic enzymes including *glyceraldehyde 3-phosphate dehydrogenase (gapdh)* (254). Phenotypically, M1-polarised macrophages have increased cellular adhesion due to an increased abundance of integrin receptors on the cell surface, which facilitates the anchoring of macrophages to endothelial cells expressing VCAM-1 and ICAM-1 (257).

In addition to undergoing transcriptional and metabolic changes in response to stimuli, monocytes and macrophages possess an innate immune 'memory', where cells respond differently to repeated stimulations compared to naïve cells (258, 259). For example, repeated β-glucan exposure yields an exaggerated immune response, known as trained immunity, whereas multiple exposures to LPS dampens the immune response, known as tolerance. Chronic inflammatory diseases such as prolonged hyperglycaemia also induce reprogramming in monocytes and these effects are conserved after the cells return to a normoglycaemic environment (252). Several studies have shown that an MI primes the bone marrow and promotes worse breast cancer outcomes in patients (87), and drives cardiac dysfunction and fibrosis in naïve mice that receive a bone marrow transplant from post-MI mice (83). Each case mentioned has a distinct transcriptional and phenotypic profile but is mediated by pro-inflammatory M1 macrophages derived from the bone marrow that undergo long-term transcriptional changes in response to an initial MI stimulus.

However, it is not currently known whether macrophages in the bone marrow can be primed by MI through EV from activated endothelial cells, and how this process occurs mechanistically. Previous work that established plasma EV-mediated monocyte mobilisation from the spleen but not the bone marrow also raises questions over the effect on monocytes in the bone marrow. Therefore, this chapter hypothesises that

EC-EV from TNF-α-stimulated endothelial cells reprogramme BMDM to modify the inflammatory profile of macrophages, including changes in cytokine expression and secretion, changes in MAPK phosphorylation signalling, and changes in cell adhesion.

5.2 List of Methods Used in This Chapter

- *2.1 Media Preparations*
- *2.2 Endothelial Cell Culture*
- *2.3 Extracellular Vesicle Isolation Using Ultracentrifugation*
- *2.4 Extracellular Vesicle Characterisation*
- *2.9 Protein Analysis by Enzyme-Linked Immunosorbent Assay (ELISA)*
- *2.13 Gene Expression Analysis by RT-qPCR*
- *2.16 Isolation and Culturing of Bone Marrow Cells to Generate Bone Marrow-Derived Macrophages*
- *2.17 Bone Marrow-Derived Macrophage Characterisation Using Flow Cytometry*
- *2.18 Bone Marrow-Derived Macrophage In Vitro Tolerance Model*
- *2.19 Static Adhesion Assay to Assess Bone Marrow-Derived Macrophages*
- *2.20 Isolation & Culturing of Peritoneal Macrophages for Protein Studies*
- *2.21 Generating Denatured Endothelial Cell-Extracellular Vesicles*
- *2.22 Human Monocyte-Derived Macrophage In Vitro Tolerance Model*
- *2.23 Statistical Analysis*

5.3 Characterisation of Mouse Bone Marrow-Derived Macrophages

Mouse BMDM were generated *in vitro* following isolation and culture of primary bone marrow cells (**Method 2.16**) (**Figure 39A**). BMDM were analysed by flow cytometry to confirm their macrophage characteristics (**Figure 39B**). Macrophages were positive for the pan-haematopoietic marker, CD45, the pan-myeloid marker, CD11b, and the macrophage marker, F4/80, which confirmed the macrophages had a sample purity of ~93.6%.

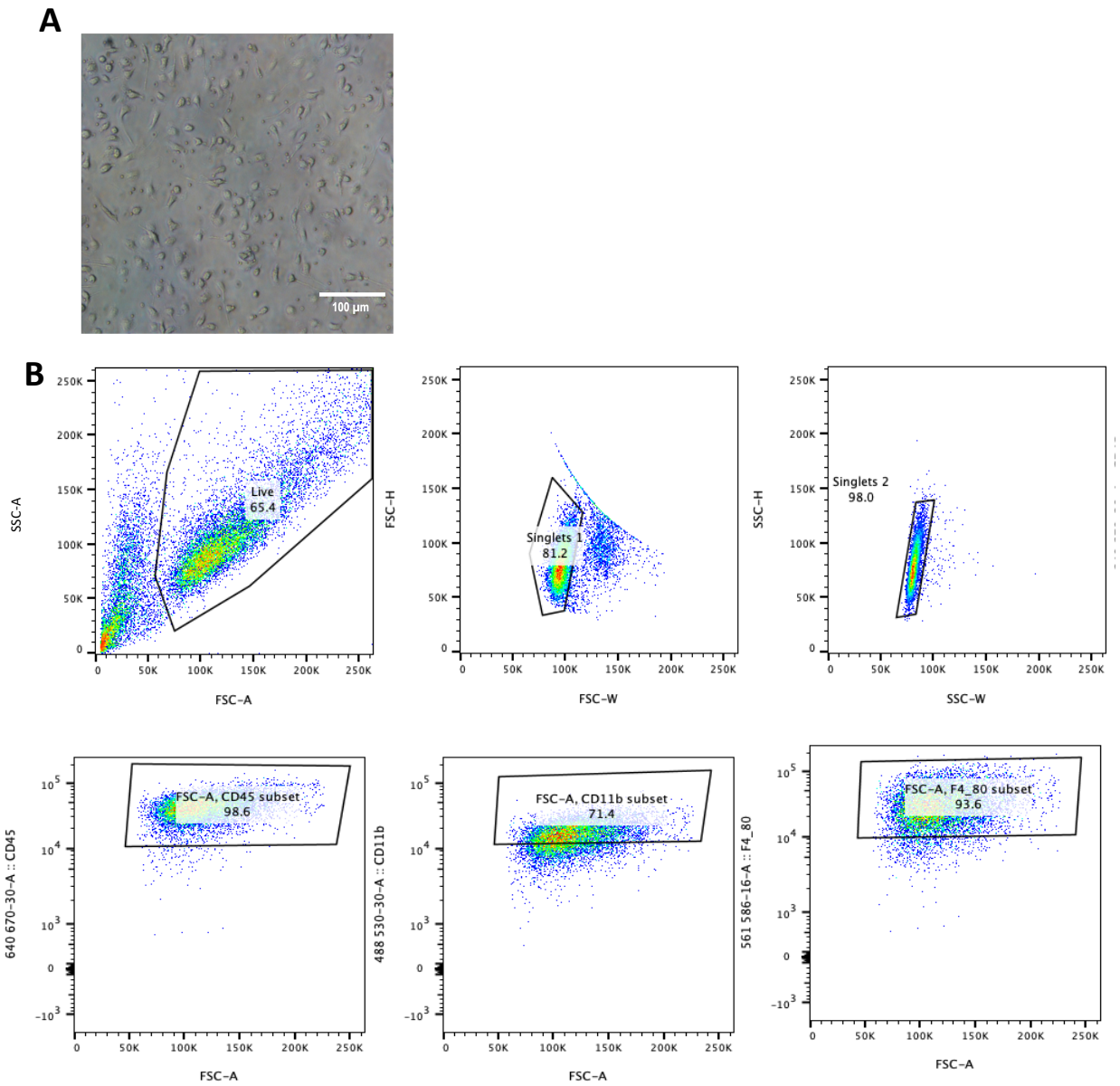

Figure 39. Characterisation of Mouse Bone Marrow-Derived Macrophages. *(**A**) Brightfield microscopy image of BMDM (10x magnification, scale bar 100 μm). (**B**) Flow cytometry plots showing the gating strategy for BMDM characterisation using CD45 (left), CD11b (centre) and F4/80 (right). n = 4. n = Number of replicates.*

5.4 Endothelial Cell-Extracellular Vesicles Induce a Tolerance Phenotype in Pro-Inflammatory Bone Marrow-Derived Macrophages

Studies in the literature show that macrophages have different states depending on the stimuli they receive (258, 259). Innate immune memory contributes to this phenotype and can promote an exaggerated immune response (trained immunity) or a lower immune response (tolerance) depending on the stimulus (258). To optimise a model of trained immunity and tolerance, the inflammatory cytokine response of BMDM was analysed following exposure to either vehicle-control, LPS (100 ng / mL), β-glucan (10 μg / mL), hyperglycaemia (20 mM) or the osmotic control (5 mM glucose + 15 mM mannitol), followed by treatment with M1-polarising agents LPS and IFN-γ (**Figure 40A**). The data showed LPS ($p<0.0001$) or hyperglycaemia ($p<0.05$) priming lowered TNF-α secretion from BMDM whilst β-glucan ($p<0.05$) priming elevated TNF-α relative to the vehicle-control group. The tolerance response of BMDM to LPS and the trained immunity response to β-glucan stimulation aligns with findings from the literature and therefore validate the BMDM model is functional for further trained immunity and tolerance studies (260-262).

To test whether EC-EV modify the inflammatory cytokine response in BMDM, macrophages were exposed to either vehicle-control, LPS, control EC-EV or TNF-α

EC-EV for 18 hours, were rested for 24 hours and then were treated with LPS and IFN-γ as M1-polarising agents for 18 hours (**Figure 40B**). TNF-α protein cytokine secretion from BMDM decreased following priming with TNF-α EC-EV ($p<0.001$, **Figure 40C**), but control EC-EV priming did not affect TNF-α secretion relative to the vehicle-control. LPS priming also decreased TNF-α secretion in BMDM and acted as a control since repeated LPS exposure is known to induce immune cell tolerance in macrophages (258, 263). This data indicates the macrophage response to EC-EV was dependent on the EV being derived from a pro-inflammatory environment.

Gene expression analysis was then performed on the same BMDM primed with vehicle-control, LPS, control EC-EV, or TNF-α EC-EV for 18 hours, rested for 24 hours and then treated with LPS and IFN-γ for 18 hours (**Figure 40D-F**). TNF-α EC-EV increased *tnf* ($p<0.05$) in macrophages relative to control EC-EV and there was no significant difference in the M2-associated macrophage markers *ym1* or *nos2 (264, 265)*. The differences between *tnf* gene expression and the TNF-α protein secretion response to TNF-α EC-EV priming suggests *tnf* is being regulated at the post-transcriptional or post-translational level, prior to secretion.

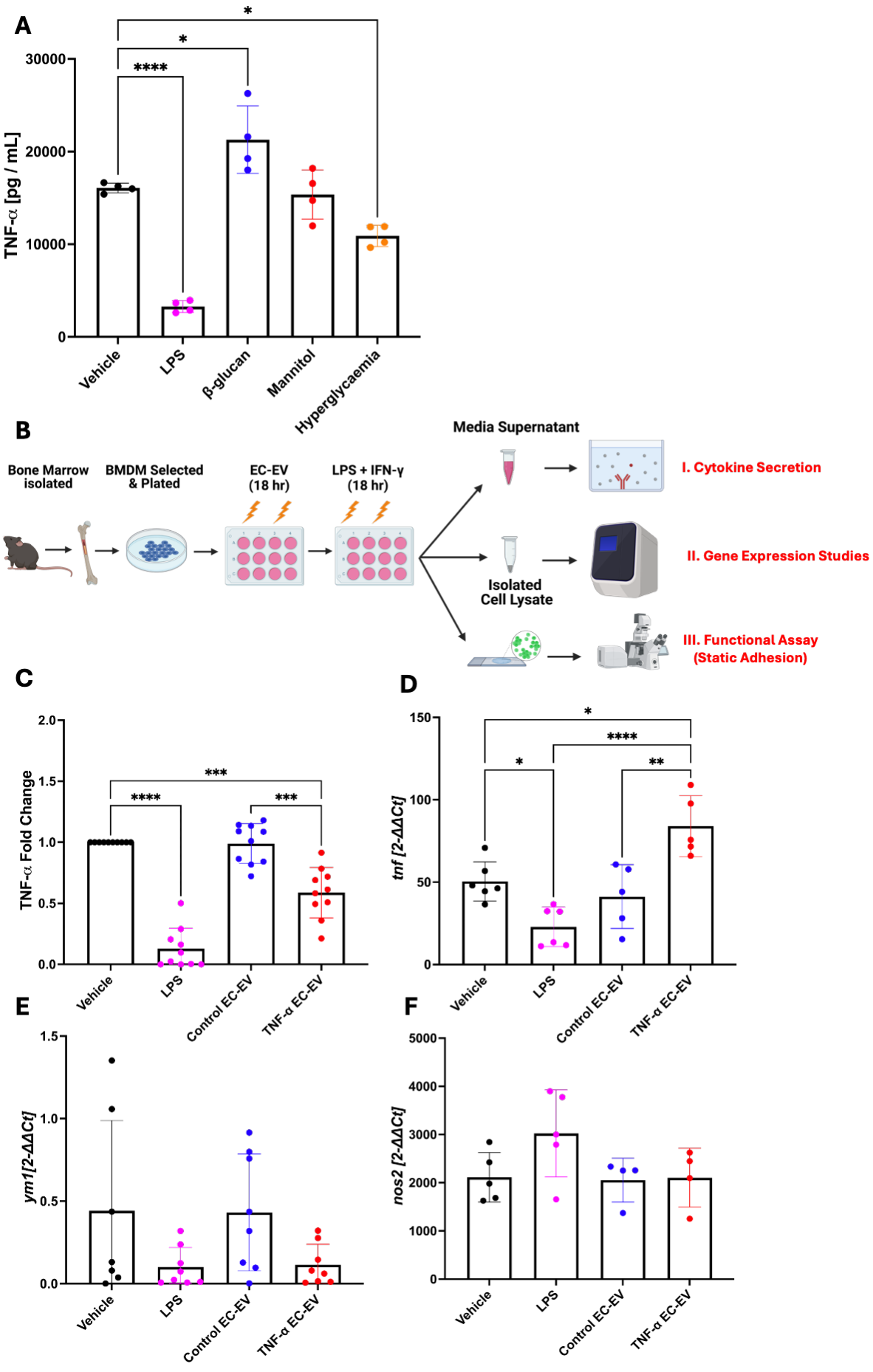
A
TNF-α [pg / mL]
30000
20000
10000
0
Vehicle
LPS
β-glucan
Mannitol
Hyperglycaemia
B
Bone Marrow isolated
BMDM Selected & Plated
EC-EV (18 hr)
LPS + IFN-γ (18 hr)
Media Supernatant
I. Cytokine Secretion
II. Gene Expression Studies
Isolated Cell Lysate
III. Functional Assay (Static Adhesion)
C
TNF-α Fold Change
2.0
1.5
1.0
0.5
0.0
Vehicle
LPS
Control EC-EV
TNF-α EC-EV
D
tnf [2-ΔΔCt]
150
100
50
0
E
ym1[2-ΔΔCt]
F
nos2 [2-ΔΔCt]
5000
4000
3000
2000
1000

Figure 40. Mouse Bone Marrow-Derived Macrophages Have a Modified Inflammatory Response to TNF-α Endothelial Cell-Extracellular Vesicles. *(**A**) TNF-α protein secretion in cell culture supernatants by BMDM exposed to vehicle-control (sterile PBS), LPS (100 ng / mL), β-glucan (10 μg / mL), mannitol (15 mM) or hyperglycaemia (20 mM glucose) for 18 hours followed by treatment with LPS (100 ng / mL) and IFN-γ (10 ng / mL) for 18 hours (n = 4 per group). (**B**) Schematic overview of the BMDM-EC-EV priming experiment. (**C**) TNF-α protein secretion in cell culture supernatants by BMDM exposed to vehicle-control (sterile PBS), LPS (100 ng / mL), control EC-EV (1 x 10^9 particles) or TNF-α EC-EV (1 x 10^9 particles) for 18 hours before treatment with LPS (100 ng / mL) and IFN-γ (10 ng / mL) for 18 hours (n = 10 per group). mRNA expression changes for (**D**) tnf, (**E**) ym1, and (**F**) nos2 in BMDM exposed to vehicle-control (sterile PBS), LPS (100 ng / mL), control EC-EV (1 x 10^9 particles) or TNF-α EC-EV (1 x 10^9 particles) followed by treatment with LPS (100 ng / mL) and IFN-γ (10 ng / mL) for 18 hours (n = 4 per group). RT-qPCR values are normalised to cyclophilin. n = Number of replicates. Data are reported as mean $\pm$ standard deviation. A Shapiro-Wilk test was used to determine data normality (α = 0.05, p<0.05), and a Grubbs test was used to identify outliers (α = 0.05). Data was parametric and one-way ANOVA with Bonferroni post-hoc correction was used to determine the statistical significance of differences between the groups. Significance is represented on the graph by *p<0.05, **p<0.01, ***p<0.001 or ****p<0.0001.*

Macrophages constitutively produce *tnf* mRNA, which is stabilised and translated through post-transcriptional modifications in response to pro-inflammatory signals mediated by TLR4 (266). Studies elsewhere indicate macrophages have the capacity

to store inflammatory cytokine proteins in the inactive precursor state within the Golgi network (267). Therefore, it was hypothesised that inflammatory cytokine production may not directly equate to secretion from the cell and that TNF-α may be stored within BMDM exposed to TNF-α EC-EV. To test this, the cell lysate was assessed for TNF-α after BMDM were primed with vehicle-control, LPS, control EC-EV, or TNF-α EC-EV, were rested for 24 hours and then were treated with LPS and IFN-γ for 18 hours (**Figure 41**). As shown in **Figure 40**, TNF-α secretion decreased following exposure to TNF-α EC-EV ($p<0.01$, **Figure 41A**) compared to control EC-EV. Cell lysate analysis showed a decrease in TNF-α at 1 hour (**Figure 41C**) and 18 hours ($p<0.01$, **Figure 41D**) of LPS-IFN-γ treatment. This suggests inflammatory cytokines are not stored within macrophages in response to TNF-α EC-EV and therefore disproves this hypothesis.

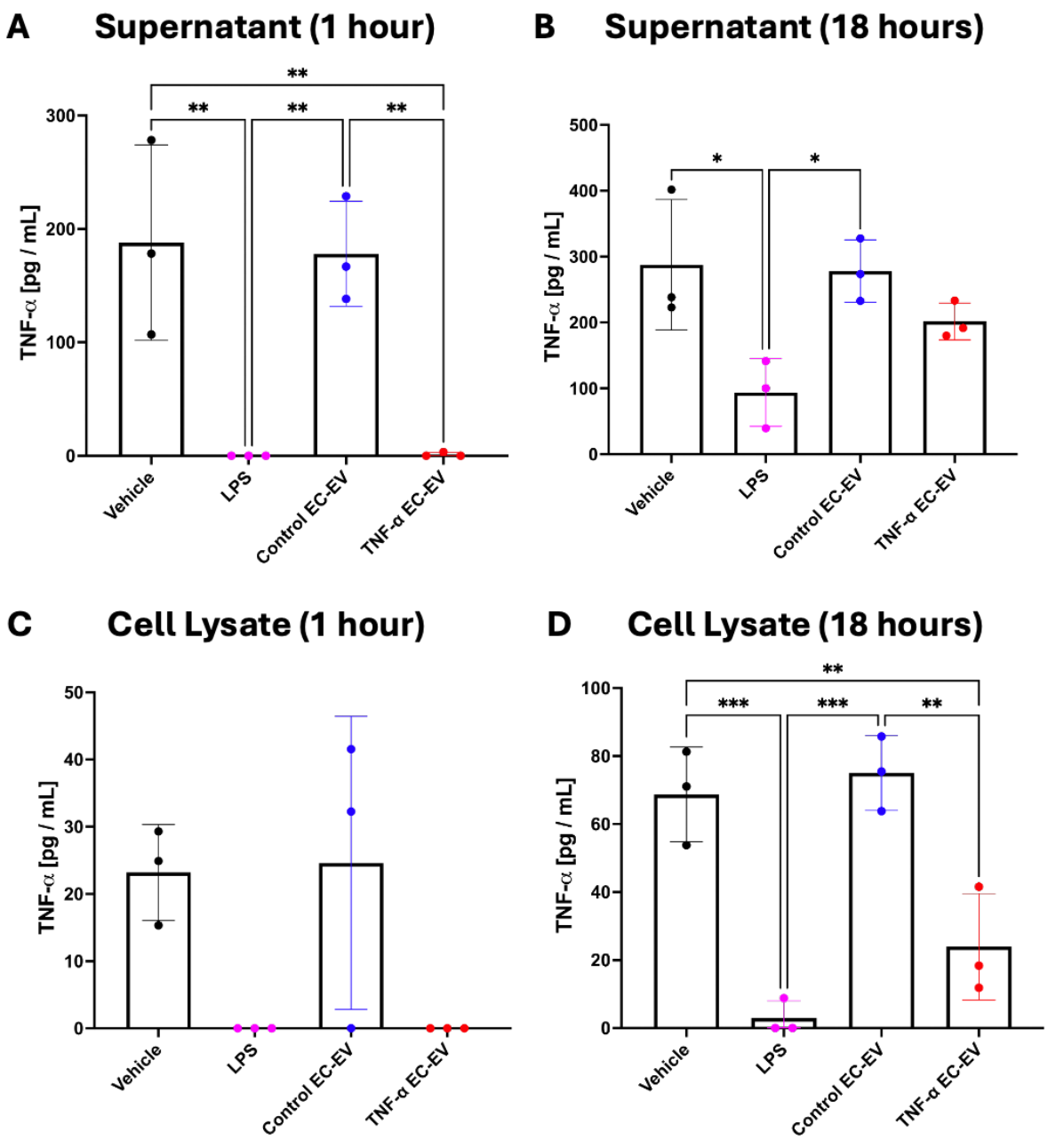

Figure 41. Pro-inflammatory Cytokines Are Not Stored Within Bone Marrow-Derived Macrophages in Response to TNF-α Endothelial Cell-Extracellular Vesicles. *TNF-α protein secreted by BMDM following priming with vehicle-control (sterile PBS), LPS (100 ng / mL), control EC-EV (1 x 10^9 particles) or TNF-α EC-EV (1 x 10^9 particles) for 18 hours before treatment with LPS (100 ng / mL) and IFN-γ (10 ng / mL) for (**A**) 1 hour, or (**B**) 18 hours. TNF-α protein was also assessed in BMDM*

*cell lysates after (**C**) 1 hour and (**D**) 18 hours. (n = 3 per group). n = Number of replicates. Data are reported as mean ± standard deviation. A Shapiro-Wilk test was used to determine data normality (α = 0.05, p<0.05), and a Grubbs test was used to identify outliers (α = 0.05). Data was parametric and one-way ANOVA with Bonferroni post-hoc correction was used to determine the statistical significance of differences between the groups. Significance is represented on the graph by *p<0.05, **p<0.01, or ***p<0.001.*

Functional changes in BMDM were then assessed using a static adhesion assay to determine whether the transcriptional changes in response to TNF-α EC-EV priming translate into changes in macrophage function. The ability of macrophages to adhere to a monolayer of sEND.1 endothelial cells, which were activated through TNF-α stimulation for 18 hours, was assessed by priming BMDM with vehicle-control, LPS, control EC-EV, or TNF-α EC-EV for 18 hours, resting cells for 24 hours, and then treating cells with LPS and IFN-γ for 18 hours. **Figure 42** showed that BMDM primed with TNF-α EC-EV adhered less (p<0.0001) to activated endothelial cells relative to the control EC-EV. This corroborates with the inflammatory cytokine secretion data (**Figure 40C**) that the pro-inflammatory profile of BMDM is suppressed following priming with TNF-α EC-EV and supports findings from the literature that cells in the bone marrow have reduced cell adhesion in response to EV (96).

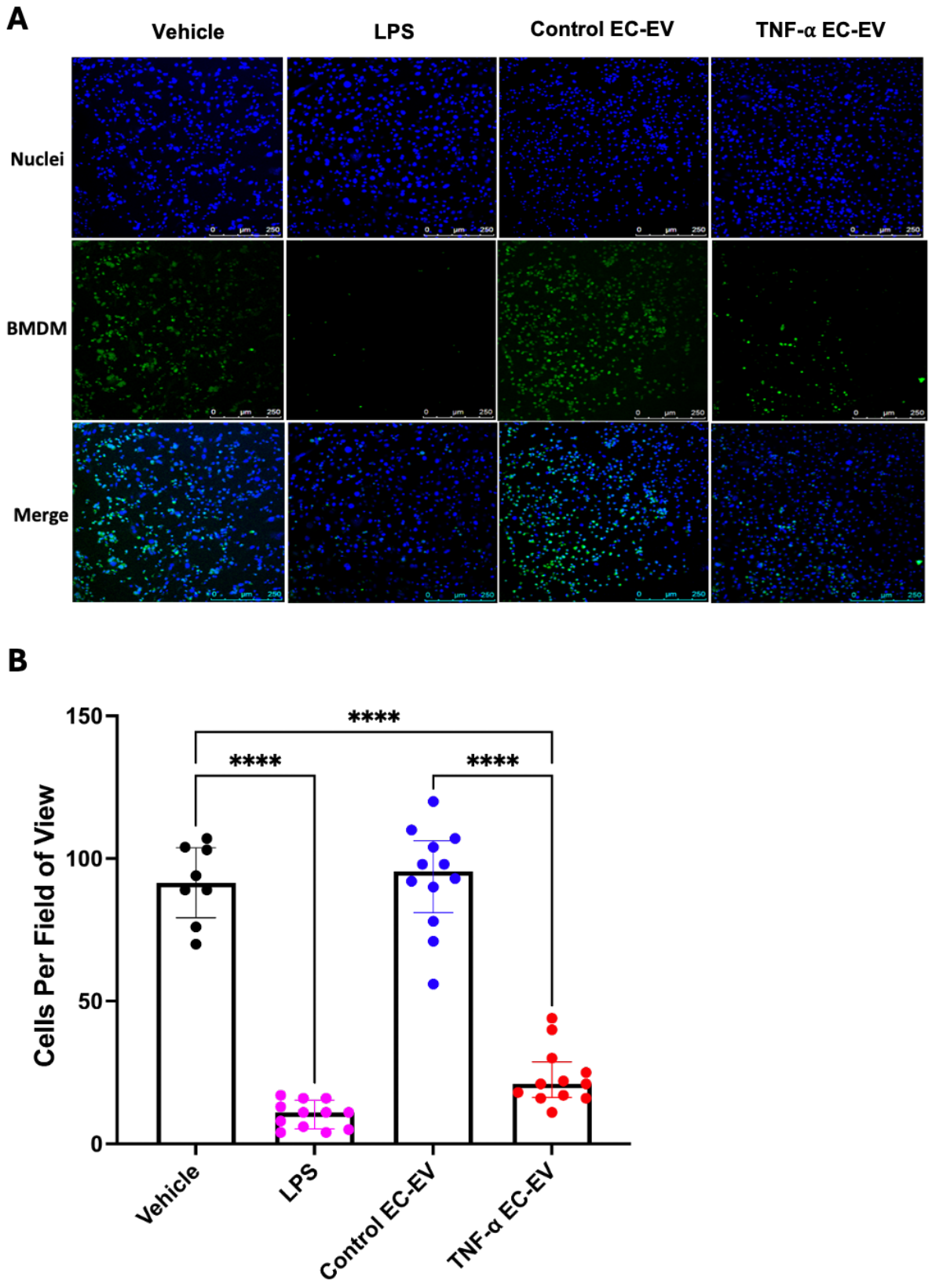
A
Vehicle
LPS
Control EC-EV
TNF-α EC-EV
Nuclei
BMDM
Merge
B
Cells Per Field of View
150
100
50
0
****
****
****
Vehicle
LPS
Control EC-EV
TNF-α EC-EV

Figure 42. TNF-α Endothelial Cell-Extracellular Vesicles Lower Macrophage Adhesion to Activated Endothelial Cell Monolayers. *(**A**) Representative images from static adhesion assay representing nuclei staining (DAPI / Blue), BMDM (FITC / Green) and Merge. (**B**) Macrophage adhesion to TNF-α-activated endothelial cell monolayers in BMDM primed with vehicle-control (sterile PBS), LPS (100 ng / mL), control EC-EV (1 x 10^9 particles) or TNF-α EC-EV (1 x 10^9 particles) for 18 hours before treatment with LPS (100 ng / mL) and IFN-γ (10 ng / mL) for 18 hours (n = 8-12). n = Number of replicates. Data are reported as median and interquartile ranges. A Shapiro-Wilk test was used to determine data normality (α = 0.05, p<0.05), and a Grubbs test was used to identify outliers (α = 0.05). Data was non-parametric and a Kruskal-Wallis test with Dunn's post-hoc correction analysis was used to determine statistical significance of differences between the groups. Significance is represented on the graph by ****p<0.0001.*

5.5 The Endothelial Cell-Extracellular Vesicle Bone Marrow-Derived Macrophage Tolerance Phenotype is Conserved Between Mouse and Human Models

To better understand the immune cell tolerance phenotype of TNF-α EC-EV on BMDM and the translatability of this model, a human monocyte-derived macrophage (MDM) model was established using PBMC from healthy volunteers. Macrophages were primed with vehicle-control, control EC-EV or TNF-α EC-EV for 18 hours, were rested for 24 hours and then were treated with LPS and IFN-γ for either 6 hours or 18 hours (**Figure 43**). The additional 6-hour timepoint was used to capture earlier spikes that may occur in inflammatory cytokine gene expression and secretion.

TNF-α secretion at 6 hours was lower in MDM exposed to TNF-α EC-EV ($p<0.0001$, **Figure 43A**) compared to control EC-EV, and this observation was also found in TNF-α EC-EV MDM at the 18-hour timepoint ($p<0.0001$, **Figure 43B**). For IL-6, lower levels of secretion were detected at 6 hours (**Figure 43C**) compared to 18 hours (**Figure 43D**). There were no significant differences in IL-6 secretion across all groups at 6 hours (**Figure 43C**). TNF-α EC-EV priming lowered TNF-α secretion from MDM at 18 hours compared to control EC-EV ($p<0.0001$, **Figure 43D**).

Gene expression analysis of *tnf* at 6 hours (**Figure 43E**) showed an increase in expression in TNF-α EC-EV-primed MDM compared to control EC-EV ($p<0.05$). *tnf* expression was significantly elevated in control EC-EV-primed MDM compared to the M1 (LPS and IFN-γ) group ($p<0.05$). At 18 hours, *tnf* expression was also significantly higher in TNF-α EC-EV-primed MDM compared to control EC-EV-primed MDM ($p<0.05$, **Figure 43F**). These data corroborate the findings from the mouse BMDM model (**Figure 40D**) and suggests the effects of TNF-α EC-EV may be consistent across the mouse and human macrophage models. *il6* expression also increased in TNF-α EC-EV-primed MDM at 6 hours compared with the control EC-EV group ($p<0.001$, **Figure 43G**), although there were no significant differences in *il6* expression at 18 hours between the TNF-α EC-EV and control EC-EV groups (**Figure 43H**). Combined, these data suggest the mouse BMDM and human MDM models respond comparably to TNF-α EC-EV priming *in vitro*.

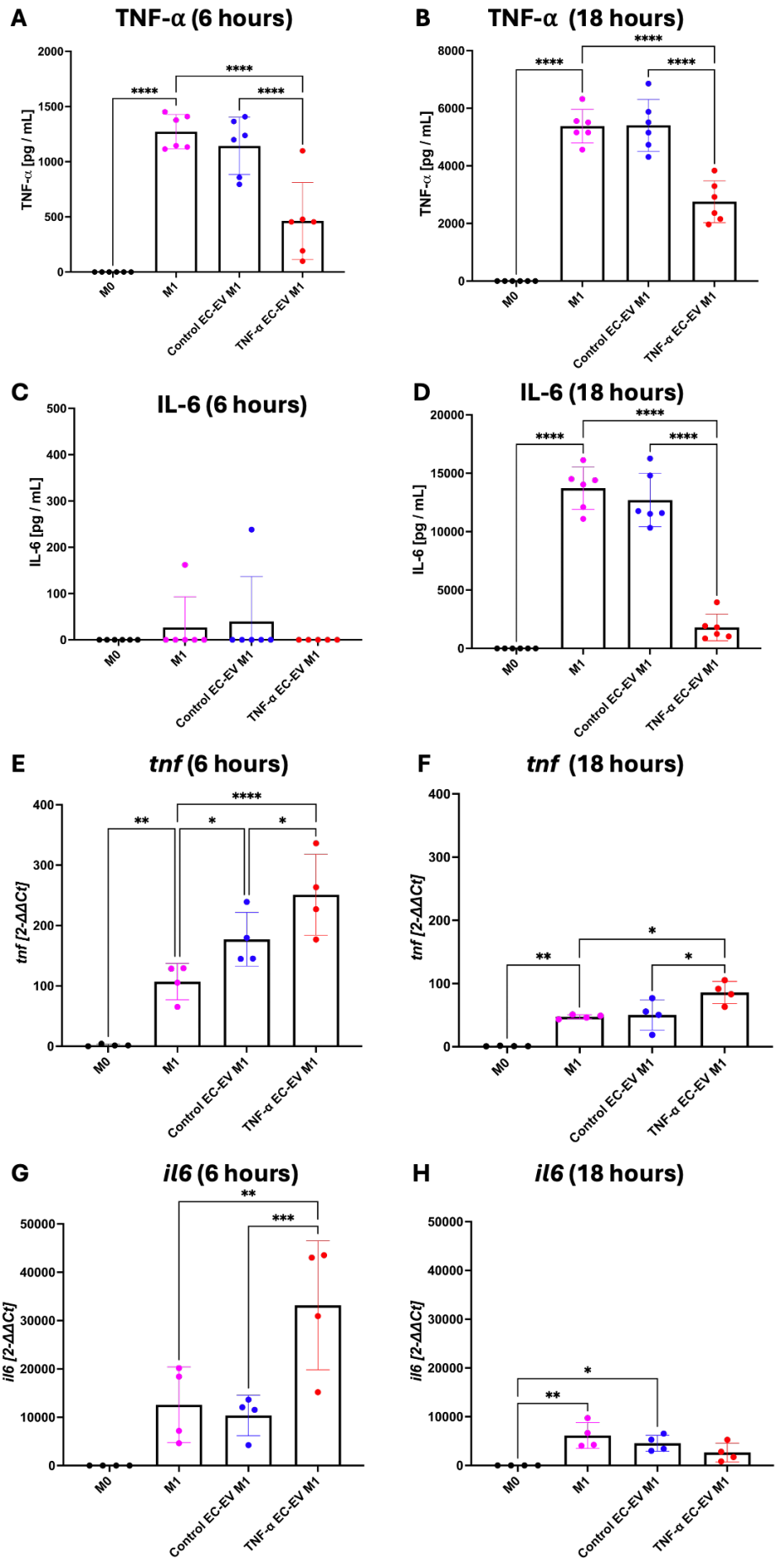
A
TNF-α (6 hours)
TNF-α [pg / mL]
2000
1500
1000
500
0
****
****
****
M0
M1
Control EC-EV M1
TNF-α EC-EV M1
B
TNF-α (18 hours)
TNF-α [pg / mL]
8000
6000
4000
2000
0
****
****
****
M0
M1
Control EC-EV M1
TNF-α EC-EV M1
C
IL-6 (6 hours)
IL-6 [pg / mL]
500
400
300
200
100
0
M0
M1
Control EC-EV M1
TNF-α EC-EV M1
D
IL-6 (18 hours)
IL-6 [pg / mL]
20000
15000
10000
5000
0
****
****
****
M0
M1
Control EC-EV M1
TNF-α EC-EV M1
E
tnf (6 hours)
tnf [2-ΔΔCt]
400
300
200
100
0
**
*
*
****
M0
M1
Control EC-EV M1
TNF-α EC-EV M1
F
tnf (18 hours)
tnf [2-ΔΔCt]
400
300
200
100
0
**
*
*
M0
M1
Control EC-EV M1
TNF-α EC-EV M1
G
il6 (6 hours)
il6 [2-ΔΔCt]
50000
40000
30000
20000
10000
0
**
***
M0
M1
Control EC-EV M1
TNF-α EC-EV M1
H
il6 (18 hours)
il6 [2-ΔΔCt]
50000
40000
30000
20000
10000
0
*
**
M0
M1
Control EC-EV M1
TNF-α EC-EV M1

Figure 43. Human Monocyte-Derived Macrophages Have a Lower Inflammatory Cytokine Response to TNF-α Endothelial Cell-Extracellular Vesicle Priming. *TNF-α protein secretion in cell culture supernatants by MDM exposed to M0 (sterile PBS), M1 (100 ng / mL LPS + 10 µg / mL IFN-γ), control EC-EV (1 x 10^9 particles) or TNF-α EC-EV (1 x 10^9 particles) for 18 hours before the control EC-EV and TNF-α EC-EV groups were treated with LPS (100 ng / mL) and IFN-γ (10 ng / mL) for (**A**) 6 hours and (**B**) 18 hours (n = 6 per group). IL-6 protein secretion analysis was also performed on these cell culture supernatants at (**C**) 6 hours and (**D**) 18 hours (n = 6 per group). mRNA expression changes for tnf in MDM exposed to M0 (PBS), M1 (100 ng / mL LPS + 10 µg / mL IFN-γ), control EC-EV (1 x 10^9 particles) or TNF-α EC-EV (1 x 10^9 particles) for 18 hours before the control EC-EV and TNF-α EC-EV groups were treated with LPS (100 ng / mL) and IFN-γ (10 ng / mL) for (**E**) 6 hours and (**F**) 18 hours (n = 3 per group). mRNA expression changes for il6 were also performed on MDM cell lysates (**G**) 6 hours and (**H**) 18 hours (n = 3 per group). RT-qPCR Ct values are normalised to cyclophilin. n = Number of replicates. Data are reported as mean $\pm$ standard deviation. A Shapiro-Wilk test was used to determine data normality (α = 0.05, p<0.05), and a Grubbs test was used to identify outliers (α = 0.05). Data was parametric and one-way ANOVA with Bonferroni post-hoc correction was used to determine the statistical significance of differences between the groups. Significance is represented on the graph by *p<0.05, **p<0.01, ***p<0.001 or ****p<0.0001.*

5.6 Mouse Bone Marrow-Derived Macrophages Undergo a Pro-Inflammatory Metabolic & Phosphorylation Shift in Response to TNF-α Endothelial Cell-Extracellular Vesicle Priming

During M1 polarisation, macrophage metabolism shifts towards glycolysis (268), and is associated with the upregulation of glycolytic genes and hypoxia response genes such as *hif1-α* and *irg1* (269-273). To investigate the metabolic changes in BMDM in response to TNF-α EC-EV priming, changes in the expression of genes associated with cell metabolism were examined (**Figure 44**). Gene expression analysis showed that both control EC-EV and TNF-α EC-EV priming promotes an increase in *hif1-α* ($p<0.001$, **Figure 44A**) and *gapdh* ($p<0.05$, **Figure 44B**) expression relative to the vehicle-control. However, there were no significant differences between the control EC-EV and TNF-α EC-EV groups. There were also no significant differences across all groups for *irg1* expression (**Figure 44C**). Further analysis into differences in key metabolites and the cellular respiration rate of BMDM are required to fully elucidate this response.

Macrophage activation in response to stimuli such as LPS leads to an upregulation in inflammatory cytokine expression and secretion and is mediated by intracellular MAPK phosphorylation cascades (27, 28). Key components of this cascade include ERK1/2, p38-MAPK and NF-κB and therefore changes in protein phosphorylation were assessed to determine if TNF-α EC-EV priming reprogrammes BMDM through modified MAPK phosphorylation signalling.

Western blotting analysis of BMDM stimulated with vehicle-control, LPS, control EC-EV, or TNF-α EC-EV for 18 hours, rested for 24 hours and treated with LPS showed a

decrease in phosphorylated NF-κB at 30 minutes, 60 minutes and 120 minutes for the TNF-α EC-EV group relative to control EC-EV (**Figure 44D-E**). Unphosphorylated NF-κB was unchanged across all groups (**Figure 44D**), indicating the phosphorylation changes in **Figure 44E** are not simply due to increased production of NF-κB. There appeared to be no change in phosphorylated ERK1/2 and p38-MAPK across all groups, indicating TNF-α EC-EV may target NF-κB through a mechanism independent of MAPK, although further studies are necessary to fully elucidate this mechanism.

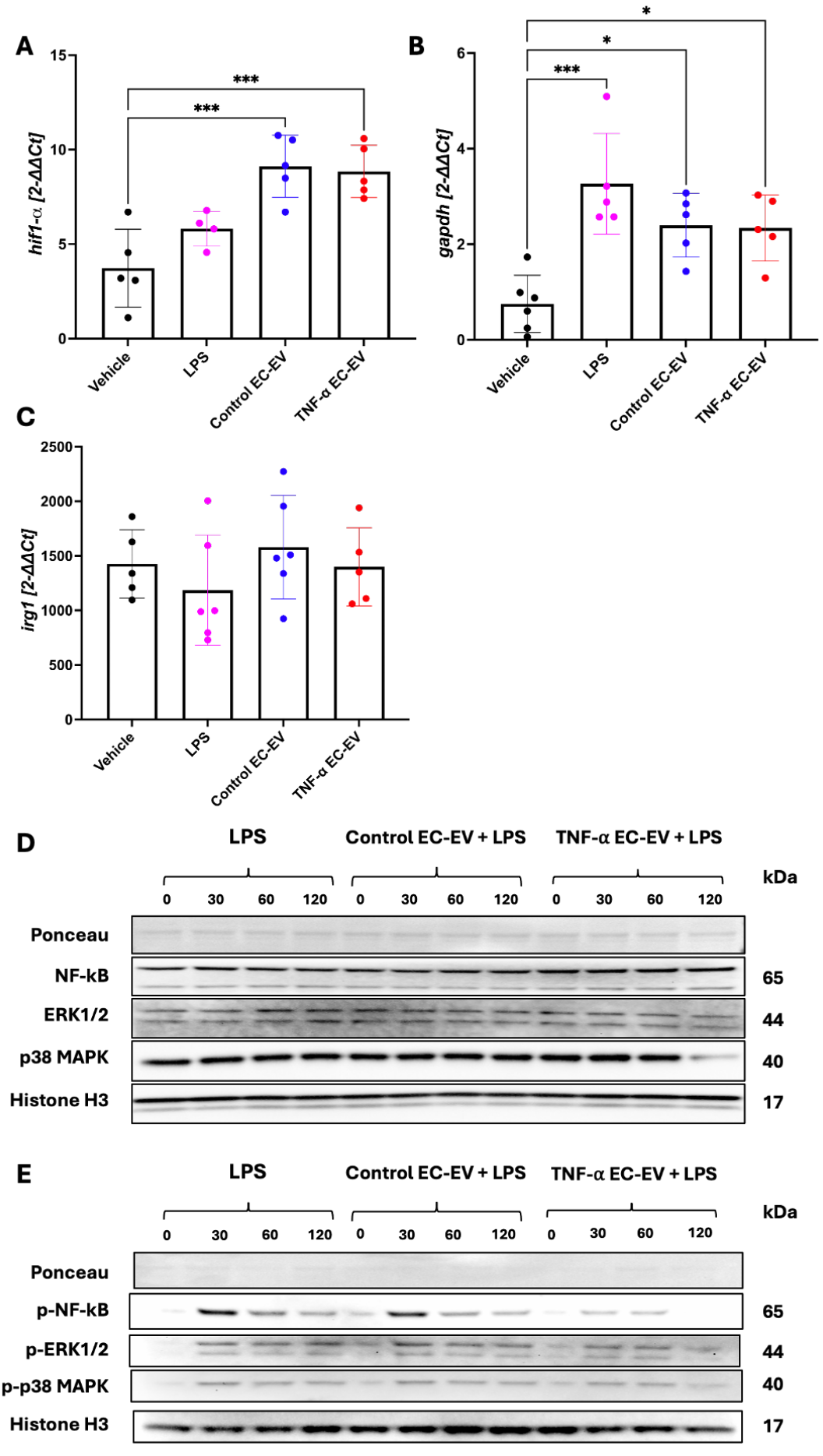
A
hif1-α [2-ΔΔCt]
15
10
5
0
***
***
Vehicle
LPS
Control EC-EV
TNF-α EC-EV
B
gapdh [2-ΔΔCt]
6
4
2
0
*
*
***
Vehicle
LPS
Control EC-EV
TNF-α EC-EV
C
irg1 [2-ΔΔCt]
2500
2000
1500
1000
500
0
Vehicle
LPS
Control EC-EV
TNF-α EC-EV
D
LPS
Control EC-EV + LPS
TNF-α EC-EV + LPS
kDa
0 30 60 120 0 30 60 120 0 30 60 120
Ponceau
NF-kB
ERK1/2
p38 MAPK
Histone H3
65
44
40
17
E
LPS
Control EC-EV + LPS
TNF-α EC-EV + LPS
kDa
0 30 60 120 0 30 60 120 0 30 60 120
Ponceau
p-NF-kB
p-ERK1/2
p-p38 MAPK
Histone H3
65
44
40
17

Figure 44. Mouse Bone Marrow-Derived Macrophages Undergo Changes in Metabolic and Phosphorylation Processes in Response to TNF-α Endothelial Cell-Extracellular Vesicles. *mRNA expression changes for (**A**) hif1-α, (**B**) gapdh, and (**C**) irg1 in BMDM primed with vehicle-control (sterile PBS), LPS (100 ng / mL), control EC-EV (1 x 10^9 particles) or TNF-α EC-EV (1 x 10^9 particles) for 18 hours before treatment with LPS (100 ng / mL) and IFN-γ (10 ng / mL) for 18 hours (n = 4-6). Changes in (**D**) unphosphorylated and (**E**) phosphorylated proteins in BMDM in response to LPS (100 ng / mL), control EC-EV (1 x 10^9 particles) and TNF-α EC-EV (1 x 10^9 particles) for 18 hours before treatment with LPS (100 ng / mL) for 0 minutes, 30 minutes, 60 minutes or 120 minutes. RT-qPCR Ct values are normalised to cyclophilin. n = Number of replicates. Data are reported as mean $\pm$ standard deviation. A Shapiro-Wilk test was used to determine data normality (α = 0.05, p<0.05), and a Grubbs test was used to identify outliers (α = 0.05). Data was parametric and one-way ANOVA with Bonferroni post-hoc correction was used to determine the statistical significance of differences between the groups. Significance is represented on the graph by *p<0.05 or ***p<0.001.*

5.7 Endothelial Cell-Extracellular Vesicle Priming Does Not Induce a Tolerance Response in Peritoneal Macrophages

To determine whether the innate immune tolerance response of BMDM to TNF-α EC-EV priming is specific to myeloid-derived macrophages or is present in all macrophage populations, the BMDM EC-EV priming model was tested on peritoneal macrophages. These macrophages were isolated and treated with either vehicle-control, LPS or β-glucan (**Figure 45A**) for 18 hours, were rested for 24 hours and then stimulated with

LPS and IFN-γ for 18 hours. Unlike BMDM, which are myeloid-derived and generated from bone marrow HSC, tissue-resident macrophages are yolk sac-derived and form during embryonic development (274, 275). As observed in the BMDM model in **Figure 40**, LPS exposure suppresses TNF-α secretion ($p<0.01$) from peritoneal macrophages after treatment with LPS and IFN-γ, whilst β-glucan amplifies ($p<0.05$) the inflammatory cytokine response. By contrast, priming peritoneal macrophages with control EC-EV or TNF-α EC-EV for 18 hours, followed by a rest for 24 hours, and second stimulation with LPS and IFN-γ for 18 hours (**Figure 45B**) had no effect on TNF-α secretion, indicating the inflammatory cytokine response to TNF-α EC-EV may be unique to specific macrophage populations, such as myeloid-derived BMDM.

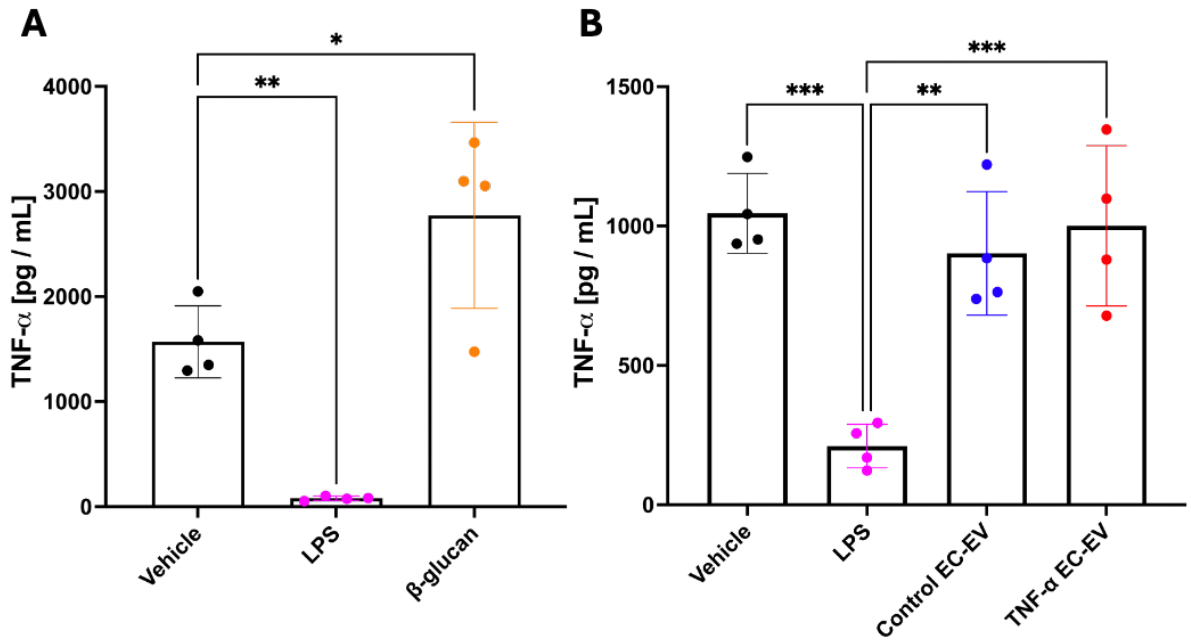

Figure 45. Mouse Peritoneal Macrophages Do Not Have a Modified Inflammatory Response to TNF-α Endothelial Cell-Extracellular Vesicles. *(**A**) Change in TNF-α secretion in peritoneal macrophages exposed to vehicle-control (sterile PBS), LPS*

*(100 ng / mL) or β-glucan (10 μg / mL) for 18 hours followed by treatment with LPS (100 ng / mL) and IFN-γ (10 μg / mL) for 18 hours (n = 4 per group). (**B**) TNF-α response in peritoneal macrophages following priming with vehicle-control (sterile PBS), LPS (100 ng / mL), control EC-EV (1 x 10^9 particles) and TNF-α EC-EV (1 x 10^9 particles) for 18 hours followed by LPS (100 ng / mL) and IFN-γ (10 μg / mL) for 18 hours (n = 4 per group). n = Number of replicates. Data are reported as mean ± standard deviation. A Shapiro-Wilk test was used to determine data normality (α = 0.05, p<0.05), and a Grubbs test was used to identify outliers (α = 0.05). Data was parametric and one-way ANOVA with Bonferroni post-hoc correction was used to determine the statistical significance of differences between the groups. Significance is represented on the graph by *p<0.05, **p<0.01, or ***p<0.001.*

5.8 Denaturing Endothelial Cell-Extracellular Vesicles Mitigates the Tolerance Phenotype in Bone Marrow-Derived Macrophages

EV are abundant in protein, RNA and lipids which can contribute to intercellular signalling (99, 102, 276). To determine whether the effects of TNF-α EC-EV priming on BMDM are mediated by an active biomolecule, the TNF-α EC-EV were isolated and denatured through boiling at 95 °C, followed by characterisation (**Figure 46**). Overall, there were no significant differences in particle count (**Figure 46A**) or the particle size distribution (**Figure 46B**) between denatured and non-denatured groups, indicating the denatured particles were not ruptured.

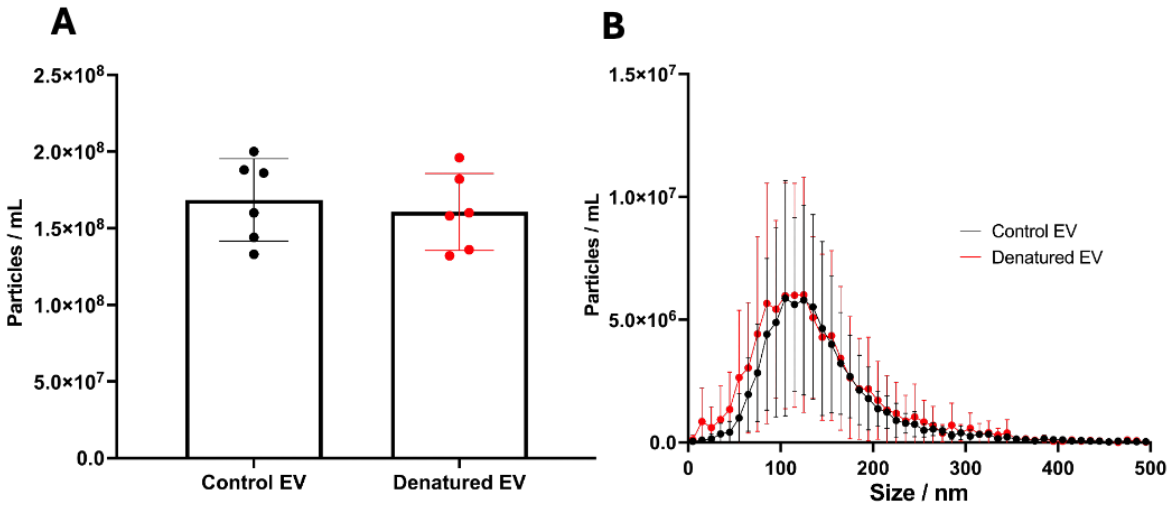

Figure 46. Characterisation of Denatured Mouse sEND.1 Endothelial Cell-Extracellular Vesicles. *(**A**) Particle count of untreated control and denatured sEND.1 endothelial cell-derived particles (n = 6 per group). (**B**) Size and concentration profile of untreated control and denatured endothelial cell-derived particles (n = 6 per group). n = Number of replicates. Data are reported as mean ± standard deviation. A Shapiro-Wilk test was used to determine data normality (α = 0.05, p<0.05), and a Grubbs test was used to identify outliers (α = 0.05). Data was parametric and a two-tailed unpaired t-test was used to determine the statistical significance of differences between the groups.*

The cell adhesion molecule, VCAM-1, mediates the anchoring of leukocytes to endothelial cells (143) and is required for the mobilisation effects of EC-EV on the spleen (89). To determine the effects of VCAM-1 in the EC-EV BMDM model, TNF-α-stimulated VCAM-1 knockout EC-EV (89) were given to BMDM for 18 hours alongside vehicle-control, LPS, control EC-EV, or TNF-α EC-EV. Denatured EC-EV from each group (control EC-EV, TNF-α EC-EV, or VCAM-1 knockout TNF-α EC-EV) were also

given to BMDM. After 18 hours, the stimulus was removed, BMDM were rested for 24 hours and were stimulated with LPS and IFN-γ for 18 hours (**Figure 47**).

Inflammatory cytokine secretion analysis showed that TNF-α EC-EV priming lowered TNF-α secretion ($p<0.0001$, **Figure 47A**) relative to the control EC-EV group. However, this property was lost when TNF-α EC-EV were denatured prior to priming treatment ($p<0.0001$). Interestingly, there were no significant differences in TNF-α secretion between the TNF-α EC-EV and the VCAM-1 knockout EC-EV groups.

IL-6 secretion from BMDM was also analysed (**Figure 47B**) and was suppressed in response to TNF-α EC-EV priming ($p<0.001$) relative to control EC-EV priming, but not in the denatured TNF-α EC-EV group. This indicates an active biomolecule within TNF-α EC-EV contributes to immune cell tolerance and is lost through denaturing EC-EV. Furthermore, this biomolecule is not active within control EC-EV. Unlike TNF-α secretion, changes in IL-6 secretion appear to be mediated by VCAM-1 since the VCAM-1 knockout EC-EV has no effect on IL-6 secretion relative to the vehicle-control in BMDM.

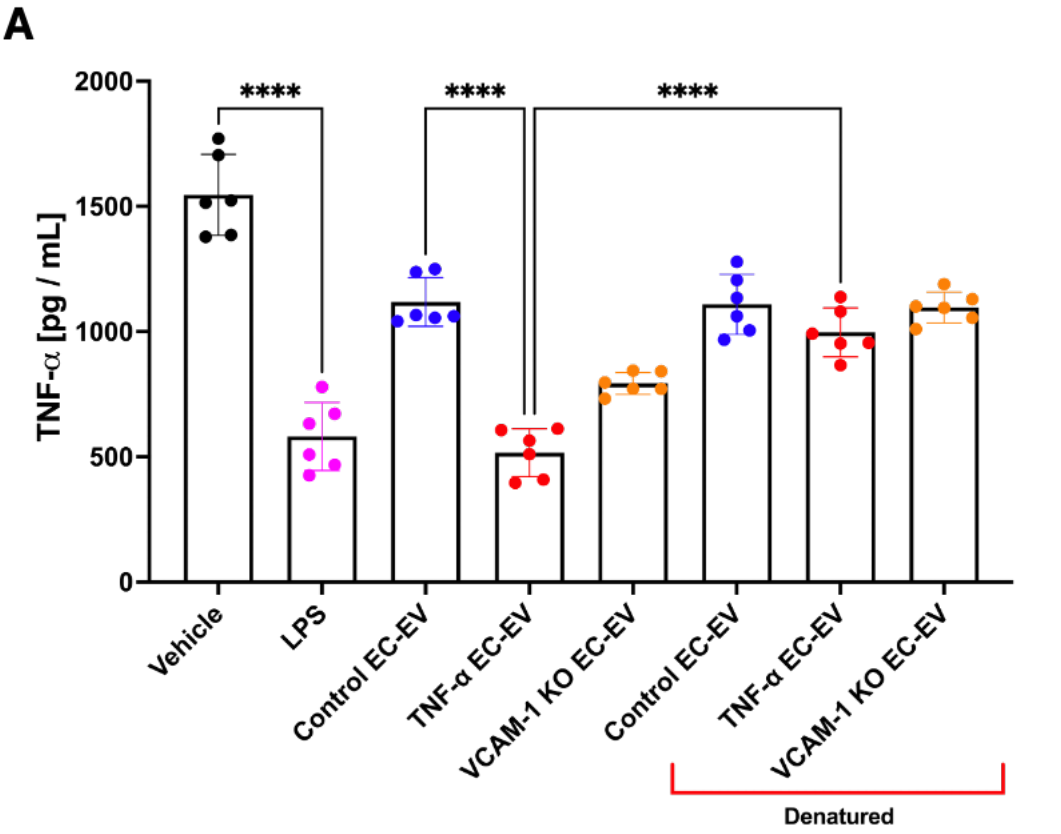
A
2000
1500
1000
500
0
TNF-α [pg / mL]
****
****
****
Vehicle
LPS
Control EC-EV
TNF-α EC-EV
VCAM-1 KO EC-EV
Control EC-EV
TNF-α EC-EV
VCAM-1 KO EC-EV
Denatured

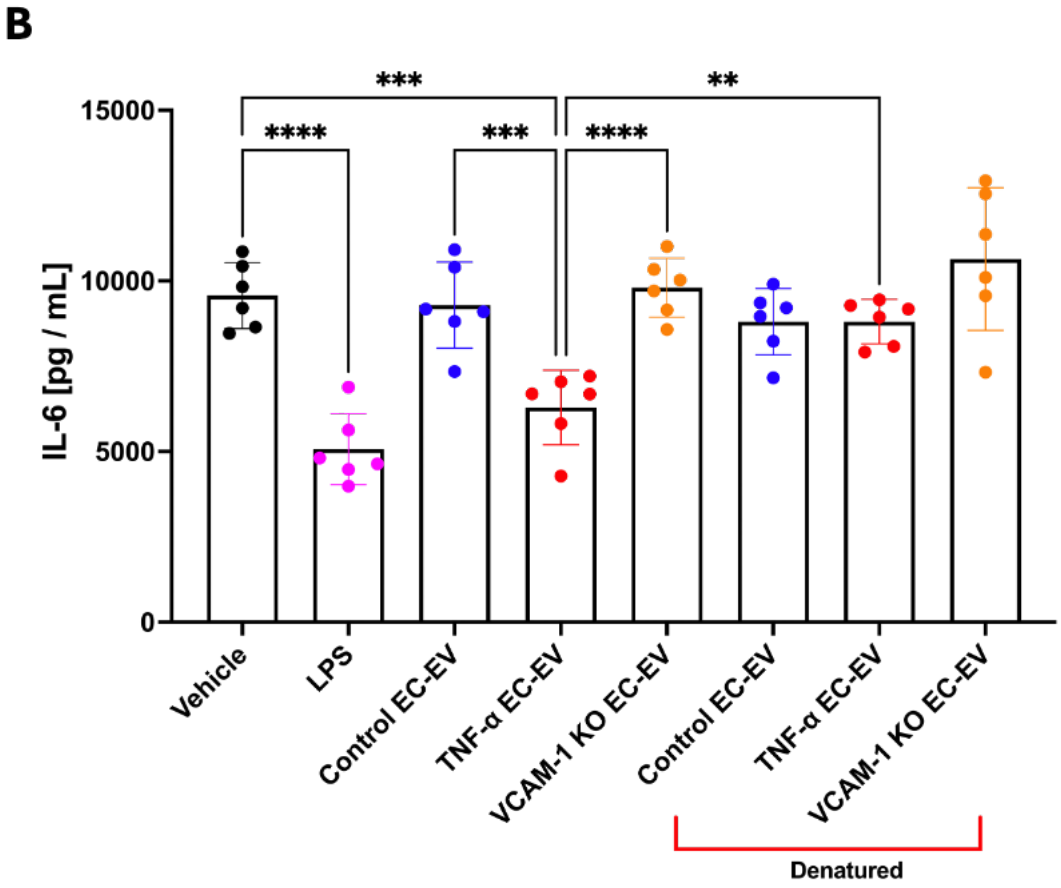
B
15000
10000
5000
0
IL-6 [pg / mL]
***
**
****
***
****
Vehicle
LPS
Control EC-EV
TNF-α EC-EV
VCAM-1 KO EC-EV
Control EC-EV
TNF-α EC-EV
VCAM-1 KO EC-EV
Denatured

Figure 47. Denaturation Mitigates the Effects of TNF-α Endothelial Cell-Extracellular Vesicles on Bone Marrow-Derived Macrophages. *Changes in (**A**) TNF-α and (**B**) IL-6 secretion in BMDM primed with vehicle-control (sterile PBS), LPS (100 ng / mL), control EC-EV (1 x 10^9 particles), TNF-α EC-EV (1 x 10^9 particles), VCAM-1 knockout TNF-α EC-EV (1 x 10^9 particles), either untreated or boiled, for 18 hours, before treatment with LPS (100 ng / mL) and IFN-γ (10 μg / mL) for 18 hours (n = 6 per group). n = Number of replicates. Data are reported as mean ± standard deviation. A Shapiro-Wilk test was used to determine data normality (α = 0.05, p<0.05), and a Grubbs test was used to identify outliers (α = 0.05). Data was parametric and one-way ANOVA with Bonferroni post-hoc correction was used to determine the statistical significance of differences between the groups. Significance is represented on the graph by **p<0.01, ***p<0.001 or ****p<0.0001.*

Next, gene expression analysis was performed on the BMDM primed with vehicle-control, LPS, control EC-EV, TNF-α EC-EV, VCAM-1 knockout EC-EV, denatured control EC-EV, denatured TNF-α EC-EV, or denatured VCAM-1 knockout EC-EV, all for 18 hours, followed by a 24-hour rest period and treatment with LPS and IFN-γ for 18 hours. In support of the data from **Figure 28**, TNF-α EC-EV priming increased *tnf* (p<0.05, **Figure 48A**) and *il6* (p<0.05, **Figure 48B**) expression relative to control EC-EV priming, and these effects were mitigated by denaturing TNF-α EC-EV, or by using the VCAM-1 knockout TNF-α EC-EV model. This data indicates the changes in inflammatory cytokine gene expression induced by TNF-α EC-EV priming are dependent on VCAM-1.

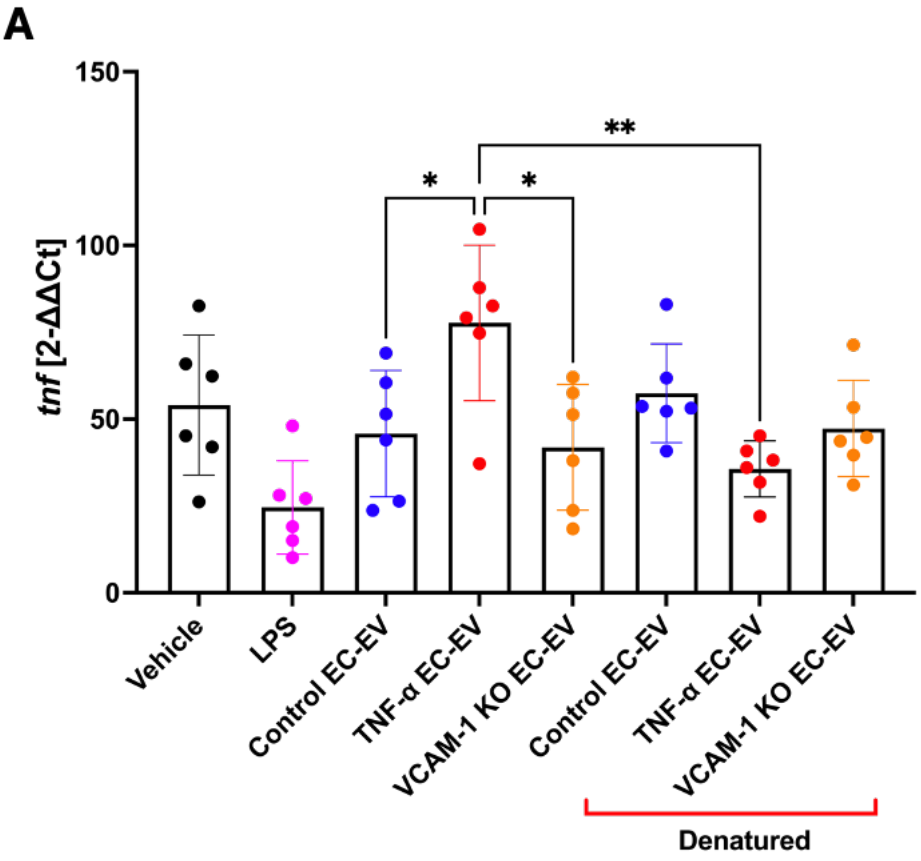
A
150
100
50
0
tnf [2-ΔΔCt]
*
*
**
Vehicle
LPS
Control EC-EV
TNF-α EC-EV
VCAM-1 KO EC-EV
Control EC-EV
TNF-α EC-EV
VCAM-1 KO EC-EV
Denatured

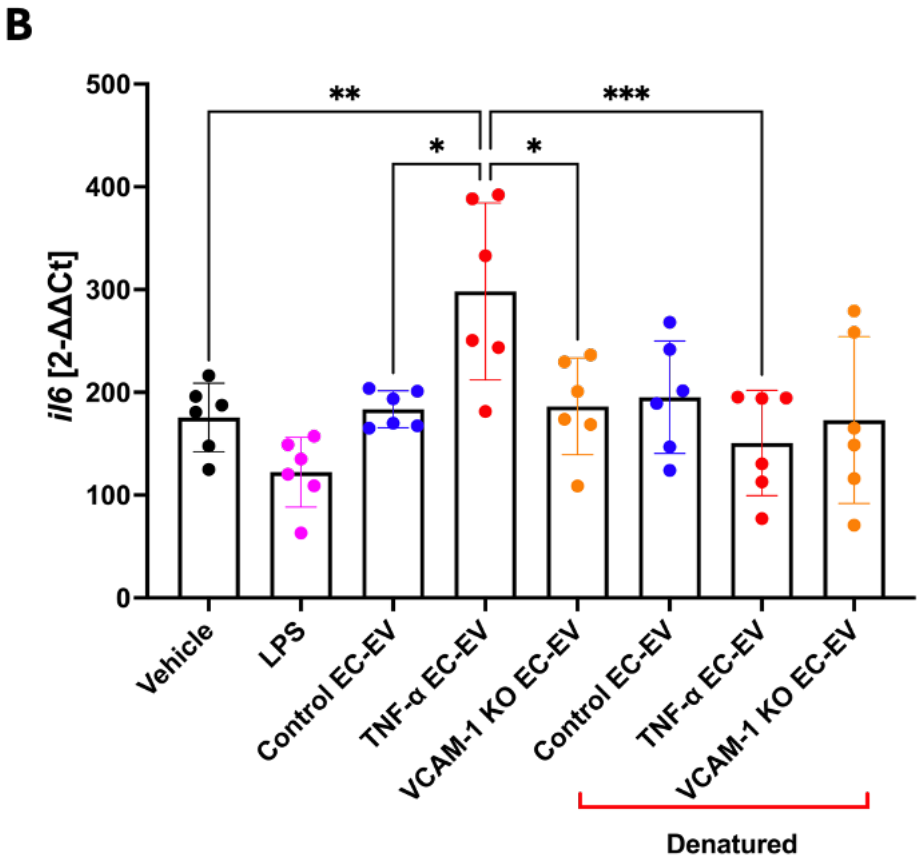
B
500
400
300
200
100
0
il6 [2-ΔΔCt]
**
*
*
***
Vehicle
LPS
Control EC-EV
TNF-α EC-EV
VCAM-1 KO EC-EV
Control EC-EV
TNF-α EC-EV
VCAM-1 KO EC-EV
Denatured

Figure 48. Denaturation Mitigates the Effects of TNF-α Endothelial Cell-Extracellular Vesicle Priming on Bone Marrow-Derived Macrophage Gene Expression. *Gene expression changes for (**A**) tnf, and (**B**) il6 in BMDM primed with vehicle-control (sterile PBS), LPS (100 ng / mL), control EC-EV (1 x 10^9 particles), TNF-α EC-EV (1 x 10^9 particles), VCAM-1 knockout TNF-α EC-EV (1 x 10^9 particles), either untreated or boiled, for 18 hours before treatment with LPS (100 ng / mL) and IFN-γ (10 μg / mL) for 18 hours (n = 6 per group). n = Number of replicates. RT-qPCR Ct values are normalised to cyclophilin. Data are reported as mean ± standard deviation. A Shapiro-Wilk test was used to determine data normality (α = 0.05, p<0.05), and a Grubbs test was used to identify outliers (α = 0.05). Data was parametric and one-way ANOVA with Bonferroni post-hoc correction was used to determine the statistical significance of differences between the groups. Significance is represented on the graph by *p<0.05, **p<0.01, or ***p<0.001.*

There was no significant response in BMDM *il1β* expression (**Figure 49A**) following priming with TNF-α EC-EV relative to the vehicle-control group, although the control EC-EV group had increased *il1β* expression compared to the vehicle-control group (p<0.001) and the TNF-α EC-EV (p<0.0001) group. Zeb1 is a transcription factor associated with macrophage plasticity and has been shown to both initiate inflammation, by upregulating pro-inflammatory genes including *il6 (277)***,** and also resolve inflammation by inhibiting mitochondrial protein translation and restricting amino acid transport into macrophages (277). In BMDM primed with TNF-α EC-EV, *zeb1* expression was not significantly different to the control EC-EV group (**Figure 49B**). Finally, BMDM primed with LPS had significantly elevated levels of *zeb1*

expression relative to vehicle-control ($p<0.01$). These data do not indicate that *zeb1* expression in BMDM is altered by EC-EV priming.

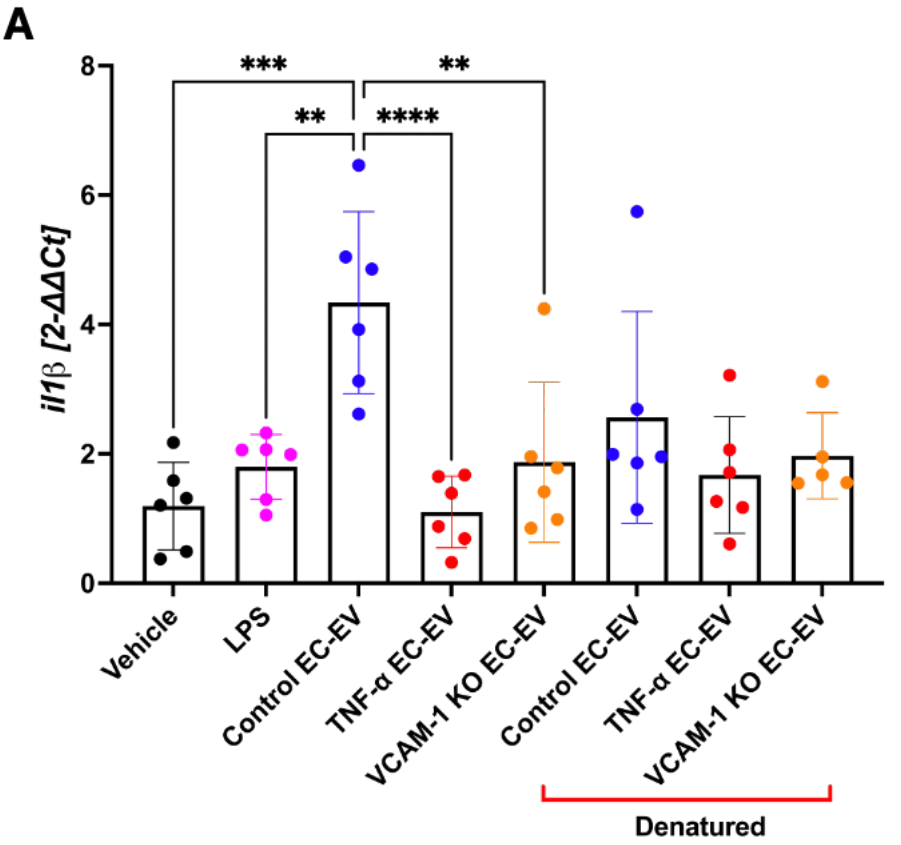
A
***
**
**
****
8
6
4
2
0
il1β [2-ΔΔCt]
Vehicle
LPS
Control EC-EV
TNF-α EC-EV
VCAM-1 KO EC-EV
Control EC-EV
TNF-α EC-EV
VCAM-1 KO EC-EV
Denatured

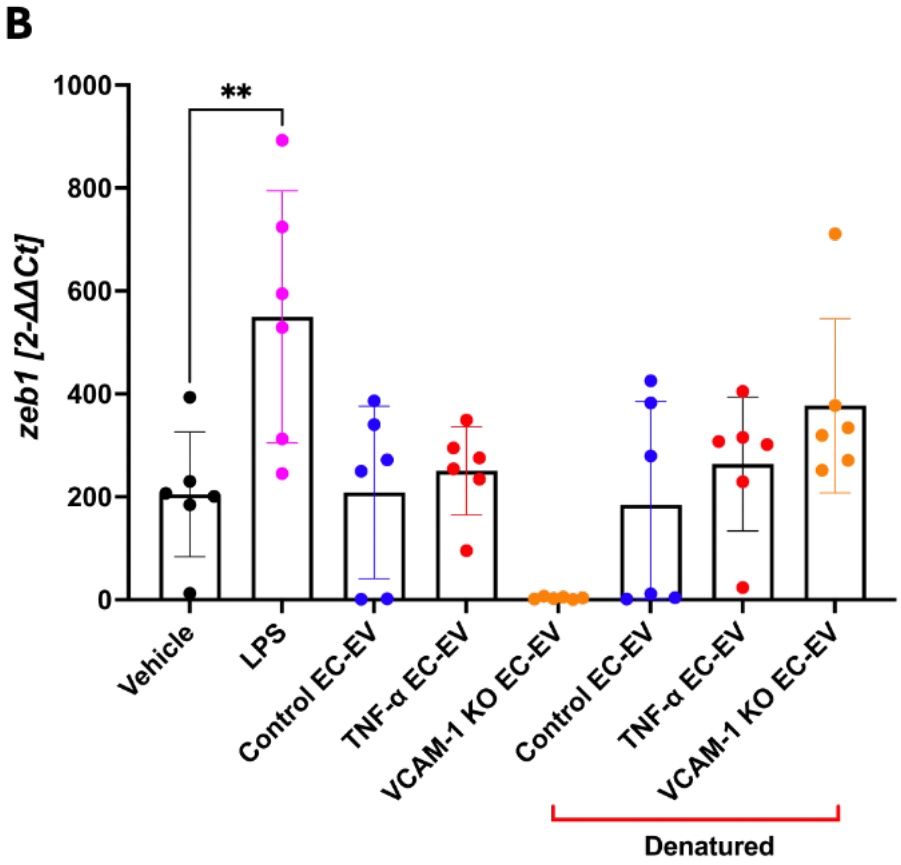
B
**
1000
800
600
400
200
0
zeb1 [2-ΔΔCt]
Vehicle
LPS
Control EC-EV
TNF-α EC-EV
VCAM-1 KO EC-EV
Control EC-EV
TNF-α EC-EV
VCAM-1 KO EC-EV
Denatured

Figure 49. Denaturation Mitigates the Effects of TNF-α Endothelial Cell-Extracellular Vesicle Priming on Bone Marrow-Derived Macrophage Gene Expression*. Gene expression changes for (**A**) il1β, and (**B**) zeb1 in BMDM primed with vehicle-control (sterile PBS), LPS (100 ng / mL), control EC-EV (1 x 10^9 particles), TNF-α EC-EV (1 x 10^9 particles), VCAM-1 knockout TNF-α EC-EV (1 x 10^9 particles), either untreated or boiled, for 18 hours before treatment with LPS (100 ng / mL) and IFN-γ (10 μg / mL) for 18 hours (n = 6 per group). n = Number of replicates. RT-qPCR Ct values are normalised to cyclophilin. Data are reported as mean ± standard deviation. A Shapiro-Wilk test was used to determine data normality (α = 0.05, p<0.05), and a Grubbs test was used to identify outliers (α = 0.05). Data was parametric and one-way ANOVA with Bonferroni post-hoc correction was used to determine the statistical significance of differences between the groups. Significance is represented on the graph by **p<0.01, ***p<0.001, or ****p<0.0001.*

5.9 Discussion

MI is known to induce reprogramming of the bone marrow in diseases such as heart failure and cancer (83, 87), and also lowers haematopoiesis in mouse models of recurrent MI (82). EC-EV transcriptionally reprogramme innate immune cells in the spleen (89) and may function in the bone marrow post-MI, but it is not clear whether EC-EV transcriptionally reprogramme innate immune cells in the bone marrow and how this process is mediated.

This chapter shows that; (I) TNF-α EC-EV priming induces a tolerance phenotype in BMDM, through the suppression of inflammatory cytokine secretion, macrophage

cellular adhesion, changes in metabolic gene expression, and in MAPK phosphorylation signalling. (II) These findings are consistent in both mouse and human models. (III) There is a disparity in the gene expression and protein secretion responses in BMDM primed with TNF-α EC-EV. (IV) The findings observed are specific to myeloid-derived cells. (V) Denaturing TNF-α EC-EV or knocking out VCAM-1 mitigates the effects of TNF-α EC-EV on BMDM. The key findings are summarised in **Figure 50**.

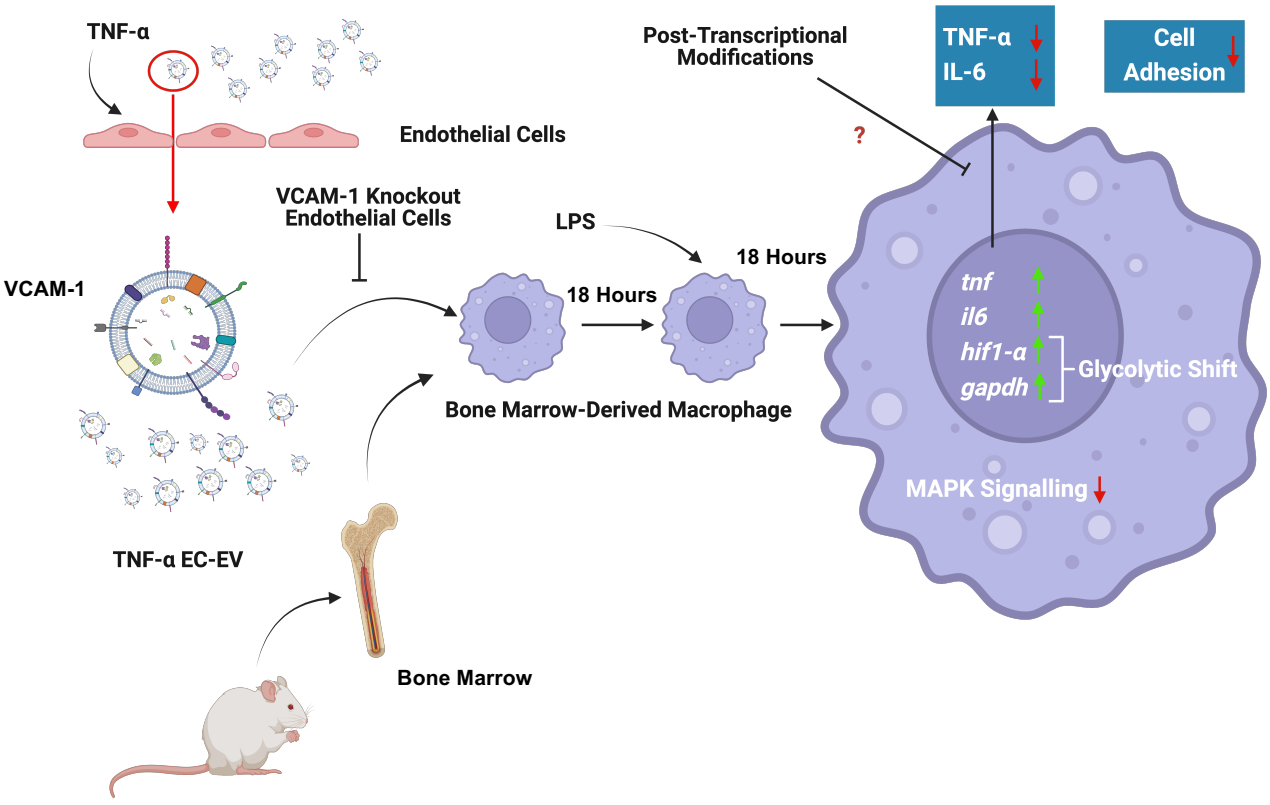

Figure 50. TNF-α Endothelial Cell-Extracellular Vesicles Modulate the Inflammatory Profile of Bone Marrow-Derived Macrophages in a VCAM-1-Dependent Manner. *Green arrow = increased production. Red arrow = decreased production.*

Previous data show that MI can reprogramme the bone marrow and promote an exaggerated monocyte-mediated response in cardiovascular disease and co-morbidities such as cancer and chronic kidney disease (82, 83, 87). However, these studies have largely focused on reprogramming at the HSPC level and not on modifications to mature cells, such as macrophages. Furthermore, few have considered the role of EC-EV in mediating the crosstalk between the damaged myocardium and the bone marrow.

This chapter has shown EC-EV derived from activated endothelium induce a tolerance phenotype in macrophages treated with LPS and IFN-γ and this finding is conserved between mouse BMDM (**Figure 40** and **Figure 42**) and human MDM (**Figure 43**) models. LPS-mediated immune cell tolerance is associated with the inhibited secretion of pro-inflammatory cytokines including TNF-α and IL-6 (278, 279), which was also found in the TNF-α EC-EV model in this chapter. Production of TNF-α and IL-6 are mediated by NF-κB signalling (280) and therefore the abrogation of NF-κB phosphorylation by TNF-α EC-EV (as observed in **Figure 44**) may also provide an explanation for lower TNF-α and IL-6 secretion. In sepsis models of immune cell tolerance, the LPS-TLR4 signalling cascade is repressed, leading to a downregulation of TLR4-associated genes including *tnf, il6* and *il1*β (278, 281, 282). Histones at the promoter sites of these genes have modifications including repressed H3K27ac and H3K4me3, which are both associated with active promoter sites (281, 282).

Data in this chapter demonstrate that TNF-α EC-EV priming upregulates gene expression of both *tnf* and *il6* in BMDM, creating a paradox where gene expression is upregulated, but the corresponding protein secretion is downregulated. The interplay between different stimuli and how they modify macrophage gene expression and

function contributes to the complexity of immune cell tolerance. IFN-γ was used in combination with LPS in the mouse BMDM and human MDM models as M1-polarising agents after TNF-α EC-EV treatment, and has been shown to partially abrogate the tolerance effects of LPS (283). Although the mechanism of action for IFN-γ has not been elucidated, one study showed that treating pre-tolerised cells with IFN-γ reversed the downregulation of *tnf* and *il6* through chromatin remodelling (283). The interplay between the different M1 polarising agents in the BMDM and MDM models could therefore explain the discrepancy in the gene expression and protein secretion data for pro-inflammatory cytokines. Comparing changes in inflammatory cytokine gene expression from the TNF-α EC-EV-LPS and IFN-γ model with a TNF-α EC-EV-LPS model would be useful to understand the role of IFN-γ in this process.

Alternatively, the reprogramming effects of TNF-α EC-EV priming on pro-inflammatory cytokine expression and protein synthesis may occur at the post-transcriptional level (284). Several studies have shown the translation of *tnf* mRNA is regulated by adenine and uridine-rich elements (ARE), which are present in the 3' untranslated region of *tnf* mRNA transcripts (285-287). ARE binding proteins regulate translation either through stabilising the *tnf* mRNA transcript or by promoting degradation and therefore may promote the accumulation of *tnf* mRNA transcripts that are not translated into TNF-α protein. Furthermore, post-transcriptional regulation may occur through specific miRNA targeting of *tnf* mRNA. For example, studies have shown miRNA-126 suppresses inflammatory cytokine mRNA production (288), including in monocytes (289), and therefore the inflammatory cytokine transcripts may be suppressed from translation through this mechanism.

In addition to modifying the pro-inflammatory cytokine profile of macrophages, EC-EV also affected the metabolic profile of BMDM (**Figure 44**). Gene expression data show a significant enrichment in *hif1-α* and *gapdh* mRNA, although this effect was not specific to TNF-α EC-EV. Cellular reprogramming of macrophages into pro-inflammatory M1 phenotypes promotes a shift in cellular metabolism to favour anaerobic glycolysis in order to meet the increased energy demands of the cell for processes such as pro-inflammatory cytokine production, increased cell motility, and phagocytosis (268). The switch to favouring glycolysis involves an upregulation of glycolytic enzyme gene expression including *gapdh*, *hexokinase*, and *pyruvate kinase M2* (270, 290) as well as an accumulation of succinate in the tricarboxylic acid (TCA) cycle which promotes the stabilisation of Hif1-α (291). The increase in *gapdh* and *hif1-α* in TNF-α EC-EV primed BMDM therefore suggests a shift in metabolism which favours glycolysis. To fully elucidate the changes in BMDM metabolism in response to TNF-α EC-EV, the respiratory rate of these cells could be tracked using a Seahorse assay (292), or a lactate accumulation to track the rate of anaerobic respiration (293).

Interestingly, Hif1-α has also been described in mediating immune cell tolerance in macrophages by preventing the accumulation of H3K27ac-modified histones at gene promoter sites (281). Furthermore, *hif1-α* gene expression increases in LPS-induced tolerised monocytes and was shown to attenuate the inflammatory response through *interleukin-1 receptor associated kinase M*, which negatively regulates TLR signalling (282). This data indicates an important role for Hif1-α as part of a shift towards glycolysis, but also in reprogramming monocytes towards a tolerance phenotype by restricting H3K27 acetylation. Comparing histone acetylation changes in TNF-α EC-EV primed BMDM with those of LPS-tolerised BMDM at Hif1-α transcription factor

binding sites would be a useful next experiment to identify a role for Hif1-α in this process.

The reprogramming effects of TNF-α EC-EV were perturbed by boiling the TNF-α EC-EV at 95 °C prior to treatment, or through the use of a VCAM-1 knockout EC-EV model (**Figure 47-49**). VCAM-1 is important in leukocyte docking to endothelial cells through integrin Very Late Antigen-4 (VLA-4), which is primarily expressed on leukocytes and undergoes a conformational change upon leukocyte activation to enable VCAM-1 binding (294). Future experiments should investigate the mechanism of interaction between EC-EV and macrophages. The enrichment of VCAM-1 in TNF-α EC-EV and the requirement for VCAM-1 in TNF-α EC-EV reprogramming of BMDM suggests interactions between VCAM-1 and VLA-4 are likely. However, it is not clear whether the EV are internalised within the macrophage, or reprogramming is driven by the binding of EV to the cell surface. High-resolution imaging would provide insight into how TNF-α EC-EV interact with BMDM and also the kinetics of this interaction.

The induction of immune cell tolerance in BMDM has interesting therapeutic potential in cardiovascular disease, especially in regulating the initial pro-injury phase of monocytosis post-MI (32, 58) and chronic inflammatory diseases such as sepsis (295). However, this process must be tightly controlled as excessive immune cell tolerance creates immunoparalysis, as is seen in sepsis patients (263, 296).

This chapter highlighted that TNF-α EC-EV target macrophages in the bone marrow and induce an immunosuppressive phenotype through lowering inflammatory cytokine secretion and lowering macrophage adhesion to endothelial cells. These effects appear to be dependent on VCAM-1 and therefore VCAM-1^{+} EC-EV may be of

therapeutic importance in neutralising pro-inflammatory macrophages in chronic inflammatory diseases, and also as part of post-MI interventions.

Chapter 6- Discussion

6.1 Key Findings

This thesis has demonstrated that: (I) TNF-α EC-EV induce haematopoiesis in the bone marrow and skews haematopoiesis towards the myeloid lineages, resulting in an increased production of neutrophils and monocytes in the bone marrow, and in circulation. (II) Transcriptional analysis of bone marrow HSC in response to treatment with TNF-α EC-EV show distinct patterns of gene expression, compared to control EC-EV exposure. These patterns include the positive regulation of haematopoiesis, MAPK signalling and cellular migration. Pathway analysis of miRNA-126-3p and miRNA-320b targets correlate with the HSC transcriptomics data, indicating a potential mechanism of reprogramming through miRNA-126-3p and miRNA-320b. (III) The development of an EV-priming model showed that exposing the bone marrow to TNF-α EC-EV followed by treatment with LPS and IFN-γ lowered the number of GMP, which produce neutrophils and monocytes, indicating a dampening of the innate immune response. Finally, (IV) TNF-α EC-EV priming can modify the inflammatory profile of BMDM through a mechanism that targets the ERK1/2-NF-κB signalling pathway and is dependent on VCAM-1. The key findings are outlined in **Figure 51**.

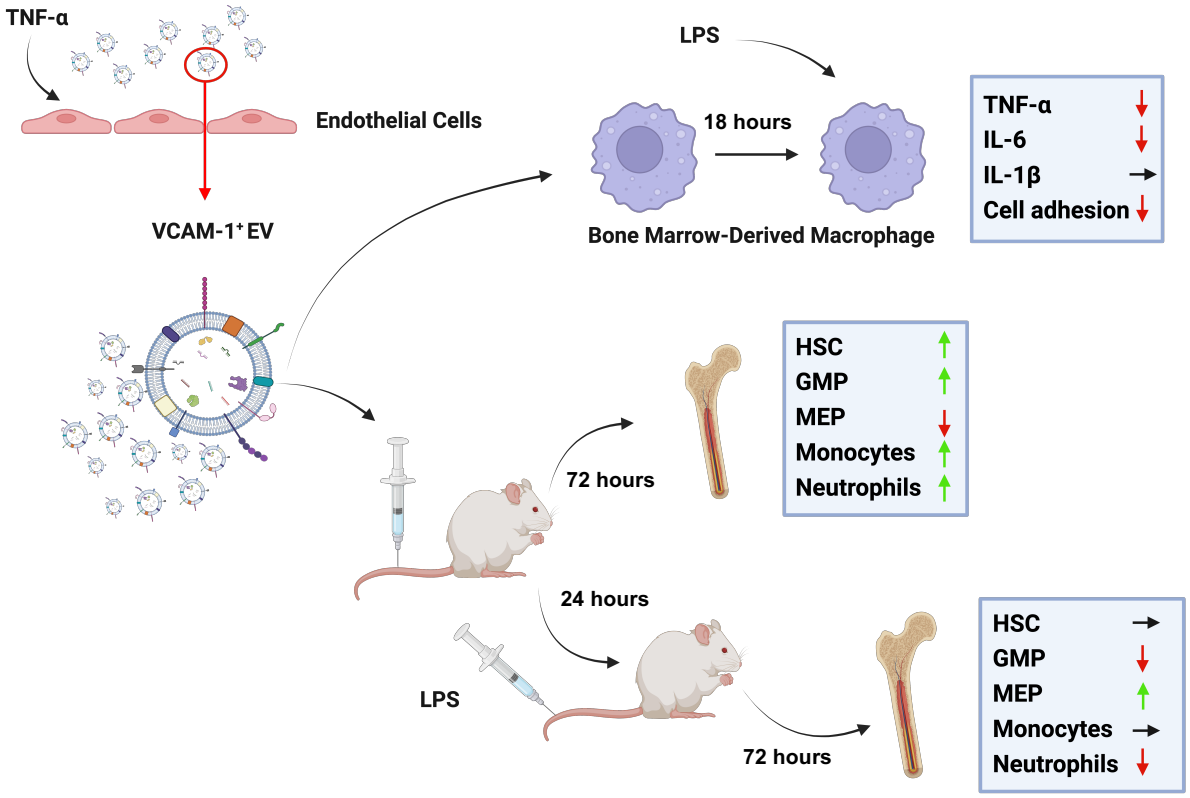

Figure 51. Overview Schematic Highlighting the Key Findings from This Thesis.

Research in this thesis shows that injection of TNF-α EC-EV modifies the contents of the bone marrow, including the quantity of different HSPC subpopulations, monocytes and neutrophils. Previous work attempting to understand communication between the spleen and injured heart post-MI investigated the role of circulating EC-EV and demonstrated that TNF-α EC-EV localise to the spleen (88) and promote the mobilisation of monocytes and neutrophils in a VCAM-1-dependent manner (88, 89). Despite showing haematopoiesis in the bone marrow is activated following MI (82, 83, 86), no studies to date have considered the role of EC-EV in this process. An increase in the number of bone marrow HSC and GMP indicated haematopoiesis was induced and skewed towards granulocyte and monocyte production, which was replicated *in*

vitro. These findings provide a potential mechanism for bone marrow-myocardial communication through EC-EV post-MI which leads to the increased supply of monocytes and neutrophils downstream which are recruited to the injury site.

Having provided evidence to support the hypothesis of modified bone marrow haematopoiesis in response to TNF-α EC-EV, it was important to determine the transcriptional changes that occur within bone marrow HSC to fully elucidate this mechanism. Transcriptomic analysis identified several potential genes of interest, which were differentially expressed in TNF-α EC-EV compared to control EC-EV and were associated with regulating MAPK-NF-κB signalling, cell adhesion, and stem cell proliferation and maintenance. This aligns with our existing understanding of HSC proliferation in the bone marrow and how HSC respond to stimuli such as LPS and ROS (77, 78), which induce the phospho-activation of NF-κB. Nevertheless, further insight will be required to validate this model, including the role of HSC heterogeneity, which has been studied elsewhere using genetic lineage tracing (67, 68), to understand how TNF-α EC-EV reprogramming affects different subpopulations of HSC within the bone marrow.

Several studies in the literature have suggested a role for MI in reprogramming the bone marrow, including in a model of breast cancer which elevated pro-inflammatory monocytes and accelerated breast cancer progression (87). In Cremer et al., a recurrent MI model was developed to show restricted haematopoiesis in the bone marrow, including when an MI was followed by LPS in a sepsis model (82). This thesis assessed whether TNF-α EC-EV could induce a 'primed' haematopoiesis phenotype followed by LPS stimulation and found fewer GMP in the bone marrow and fewer neutrophils in the bone marrow and spleen. Interestingly, this phenotype appears to

be mitigated in VCAM-1 knockout EC-EV and therefore is VCAM-1-dependent. The impact of suppressing VCAM-1 has been studied in splenic reprogramming (89) and highlights that VCAM-1 has an important regulatory function in the innate immune response. In the context of MI, studies have shown EC-EV stimulate ERK1/2 activation in cardiomyocytes (297), and that VCAM-1 is positively associated with heart failure (142), however, the mechanisms which govern VCAM-1 functionality are not fully understood and must be studied further.

The phenomenon of innate immune cell 'memory' has been studied in the literature with several stimuli including β-glucan and LPS (258, 261), and more recently with hyperglycaemia (252). MI has also been studied as a potential stimulus for inducing trained immunity (85, 86) and therefore we hypothesised that TNF-α EC-EV may mediate these effects in the bone marrow on bone marrow-derived macrophages. Macrophages were primed with EC-EV followed by treatment with LPS and IFN-γ as M1-polarising agents and had a diminished inflammatory cytokine response. Furthermore, macrophage adhesion to activated endothelial cells was also reduced, suggesting TNF-α EC-EV priming induces a state of tolerance in BMDM. These effects were also VCAM-1-dependent, indicating a mechanistic role for VCAM-1 in this process, and appeared to lower NF-κB phosphorylation in macrophages. NF-κB phosphorylation is crucial in the induction of pro-inflammatory cytokine expression in pro-inflammatory M1 macrophages (17, 25, 57) and therefore EC-EV priming may regulate macrophage activity through this pathway, although further studies are required to investigate the specific pathway components which are involved.

6.2 Study Limitations & Future Work

This thesis has uncovered a novel role for EC-EV in modulating the bone marrow. However, there are many aspects of the models developed in these studies which need to be elaborated on. The *in vivo* findings that TNF-α EC-EV induce haematopoiesis in bone marrow focus on changes in HSPC populations but do not track the location of EC-EV post-injection. Tracking EV in this model would provide information on EC-EV kinetics such as the rate of EV uptake into the bone marrow as well as the rate of clearance. The latter is important in understanding whether the effects of EC-EV are lost immediately after clearance or if the transcriptional effects are retained.

Importantly, tracking EC-EV would also provide mechanistic insight into which cells within the bone marrow absorb EV and whether uptake is biased to specific cell types. For example, studies show bone marrow adipocytes are able to induce haematopoiesis post-MI (198), and therefore may regulate the bone marrow response to TNF-α EC-EV. Secondly, stromal cells in the bone marrow regulate haematopoiesis in response to infection by transferring mitochondria to HSC (78). Together these studies highlight the tight regulation of haematopoiesis in the bone marrow which is coordinated by several cell types and therefore TNF-α EC-EV may act on the bone marrow directly through HSC or be absorbed by intermediary cell types such as stromal, adipocyte or endothelial cells.

TNF-α EC-EV induce changes in the transcriptional profile of bone marrow HSC, however experiments confirming the specific component of EV which mediate these changes are required to better understand this model. Studies in this thesis highlight

an enrichment in miRNAs including miRNA-126-3p and miRNA-320b in TNF-α EC-EV and that the mRNA targets of these miRNA have overlapping GO terms with differentially expressed genes of HSC. Therefore, it is hypothesised that miRNA-126-3p and miRNA-320b regulate the transcriptional changes in bone marrow HSC induced by TNF-α EC-EV. To test this, miRNA-126-3p and miRNA-320 should be silenced or knocked-down from TNF-α EC-EV using specific antagomirs for each miRNA and assess whether the transcriptional effects of the EV are lost. Going further, a rescue assay could also be performed by administering miRNA-126-3p and miRNA-320b to induce transcriptional changes in HSC. Previous studies analysing the role of miRNA-126 in splenic mobilisation of neutrophils following MI successfully inhibited miRNA-126 using antagomirs which lowered the infarct size in mice and demonstrated the potent physiological effects of eliminating miRNA-126 (89).

Furthermore, given the importance of VCAM-1 in regulating the activity of TNF-α EC-EV in the BMDM model, it would be interesting to use VCAM-1 knockout EC-EV in the haematopoiesis model to assess if the effects on the transcriptional profile of bone marrow HSC are dependent on VCAM-1. To better replicate the EV model in this experiment and protect the miRNA from degradation, the miRNA could be packaged into liposomes prior to administration. This method would also test the importance of EV targeting specific cells since liposomes lack the surface proteins, including VCAM-1, which allow EV to target specific cell populations. If liposome-miRNA complexes were found to have the same effects as TNF-α EC-EV on bone marrow HSC, it would suggest the TNF-α EC-EV reprogramming may not be mediated by targeting specific cell types within the bone marrow.

The studies described in this thesis assume that the TNF-α EC-EV model replicates the effects of MI on the bone marrow. This was used on the basis that plasma VCAM-1$^+$-EV are enriched following MI, and the extent of injury positively correlates with the number of plasma VCAM-1$^+$-EV (88, 89). Future studies could test this model *in vivo* by generating a mouse strain which is deficient in VCAM-1, and assess the transcriptional changes in bone marrow HSC post-MI. The extensive role of VCAM-1 physiologically makes the use of a VCAM-1 knockout mouse model challenging (298) and therefore an inducible knockdown may be preferred for this experiment (299).

In addition to assessing whether the TNF-α EC-EV model is physiologically relevant to MI, it is important to establish the translatability from mouse to human models. Data in this thesis shows that human PBMC-derived macrophages respond to human TNF-α EC-EV by lowering inflammatory cytokine secretion, which is consistent with the mouse BMDM model, and therefore determining whether TNF-α EC-EV reprogramme human bone marrow cells will provide useful therapeutic insight. Due to the ethical implications of isolating bone marrow from healthy human patients, commercial CD34$^+$ bone marrow cells can be used for this investigation (300), but more recent developments in organoid technology increases the possibility of stimulating a three-dimensional, multi-lineage, vascularised bone marrow organoid model to TNF-α EC-EV (301). Bone marrow organoids are an exciting technology which offer significant improvements to previous *in vitro* models, which studied homogenous cell lines in two-dimensional cell culture plates and provided limited biophysical and cellular relevance to physiological bone marrow conditions and therefore had little translatability (302). Interestingly, these novel model systems can be generated from human induced

pluripotent stem cells meaning they can be personalised for each individual patient (301).

Another model used in this thesis which may benefit from bone marrow organoid research is the *in vivo* TNF-α EC-EV-sepsis model, which showed exposure to TNF-α EC-EV followed by LPS diminished haematopoiesis as well as neutrophil production. In this model, the time between EV priming and the LPS exposure was 24 hours, but the optimal time between these stimulations and the long-term implications of immune cell tolerance remain unclear. From similar studies elsewhere, the 10-day timepoint between MI and LPS stimulation suggests a stronger response may be generated with longer stimulation gaps (82). To understand the longevity of the TNF-α EC-EV-induced tolerance model, future studies should establish how long the diminished haematopoiesis phenotype is retained by tracking changes in HSPC subpopulations. Furthermore, studies elsewhere have shown bone marrow HSC memory post-MI is retained after transplantation into naïve mice (83). To determine if the immune cell 'memory' produced by exposure to TNF-α EC-EV is also preserved, transplantation studies should be performed from TNF-α EC-EV-treated mice to naïve mice.

The method used to generate and isolate EC-EV allows the rapid production of disease-relevant EV in a robust manner. However, the high degree of variability between endothelial cells within and between tissues (218, 220) mean there are considerations over which endothelial cells are the most appropriate to use. sEND.1 cells were created using an immortalised endothelioma cell line and therefore the use of primary endothelial cells with more physiological relevance would be a useful method of validating this model. The lower yield of VCAM-1^{+}-EV from plasma limits

the ability of using mouse plasma as a source of EC-EV for these studies, although this would be the most physiologically relevant.

Lastly, a key component of endothelial cell homeostasis *in vivo* is consistent fluid shear stress with fluctuations in shear stress occurring in atherosclerosis-prone regions (303). *In vitro* cell culture can overcome the lack of flowing blood to generate fluid shear stress using flow chambers (215). Isolating EC-EV from cells undergoing fluid shear stress could therefore improve the physiological relevance of the current model. The endothelial cells used in this thesis were cultured in a physiologically healthy environment and disrupting fluid sheer stress could be one way of introducing endothelial cell dysfunction into the EC-EV model. Another stress signal which induces *in vivo* endothelial cell dysfunction is oxidative stress, which has been recreated *in vitro* in models of metabolic diseases such as diabetes and atherosclerosis (304). One study showed that RAGE is activated in the endothelial cells of patients with diabetes and induces oxidative stress (304). This receptor is also expressed on the surface of HUVEC and modifies VCAM-1 expression and endothelial cell permeability (305, 306). Therefore, comparing the response of dysfunctional and comparatively healthy endothelial cells to TNF-α stimulation through parameters such as RAGE activation would be an important step in measuring the robustness of the current TNF-α EC-EV model described here.

6.3 Conclusions

In conclusion, this thesis has uncovered novel roles of reprogramming the bone marrow through TNF-α EC-EV with relevance to cardiovascular disease. Knowledge

of the communication mechanisms between the infarcted heart and the bone marrow are constantly improving, and these findings showcase that haematopoiesis can be regulated by EC-EV to increase the production of myeloid cells. Despite the current unknowns highlighted in this section, the discovery of a link between the injured heart and bone marrow via EC-EV may be of great diagnostic and therapeutic importance to improve patient outcomes following MI.

References

1. Mensah GA, Fuster V, Murray CJL, Roth GA, Collaborators GBoCDaR. Global Burden of Cardiovascular Diseases and Risks, 1990-2022. J Am Coll Cardiol. 2023;82(25):2350-473.
2. Andersson C, Vasan RS. Epidemiology of cardiovascular disease in young individuals. Nat Rev Cardiol. 2018;15(4):230-40.
3. Vaduganathan M, Mensah GA, Turco JV, Fuster V, Roth GA. The Global Burden of Cardiovascular Diseases and Risk: A Compass for Future Health. J Am Coll Cardiol. 2022;80(25):2361-71.
4. Ibanez B, James S, Agewall S, Antunes MJ, Bucciarelli-Ducci C, Bueno H, et al. 2017 ESC Guidelines for the management of acute myocardial infarction in patients presenting with ST-segment elevation: The Task Force for the management of acute myocardial infarction in patients presenting with ST-segment elevation of the European Society of Cardiology (ESC). Eur Heart J. 2018;39(2):119-77.
5. de Torbal A, Boersma E, Kors JA, van Herpen G, Deckers JW, van der Kuip DA, et al. Incidence of recognized and unrecognized myocardial infarction in men and women aged 55 and older: the Rotterdam Study. Eur Heart J. 2006;27(6):729-36.
6. Townsend N, Wilson L, Bhatnagar P, Wickramasinghe K, Rayner M, Nichols M. Cardiovascular disease in Europe: epidemiological update 2016. Eur Heart J. 2016;37(42):3232-45.
7. Gale CP, Allan V, Cattle BA, Hall AS, West RM, Timmis A, et al. Trends in hospital treatments, including revascularisation, following acute myocardial infarction, 2003-2010: a multilevel and relative survival analysis for the National Institute for Cardiovascular Outcomes Research (NICOR). Heart. 2014;100(7):582-9.
8. Puymirat E, Simon T, Steg PG, Schiele F, Guéret P, Blanchard D, et al. Association of changes in clinical characteristics and management with improvement in survival among patients with ST-elevation myocardial infarction. JAMA. 2012;308(10):998-1006.
9. Valgimigli M, Bueno H, Byrne RA, Collet JP, Costa F, Jeppsson A, et al. 2017 ESC focused update on dual antiplatelet therapy in coronary artery disease developed in collaboration with EACTS: The Task Force for dual antiplatelet therapy in coronary artery disease of the European Society of Cardiology (ESC) and of the European Association for Cardio-Thoracic Surgery (EACTS). Eur Heart J. 2018;39(3):213-60.

10. Dans AL, Connolly SJ, Wallentin L, Yang S, Nakamya J, Brueckmann M, et al. Concomitant use of antiplatelet therapy with dabigatran or warfarin in the Randomized Evaluation of Long-Term Anticoagulation Therapy (RE-LY) trial. Circulation. 2013;127(5):634-40.
11. Sørensen R, Hansen ML, Abildstrom SZ, Hvelplund A, Andersson C, Jørgensen C, et al. Risk of bleeding in patients with acute myocardial infarction treated with different combinations of aspirin, clopidogrel, and vitamin K antagonists in Denmark: a retrospective analysis of nationwide registry data. Lancet. 2009;374(9706):1967-74.
12. Piepoli MF, Hoes AW, Agewall S, Albus C, Brotons C, Catapano AL, et al. 2016 European Guidelines on cardiovascular disease prevention in clinical practice: The Sixth Joint Task Force of the European Society of Cardiology and Other Societies on Cardiovascular Disease Prevention in Clinical Practice (constituted by representatives of 10 societies and by invited experts): Developed with the special contribution of the European Association for Cardiovascular Prevention & Rehabilitation (EACPR). Eur J Prev Cardiol. 2016;23(11):NP1-NP96.
13. Mach F, Baigent C, Catapano AL, Koskinas KC, Casula M, Badimon L, et al. 2019 ESC/EAS Guidelines for the management of dyslipidaemias: lipid modification to reduce cardiovascular risk. Eur Heart J. 2020;41(1):111-88.
14. Visseren FLJ, Mach F, Smulders YM, Carballo D, Koskinas KC, Bäck M, et al. 2021 ESC Guidelines on cardiovascular disease prevention in clinical practice. Eur Heart J. 2021;42(34):3227-337.
15. Yellon DM, Hausenloy DJ. Myocardial reperfusion injury. N Engl J Med. 2007;357(11):1121-35.
16. Algoet M, Janssens S, Himmelreich U, Gsell W, Pusovnik M, Van den Eynde J, et al. Myocardial ischemia-reperfusion injury and the influence of inflammation. Trends Cardiovasc Med. 2023;33(6):357-66.
17. Ong SB, Hernández-Reséndiz S, Crespo-Avilan GE, Mukhametshina RT, Kwek XY, Cabrera-Fuentes HA, et al. Inflammation following acute myocardial infarction: Multiple players, dynamic roles, and novel therapeutic opportunities. Pharmacol Ther. 2018;186:73-87.
18. Tombor LS, John D, Glaser SF, Luxán G, Forte E, Furtado M, et al. Single cell sequencing reveals endothelial plasticity with transient mesenchymal activation after myocardial infarction. Nat Commun. 2021;12(1):681.

19. Zeisberg EM, Tarnavski O, Zeisberg M, Dorfman AL, McMullen JR, Gustafsson E, et al. Endothelial-to-mesenchymal transition contributes to cardiac fibrosis. Nat Med. 2007;13(8):952-61.
20. Görlach A, Dimova EY, Petry A, Martínez-Ruiz A, Hernansanz-Agustín P, Rolo AP, et al. Reactive oxygen species, nutrition, hypoxia and diseases: Problems solved? Redox Biol. 2015;6:372-85.
21. Frangogiannis NG. Pathophysiology of Myocardial Infarction. Compr Physiol. 2015;5(4):1841-75.
22. Tian M, Yuan YC, Li JY, Gionfriddo MR, Huang RC. Tumor necrosis factor-α and its role as a mediator in myocardial infarction: A brief review. Chronic Dis Transl Med. 2015;1(1):18-26.
23. Kohno T, Anzai T, Naito K, Miyasho T, Okamoto M, Yokota H, et al. Role of high-mobility group box 1 protein in post-infarction healing process and left ventricular remodelling. Cardiovasc Res. 2009;81(3):565-73.
24. Dillmann WH, Mestril R. Heat shock proteins in myocardial stress. Z Kardiol. 1995;84 Suppl 4:87-90.
25. Komal S, Komal N, Mujtaba A, Wang SH, Zhang LR, Han SN. Potential therapeutic strategies for myocardial infarction: the role of Toll-like receptors. Immunol Res. 2022;70(5):607-23.
26. Toldo S, Abbate A. The NLRP3 inflammasome in acute myocardial infarction. Nat Rev Cardiol. 2018;15(4):203-14.
27. Martínez GJ, Celermajer DS, Patel S. The NLRP3 inflammasome and the emerging role of colchicine to inhibit atherosclerosis-associated inflammation. Atherosclerosis. 2018;269:262-71.
28. Swirski F, Nahrendorf M. Leukocyte Behavior in Atherosclerosis, Myocardial Infarction, and Heart Failure. 2013.
29. Ruparelia N, Godec J, Lee R, Chai JT, Dall'Armellina E, McAndrew D, et al. Acute myocardial infarction activates distinct inflammation and proliferation pathways in circulating monocytes, prior to recruitment, and identified through conserved transcriptional responses in mice and humans. Eur Heart J. 2015;36(29):1923-34.
30. Swirski FK, Nahrendorf M, Etzrodt M, Wildgruber M, Cortez-Retamozo V, Panizzi P, et al. Identification of splenic reservoir monocytes and their deployment to inflammatory sites. Science. 2009;325(5940):612-6.

31. Panizzi P, Swirski FK, Figueiredo JL, Waterman P, Sosnovik DE, Aikawa E, et al. Impaired infarct healing in atherosclerotic mice with Ly-6C(hi) monocytosis. J Am Coll Cardiol. 2010;55(15):1629-38.
32. Nahrendorf M, Swirski FK, Aikawa E, Stangenberg L, Wurdinger T, Figueiredo JL, et al. The healing myocardium sequentially mobilizes two monocyte subsets with divergent and complementary functions. J Exp Med. 2007;204(12):3037-47.
33. Schloss MJ, Horckmans M, Nitz K, Duchene J, Drechsler M, Bidzhekov K, et al. The time-of-day of myocardial infarction onset affects healing through oscillations in cardiac neutrophil recruitment. EMBO Mol Med. 2016;8(8):937-48.
34. Horckmans M, Ring L, Duchene J, Santovito D, Schloss MJ, Drechsler M, et al. Neutrophils orchestrate post-myocardial infarction healing by polarizing macrophages towards a reparative phenotype. Eur Heart J. 2017;38(3):187-97.
35. Chia S, Nagurney JT, Brown DF, Raffel OC, Bamberg F, Senatore F, et al. Association of leukocyte and neutrophil counts with infarct size, left ventricular function and outcomes after percutaneous coronary intervention for ST-elevation myocardial infarction. Am J Cardiol. 2009;103(3):333-7.
36. Martin C, Burdon PC, Bridger G, Gutierrez-Ramos JC, Williams TJ, Rankin SM. Chemokines acting via CXCR2 and CXCR4 control the release of neutrophils from the bone marrow and their return following senescence. Immunity. 2003;19(4):583-93.
37. Terashima T, English D, Hogg JC, van Eeden SF. Release of polymorphonuclear leukocytes from the bone marrow by interleukin-8. Blood. 1998;92(3):1062-9.
38. Sokol CL, Luster AD. The chemokine system in innate immunity. Cold Spring Harb Perspect Biol. 2015;7(5).
39. Hernández-Reséndiz S, Muñoz-Vega M, Contreras WE, Crespo-Avilan GE, Rodriguez-Montesinos J, Arias-Carrión O, et al. Responses of Endothelial Cells Towards Ischemic Conditioning Following Acute Myocardial Infarction. Cond Med. 2018;1(5):247-58.
40. Muller WA. Leukocyte-endothelial-cell interactions in leukocyte transmigration and the inflammatory response. Trends Immunol. 2003;24(6):327-34.
41. Furze RC, Rankin SM. Neutrophil mobilization and clearance in the bone marrow. Immunology. 2008;125(3):281-8.

42. Lörchner H, Pöling J, Gajawada P, Hou Y, Polyakova V, Kostin S, et al. Myocardial healing requires Reg3β-dependent accumulation of macrophages in the ischemic heart. Nat Med. 2015;21(4):353-62.
43. Leuschner F, Panizzi P, Chico-Calero I, Lee WW, Ueno T, Cortez-Retamozo V, et al. Angiotensin-converting enzyme inhibition prevents the release of monocytes from their splenic reservoir in mice with myocardial infarction. Circ Res. 2010;107(11):1364-73.
44. Peet C, Ivetic A, Bromage DI, Shah AM. Cardiac monocytes and macrophages after myocardial infarction. Cardiovasc Res. 2020;116(6):1101-12.
45. O'Rourke SA, Dunne A, Monaghan MG. The Role of Macrophages in the Infarcted Myocardium: Orchestrators of ECM Remodeling. Front Cardiovasc Med. 2019;6:101.
46. Biswas SK, Mantovani A. Macrophage plasticity and interaction with lymphocyte subsets: cancer as a paradigm. Nat Immunol. 2010;11(10):889-96.
47. Leuschner F, Dutta P, Gorbatov R, Novobrantseva TI, Donahoe JS, Courties G, et al. Therapeutic siRNA silencing in inflammatory monocytes in mice. Nat Biotechnol. 2011;29(11):1005-10.
48. Majmudar MD, Keliher EJ, Heidt T, Leuschner F, Truelove J, Sena BF, et al. Monocyte-directed RNAi targeting CCR2 improves infarct healing in atherosclerosis-prone mice. Circulation. 2013;127(20):2038-46.
49. Matter MA, Tschaikowsky T, Stähli BE, Matter CM. Acute-on-chronic inflammation in acute myocardial infarction. Curr Opin Cardiol. 2024.
50. Seropian IM, Toldo S, Van Tassell BW, Abbate A. Anti-inflammatory strategies for ventricular remodeling following ST-segment elevation acute myocardial infarction. J Am Coll Cardiol. 2014;63(16):1593-603.
51. Mitsis A, Kyriakou M, Sokratous S, Karmioti G, Drakomathioulakis M, Myrianthefs M, et al. Exploring the Landscape of Anti-Inflammatory Trials: A Comprehensive Review of Strategies for Targeting Inflammation in Acute Myocardial Infraction. Biomedicines. 2024;12(3).
52. Rieckmann M, Delgobo M, Gaal C, Büchner L, Steinau P, Reshef D, et al. Myocardial infarction triggers cardioprotective antigen-specific T helper cell responses. J Clin Invest. 2019;129(11):4922-36.

53. Hofmann U, Beyersdorf N, Weirather J, Podolskaya A, Bauersachs J, Ertl G, et al. Activation of CD4+ T lymphocytes improves wound healing and survival after experimental myocardial infarction in mice. Circulation. 2012;125(13):1652-63.
54. Bansal SS, Ismahil MA, Goel M, Patel B, Hamid T, Rokosh G, et al. Activated T Lymphocytes are Essential Drivers of Pathological Remodeling in Ischemic Heart Failure. Circ Heart Fail. 2017;10(3):e003688.
55. Tang TT, Zhu YC, Dong NG, Zhang S, Cai J, Zhang LX, et al. Pathologic T-cell response in ischaemic failing hearts elucidated by T-cell receptor sequencing and phenotypic characterization. Eur Heart J. 2019;40(48):3924-33.
56. McKim DB, Yin W, Wang Y, Cole SW, Godbout JP, Sheridan JF. Social Stress Mobilizes Hematopoietic Stem Cells to Establish Persistent Splenic Myelopoiesis. Cell Rep. 2018;25(9):2552-62.e3.
57. Nahrendorf M. Myeloid cell contributions to cardiovascular health and disease. Nat Med. 2018;24(6):711-20.
58. Dutta P, Nahrendorf M. Regulation and consequences of monocytosis. Immunol Rev. 2014;262(1):167-78.
59. Fröbel J, Landspersky T, Percin G, Schreck C, Rahmig S, Ori A, et al. The Hematopoietic Bone Marrow Niche Ecosystem. Front Cell Dev Biol. 2021;9:705410.
60. Baccin C, Al-Sabah J, Velten L, Helbling PM, Grünschläger F, Hernández-Malmierca P, et al. Combined single-cell and spatial transcriptomics reveal the molecular, cellular and spatial bone marrow niche organization. Nat Cell Biol. 2020;22(1):38-48.
61. Höfer T, Rodewald HR. Differentiation-based model of hematopoietic stem cell functions and lineage pathways. Blood. 2018;132(11):1106-13.
62. Yamamoto R, Morita Y, Ooehara J, Hamanaka S, Onodera M, Rudolph KL, et al. Clonal analysis unveils self-renewing lineage-restricted progenitors generated directly from hematopoietic stem cells. Cell. 2013;154(5):1112-26.
63. Busch K, Klapproth K, Barile M, Flossdorf M, Holland-Letz T, Schlenner SM, et al. Fundamental properties of unperturbed haematopoiesis from stem cells in vivo. Nature. 2015;518(7540):542-6.
64. Pietras EM, Reynaud D, Kang YA, Carlin D, Calero-Nieto FJ, Leavitt AD, et al. Functionally Distinct Subsets of Lineage-Biased Multipotent Progenitors Control Blood Production in Normal and Regenerative Conditions. Cell Stem Cell. 2015;17(1):35-46.

65. Cabezas-Wallscheid N, Klimmeck D, Hansson J, Lipka DB, Reyes A, Wang Q, et al. Identification of regulatory networks in HSCs and their immediate progeny via integrated proteome, transcriptome, and DNA methylome analysis. Cell Stem Cell. 2014;15(4):507-22.
66. Kang YA, Pietras EM, Passegué E. Deregulated Notch and Wnt signaling activates early-stage myeloid regeneration pathways in leukemia. J Exp Med. 2020;217(3).
67. Yamamoto R, Wilkinson AC, Ooehara J, Lan X, Lai CY, Nakauchi Y, et al. Large-Scale Clonal Analysis Resolves Aging of the Mouse Hematopoietic Stem Cell Compartment. Cell Stem Cell. 2018;22(4):600-7.e4.
68. Notta F, Zandi S, Takayama N, Dobson S, Gan OI, Wilson G, et al. Distinct routes of lineage development reshape the human blood hierarchy across ontogeny. Science. 2016;351(6269):aab2116.
69. Qin P, Pang Y, Hou W, Fu R, Zhang Y, Wang X, et al. Integrated decoding hematopoiesis and leukemogenesis using single-cell sequencing and its medical implication. Cell Discov. 2021;7(1):2.
70. Bryder D, Rossi DJ, Weissman IL. Hematopoietic stem cells: the paradigmatic tissue-specific stem cell. Am J Pathol. 2006;169(2):338-46.
71. Ding L, Morrison SJ. Haematopoietic stem cells and early lymphoid progenitors occupy distinct bone marrow niches. Nature. 2013;495(7440):231-5.
72. Greenbaum A, Hsu YM, Day RB, Schuettpelz LG, Christopher MJ, Borgerding JN, et al. CXCL12 in early mesenchymal progenitors is required for haematopoietic stem-cell maintenance. Nature. 2013;495(7440):227-30.
73. Kiel MJ, Yilmaz OH, Iwashita T, Terhorst C, Morrison SJ. SLAM family receptors distinguish hematopoietic stem and progenitor cells and reveal endothelial niches for stem cells. Cell. 2005;121(7):1109-21.
74. Kiel MJ, Radice GL, Morrison SJ. Lack of evidence that hematopoietic stem cells depend on N-cadherin-mediated adhesion to osteoblasts for their maintenance. Cell Stem Cell. 2007;1(2):204-17.
75. Wright DE, Wagers AJ, Gulati AP, Johnson FL, Weissman IL. Physiological migration of hematopoietic stem and progenitor cells. Science. 2001;294(5548):1933-6.
76. Takizawa H, Fritsch K, Kovtonyuk LV, Saito Y, Yakkala C, Jacobs K, et al. Pathogen-Induced TLR4-TRIF Innate Immune Signaling in Hematopoietic Stem Cells

Promotes Proliferation but Reduces Competitive Fitness. Cell Stem Cell. 2017;21(2):225-40.e5.
77. Vandoorne K, Rohde D, Kim HY, Courties G, Wojtkiewicz G, Honold L, et al. Imaging the Vascular Bone Marrow Niche During Inflammatory Stress. Circ Res. 2018;123(4):415-27.
78. Mistry JJ, Marlein CR, Moore JA, Hellmich C, Wojtowicz EE, Smith JGW, et al. ROS-mediated PI3K activation drives mitochondrial transfer from stromal cells to hematopoietic stem cells in response to infection. Proc Natl Acad Sci U S A. 2019;116(49):24610-9.
79. Nagareddy PR, Kraakman M, Masters SL, Stirzaker RA, Gorman DJ, Grant RW, et al. Adipose tissue macrophages promote myelopoiesis and monocytosis in obesity. Cell Metab. 2014;19(5):821-35.
80. Nagareddy PR, Murphy AJ, Stirzaker RA, Hu Y, Yu S, Miller RG, et al. Hyperglycemia promotes myelopoiesis and impairs the resolution of atherosclerosis. Cell Metab. 2013;17(5):695-708.
81. Thune JJ, Signorovitch JE, Kober L, McMurray JJ, Swedberg K, Rouleau J, et al. Predictors and prognostic impact of recurrent myocardial infarction in patients with left ventricular dysfunction, heart failure, or both following a first myocardial infarction. Eur J Heart Fail. 2011;13(2):148-53.
82. Cremer S, Schloss MJ, Vinegoni C, Foy BH, Zhang S, Rohde D, et al. Diminished Reactive Hematopoiesis and Cardiac Inflammation in a Mouse Model of Recurrent Myocardial Infarction. J Am Coll Cardiol. 2020;75(8):901-15.
83. Nakayama Y, Fujiu K, Oshima T, Matsuda J, Sugita J, Matsubara TJ, et al. Heart failure promotes multimorbidity through innate immune memory. Sci Immunol. 2024;9(95):eade3814.
84. Saeed S, Quintin J, Kerstens HH, Rao NA, Aghajanirefah A, Matarese F, et al. Epigenetic programming of monocyte-to-macrophage differentiation and trained innate immunity. Science. 2014;345(6204):1251086.
85. Christ A, Günther P, Lauterbach MAR, Duewell P, Biswas D, Pelka K, et al. Western Diet Triggers NLRP3-Dependent Innate Immune Reprogramming. Cell. 2018;172(1-2):162-75.e14.
86. Mitroulis I, Ruppova K, Wang B, Chen LS, Grzybek M, Grinenko T, et al. Modulation of Myelopoiesis Progenitors Is an Integral Component of Trained Immunity. Cell. 2018;172(1-2):147-61.e12.

87. Koelwyn GJ, Newman AAC, Afonso MS, van Solingen C, Corr EM, Brown EJ, et al. Myocardial infarction accelerates breast cancer via innate immune reprogramming. Nat Med. 2020;26(9):1452-8.
88. Akbar N, Digby JE, Cahill TJ, Tavare AN, Corbin AL, Saluja S, et al. Endothelium-derived extracellular vesicles promote splenic monocyte mobilization in myocardial infarction. 2017.
89. Akbar N, Braithwaite AT, Corr EM, Koelwyn GJ, van Solingen C, Cochain C, et al. Rapid neutrophil mobilization by VCAM-1+ endothelial cell-derived extracellular vesicles. Cardiovasc Res. 2023;119(1):236-51.
90. Welsh JA, Goberdhan DCI, O'Driscoll L, Buzas EI, Blenkiron C, Bussolati B, et al. Minimal information for studies of extracellular vesicles (MISEV2023): From basic to advanced approaches. J Extracell Vesicles. 2024;13(2):e12404.
91. Akbar N, Azzimato V, Choudhury RP, Aouadi M. Extracellular vesicles in metabolic disease. Diabetologia. 2019;62(12):2179-87.
92. Russell AE, Sneider A, Witwer KW, Bergese P, Bhattacharyya SN, Cocks A, et al. Biological membranes in EV biogenesis, stability, uptake, and cargo transfer: an ISEV position paper arising from the ISEV membranes and EVs workshop. J Extracell Vesicles. 2019;8(1):1684862.
93. Doyle LM, Wang MZ. Overview of Extracellular Vesicles, Their Origin, Composition, Purpose, and Methods for Exosome Isolation and Analysis. Cells. 2019;8(7).
94. Loyer X, Zlatanova I, Devue C, Yin M, Howangyin KY, Klaihmon P, et al. Intra-Cardiac Release of Extracellular Vesicles Shapes Inflammation Following Myocardial Infarction. Circ Res. 2018;123(1):100-6.
95. Sluijter JP, Verhage V, Deddens JC, van den Akker F, Doevendans PA. Microvesicles and exosomes for intracardiac communication. Cardiovasc Res. 2014;102(2):302-11.
96. Cheng M, Yang J, Zhao X, Zhang E, Zeng Q, Yu Y, et al. Circulating myocardial microRNAs from infarcted hearts are carried in exosomes and mobilise bone marrow progenitor cells. Nat Commun. 2019;10(1):959.
97. Villarroya-Beltri C, Gutiérrez-Vázquez C, Sánchez-Madrid F, Mittelbrunn M. Analysis of microRNA and protein transfer by exosomes during an immune synapse. Methods Mol Biol. 2013;1024:41-51.

98. Paget D, Checa A, Zöhrer B, Heilig R, Shanmuganathan M, Dhaliwal R, et al. Comparative and integrated analysis of plasma extracellular vesicle isolation methods in healthy volunteers and patients following myocardial infarction. J Extracell Biol. 2022;1(11):e66.
99. O'Brien K, Breyne K, Ughetto S, Laurent LC, Breakefield XO. RNA delivery by extracellular vesicles in mammalian cells and its applications. Nat Rev Mol Cell Biol. 2020;21(10):585-606.
100. Elzanowska J, Semira C, Costa-Silva B. DNA in extracellular vesicles: biological and clinical aspects. Mol Oncol. 2021;15(6):1701-14.
101. Liang W, Sagar S, Ravindran R, Najor RH, Quiles JM, Chi L, et al. Mitochondria are secreted in extracellular vesicles when lysosomal function is impaired. Nat Commun. 2023;14(1):5031.
102. Dixson AC, Dawson TR, Di Vizio D, Weaver AM. Context-specific regulation of extracellular vesicle biogenesis and cargo selection. Nat Rev Mol Cell Biol. 2023;24(7):454-76.
103. Petersen JD, Mekhedov E, Kaur S, Roberts DD, Zimmerberg J. Endothelial cells release microvesicles that harbour multivesicular bodies and secrete exosomes. J Extracell Biol. 2023;2(4):e79.
104. Ludwig N, Whiteside TL, Reichert TE. Challenges in Exosome Isolation and Analysis in Health and Disease. Int J Mol Sci. 2019;20(19).
105. Karimi N, Cvjetkovic A, Jang SC, Crescitelli R, Hosseinpour Feizi MA, Nieuwland R, et al. Detailed analysis of the plasma extracellular vesicle proteome after separation from lipoproteins. Cell Mol Life Sci. 2018;75(15):2873-86.
106. Bellin G, Gardin C, Ferroni L, Chachques JC, Rogante M, Mitrečić D, et al. Exosome in Cardiovascular Diseases: A Complex World Full of Hope. Cells. 2019;8(2).
107. Kowal J, Arras G, Colombo M, Jouve M, Morath JP, Primdal-Bengtson B, et al. Proteomic comparison defines novel markers to characterize heterogeneous populations of extracellular vesicle subtypes. Proc Natl Acad Sci U S A. 2016;113(8):E968-77.
108. Gardiner C, Ferreira YJ, Dragovic RA, Redman CW, Sargent IL. Extracellular vesicle sizing and enumeration by nanoparticle tracking analysis. J Extracell Vesicles. 2013;2.

109. Welsh JA, Van Der Pol E, Arkesteijn GJA, Bremer M, Brisson A, Coumans F, et al. MIFlowCyt-EV: a framework for standardized reporting of extracellular vesicle flow cytometry experiments. J Extracell Vesicles. 2020;9(1):1713526.
110. Vogel R, Coumans FA, Maltesen RG, Böing AN, Bonnington KE, Broekman ML, et al. A standardized method to determine the concentration of extracellular vesicles using tunable resistive pulse sensing. J Extracell Vesicles. 2016;5:31242.
111. Tian Y, Gong M, Hu Y, Liu H, Zhang W, Zhang M, et al. Quality and efficiency assessment of six extracellular vesicle isolation methods by nano-flow cytometry. J Extracell Vesicles. 2020;9(1):1697028.
112. Yuana Y, Koning RI, Kuil ME, Rensen PC, Koster AJ, Bertina RM, et al. Cryo-electron microscopy of extracellular vesicles in fresh plasma. J Extracell Vesicles. 2013;2.
113. Cavallaro S, Hååg P, Viktorsson K, Krozer A, Fogel K, Lewensohn R, et al. Comparison and optimization of nanoscale extracellular vesicle imaging by scanning electron microscopy for accurate size-based profiling and morphological analysis. Nanoscale Adv. 2021;3(11):3053-63.
114. Théry C, Amigorena S, Raposo G, Clayton A. Isolation and characterization of exosomes from cell culture supernatants and biological fluids. Curr Protoc Cell Biol. 2006;Chapter 3:Unit 3.22.
115. Sharma S, LeClaire M, Gimzewski JK. Ascent of atomic force microscopy as a nanoanalytical tool for exosomes and other extracellular vesicles. Nanotechnology. 2018;29(13):132001.
116. Arraud N, Linares R, Tan S, Gounou C, Pasquet JM, Mornet S, et al. Extracellular vesicles from blood plasma: determination of their morphology, size, phenotype and concentration. J Thromb Haemost. 2014;12(5):614-27.
117. Greening DW, Simpson RJ. Understanding extracellular vesicles. Proteomics. 2021;21(13-14):e2100126.
118. Poe AJ, Knowlton AA. Exosomes and cardiovascular cell-cell communication. Essays Biochem. 2018;62(2):193-204.
119. Couch Y, Akbar N, Roodselaar J, Evans MC, Gardiner C, Sargent I, et al. Circulating endothelial cell-derived extracellular vesicles mediate the acute phase response and sickness behaviour associated with CNS inflammation. Sci Rep. 2017;7(1):9574.

120. Kong DH, Kim YK, Kim MR, Jang JH, Lee S. Emerging Roles of Vascular Cell Adhesion Molecule-1 (VCAM-1) in Immunological Disorders and Cancer. Int J Mol Sci. 2018;19(4).
121. Li D, Xue W, Li M, Dong M, Wang J, Wang X, et al. VCAM-1. Nature. 2018;564(7734):119-24.
122. Gkaliagkousi E, Gavriilaki E, Vasileiadis I, Nikolaidou B, Yiannaki E, Lazaridis A, et al. Endothelial Microvesicles Circulating in Peripheral and Coronary Circulation Are Associated With Central Blood Pressure in Coronary Artery Disease. Am J Hypertens. 2019;32(12):1199-205.
123. Vagida M, Arakelyan A, Lebedeva A, Grivel JC, Shpektor A, Vasilieva E, et al. Flow analysis of individual blood extracellular vesicles in acute coronary syndrome. Platelets. 2017;28(2):165-73.
124. Vicencio JM, Yellon DM, Sivaraman V, Das D, Boi-Doku C, Arjun S, et al. Plasma exosomes protect the myocardium from ischemia-reperfusion injury. J Am Coll Cardiol. 2015;65(15):1525-36.
125. Cheng XF, He ST, Zhong GQ, Meng JJ, Wang M, Bi Q, et al. Exosomal HSP90 induced by remote ischemic preconditioning alleviates myocardial ischemia/reperfusion injury by inhibiting complement activation and inflammation. BMC Cardiovasc Disord. 2023;23(1):58.
126. Malik ZA, Kott KS, Poe AJ, Kuo T, Chen L, Ferrara KW, et al. Cardiac myocyte exosomes: stability, HSP60, and proteomics. Am J Physiol Heart Circ Physiol. 2013;304(7):H954-65.
127. Yang J, Yu X, Xue F, Li Y, Liu W, Zhang S. Exosomes derived from cardiomyocytes promote cardiac fibrosis via myocyte-fibroblast cross-talk. Am J Transl Res. 2018;10(12):4350-66.
128. Almeida Paiva R, Martins-Marques T, Jesus K, Ribeiro-Rodrigues T, Zuzarte M, Silva A, et al. Ischaemia alters the effects of cardiomyocyte-derived extracellular vesicles on macrophage activation. J Cell Mol Med. 2019;23(2):1137-51.
129. Zhang C, Wu J, Xu X, Potter BJ, Gao X. Direct relationship between levels of TNF-alpha expression and endothelial dysfunction in reperfusion injury. Basic Res Cardiol. 2010;105(4):453-64.
130. Li J, Salvador AM, Li G, Valkov N, Ziegler O, Yeri A, et al. Mir-30d Regulates Cardiac Remodeling by Intracellular and Paracrine Signaling. Circ Res. 2021;128(1):e1-e23.

131. Liu S, Chen J, Shi J, Zhou W, Wang L, Fang W, et al. M1-like macrophage-derived exosomes suppress angiogenesis and exacerbate cardiac dysfunction in a myocardial infarction microenvironment. Basic Res Cardiol. 2020;115(2):22.
132. Wang C, Zhang C, Liu L, A X, Chen B, Li Y, et al. Macrophage-Derived mir-155-Containing Exosomes Suppress Fibroblast Proliferation and Promote Fibroblast Inflammation during Cardiac Injury. Mol Ther. 2017;25(1):192-204.
133. Luo H, Li X, Li T, Zhao L, He J, Zha L, et al. microRNA-423-3p exosomes derived from cardiac fibroblasts mediates the cardioprotective effects of ischaemic post-conditioning. Cardiovasc Res. 2019;115(7):1189-204.
134. Burrello J, Biemmi V, Dei Cas M, Amongero M, Bolis S, Lazzarini E, et al. Sphingolipid composition of circulating extracellular vesicles after myocardial ischemia. Sci Rep. 2020;10(1):16182.
135. Sturtzel C. Endothelial Cells. Adv Exp Med Biol. 2017;1003:71-91.
136. Trimm E, Red-Horse K. Vascular endothelial cell development and diversity. Nat Rev Cardiol. 2023;20(3):197-210.
137. Zhang C. The role of inflammatory cytokines in endothelial dysfunction. Basic Res Cardiol. 2008;103(5):398-406.
138. Cook-Mills JM, Marchese ME, Abdala-Valencia H. Vascular cell adhesion molecule-1 expression and signaling during disease: regulation by reactive oxygen species and antioxidants. Antioxid Redox Signal. 2011;15(6):1607-38.
139. Cai H, Harrison DG. Endothelial dysfunction in cardiovascular diseases: the role of oxidant stress. Circ Res. 2000;87(10):840-4.
140. Hunt BJ, Jurd KM. Endothelial cell activation. A central pathophysiological process. BMJ. 1998;316(7141):1328-9.
141. Singhal AK, Symons JD, Boudina S, Jaishy B, Shiu YT. Role of Endothelial Cells in Myocardial Ischemia-Reperfusion Injury. Vasc Dis Prev. 2010;7:1-14.
142. Wang T, Tian J, Jin Y. VCAM1 expression in the myocardium is associated with the risk of heart failure and immune cell infiltration in myocardium. Sci Rep. 2021;11(1):19488.
143. Hauser IA, Johnson DR, Madri JA. Differential induction of VCAM-1 on human iliac venous and arterial endothelial cells and its role in adhesion. J Immunol. 1993;151(10):5172-85.
144. Boon RA, Dimmeler S. MicroRNA-126 in atherosclerosis. Arterioscler Thromb Vasc Biol. 2014;34(7):e15-6.

145. Schober A, Nazari-Jahantigh M, Wei Y, Bidzhekov K, Gremse F, Grommes J, et al. MicroRNA-126-5p promotes endothelial proliferation and limits atherosclerosis by suppressing Dlk1. Nat Med. 2014;20(4):368-76.
146. Wang S, Aurora AB, Johnson BA, Qi X, McAnally J, Hill JA, et al. The endothelial-specific microRNA miR-126 governs vascular integrity and angiogenesis. Dev Cell. 2008;15(2):261-71.
147. Ling H, Guo Z, Shi Y, Zhang L, Song C. Serum Exosomal MicroRNA-21, MicroRNA-126, and PTEN Are Novel Biomarkers for Diagnosis of Acute Coronary Syndrome. Front Physiol. 2020;11:654.
148. Anderson JL, Morrow DA. Acute Myocardial Infarction. N Engl J Med. 2017;376(21):2053-64.
149. Mastronarde DN. Automated electron microscope tomography using robust prediction of specimen movements. Journal of Structural Biology. 2005;152(1):36-51.
150. Boettcher S, Ziegler P, Schmid MA, Takizawa H, van Rooijen N, Kopf M, et al. Cutting edge: LPS-induced emergency myelopoiesis depends on TLR4-expressing nonhematopoietic cells. J Immunol. 2012;188(12):5824-8.
151. Mortazavi A, Williams BA, McCue K, Schaeffer L, Wold B. Mapping and quantifying mammalian transcriptomes by RNA-Seq. Nat Methods. 2008;5(7):621-8.
152. Pertea M, Pertea GM, Antonescu CM, Chang TC, Mendell JT, Salzberg SL. StringTie enables improved reconstruction of a transcriptome from RNA-seq reads. Nat Biotechnol. 2015;33(3):290-5.
153. Subramanian A, Tamayo P, Mootha VK, Mukherjee S, Ebert BL, Gillette MA, et al. Gene set enrichment analysis: a knowledge-based approach for interpreting genome-wide expression profiles. Proc Natl Acad Sci U S A. 2005;102(43):15545-50.
154. Mootha VK, Lindgren CM, Eriksson KF, Subramanian A, Sihag S, Lehar J, et al. PGC-1alpha-responsive genes involved in oxidative phosphorylation are coordinately downregulated in human diabetes. Nat Genet. 2003;34(3):267-73.
155. Szklarczyk D, Kirsch R, Koutrouli M, Nastou K, Mehryary F, Hachilif R, et al. The STRING database in 2023: protein-protein association networks and functional enrichment analyses for any sequenced genome of interest. Nucleic Acids Res. 2023;51(D1):D638-D46.
156. Chen Y, Wang X. miRDB: an online database for prediction of functional microRNA targets. Nucleic Acids Res. 2020;48(D1):D127-D31.

157. Sticht C, De La Torre C, Parveen A, Gretz N. miRWalk: An online resource for prediction of microRNA binding sites. PLoS One. 2018;13(10):e0206239.
158. Agarwal V, Bell GW, Nam JW, Bartel DP. Predicting effective microRNA target sites in mammalian mRNAs. Elife. 2015;4.
159. Golia E, Limongelli G, Natale F, Fimiani F, Maddaloni V, Pariggiano I, et al. Inflammation and Cardiovascular Disease: From Pathogenesis to Therapeutic Target. Current Atherosclerosis Reports. 2014;16(9):1-7.
160. Hansson GK, Hermansson A. The immune system in atherosclerosis. Nat Immunol. 2011;12(3):204-12.
161. Ruparelia N, Chai JT, Fisher EA, Choudhury RP. Inflammatory processes in cardiovascular disease: a route to targeted therapies. Nat Rev Cardiol. 2017;14(5):314.
162. Williams JW, Huang LH, Randolph GJ. Cytokine Circuits in Cardiovascular Disease. Immunity. 2019;50(4):941-54.
163. Vafadarnejad E, Rizzo G, Krampert L, Arampatzi P, Arias-Loza AP, Nazzal Y, et al. Dynamics of Cardiac Neutrophil Diversity in Murine Myocardial Infarction. Circ Res. 2020;127(9):e232-e49.
164. Kubota A, Frangogiannis NG. Macrophages in myocardial infarction. Am J Physiol Cell Physiol. 2022;323(4):C1304-C24.
165. Dutta P, Sager HB, Stengel KR, Naxerova K, Courties G, Saez B, et al. Myocardial Infarction Activates CCR2(+) Hematopoietic Stem and Progenitor Cells. Cell Stem Cell. 2015;16(5):477-87.
166. Sager HB, Hulsmans M, Lavine KJ, Moreira MB, Heidt T, Courties G, et al. Proliferation and Recruitment Contribute to Myocardial Macrophage Expansion in Chronic Heart Failure. Circ Res. 2016;119(7):853-64.
167. Yap J, Irei J, Lozano-Gerona J, Vanapruks S, Bishop T, Boisvert WA. Macrophages in cardiac remodelling after myocardial infarction. Nat Rev Cardiol. 2023;20(6):373-85.
168. Ma Y. Role of Neutrophils in Cardiac Injury and Repair Following Myocardial Infarction. Cells. 2021;10(7).
169. Fielding C, Méndez-Ferrer S. Neuronal regulation of bone marrow stem cell niches. F1000Res. 2020;9.
170. Ho NP, Takizawa H. Inflammation Regulates Haematopoietic Stem Cells and Their Niche. Int J Mol Sci. 2022;23(3).

171. Liu P, Sun M, Sader S. Matrix metalloproteinases in cardiovascular disease. Can J Cardiol. 2006;22 Suppl B(Suppl B):25B-30B.
172. Harris TA, Yamakuchi M, Ferlito M, Mendell JT, Lowenstein CJ. MicroRNA-126 regulates endothelial expression of vascular cell adhesion molecule 1. Proc Natl Acad Sci U S A. 2008;105(5):1516-21.
173. Feng B, Chakrabarti S. miR-320 Regulates Glucose-Induced Gene Expression in Diabetes. ISRN Endocrinol. 2012;2012:549875.
174. Wang XH, Qian RZ, Zhang W, Chen SF, Jin HM, Hu RM. MicroRNA-320 expression in myocardial microvascular endothelial cells and its relationship with insulin-like growth factor-1 in type 2 diabetic rats. Clin Exp Pharmacol Physiol. 2009;36(2):181-8.
175. Rosenson RS. Myocardial injury: the acute phase response and lipoprotein metabolism. J Am Coll Cardiol. 1993;22(3):933-40.
176. Sun JY, Du LJ, Shi XR, Zhang YY, Liu Y, Wang YL, et al. An IL-6/STAT3/MR/FGF21 axis mediates heart-liver cross-talk after myocardial infarction. Sci Adv. 2023;9(14):eade4110.
177. Heusch G. The Spleen in Myocardial Infarction. Circ Res. 2019;124(1):26-8.
178. Wang P, Wang J, Li YH, Wang L, Shang HC, Wang JX. Phenotypical Changes of Hematopoietic Stem and Progenitor Cells in Sepsis Patients: Correlation With Immune Status? Front Pharmacol. 2020;11:640203.
179. Zhang H, Rodriguez S, Wang L, Wang S, Serezani H, Kapur R, et al. Sepsis Induces Hematopoietic Stem Cell Exhaustion and Myelosuppression through Distinct Contributions of TRIF and MYD88. Stem Cell Reports. 2016;6(6):940-56.
180. Nguyen TH, Abidin BM, Heinonen KM. Frizzled-6 promotes hematopoietic stem/progenitor cell mobilization and survival during LPS-induced emergency myelopoiesis. Stem Cell Reports. 2022;17(10):2303-17.
181. Abidin BM, Owusu Kwarteng E, Heinonen KM. Frizzled-6 Regulates Hematopoietic Stem/Progenitor Cell Survival and Self-Renewal. J Immunol. 2015;195(5):2168-76.
182. Orphanidou-Vlachou E, Tziakouri-Shiakalli C, Georgiades CS. Extramedullary hemopoiesis. Semin Ultrasound CT MR. 2014;35(3):255-62.
183. Cenariu D, Iluta S, Zimta AA, Petrushev B, Qian L, Dirzu N, et al. Extramedullary Hematopoiesis of the Liver and Spleen. J Clin Med. 2021;10(24).

184. Ruparelia N, Division of Cardiovascular Medicine RDoM, John Radcliffe Hospital, University of Oxford, Headley Way, Oxford OX3 9DU, UK, Oxford Heart Centre JRH, Headley Way, Oxford OX3 9DU, UK, Godec J, Dana-Farber Cancer Institute HMS, 44 Binney Street, Boston, MA 02115, USA, Lee R, et al. Acute myocardial infarction activates distinct inflammation and proliferation pathways in circulating monocytes, prior to recruitment, and identified through conserved transcriptional responses in mice and humans. European Heart Journal. 2021;36(29):1923-34.
185. Fagher B, Sjögren A, Sjögren U. Platelet counts in myocardial infarction, angina pectoris and peripheral artery disease. Acta Med Scand. 1985;217(1):21-6.
186. Haase VH. Regulation of erythropoiesis by hypoxia-inducible factors. Blood Rev. 2013;27(1):41-53.
187. Neumann FJ, Ott I, Gawaz M, Richardt G, Holzapfel H, Jochum M, et al. Cardiac release of cytokines and inflammatory responses in acute myocardial infarction. Circulation. 1995;92(4):748-55.
188. Deten A, Volz HC, Briest W, Zimmer HG. Cardiac cytokine expression is upregulated in the acute phase after myocardial infarction. Experimental studies in rats. Cardiovasc Res. 2002;55(2):329-40.
189. Bouchareychas L, Duong P, Covarrubias S, Alsop E, Phu TA, Chung A, et al. Macrophage Exosomes Resolve Atherosclerosis by Regulating Hematopoiesis and Inflammation via MicroRNA Cargo. Cell Rep. 2020;32(2):107881.
190. Bouchareychas L. High glucose macrophage exosomes enhance atherosclerosis by driving cellular proliferation & hematopoiesis. iScience. 2021.
191. Pinho S, Frenette PS. Haematopoietic stem cell activity and interactions with the niche. Nat Rev Mol Cell Biol. 2019;20(5):303-20.
192. Shefler I, Salamon P, Mekori YA. Extracellular Vesicles as Emerging Players in Intercellular Communication: Relevance in Mast Cell-Mediated Pathophysiology. Int J Mol Sci. 2021;22(17).
193. Valent P, Akin C, Hartmann K, Nilsson G, Reiter A, Hermine O, et al. Mast cells as a unique hematopoietic lineage and cell system: From Paul Ehrlich's visions to precision medicine concepts. Theranostics. 2020;10(23):10743-68.
194. Srivastava J, Katiyar S, Chaturvedi CP, Nityanand S. Extracellular vesicles from bone marrow mesenchymal stromal cells of severe aplastic anemia patients attenuate hematopoietic functions of CD34. Cell Biol Int. 2022;46(11):1970-6.

195. Budgude P, Kale V, Vaidya A. Mesenchymal stromal cell-derived extracellular vesicles as cell-free biologics for the ex vivo expansion of hematopoietic stem cells. Cell Biol Int. 2020;44(5):1078-102.
196. Calcagno DM, Ng RP, Toomu A, Zhang C, Huang K, Aguirre AD, et al. The myeloid type I interferon response to myocardial infarction begins in bone marrow and is regulated by Nrf2-activated macrophages. Sci Immunol. 2020;5(51).
197. Justicia C, Martín A, Rojas S, Gironella M, Cervera A, Panés J, et al. Anti-VCAM-1 antibodies did not protect against ischemic damage either in rats or in mice. J Cereb Blood Flow Metab. 2006;26(3):421-32.
198. Zhang S, Paccalet A, Rohde D, Cremer S, Hulsmans M, Lee IH, et al. Bone marrow adipocytes fuel emergency hematopoiesis after myocardial infarction. Nat Cardiovasc Res. 2023;2(12):1277-90.
199. Sreejit G, Abdel-Latif A, Athmanathan B, Annabathula R, Dhyani A, Noothi SK, et al. Neutrophil-Derived S100A8/A9 Amplify Granulopoiesis After Myocardial Infarction. Circulation. 2020;141(13):1080-94.
200. Tsiftsoglou AS. Erythropoietin (EPO) as a Key Regulator of Erythropoiesis, Bone Remodeling and Endothelial Transdifferentiation of Multipotent Mesenchymal Stem Cells (MSCs): Implications in Regenerative Medicine. Cells. 2021;10(8).
201. Brines ML, Ghezzi P, Keenan S, Agnello D, de Lanerolle NC, Cerami C, et al. Erythropoietin crosses the blood-brain barrier to protect against experimental brain injury. Proc Natl Acad Sci U S A. 2000;97(19):10526-31.
202. Moon C, Krawczyk M, Ahn D, Ahmet I, Paik D, Lakatta EG, et al. Erythropoietin reduces myocardial infarction and left ventricular functional decline after coronary artery ligation in rats. Proc Natl Acad Sci U S A. 2003;100(20):11612-7.
203. Hofmann U, Frantz S. Role of lymphocytes in myocardial injury, healing, and remodeling after myocardial infarction. Circ Res. 2015;116(2):354-67.
204. Feng Q, Li Q, Zhou H, Sun L, Lin C, Jin Y, et al. The role of major immune cells in myocardial infarction. Front Immunol. 2022;13:1084460.
205. Rochman Y, Spolski R, Leonard WJ. New insights into the regulation of T cells by gamma(c) family cytokines. Nat Rev Immunol. 2009;9(7):480-90.
206. Chen L, Flies DB. Molecular mechanisms of T cell co-stimulation and co-inhibition. Nat Rev Immunol. 2013;13(4):227-42.
207. Kurose H. Cardiac Fibrosis and Fibroblasts. Cells. 2021;10(7).

208. Yang W, Lin J, Zhou J, Zheng Y, Jiang S, He S, et al. Innate Lymphoid Cells and Myocardial Infarction. Front Immunol. 2021;12:758272.
209. Knorr M, Münzel T, Wenzel P. Interplay of NK cells and monocytes in vascular inflammation and myocardial infarction. Front Physiol. 2014;5:295.
210. Delgobo M, Weiß E, Ashour D, Richter L, Popiolkowski L, Arampatzi P, et al. Myocardial Milieu Favors Local Differentiation of Regulatory T Cells. Circ Res. 2023;132(5):565-82.
211. Souilhol C, Serbanovic-Canic J, Fragiadaki M, Chico TJ, Ridger V, Roddie H, et al. Endothelial responses to shear stress in atherosclerosis: a novel role for developmental genes. Nat Rev Cardiol. 2020;17(1):52-63.
212. Sorescu GP, Song H, Tressel SL, Hwang J, Dikalov S, Smith DA, et al. Bone morphogenic protein 4 produced in endothelial cells by oscillatory shear stress induces monocyte adhesion by stimulating reactive oxygen species production from a nox1-based NADPH oxidase. Circ Res. 2004;95(8):773-9.
213. Passerini AG, Polacek DC, Shi C, Francesco NM, Manduchi E, Grant GR, et al. Coexisting proinflammatory and antioxidative endothelial transcription profiles in a disturbed flow region of the adult porcine aorta. Proc Natl Acad Sci U S A. 2004;101(8):2482-7.
214. Sedlak J, Clyne A. Application of Shear Stress to Endothelial Cells Using a Parallel Plate Flow Chamber. Methods Mol Biol. 2023;2600:81-90.
215. Fallon ME, Mathews R, Hinds MT. In Vitro Flow Chamber Design for the Study of Endothelial Cell (Patho)Physiology. J Biomech Eng. 2022;144(2).
216. Scott DW, Vallejo MO, Patel RP. Heterogenic endothelial responses to inflammation: role for differential N-glycosylation and vascular bed of origin. J Am Heart Assoc. 2013;2(4):e000263.
217. Kalucka J, de Rooij LPMH, Goveia J, Rohlenova K, Dumas SJ, Meta E, et al. Single-Cell Transcriptome Atlas of Murine Endothelial Cells. Cell. 2020;180(4):764-79.e20.
218. Madonna R. Endothelial heterogeneity and their relevance in cardiac development and coronary artery disease. Vascul Pharmacol. 2023;153:107242.
219. Li Z, Solomonidis EG, Meloni M, Taylor RS, Duffin R, Dobie R, et al. Single-cell transcriptome analyses reveal novel targets modulating cardiac neovascularization by resident endothelial cells following myocardial infarction. Eur Heart J. 2019;40(30):2507-20.

220. Aird WC. Endothelial cell heterogeneity. Cold Spring Harb Perspect Med. 2012;2(1):a006429.
221. Ulyanova T, Scott LM, Priestley GV, Jiang Y, Nakamoto B, Koni PA, et al. VCAM-1 expression in adult hematopoietic and nonhematopoietic cells is controlled by tissue-inductive signals and reflects their developmental origin. Blood. 2005;106(1):86-94.
222. Ma S, Xing X, Huang H, Gao X, Xu X, Yang J, et al. Skeletal muscle-derived extracellular vesicles transport glycolytic enzymes to mediate muscle-to-bone crosstalk. Cell Metab. 2023;35(11):2028-43.e7.
223. Liu B, Jin Y, Yang J, Han Y, Shan H, Qiu M, et al. Extracellular vesicles from lung tissue drive bone marrow neutrophil recruitment in inflammation. J Extracell Vesicles. 2022;11(5):e12223.
224. French SL, Butov KR, Allaeys I, Canas J, Morad G, Davenport P, et al. Platelet-derived extracellular vesicles infiltrate and modify the bone marrow during inflammation. Blood Adv. 2020;4(13):3011-23.
225. Goldberg LR. Extracellular Vesicles and Hematopoietic Stem Cell Aging. Arterioscler Thromb Vasc Biol. 2021;41(8):e399-e416.
226. Preciado S, Muntión S, Corchete LA, Ramos TL, de la Torre AG, Osugui L, et al. The Incorporation of Extracellular Vesicles from Mesenchymal Stromal Cells Into CD34. Stem Cells. 2019;37(10):1357-68.
227. Zhang J, Li S, Li L, Li M, Guo C, Yao J, et al. Exosome and exosomal microRNA: trafficking, sorting, and function. Genomics Proteomics Bioinformatics. 2015;13(1):17-24.
228. Babuta M, Szabo G. Extracellular vesicles in inflammation: Focus on the microRNA cargo of EVs in modulation of liver diseases. J Leukoc Biol. 2022;111(1):75-92.
229. Cheng M, Yang J, Zhao X, Zhang E, Zeng Q, Yu Y, et al. Circulating myocardial microRNAs from infarcted hearts are carried in exosomes and mobilise bone marrow progenitor cells. Nature Communications. 2019;10(1):1-9.
230. Xie H, Sun L, Zhang L, Liu T, Chen L, Zhao A, et al. Mesenchymal Stem Cell-Derived Microvesicles Support Ex Vivo Expansion of Cord Blood-Derived CD34(+) Cells. Stem Cells Int. 2016;2016:6493241.

231. Sturgeon CM, Chicha L, Ditadi A, Zhou Q, McGrath KE, Palis J, et al. Primitive erythropoiesis is regulated by miR-126 via nonhematopoietic Vcam-1+ cells. Dev Cell. 2012;23(1):45-57.
232. Garcia A, Dunoyer-Geindre S, Zapilko V, Nolli S, Reny JL, Fontana P. Functional Validation of microRNA-126-3p as a Platelet Reactivity Regulator Using Human Haematopoietic Stem Cells. Thromb Haemost. 2019;119(2):254-63.
233. Salvucci O, Jiang K, Gasperini P, Maric D, Zhu J, Sakakibara S, et al. MicroRNA126 contributes to granulocyte colony-stimulating factor-induced hematopoietic progenitor cell mobilization by reducing the expression of vascular cell adhesion molecule 1. Haematologica. 2012;97(6):818-26.
234. Parajuli N, Yuan Y, Zheng X, Bedja D, Cai ZP. Phosphatase PTEN is critically involved in post-myocardial infarction remodeling through the Akt/interleukin-10 signaling pathway. Basic Res Cardiol. 2012;107(2):248.
235. Hu H, Wu J, Li D, Zhou J, Yu H, Ma L. Knockdown of lncRNA MALAT1 attenuates acute myocardial infarction through miR-320-Pten axis. Biomed Pharmacother. 2018;106:738-46.
236. Zhu XA, Gao LF, Zhang ZG, Xiang DK. Down-regulation of miR-320 exerts protective effects on myocardial I-R injury via facilitating Nrf2 expression. Eur Rev Med Pharmacol Sci. 2019;23(4):1730-41.
237. Tian ZQ, Jiang H, Lu ZB. MiR-320 regulates cardiomyocyte apoptosis induced by ischemia-reperfusion injury by targeting AKIP1. Cell Mol Biol Lett. 2018;23:41.
238. Chambers SM, Boles NC, Lin KY, Tierney MP, Bowman TV, Bradfute SB, et al. Hematopoietic fingerprints: an expression database of stem cells and their progeny. Cell Stem Cell. 2007;1(5):578-91.
239. Kim YC, Wu Q, Chen J, Xuan Z, Jung YC, Zhang MQ, et al. The transcriptome of human CD34+ hematopoietic stem-progenitor cells. Proc Natl Acad Sci U S A. 2009;106(20):8278-83.
240. Sayed AS, Xia K, Yang TL, Peng J. Circulating microRNAs: a potential role in diagnosis and prognosis of acute myocardial infarction. Dis Markers. 2013;35(5):561-6.
241. Sayed AS, Xia K, Salma U, Yang T, Peng J. Diagnosis, prognosis and therapeutic role of circulating miRNAs in cardiovascular diseases. Heart Lung Circ. 2014;23(6):503-10.

242. Wang GK, Zhu JQ, Zhang JT, Li Q, Li Y, He J, et al. Circulating microRNA: a novel potential biomarker for early diagnosis of acute myocardial infarction in humans. Eur Heart J. 2010;31(6):659-66.
243. Fabbiano F, Corsi J, Gurrieri E, Trevisan C, Notarangelo M, D'Agostino VG. RNA packaging into extracellular vesicles: An orchestra of RNA-binding proteins? J Extracell Vesicles. 2020;10(2):e12043.
244. Németh A, Orgovan N, Sódar BW, Osteikoetxea X, Pálóczi K, Szabó-Taylor K, et al. Antibiotic-induced release of small extracellular vesicles (exosomes) with surface-associated DNA. Sci Rep. 2017;7(1):8202.
245. McGeary SE, Lin KS, Shi CY, Pham TM, Bisaria N, Kelley GM, et al. The biochemical basis of microRNA targeting efficacy. Science. 2019;366(6472).
246. Ashburner M, Ball CA, Blake JA, Botstein D, Butler H, Cherry JM, et al. Gene ontology: tool for the unification of biology. The Gene Ontology Consortium. Nat Genet. 2000;25(1):25-9.
247. Consortium GO. The Gene Ontology resource: enriching a GOld mine. Nucleic Acids Res. 2021;49(D1):D325-D34.
248. Berman JN, Kanki JP, Look AT. Zebrafish as a model for myelopoiesis during embryogenesis. Exp Hematol. 2005;33(9):997-1006.
249. Zhang T, Wang Z, Liu Y, Huo Y, Liu H, Xu C, et al. Plastin 1 drives metastasis of colorectal cancer through the IQGAP1/Rac1/ERK pathway. Cancer Sci. 2020;111(8):2861-71.
250. Heissig B, Hattori K, Dias S, Friedrich M, Ferris B, Hackett NR, et al. Recruitment of stem and progenitor cells from the bone marrow niche requires MMP-9 mediated release of kit-ligand. Cell. 2002;109(5):625-37.
251. Yang F, Wang T, Du P, Fan H, Dong X, Guo H. M2 bone marrow-derived macrophage-derived exosomes shuffle microRNA-21 to accelerate immune escape of glioma by modulating PEG3. Cancer Cell Int. 2020;20:93.
252. Edgar L, Akbar N, Braithwaite AT, Krausgruber T, Gallart-Ayala H, Bailey J, et al. Hyperglycaemia Induces Trained Immunity in Macrophages and Their Precursors and Promotes Atherosclerosis. Circulation. 2021.
253. Ghafouri-Fard S, Abak A, Tavakkoli Avval S, Shoorei H, Taheri M, Samadian M. The impact of non-coding RNAs on macrophage polarization. Biomed Pharmacother. 2021;142:112112.

254. Wang S, Liu G, Li Y, Pan Y. Metabolic Reprogramming Induces Macrophage Polarization in the Tumor Microenvironment. Front Immunol. 2022;13:840029.
255. Boutilier AJ, Elsawa SF. Macrophage Polarization States in the Tumor Microenvironment. Int J Mol Sci. 2021;22(13).
256. Martinez FO, Sica A, Mantovani A, Locati M. Macrophage activation and polarization. Front Biosci. 2008;13:453-61.
257. Ley K, Laudanna C, Cybulsky MI, Nourshargh S. Getting to the site of inflammation: the leukocyte adhesion cascade updated. Nat Rev Immunol. 2007;7(9):678-89.
258. Divangahi M, Aaby P, Khader SA, Barreiro LB, Bekkering S, Chavakis T, et al. Trained immunity, tolerance, priming and differentiation: distinct immunological processes. Nature Immunology. 2020;22(1):2-6.
259. Netea MG, Domínguez-Andrés J, Barreiro LB, Chavakis T, Divangahi M, Fuchs E, et al. Defining trained immunity and its role in health and disease. Nature Reviews Immunology. 2020;20(6):375-88.
260. Netea MG, Quintin J, van der Meer JW. Trained immunity: a memory for innate host defense. Cell Host Microbe. 2011;9(5):355-61.
261. Netea MG, Joosten LAB, Latz E, Mills KHG, Natoli G, Stunnenberg HG, et al. Trained immunity: A program of innate immune memory in health and disease. Science. 2016;352(6284):aaf1098-aaf.
262. Di Luzio NR, Williams DL. Protective effect of glucan against systemic Staphylococcus aureus septicemia in normal and leukemic mice. Infect Immun. 1978;20(3):804-10.
263. Hotchkiss RS, Monneret G, Payen D. Sepsis-induced immunosuppression: from cellular dysfunctions to immunotherapy. Nat Rev Immunol. 2013;13(12):862-74.
264. Raes G, Noël W, Beschin A, Brys L, de Baetselier P, Hassanzadeh GH. FIZZ1 and Ym as tools to discriminate between differentially activated macrophages. Dev Immunol. 2002;9(3):151-9.
265. Kang Q, Li L, Pang Y, Zhu W, Meng L. An update on Ym1 and its immunoregulatory role in diseases. Front Immunol. 2022;13:891220.
266. Anderson P, Phillips K, Stoecklin G, Kedersha N. Post-transcriptional regulation of proinflammatory proteins. J Leukoc Biol. 2004;76(1):42-7.
267. Murray RZ, Stow JL. Cytokine Secretion in Macrophages: SNAREs, Rabs, and Membrane Trafficking. Front Immunol. 2014;5:538.

268. Zhu L, Zhao Q, Yang T, Ding W, Zhao Y. Cellular metabolism and macrophage functional polarization. Int Rev Immunol. 2015;34(1):82-100.
269. Corcoran SE, O'Neill LA. HIF1α and metabolic reprogramming in inflammation. J Clin Invest. 2016;126(10):3699-707.
270. Palsson-McDermott EM, Curtis AM, Goel G, Lauterbach MAR, Sheedy FJ, Gleeson LE, et al. Pyruvate Kinase M2 Regulates Hif-1α Activity and IL-1β Induction and Is a Critical Determinant of the Warburg Effect in LPS-Activated Macrophages. Cell Metab. 2015;21(2):347.
271. Dang B, Gao Q, Zhang L, Zhang J, Cai H, Zhu Y, et al. The glycolysis/HIF-1α axis defines the inflammatory role of IL-4-primed macrophages. Cell Rep. 2023;42(5):112471.
272. Liao ST, Han C, Xu DQ, Fu XW, Wang JS, Kong LY. 4-Octyl itaconate inhibits aerobic glycolysis by targeting GAPDH to exert anti-inflammatory effects. Nat Commun. 2019;10(1):5091.
273. De Jesus A, Keyhani-Nejad F, Pusec CM, Goodman L, Geier JA, Stoolman JS, et al. Hexokinase 1 cellular localization regulates the metabolic fate of glucose. Mol Cell. 2022;82(7):1261-77.e9.
274. Splichalova I, Mass E. Fate-Mapping of Yolk Sac-Derived Macrophages. Methods Mol Biol. 2024;2713:129-37.
275. Gomez Perdiguero E, Klapproth K, Schulz C, Busch K, Azzoni E, Crozet L, et al. Tissue-resident macrophages originate from yolk-sac-derived erythro-myeloid progenitors. Nature. 2015;518(7540):547-51.
276. Bonsergent E, Grisard E, Buchrieser J, Schwartz O, Théry C, Lavieu G. Quantitative characterization of extracellular vesicle uptake and content delivery within mammalian cells. Nat Commun. 2021;12(1):1864.
277. Cortés M, Brischetto A, Martinez-Campanario MC, Ninfali C, Domínguez V, Fernández S, et al. Inflammatory macrophages reprogram to immunosuppression by reducing mitochondrial translation. Nat Commun. 2023;14(1):7471.
278. Biswas SK, Lopez-Collazo E. Endotoxin tolerance: new mechanisms, molecules and clinical significance. Trends Immunol. 2009;30(10):475-87.
279. Park SH, Park-Min KH, Chen J, Hu X, Ivashkiv LB. Tumor necrosis factor induces GSK3 kinase-mediated cross-tolerance to endotoxin in macrophages. Nat Immunol. 2011;12(7):607-15.

280. Kalliolias GD, Ivashkiv LB. TNF biology, pathogenic mechanisms and emerging therapeutic strategies. Nat Rev Rheumatol. 2016;12(1):49-62.
281. Novakovic B, Habibi E, Wang SY, Arts RJW, Davar R, Megchelenbrink W, et al. β-Glucan Reverses the Epigenetic State of LPS-Induced Immunological Tolerance. Cell. 2016;167(5):1354-68.e14.
282. Shalova IN, Lim JY, Chittezhath M, Zinkernagel AS, Beasley F, Hernández-Jiménez E, et al. Human monocytes undergo functional re-programming during sepsis mediated by hypoxia-inducible factor-1α. Immunity. 2015;42(3):484-98.
283. Chen J, Ivashkiv LB. IFN-γ abrogates endotoxin tolerance by facilitating Toll-like receptor-induced chromatin remodeling. Proc Natl Acad Sci U S A. 2010;107(45):19438-43.
284. Anderson P. Post-transcriptional regulation of tumour necrosis factor alpha production. Ann Rheum Dis. 2000;59 Suppl 1(Suppl 1):i3-5.
285. Caput D, Beutler B, Hartog K, Thayer R, Brown-Shimer S, Cerami A. Identification of a common nucleotide sequence in the 3'-untranslated region of mRNA molecules specifying inflammatory mediators. Proc Natl Acad Sci U S A. 1986;83(6):1670-4.
286. Kruys V, Marinx O, Shaw G, Deschamps J, Huez G. Translational blockade imposed by cytokine-derived UA-rich sequences. Science. 1989;245(4920):852-5.
287. Lewis T, Gueydan C, Huez G, Toulmé JJ, Kruys V. Mapping of a minimal AU-rich sequence required for lipopolysaccharide-induced binding of a 55-kDa protein on tumor necrosis factor-alpha mRNA. J Biol Chem. 1998;273(22):13781-6.
288. Arderiu G, Peña E, Civit-Urgell A, Badimon L. Endothelium-Released Microvesicles Transport miR-126 That Induces Proangiogenic Reprogramming in Monocytes. Front Immunol. 2022;13:836662.
289. Zeinali F, Aghaei Zarch SM, Jahan-Mihan A, Kalantar SM, Vahidi Mehrjardi MY, Fallahzadeh H, et al. Circulating microRNA-122, microRNA-126-3p and microRNA-146a are associated with inflammation in patients with pre-diabetes and type 2 diabetes mellitus: A case control study. PLoS One. 2021;16(6):e0251697.
290. Newsholme P, Curi R, Gordon S, Newsholme EA. Metabolism of glucose, glutamine, long-chain fatty acids and ketone bodies by murine macrophages. Biochem J. 1986;239(1):121-5.

291. Tannahill GM, Curtis AM, Adamik J, Palsson-McDermott EM, McGettrick AF, Goel G, et al. Succinate is an inflammatory signal that induces IL-1β through HIF-1α. Nature. 2013;496(7444):238-42.
292. Li X, Shen H, Zhang M, Teissier V, Huang EE, Gao Q, et al. Glycolytic reprogramming in macrophages and MSCs during inflammation. Front Immunol. 2023;14:1199751.
293. Xu B, Liu Y, Li N, Geng Q. Lactate and lactylation in macrophage metabolic reprogramming: current progress and outstanding issues. Front Immunol. 2024;15:1395786.
294. Imai Y, Shimaoka M, Kurokawa M. Essential roles of VLA-4 in the hematopoietic system. Int J Hematol. 2010;91(4):569-75.
295. Huber R, Bikker R, Welz B, Christmann M, Brand K. TNF Tolerance in Monocytes and Macrophages: Characteristics and Molecular Mechanisms. J Immunol Res. 2017;2017:9570129.
296. Hotchkiss RS, Moldawer LL, Opal SM, Reinhart K, Turnbull IR, Vincent JL. Sepsis and septic shock. Nat Rev Dis Primers. 2016;2:16045.
297. Davidson SM, Riquelme JA, Zheng Y, Vicencio JM, Lavandero S, Yellon DM. Endothelial cells release cardioprotective exosomes that may contribute to ischaemic preconditioning. Sci Rep. 2018;8(1):15885.
298. Kwee L, Baldwin HS, Shen HM, Stewart CL, Buck C, Buck CA, et al. Defective development of the embryonic and extraembryonic circulatory systems in vascular cell adhesion molecule (VCAM-1) deficient mice. Development. 1995;121(2):489-503.
299. Marschall AL, Single FN, Schlarmann K, Bosio A, Strebe N, van den Heuvel J, et al. Functional knock down of VCAM1 in mice mediated by endoplasmatic reticulum retained intrabodies. MAbs. 2014;6(6):1394-401.
300. Mahalingaiah PK, Palenski T, Van Vleet TR. An In Vitro Model of Hematotoxicity: Differentiation of Bone Marrow-Derived Stem/Progenitor Cells into Hematopoietic Lineages and Evaluation of Lineage-Specific Hematotoxicity. Curr Protoc Toxicol. 2018;76(1):e45.
301. Olijnik AA, Rodriguez-Romera A, Wong ZC, Shen Y, Reyat JS, Jooss NJ, et al. Generating human bone marrow organoids for disease modeling and drug discovery. Nat Protoc. 2024;19(7):2117-46.
302. Khan AO, Rodriguez-Romera A, Reyat JS, Olijnik AA, Colombo M, Wang G, et al. Human Bone Marrow Organoids for Disease Modeling, Discovery, and Validation

of Therapeutic Targets in Hematologic Malignancies. Cancer Discov. 2023;13(2):364-85.
303. Souilhol C, Serbanovic-Canic J, Fragiadaki M, Chico TJ, Ridger V, Roddie H, et al. Endothelial responses to shear stress in atherosclerosis: a novel role for developmental genes. Nature Reviews Cardiology. 2019;17(1):52-63.
304. Onat D, Brillon D, Colombo PC, Schmidt AM. Human vascular endothelial cells: a model system for studying vascular inflammation in diabetes and atherosclerosis. Curr Diab Rep. 2011;11(3):193-202.
305. Wautier JL, Wautier MP, Schmidt AM, Anderson GM, Hori O, Zoukourian C, et al. Advanced glycation end products (AGEs) on the surface of diabetic erythrocytes bind to the vessel wall via a specific receptor inducing oxidant stress in the vasculature: a link between surface-associated AGEs and diabetic complications. Proc Natl Acad Sci U S A. 1994;91(16):7742-6.
306. Schmidt AM, Hori O, Chen JX, Li JF, Crandall J, Zhang J, et al. Advanced glycation endproducts interacting with their endothelial receptor induce expression of vascular cell adhesion molecule-1 (VCAM-1) in cultured human endothelial cells and in mice. A potential mechanism for the accelerated vasculopathy of diabetes. J Clin Invest. 1995;96(3):1395-403.